SCALING OF BURIED PIPE RESPONSE IN SAND TO SURFACE LOADS

GERALD PIERCEY

Your file Votre référence
ISBN: 978-0-494-42086-7
Our file Notre référence
ISBN: 978-0-494-42086-7

SCALING OF BURIED PIPE RESPONSE IN SAND TO SURFACE LOADS

by

© Gerald Piercey

A thesis submitted to the School of Graduate Studies in partial fulfillment of the requirements for the degree of Master of Engineering

Faculty of Engineering and Applied Science
Memorial University of Newfoundland

December 2005

St. John's Newfoundland

Abstract

The extent to which pipelines are stressed or damaged when heavy equipment such as bulldozers, excavators, or backhoes traverse or run parallel to the backfilled ditch of the pipeline right of way is not well known. Full-scale studies of buried pipes are expensive and time consuming. Finite element analysis, numerical and analytical studies have uncertainties due to generalized assumptions. Three test programs were carried out at the C-CORE Geotechnical Centrifuge Center in an attempt to validate the centrifuge as an effective tool to model the mechanical response of buried pipes to surface loads. In the first program, twenty four surface loading tests were carried out on an aluminum model pipe in the centrifuge. The second program included three tests at full-scale, varying the soil cover on a steel pipe. For direct comparison to the full-scale tests, a third program consisted of applying surface loads to six model steel pipes in the centrifuge. In a test bed of silica sand, cover depths, internal pressures, soil density and loading position were among the parameters varied. The model and full-scale pipes were instrumented with strain gages and ovalization transducers. Comparisons of the test data from each program validate the centrifuge as an effective and accurate tool to study the response of a buried pipe to surface loading. The test program also highlighted several common characteristics of the pipe response. The main modes of pipe deformation identified under surface loading were ovalization of the pipe cross-section and bending in the long section. The ovalization mode was not associated with the traditional elliptical pipe shape, but was characterized by the pipe crown deflecting significantly with smaller deformations of the pipe haunch. The second mode demonstrated the axial strain response was dominated by longitudinal deformation at the pipeline crown (local bending) with a limited axial strain response to load at the pipeline invert (limited global bending).

This thesis was made possible by data from C-CORE contracts for PRCI (Pipeline Research Council International) and GRI (Gas Research Institute). The test data and contents of this thesis are to be held confidential with the thesis not to be published or distributed for a period of 2 years.

Acknowledgements:

I would like to thank my supervisor, Dr. Ryan Phillips for his helpful guidance and advice while working on this project.

I would like to acknowledge the Gas Research Institute and the Pipeline Research Council International, for allowing me to use the data collected during C-CORE contracts they funded that allowed me to have a basis for this thesis.

My colleagues at the C-CORE Centrifuge Center also deserve a note of thanks. Thank you to the numerous staff that assisted in both time and advice during the testing, analysis and data interpretation phases of this work.

On a personal note I would like to thank my parents for the encouragement and motivation to pursue a post secondary degree. I would like to thank my wife, Sonya for her love and encouragement during this entire process, without her, outside motivators alone would not have been sufficient to complete this work.

Table of Contents

List of Tables

List of Figures

List of Appendices

List of Abbreviations and Symbols

B_c = diameter of a pipe

C_c = embankment conditions

C_f = pipe construction factor

dy = change in vertical diameter of a pipe

D = the inside diameter of pipe

D_f = pipe design factor

D_l = deflection lag factor

D/t = pipe diameter / pipe thickness ratio

e_{max} = maximum soil void ratio

e_{min} = minimum soil void ratio

e = modulus of passive soil resistance

E = modulus of elasticity

E' = modulus of soil reaction

E_0 = the output voltage from a strain gage (mV)

E_s = the bridge supply voltage for a strain gage (V)

F = the gage factor of a strain gage

F_a = external load applied

g = acceleration due to gravity

Gs = the specific gravity of the soil particles

h = pipe cover depth

H_c = pipe cover depth

I = moment of inertia

I_f = pipe inspection factor.

K = pipe bedding constant

Kg = kilograms

kW = kilowatts

lbs = pounds

m = meter

M_s = constrained soil modulus

n = centrifuge scaling factor

P = pipe pressure

PS = pipe stiffness

r = mean pipe radius

rpm = revolutions per minute

S = pipe stiffness

S_f = soil stiffness factor

t = wall thickness of a pipe

T_f = time lag factor

w = soil pressure at crown of a pipe

W_c = Marston's load per unit length

γ = soil unit weight

ε = strain

ε_{hoop} = pipe hoop strain

ν = Poisson's ratio

ρ = density

ρ_w = density of water

σ = stress

σ_{hoop} = pipe hoop stress

Δ/D = pipe ovalization

Δx = horizontal deformation of the pipe at the centerline

Δy (%) = percent vertical deflection of a pipe

%RD = percent relative density of soil

FEA = finite element analysis

GRI = Gas Research Institute

NSERC = Natural Science and Engineering Research Council Canada

PRCI = Pipeline Research Council International

SMYS = specified minimum yield strength

SwRI = Southwest Research Institute

USBR = United States Bureau of Reclamation

1.0, Introduction

1.1 Background

The extent to which pipelines are stressed or damaged when heavy equipment such as bulldozers, excavators, or backhoes traverse or run parallel to the backfilled ditch of the pipeline right of way is not well known. Such activity could cause distress that could present problems, or the soil structure interaction may behave in such a way that the actual stress distribution to the pipeline is not of concern.

Interest in this area grew in the 1990's when a train derailed in California. Parallel to the rail bed was a buried pressurized gas pipeline. The train fell to the side of the rail bed opposite the pipeline and a crane outrigger was placed over the buried pipe by the rail company to upright the cars. This crane outrigger's placement was carried out without the permission of the pipeline company and the extent to which it distressed the pipeline was of great concern.

Surface loads imposed on buried pipeline systems by heavy equipment on pipeline right-of-ways represent a potential hazard to pipeline integrity. Engineering practice provides adequate guidance for the assessment of pipeline stress due to surface loads for typical design conditions. A comprehensive understanding of pipeline/soil interaction mechanisms and mechanical pipeline behavior during non-typical surface loading events

has not been well developed. An increased understanding in this area is needed to develop guidelines and engineering tools.

1.2 Objective and Incentive

While full-scale tests are very expensive and time consuming, centrifuge modelling can replicate full-scale behavior, thus providing an economical and effective means of examining the various buried pipeline conditions encountered in the real world. Centrifuge testing could be used to verify or extend full- scale data sets and numerical simulations.

C-CORE undertook a series of projects funded by PRCI (Pipeline Research Council International) and the GRI (Gas Research Institute) in the area of surface loading of buried pipes. The project objective was to validate centrifuge modeling as a viable experimental method, in assessing the pipe stress response to non-typical surface loads through comparison with compatible full-scale experiments. Centrifuge modelling was conducted to verify that the response of the model pipe (strain and ovalization) was comparable to that of full-scale prototypes studied by SwRI (Southwest Research Institute) under a PRCI project. The work from this contract is detailed in Chapter 3 of this thesis and is considered in this thesis as the first testing program. A second contract was brought about by the lack of full-scale data from the SwRI program. In the second contract, full- scale and centrifuge tests were carried out to provide data from two scales with comparable conditions allowing for a fair assessment of the centrifuge as a tool in

this research. The work from this contract is detailed in Chapters 4 and 5 of this thesis and is considered in this thesis as the second and third testing programs respectively. A third contract of centrifuge tests were added to extend the database of surface loaded pipe tests, this is beyond the scope of this thesis. The test data and contents of this thesis are to be held confidential with the thesis and are not to be published or distributed for a period of 2 years.

1.3 Author's Role

The author was project manager and design engineer for the contract work detailed in this thesis. For the test program on aluminum pipe models, he was responsible for time and cost tracking, purchasing, scheduling, design of test components and supervision of an engineering work term student and an engineering graduate student that assisted in carrying out the tests. The design work included pipe and test instrumentation layout, design of the ovalization sensors to measure diametrial deflection, design of the model pipe components and design of the pressurization system. The author carried out labor and material cost analysis and co-authored a proposal that resulted in the second phase of the surface loading work, the combined full-scale and centrifuge test comparison contract. He was also project manager for that program with duties that included supervision of engineering work term students and two laborers in conducting the full-scale tests, scheduling tasks, tracking labor and material costs and reporting to the client. He carried out design work for this second phase including instrumentation layout, pipe model design, full-scale pipe ovalization profiler and full-scale load frame design. The

data collection, synthesis, analysis and interpretation methods were the responsibility of and were carried out by the author of this thesis. The author conducted data analysis and interpretation independent from the contracted work, confirming, expanding on and in several cases correcting the initial results.

1.3 Research Facilities

1.3.1 Centrifuge Facility

The C-CORE geotechnical centrifuge center located on the campus of Memorial University of Newfoundland was established in 1993. Consisting of a soils laboratory, model preparation area and a geotechnical centrifuge the center was funded by the Canada / Newfoundland Offshore Development Fund, the Technical Outreach Program of Industry, Science and Technology Canada and NSERC (Natural Science and Engineering Research Council Canada).

The model preparation area consists of a machine shop, sand raining room, electronics lab, cold room and x-ray facility. Experimental packages are prepared in the model preparation area and are carried by a forklift and loaded onto the centrifuge platform.

The centrifuge, an Acutronic 680-2, is housed in a 13.5 meter diameter chamber with 0.3 meter thick concrete walls. The centrifuge has a radius of 5.5 meters from its rotational axis to the face of its swinging platform. It can accommodate a payload of up to 1.1 by

1.4 meters in plan and up to 1.2 meters in height and up to 2.1 meter in height in the centre of the platform. The centrifuge platform can carry a mass of 2200 kg to a rotational speed of 134 rpm, thus generating a centripetal acceleration of 100 gravities at a 5 meter radius. Due to increased self weight of the platform the payload mass must be reduced to 650 kg when a rotational speed of 189 rpm is used to generate a centripetal acceleration of 200 gravities at a 5 meter radius. The centrifuge consists of a swinging platform, two arms, a central drive box, a counterweight, electrical cabinets, pedestal, gear box, motor and drive. A schematic of the centrifuge can be seen in Figure 1.1. The swinging platform is suspended from two pivots on the end of the arms and is covered in an aluminum aerodynamic shroud to reduce drag. The arms are two parallel steel tubes held to the axis of rotation by the central drive box and held together by three spacers. The counterweight, consisting of 20,200 kg of steel, is used to balance the machine. The position of the counterweight is adjusted by gearwheels on a screw thread to a location that balances the machine against the mass in the basket. The centrifuge electrical cabinets sit on the drive box and contain components of the data acquisition and control systems. On the top of the cabinets, an electrical slip ring cabinet passes data acquisition lines, electronic control lines and power to the on arm components. The arm rotates on tapered roller bearings that are between the drive box and the pedestal mount. The pedestal mount is attached to the concrete pedestal, which is in essence the floor, by four strain gaged steel plates. These strain gages measure and monitor the imbalance in the machine. A 450kW AC variable speed motor drives a 9:1 gear box, whose output is coupled to the central vertical drive shaft that is connected to the centrifuge drive box.

The motor is powered by two parallel 250kW inverters. A fluid rotary union (FRU) is connected to the bottom of the gearbox allowing water, air, refrigerant and hydraulic lines to be connected to the rotating centrifuge. This FRU then connects to the fluid lines that pass through the hollow gearbox shaft and the hollow drive shaft to the centrifuge arm and on to the experimental package.

Instrumentation is monitored and various actuators are controlled from the centrifuge control room. Data acquisition is performed using a PC-based data acquisition system. Amplification, transducer excitation voltage, and filtering are provided using a custom designed signal-conditioning system. Transducer signals are digitized using a 16-bit data acquisition board operating through a Windows-based data acquisition program called Snapmaster.

Since the installation of C-CORE's centrifuge the usage of centrifuges worldwide has continued to grow. Academic research on these machines has been reduced because of the growth of industrial interest to use the centrifuge to help solve numerous problems. Common applications include foundation engineering, bridge piers, retaining walls, underground excavations, buried structures, earthquake engineering, contaminant transport and, as in this thesis, pipelines engineering.

1.3.2 Centrifuge Scaling Laws

Centrifuge modelling has been used in soil mechanics modeling and in a wide variety of other gravity dependent problems (Schofield, 1980). Centrifuge modelling is based on the principle of using an increased gravity field generated in a spinning centrifuge to replicate the effects of full-scale body forces on a scaled model. By decreasing the size of a structure, building a scale model, and increasing the gravitational acceleration by flying it in a centrifuge, the stress conditions resulting from body forces in the prototype are reproduced. This relationship is illustrated in Figure 1.2, showing the example of an earth embankment. The full-scale structure is referred to as the prototype while the scaled model is simply the model. Using standard centrifuge scaling laws, the model to prototype parameters can be scaled by a factor (n) as a function of the applied centrifuge acceleration field in relation to the acceleration due to Earth's gravity ($g = 9.81\ m/s^2$). These scaling laws are derived from the equation for the stress level at a particular point in the soil, defined by the equation:

$$\sigma = \rho g h \tag{1.1}$$

where ρ is the soil density, g is the acceleration due to gravity and h is the depth to the desired level of interest. The centrifuge models scaling laws are derived from the necessity to have stresses in the model equal to the stress in the prototype. The scale model built to 1 / n scale, subjected to n times earth's gravity in the centrifuge, follows the various scaling laws. The scaling laws between prototype and model for several parameters are summarized in Table 1.1.

1.3.3 Full-Scale Testing Facility

The C-CORE full-scale test facility, rented and maintained by C-CORE, is located in the laboratories of the Faculty of Engineering and Applied Science of Memorial University of Newfoundland. The main component of the facility is the concrete test tank measuring 1.4m deep, 1.5m wide and 6.5m long. A clay mixer, an overhead crane, various tamping equipment, various instrumentation including string potentiometers, LVDT's, load cells, a mobile data acquisition system and two electromechanical actuators allow a variety of test configurations to be carried out in the facility. The 25,000 lb electromechanical actuators, complete with a system of steel I beam sections can be positioned to apply a variety of loading conditions to a soil bed or directly to a buried structure.

The facility has been used by C-CORE to carry out various full-scale testing programs as discussed in Konuk *et al.* (1999) and Popescu *et al.* (2002). Backfill & Rockdump Model Testing for Technip Coflexip Stena Offshore, Dynamic Pipe Soil Interaction funded by Trans Canada Pipe Lines and NSERC, and Modelling of Pipeline/Soil Interaction for the Geological Survey of Canada are among the testing programs completed in the full-scale facility. Results from these programs were often compared to and complemented by either centrifuge model tests or numerical simulations.

Table 1-1: Centrifuge Scaling Laws

Quantity	Prototype	Model
Length	n	1
Area	n^2	1
Volume	n^3	1
Acceleration	1	n
Mass	n^3	1
Force	n^2	1
Energy	n^3	1
Stress	1	1
Strain	1	1
Mass Density	1	1

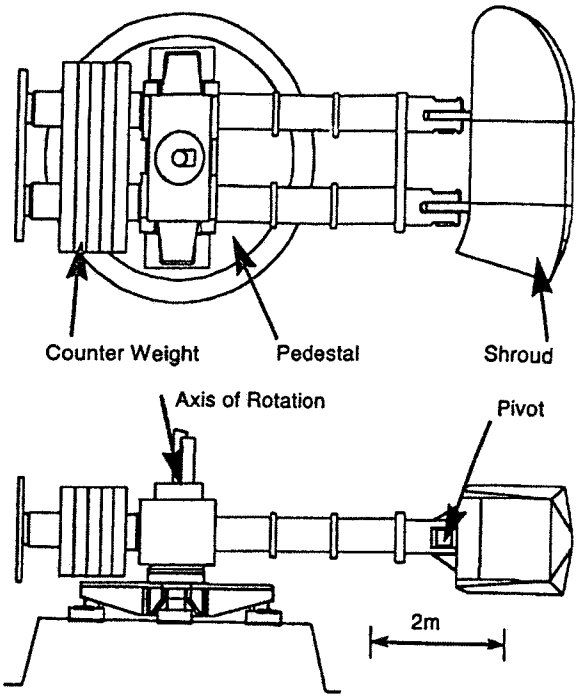

Figure 1-1: Centrifuge Schematic

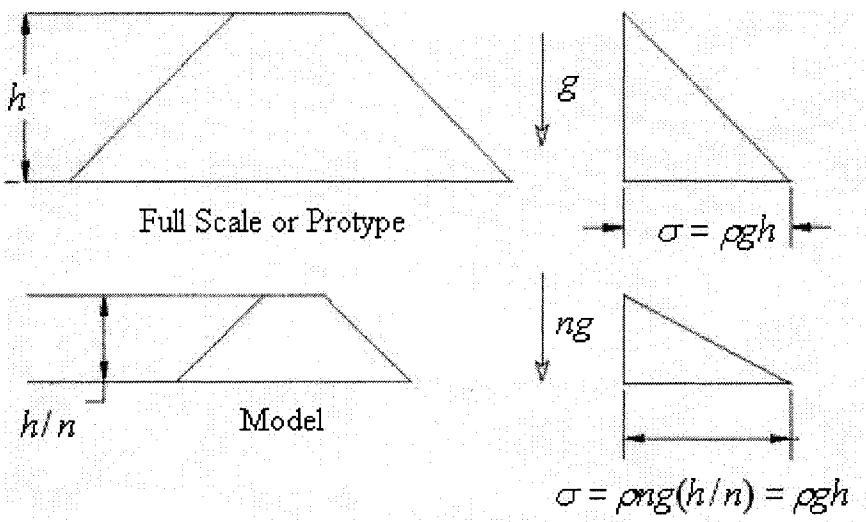

Figure 1-2: Centrifuge Scaling

2.0, Literature Review

2.1 Introduction

Underground conduits or buried pipes have improved man's existence since ancient times. Remains of water and sewer structures have been found in Europe, Asia and the Americas that date back to early civilized man. Steel pipe, formed by rolling sheets of steel, were used for water lines in the United States and Europe in early 1850's (American Water Works, 1989). The large increase in mild steel production in the later half of the 19^{th} century was followed by the mass production of steel pipes. These early pipes were manufactured by cold-forming large steel plates to a required diameter and riveting the joint. This was soon replaced by lap welding the joint, which was also replaced by electric arc-welding and later continuous arc-welding of the joint. Today underground conduits or pipes serve in diverse applications such as sewer lines, drains, oil and gas lines, electrical conduits and subway tunnels.

14,000 years ago when glaciers receded from what is now Iowa they left behind flat land with poor drainage (Spangler and Handy, 1894). At the turn of the twentieth century when farmers discovered that after draining this soil they were left with very rich farm land the need for drainage technology became important to the region. This need was part of the driving force for the culvert / buried pipe work that took place at Iowa State University first by Marston, then Spangler and others that followed. Accompanying

farmland drainage as a driving force was the development of sewage systems and the replacement of river bridges with culverts.

This increased interest in buried pipe behavior forms a large portion of the work carried out in an area known as soil / structure interaction. The nature of the soil structure interaction problem, a statically indeterminate problem, has maintained it for the past century as an area of study and debate. In studying soil structure interaction, it must be recognized that when the pressure of the soil on the structure produces deflections in the structure, the structure in turn determines that soil pressure, this resulting in non-linear behaviour.

In the past century much work has been done on analytical studies, full-scale tests, field monitoring, numerical and finite element studies and now centrifuge studies. The expansion of the buried pipe experimental database, the enhancements in finite element techniques and soil models have increased an engineer's ability to study associated problems.

2.2 Buried Pipe Design Overview

To determine the design approach for a buried pipeline, the pipe is first classified as either flexible or rigid. Rigid pipes support the load in the ground by using the resistance of the pipe as a ring. A flexible pipe uses the horizontal thrust of the soil which allows it to resist vertical loads by deforming and transferring those loads to the soil. A flexible

pipe generally deforms into an oval, increasing in horizontal diameter and reducing in vertical diameter without collapse or fracture. Some pipes that are rigid but can sustain some deformation are often called semi-flexible or intermediate. A rigid pipe's cross section cannot generally be distorted more than 0.1% without damage, semi rigid up to 3% and flexible more than 3% (Potter, 1985). A thin walled steel pipe would be flexible, a thick walled iron pipe would be semi-flexible and a concrete pipe is typically rigid.

The load supporting capability of a flexible pipe depends on the combined action of the pipe and the surrounding soil. When a flexible pipe encounters vertical load its diameter will deform, the sides or haunches may deflect outward and top or crown deflect downward. This deflection is resisted by the horizontal soil reaction forces. The combination of soil stiffness and pipe stiffness allow the pipe to have a larger load carrying capacity than the pipe by itself. Soil stiffness is affected by soil density, soil type and confining pressure. The flexible pipe develops passive soil support on the sides and through ring deflection relieves the pipe of a major portion of the vertical load which is picked up by the surrounding soil in an arching action over the pipe.

The several ways a flexible pipe can fail under load include excessive ring compression or failure of the ring by compressive loads and failure by excessive deformation caused by poor lateral restraint (Young and Trott, 1984). Also inward buckling can occur near the crown or invert when arching is lost and collapse occurs. Figure 2.1 shows a cross section of a pipe with labels indicating the locations of the crown, invert and haunch on

the pipe as they are used in this thesis. Finally local buckling can occur when the pipe is well restrained but forces are enough and wall is thin enough to cause collapse. Failure can occur in certain materials over time even if stresses are not sufficient in the short term to cause any of the failures above.

The main factors to be considered in flexible pipe design include:

- adequate compressive strength in a ring to carry the external load
- adequate stiffness of the pipe wall circumferentially to prevent local buckling
- surrounding soil that will when placed and compacted keep the deformation within the design limits, which is essentially the horizontal deflections of the pipe at the spring line (Young and Trott, 1984)

The third of the above, the deflection, is often the governing criteria in design of flexible pipes, plastics, corrugated steel or aluminum or welded steel. Factors effecting this deflection include soil type and properties (density and moisture content), bedding reactions (bedding and backfill), their placement methods, the extent of undesirable materials in the fill, the location of the water table, friction between the soil and the pipe, internal pressure, the pipe diameter and material properties, the burial depth and the type of live load on the surface.

In practice buried flexible pipes are designed to withstand internal pressure and external loads such as construction load, dead load due to soil cover, and surface load. The design of oil and gas pressurized pipes is different from gravity flow pipes. Most pressurized

flexible pipes made of steel, ductile iron or thermal plastics are designed against external loading and internal pressure independently (Moser, 2001; Prevost and Kienow, 1994). For example, pipes are designed for internal pressure without taking any account of stresses or strain due to installation or external loading. The maximum stresses from these two separate analyses are compared to the design criteria, typically the critical loads are those induced by internal pressure. In design, the maximum internal operating pressure in oil and gas pipelines is controlled by the allowable hoop stresses. The hoop stress is limited to a fraction (β) of the specified minimum yield strength (SMYS).

2.3 Historical Developments

In 1913 Professor Anson Marston published "Marston's Theory of Loads", a theory that predicts loads imposed by a soil column on a buried pipe (Moore, 1987). It assumes a flexible pipe, neglects side wall friction and using a prism load from the soil is a conservative loading calculation. He states that the total pipe load is the dead load on the pipe from the soil cover combined with the live load from the surface, depending on type of load and depth of cover. Marston's dead load on the pipe per unit length is expressed as:

$$W_c = C_c \, w \, B_c^{\,2} \tag{2.1}$$

where C_c is his coefficient of embankment conditions B_c is the diameter of the pipe and w is the unit weight of soil. For a flexible pipe the settlement ratio is assumed to be 0 and therefore $C_c = H_c/B_c$, with H_c the cover depth, the load per unit length is also expressed as:

$$W_c = w\, H_c\, B_c \tag{2.2}$$

His use of the Boussinesq solution for loads applied to a soil surface estimates stresses that develop across the top of a buried structure. Boussinesq, a French mathematician, found the load on a buried pipe, assuming the soil was an elastic homogeneous, isotropic medium. Although the assumption is not correct the formulation gives fair results (Moore, 1987).

Dr. Merlin Spangler, a student of Marston, found that the Marston theory was not adequate for flexible pipes. Spangler assumed the deformed shape of the pipe to be an ellipse based on large diameter culverts, with a soil reaction load at the invert matching the crown and the haunch loads being parabolic and equal (Spangler 1941). Spangler's work led to the Iowa formula in 1927. His methodology was based on elastic ring theory and was calibrated by empirical and numerical investigations. This formula, which has been written in several forms, is:

$$\Delta x = \frac{D_l\, K\, W_c\, r^3}{EI + 0.061\, e\, r^4} \tag{2.3}$$

where Δx is horizontal deformation of the pipe at the centerline, D_l is the deflection lag factor, K is the bedding constant (depends on the bedding angle), W_c is Marston's load per unit length, r is the mean pipe radius, E is the pipe modulus of elasticity, I is the moment of inertia of the pipe and e is the modulus of passive soil resistance (Jeyapalan and Watkins, 2004). This formulation contains three empirical constants K, D_l and e. K varies based on the width and angle of bedding and is usually assumed to be 0.1, it

accounts for the reactive force imparted from the pipe bedding material when the pipe in installed. Spangler observed that deflections could increase up to 30% over 40 years, which is why he used the deflection lag factor, commonly taken as 1.5 for conservative design. It is noted that the higher the density of the soil the shorter time of continued deflection.

Howard presents a rectangular deformation, with stiffer pipes developing plastic hinges at 60° and 270° and more flexible pipes showing hinging at 45°, 135°, 225° and 315° (Rogers, 1985). This observation adds to the pipe deformation modes including elliptical, heart shaped, inverted heart shaped and square. Howard states that the elliptical shape is correct when cyclic loads are present or the soil is not stiff, but with static loads the assumption could be in error.

The Modified Iowa Formula, 1958, was published by Dr. Reynold K. Watkins, a graduate student of Spangler. Watkins working with Spangler found that e varied with cover depth and er was not constant for a given soil so they formulated the modulus of soil reaction, E'. E' is a function of the pipe radius, r, and the modulus of passive soil resistance, e (Moser, 2001). The modified Iowa formula is written:

$$\Delta x = \frac{D_l K W_c r^3}{EI + 0.061 E' r^3} \tag{2.4}$$

Watkins presented another form of the modified Iowa formula:

$$\Delta x = \frac{D_l W_c}{1.5 PS + 0.061 E'} \tag{2.5}$$

The pipe stiffness (PS) as per ASTM D2412 is:

$$PS = \frac{E\,I}{0.149\,r^3} \tag{2.6}$$

where E is the modulus of elasticity for the pipe, I is the moment of inertia and r is the mean radius (Jeyapalan and Watkins, 2004). The pipe stiffness can also be found by carrying out parallel plate loading tests by ASTM D2414 where:

$$PS = \frac{F_a}{dy} \tag{2.7}$$

where F_a is the external load applied over a length and dy is the change in vertical diameter of the pipe wall (Jeyapalan and Watkins, 2004).

Both forms of the Modified Iowa formula require E'. Many researchers have attempted to measure E' without success. Moser (2001) gives values from 2.8MPa to 13.8MPa for fine-grained soils with slight to high degrees of compaction. Throughout history researchers found E' values, using finite element analysis, model experiments and field tests, that have ranged by several hundred percent. They all agree E' depended on soil type, density, water content and pipe geometry.

E' can be related to soil stiffness modulus in the soil surrounding the pipe. The soil stiffness modulus is in turn a function of soil confining pressure and shear stress ratio. The stress state surrounding buried pipeline is in turn a function of cover depth, pipe diameter, soil weight and surface load levels. Distributions of the confining pressure and shear stress ratio under various loading scenarios are not uniform. Thus if the confining

pressure and shear stress ratio in the soil around the pipe varies with surface load levels, cover depths and soil weight, the soil stiffness modulus varies and E' varies.

Determining deflection with the Modified Iowa formula with such a variation in E' is questionable. The most common and useful method is to back calculate E' by measuring deflections in a loaded buried pipe using the Modified Iowa formula. The problem in determining E' is that it is not a soil property alone but a property of the pipe / soil system.

Amster Howard (1977) created tables of soil types and compaction conditions and their associated E' values (Jeyapalan and Watkins, 2004). These tables were created from many lab and field measurements. Jeyapalan and Watkins (2004) say that this work created confusion and led to uses of the data that resulted in a very high degree of error. Schluter and Capossela (1998) compared field measurements of pipe deflection to their estimation from the modified Spangler's formula using E' values from Howard (1977). With field measurements on 175 different installation conditions for plastic pipe they showed significant scatter between prediction and measured (calculated E' with the Modified Iowa Formula and their data), on the order of hundreds of percent. Hartley and Duncan (1987) published E' values for various cover depths for the steel pipe industry. Most standards have not chosen to adopt these values. Their work involved finite element analysis (FEA) and the study of existing field data. They studied pipe radii from 24 to 72", cover depths from 5 to 20 ft and pipe stiffness values from 4 to 136psi. Shafer

(1948) showed remarkable variation in E' with soil depth. Jeyapalan and Jaramillo (1994) also showed E' varied with stiffness and size of the pipe. Jaramillo (1989) studied plastic pipe varying from 6 to 18" in radius, pipe cover depths from 5 to 30 ft and published varying values of E'.

Spangler and Watkins original work recommended an E' value of 700psi for typical pipe installations (Jeyapalan and Watkins, 2004). The American Society of Civil Engineers (ASCE) recommended this value when soil is compacted to a minimum 90% Proctor. The Transport Research Board (TRB) Report 225 recommends for shallow covers the listed value of E' be reduced by 50% (Chambers *et al.*,1980).

The Spangler methods and the Iowa formula, are semi-empirical methods based on parameters that are based on test results, so to use them in different cases can be inaccurate. Unless the user has the same soil and pipe conditions as in the table there can be substantial errors with only small changes in one or two properties. Watkins and Spangler (1958) noted that there is little point in evaluating E' through testing and applying this modulus to predict ring deflection since the model test provides the deflection directly (Jeyapalan and Watkins, 2004). Furthermore, the pipe ring deflection may not be the only mechanical performance criteria for the pipe.

The Iowa formula and its modified version did not consider internal pressure effects, coupled structural/soil deformation mechanisms, or relative structural/soil stiffness

effects. For flexible pipeline systems, the significance of these issues on the pipeline response due to surface loads has been investigated through a number of studies that include Moser (2001), Masada (2000), Prevost and Kienow (1994), Shmulevich *et al.*. (1986), Jeyapalan and Abdel-Magid (1984) and Gumbel & Wilson (1981).

For a pressurized flexible pipe, internal pressure stiffens the pipe considerably. The Iowa formula was extended by Prevost and Kienow (1994) to include this effect:

$$\Delta / D = \frac{0.312w}{24S + p + 1.85E'} \tag{2.8}$$

where Δ/D is pipe ovalization, w is the soil pressure at crown, S is pipe stiffness (EI/D^3) and p is internal pressure. The internal pressure of the pipe has a significant effect of reducing the stresses in the pipe from the vertical load.

Gumbel & Wilson (1981) show the simple representation of external loading on a pipe as a vertical pressure (as used in Iowa formula) is not representative of the system. First, it does not consider the free field components of horizontal soil pressure, i.e. the horizontal stress components resulting from the vertical stress due to self-weight and external loads rather than by only the load from lateral deformation. Second the lateral soil stiffness is omitted. Shmulevich *et al.* (1987) showed that both normal and tangential stresses in the soil pipe interface should also be considered for the evaluation of soil loads on buried pipes. The omission of tangential stresses leads to underestimation of the total vertical load and may result in unsafe pipe design.

The effects of surface load on pipe response have also been investigated by a number of researchers in other ways. Moore (1987) developed a semi-analytical method to estimate the response of a pipe to surface load. Both symmetric and asymmetric surface loads have been considered. In this solution, both soil and pipe are considered as elastic materials.

To avoid the problems with E' the use of the constrained soil modulus, M_s, has become common. M_s is:

$$M_s = \frac{E_s (1-\nu)}{(1+\nu)(1-2\nu)} \tag{2.9}$$

a constitutive material property taken from slope of the secant of the stress strain diagram from the confined compression test of soil or calculated from the Young's modulus E_s and Poisson's ratio, ν (Bulson, 1985). Since it is taken as the secant modulus it in part accounts for the nonlinearities in the stress strain response around the pipe.

The USBR (United States Bureau of Reclamation) equation is a method of calculating vertical deflection of a buried flexible pipe due to the soil load (Howard, 1981). Like the Iowa formulas it is an empirical relationship based on the back calculated parameters from field measurements. It can be used to predict initial, long term and average deflections. It is a modified method from the Iowa formula with several differences. It produces vertical, not horizontal deflections, it predicts deflection after installation,

predicts long term deflection, average and maximum deflections, incorporated a design factor and uses soil stiffness factor (S_f) rather than the Modulus of soil reaction E'. The equation assumes a prismatic load and a pipe wall stiffness (EI/r^3).

$$\Delta y(\%) = T_f \left[\frac{0.07 \gamma h}{EI/r^3 + S_f D_f} + C_f \right] + I_f \qquad (2.10)$$

where $\Delta y(\%)$ is the percent vertical deflection, T_f is the time lag factor, γ is the backfill density, h is the cover depth, EI/r^3 is the pipe wall stiffness factor, S_f is the soil stiffness factor, D_f is the design factor, C_f is the construction factor and I_f is the inspection factor. S_f, the soil stiffness factor, represents the resistance of the soil beside the pipe to outward movement of the pipe, it depends on the type of soil and degree of compaction and is a back calculated value (Howard, 1981).

While the problems with determining E' and its proper use within the Iowa formula have been discussed, it should be noted that the formulation of this theory has been essential to buried pipe design. Without this theory flexible pipe design would be overly conservative and inefficient.

2.4 Full-Scale Studies

Full-scale studies are very common for a variety of pipe soil interaction problems. While time consuming and expensive, if test conditions can be well controlled, issues such as scaling, model uncertainty, inaccurate assumptions and so on do not exist or are lessened

in full-scale tests. Presented are examples of several studies of buried pipe sections subjected to surface loads at full-scale.

In 1995, PRCI contracted Southwest Research Institute (SwRI) to conduct a series of full-scale experiments and analytical studies focusing on the development of guidelines for assessing shallow buried pipelines subjected to non-typical surface loadings (Waldhart *et al.*, 2001). Their program was a combination of finite element analysis and full-scale testing. Phase I of their program was to include testing of a 16" pipe, with a D/t of 43 and a 36" pipe, with a D/t of 109. These tests were to take place in 4 different test beds, 70 and 80% relative density sands and 80 and 95% Modified Proctor clays. Cover depths to be tested were between 10 and 36 inches. The pipes pressure levels were to be 5 and 80% of the pipe SMYS (specified minimum yield stress). Three types of surface loads, point loads, surcharge loads and impact tire loads, were proposed to be carried out. For Phase II of their program weak and strong clays only were to be tested, with 16, 24, 36 and 48 inch pipes, at cover depths of ½, ¾ and 1 pipe diameter. Three internal pressures of 5, 40 and 80% SMYS were to be tested. The full complement of tests they have carried out have yet to be reported to the public and were not available for discussion in this thesis. In the report referenced in this thesis, Waldhart only describes some initial testing carried out on a 16" pipe in weak sand with some limited references to the other data.

SwRI's full-scale facility, an exterior facility, is capable of applying a 180,000 lb point load or 5,000psf over a 12 foot square load pad. For the tests described in the referenced paper point loads were applied with a 22.6" diameter load pad attached to a hydraulic cylinder. This pad was sized to simulate the footprint of a heavy lift crane, such as the one mentioned in Section 1.1. To bury the pipe they excavated a stepped trench 2 ¼ pipe diameters deep and prepared a ¼ D bedding layer before laying the pipe. Waldhart carried out two types of point load tests. The first test type was where the internal pressure was kept constant for the duration of the test. The second test, a three stage pressure test, was where the internal pressure was varied while the surface load increased. This was done in an attempt to reduce the number of tests necessary to examine pipe response with varying cover depths and varying pressures. For this program's test series only partial excavations of the pipe took place, excavating to the pipe crown in the area of the load pad. The instrumentation in this program included strain gages every 90° at and adjacent to the pipe midspan on the interior and exterior of the pipe. Vertical soil pressures, vertical pipe deformations, load pad displacement, load pad load and pipe internal pressure were also measured. Waldhart's test termination criteria were 60,000 lbs of surface load and a strain level that was equivalent to 90% SMYS.

Waldhart reports a variation of 20% in the pipe stress between the weak sand, strong sand and weak clay backfills, with the weak sand producing the largest stresses. The strong clays showed a 50% reduction in stresses from the weak sand. This is why weak sand and strong clay were the two soil types selected for further study in Phase II. Waldhart

reports an 11% increase in the crown centerline hoop strain from one test to a second of the same conditions. He comments that this difference is acceptable for full-scale testing.

As the internal pressure is increased the hoop strains caused by surfacing loading decreases, showing the pipe stiffening due to internal pressure. Waldhart observes that axial strain is not as sensitive to internal pressure differences as hoop strain is. It is also stated that the variation in axial strain in the three pressure tests is so small that it may not be a result of pressure changes. Strains in the four tests decrease with increasing cover depth. In concluding the paper Waldhart remarks that 10 to 20% error seen in the measurements (crown hoop strain only) is acceptable in full-scale testing. While he reports an 11% difference in the crown centerline hoop strain, examination of the data shows over 18% difference in axial centerline strains.

Upon investigation it was determined that Waldhart's definition of relative density was a percentage of the maximum dry density, which is not the accepted geotechnical engineering definition. The accepted geotechnical engineering definition for percent relative density is:

$$\% \text{ RD} = \text{Dr} = 100 * \left[\frac{e_{max} - e}{e_{max} - e_{min}} \right] \tag{2.11}$$

where e is the void ratio, e_{max} is the maximum void ratio and e_{min} is the minimum void ratio. Then using G_s, the specific gravity of the soil particles, the dry density could be calculated using:

$$\rho = G_s \rho_w / (1 + e) \qquad (2.12)$$

where ρ_w is the density of water. Waldhart 70% 'relative density' was thereby determined to be equivalent to 40% relative density.

J.C. Potter (1985) carried out field tests measuring the effects of vehicle loads on buried high pressure pipe. This study used 10" diameter, X42 grade pipe, 31 feet long, subjected to wheeled and tracked vehicle loads. Displacement transducers were mounted inside the pipe to measure deflection. The backfill material was sandy clay with a moisture content less than 10%. Several vehicles were used with the primary test vehicle being a M51 5-ton dump truck. For each pipe section deflections were measured with dead load, static vehicle load and dynamic vehicle loads. He found pipe deflection to be directly proportional to load. Tracked vehicles created greater deformation in the pipe than wheeled ones. Deformations decreased as the cover depth increased with the deformation below 30" cover decreasing minimally.

Trott and Gaunt (1972) carried out surface loading tests on a large steel pipe at Kirtling. The 1.83 meter diameter pipe with a 12.7 mm wall was buried at a 1.6 meter cover depth. When subjected to vehicle loading they measured under one set of condition a 0.14mm vertical deformation and 0.1 mm horizontal deformation in the pipe. Using the loads they applied and several assumed values, i.e. E', they calculated an expected deflection of 16.5mm using the Spangler equation, while measuring a maximum of 0.5 mm deflection.

This discrepancy between measured and calculated was explained by the difference in installation conditions from Spangler's work and the conditions at Kirtling.

Given the increase in the use of nonmetallic pipes, PVC (polyvinyl chloride), FRP (fiber reinforced plastic), a large portion of the full-scale work carried out in recent history has concentrated on these more truly flexible pipes. Kawabata and Mohri (1995) studied full-scale FRP pipes. Rajani and Kuraoka (1995) studied full-scale instrumented PVC water pipes. Watkins *et al.* (1983) carried out full-scale tests on buried corrugated polyethylene pipe in Hamilton Ohio. Field tests on the 12" diameter corrugated polyethylene pipes with various culvert installations also varied soil densities, covers and pipe diameters were carried out. In 1985 Rogers carried out surface load tests on 160mm diameter shallow burial polyvinylchloride pipe in a reinforced box. Pipe wall strains and deflections were measured. In the less dense soils the deformation mode was roughly elliptical but in the stiffer soils the shape deviated from elliptical. Faragher *et al.* (1998) carried out a study to determine the soil stiffness data for buried plastic pipes. They applied loads to the soil surface of a buried pipe and diametrical strains were measured and Spangler's E' was back calculated. The E' values found were greater than those accepted and used in practice, implying that accepted values are conservative.

2.5 Numerical and Finite Element Analysis

Full-scale testing is costly and time consuming. Analytical calculations contain some uncertainties and unfair assumptions. Finite element analysis (FEA) and numerical

simulations are common ways to study soil structure interaction problems. FEA was originally developed to study structural systems. It was later expanded to study fluid mechanics, thermodynamics, geotechnical engineering, aerodynamics and other areas of science. FEA has also grown in the area of soil structure interaction, using one, two and three dimensional finite elements and soil models. With the ability to assign more complex constitutive behavior to different elements the modeling of a soil structure problem has become more accurate. Using incremental analysis and iterative FEA allows for the nonlinear stress strain properties of the soil. FEA can also address complex pipeline response mechanisms (i.e. ovalization), soil deformation mechanisms (e.g. shear load transfer) and soil/pipeline interaction events (e.g. variation in circumferential or longitudinal pressure distribution). As a result of these developments FEA can be carried out on a complex structure more economically than large scale testing. But these FEA solutions should be calibrated against test data. Also the FEA solutions are only as accurate as the soil models used to generate them. They are susceptible to inaccurate data input, convergence and rounding errors.

The effects of surface load on pipe response have been investigated by a number of researchers using numerical and finite element analysis. Popescu *et al.*. (2002) demonstrated the effect of internal pressure at 40% of Specified Minimum Yield Strength (SMYS), diameter to wall thickness (D/t) ratio on pipeline ovalization response and the distribution of soil pressure on the pipeline circumference. This is illustrated in Figure 2.1 for a two-dimensional continuum finite element analysis, which assumed plane strain

conditions. Numerical procedures required for the development of two-dimensional and three-dimensional continuum finite element models, which can evaluate complex pipeline/soil interaction events and pipeline response mechanisms, have been established at C-CORE through studies that include C-CORE (2003), C-CORE (2001) and C-CORE (1999) and Nobahar *et al.*. (2000). These investigations have evaluated pipeline/soil interaction events for a range of parameters, which include operational conditions, rigid and flexible pipeline behavior, pipeline collapse and post-buckling mechanisms, vertical surface loads, lateral loads and moments, and soil constitutive models. Validation and calibration of the finite element modelling procedures were based on full- scale test data where possible. These studies have provided a framework for the development of finite element models to investigate the effects of non-typical surface loads on buried pipelines that is ongoing at C-CORE.

As a continuation of the work presented in this thesis a program detailed in C-CORE (2005), carried out centrifuge tests and FEA work on buried steel pipe subjected to surface loads. They used a finite element model that was developed using the commercial software package ABAQUS/Standard. The soil was discretized using three dimensional continuum elements, the pipeline was modeled using four-node three-dimensional shell elements and the contact interface was evaluated using frictional contact surface capabilities available in ABAQUS. The analysis considered a 36" pipeline with a 0.5D and 1D cover depth buried in 80%RD sand. In order to simplify the element mesh generation process, the circular load pad investigated in the experimental

study was approximated by an equivalent square loading area. The frictional soil material was modeled using two constitutive models that included a non dilatant Mohr Coulomb model and a non dilatant Drucker Prager model. The Mohr Coulomb model is more widely used in geotechnical engineering, while it is easier to obtain convergent numerical solutions using the Drucker Prager model. For pressurized pipeline, the analysis was convergent only using Drucker Prager model.

Figures 2.2 and 2.3 show plots, surface load versus strain (microstrain), from C-CORE (2005), comparing the centrifuge tests to the FEA results. As within the remainder of this thesis a positive strain indicates tension while negative strain indicates compression. There is a good match between numerical and experimental results. The stress in the crown is significantly larger than the invert in the experimental tests and this is also shown in the finite element analysis. Analysis was also carried out on pressurized pipes with similar success. The finite element analysis procedure for pressurized pipes is similar to un-pressurized pipes; only a pressurizing step is added. They concluded that based on the centrifuge comparisons that the finite element model was able to capture the correct pipe deformation mechanism. Discussion of the centrifuge test results will be discussed more thoroughly in section 2.6.

Fernando and Carter (1998) developed a FE algorithm to analyze the buried pipes under uniformly distributed vertical patch load, simulating vehicle tires. Fernando writes that analytical solution such as the Boussinesq solution combined with a 2D FEA doesn't

account for soil structure interaction. He avoided the problems of 3D FEA being time and memory intensive by using integral transform techniques to analyze this type of 3D problem by transforming it into an equivalent 2D problem. This type of Fourier transform technique has been used on a variety of geotechnical problems. His analysis assumes the pipe is elastic and the soil is an elastic continuum with no plastic failure. The soil and pipe are assumed to be in contact with no slip between the pipe and soil when deformation begins. All field quantities and the 3D loading are transformed in the pipe longitudinal axis direction by use of the Fourier transform. A 2D mesh is used model the pipe cross section plane. To evaluate the response in the longitudinal axis the Fourier transform is inverted to find displacements and stresses. Numerical integration is used to determine displacements and stresses in the pipe cross section plane.

Fernando used similar methods to model infinitely long plate elements. This allowed the calculation of shear and axial forces and moments for the pipe or culvert. To carry out this combination of Fourier and finite element analyses a program called AFENA was used. They used symmetry and modeled half of the pipe. Cover depths of 1/10, 1/4, and 1/2 of the pipe diameter were investigated. Further increases in the cover depths found negligible forces and moments in pipes. Within 30° of the crown the maximum hoop strains were found. There were negligible strains within 45° of the invert. For non-symmetric loading, they loaded at a distance of one pipe radius from the center, and found that the hoop stresses were less than for symmetrical loading. Other observations included the stiffer the pipe and the larger the wall thickness the less the deflection and

the higher the moments. This was because the stiffer the pipe relative to the soil the more load it will attract. An increase in soil modulus lowers pipe deflections, forces and moments. They concluded that using Fourier transforms to model 3D behavior of the patch loading and conventional FEA to approximate the reactions was effective. Small and Wong used similar methods in their analysis, often called a finite strip finite prism method (Fernando and Carter, 1998)).

Through Pipeline Research Council International (PRCI) funding, several research programs have been initiated to investigate the effects of non-typical surface loads on buried pipelines. In addition to the full-scale investigations, SwRI conducted finite element analysis but data is not available for this thesis. Further efforts have been sponsored by Southern California Gas Company at the University of Texas at Austin (UT-Austin) to perform finite element analysis on buried pipelines subject to surcharge loads (C-CORE 2005). The status of these investigations, however, is not known.

Leonards *et al.*. (1985) examined the performance of buried culverts using an FEA program called Culvert Analysis and Design (CANDE). They looked at the effects of different soil models, the soil conduit interface conditions, the importance of the sequence in placement of soil layers, yielding and buckling of conduit wall and applications of analysis to practice. The results were very sensitive to the soil model used. They found that yielding was not necessarily detrimental and can allow a

redistribution of soil pressures and allow the conduit to support the overburden more effectively.

Gerbault (1995) developed a soil structure model to study the shape of the soil reaction around a buried pipe. His work attempted to show that Spangler's model where the shape is assumed parabolic is not always the case (i.e. flexible pipes). Gerbault presents an alternative model using only ring effects, such as ovalization and ignores longitudinal effects such as bending moments due to differential settlements. He assumes the pipe response linear and models the soil with springs that are perpendicular to the pipe wall.

Sharp *et al.* (1985) carried out a study where they compared their FEA results to soil box tests carried out by Knight and Moser in the Buried Structures Laboratory at Utah State University. These soil box tests were carried out on 26" and 60" strain gaged fiber reinforced plastic pipes in two soil boxes fitted with hydraulic pistons capable of generating overburdens of up to 100 feet. Their modeling was formed on the basis that FEA computer models used for soil structure investigations should incorporate non-linear properties of the soil, structural elements that transfer shear, thrust and moment and allow for movement between the soil and the structure. The authors state that while there is good correlation between the FEA and soil box tests they say calibration of the model with test data results in a better analytical tool for the evaluation of buried pipe response. Deformation response of the pipe varied between the FEA model and the soil box test

from 20 to 70%. Pipe hoop and axial strains varied from 5 to 80%. Trends in all data sets were similar.

Moore (1987) carried out FEA work studying the response of buried cylinders to surface loads. He developed a semi-analytical approach, using the Boussinesq solution, that could predict distributions of hoop force and bending moments, radial and circumferential deflection. His approximation compared well to his elastic finite element solution. Moore also analyzed the pipe response for asymmetric loads. A line load is applied on the ground surface at a horizontal distance of 1.0D from the pipe. He found compressive hoop forces with asymmetric loading, meaning compressive strains at both the crown and invert.

Fourie and Beer (1998) carried out FEA work that was compared to the centrifuge work by Trott *et al.* (1984). He used shell elements for the pipe and brick elements for the soil. He used two soil failure criteria, Drucker-Prager and Mohr-Coulomb. He compared this analysis to a full-scale study by Trott, citing very good agreement. The laboratory measurements and the simulations showed very good correlation in terms of trends but the magnitudes of the stresses and defections were shown to vary up to 60% depending on the location on the pipe circumference.

2.6 Centrifuge Studies

Full-scale pipe test programs are time consuming and expensive. Analytical models and finite element analysis, like centrifuge modelling, have inherent uncertainty due to limiting constraints and assumptions. These computer simulations also require physical test date to calibrate against. The geotechnical centrifuge provides an economical and effective means for conducting parametric studies to investigate full-scale pipeline/soil interaction behavior. The advantages and the principles of centrifuge modelling were described in more detail in section 1.2 and in section 1.3.2 respectively. In this section several examples of centrifuge modeling being used to study surface loading of buried pipe sections will be discussed.

Valsangkar and Britto (1979) reported carrying out centrifuge modelling of pipe sections subjected to surface loading. Thin-walled steel pipes with a nominal diameter, wall thickness and length of 101.6 mm, 0.152 mm, and 610 mm respectively were buried in dry sand with varying cover depths. Loading was applied using 46 mm diameter lead discs placed on the sand surface above the pipe midpoint. The pipe was instrumented to provide strain and deflection data. Loading was varied by the addition of more discs and varying the speed of the centrifuge to accelerations up to 80 g. Tests were also conducted with plastic pipe to examine the effect of pipe stiffness. They found that, because of arching, changing the stiffness had significant influence in reducing the load on the pipe. They also showed that for flexible pipes with shallow soil cover pipe failure was likely to be asymmetric with buckling at the pipe shoulder. A novel analysis of centrifuge tests

showed pipe failure due to buckling could be predicted from measured deflections using the Southwell plot method. The results of the tests were used to validate the ring compression theory for the analysis of model pipes in wide trenches or under embankments, as well as to derive load reduction factors for various conditions.

Trott *et al.* (1984) compared results obtained using a 1 m diameter prototype with a centrifuge model tested at an acceleration of approximately 10 g. The Cambridge Geotechnical Centrifuge was used for the model tests while the Transport and Road Research Laboratory (TRRL) test pit was used for the prototype tests. The test pit contained the pipe in dry sand with a 1 m bedding layer. Loading was accomplished with a series of beams and hydraulic rams which loaded seven 0.6 m by 0.6 m plates. In the centrifuge a double acting pneumatic ram was used to load the surface. They tested symmetrically and 0.25D and 0.5D from centerline. Redhill 50 sand was used, with a density of 1.71Mg/m^3 at full-scale and 1.72Mg/m^3 in the centrifuge. Pipe strains and deflections measured in the centrifuge model subjected to the same loading conditions (appropriately scaled) compared very well to the prototype. High strains in the crown were measured while the strains in the invert were very small. They found that with a cover depth of two pipe diameters there was a significant reduction in load carried by the pipe. The prototype and model had similar load deflection responses but the prototype had a stiffer response, each failed at similar loads with the same shape. Pipe permanent vertical deformations, where the diameter reduced by up to 2.3%, were seen with a slight outward movement at the spring line and significant inward deflection of the crown. For

eccentric loading the results showed more scatter in full-scale (similar for symmetric loading) than in the model. Both however showed similar trends. Comparison, of the full-scale and centrifuge pipe response to load, shows from 4 to 35% difference in strains and from 5 to 30% differences in deflections.

Many other centrifuge programs have studied the response of buried structures to surface loads. Craig and Mokrani, in 1988, studied the response of an arch culvert under a central load and a rolling load (Taylor, 1995). They achieved reasonable qualitative rather than quantitative comparison between model and prototype. Difficulties in modeling the construction of the soil around the culvert hindered the results. Stone and Newson (2002) studied square section culverts, with culvert sections of different stiffnesses, in the centrifuge. These strain gaged culverts were calibrated by applying loads (treated as a beam) and also by using a shunt calibration (a calibration resistor). Uncertainties in loading of the beam resulted in the use of the shunt calibrations for data processing. The structures saw a decrease in load in the flexible portions that yielded to the load and an increase in load in the stiff portions of the structure, demonstrating the soil arching.

As a continuation of the work presented in this thesis a program detailed in C-CORE (2005) carried out tests on steel pipes in the C-CORE centrifuge. They modeled 36" and 48" diameter pipe with a D/t of 95. The model pipes were buried in a sand test bed with a relative density of 80%. The cover depths tested were 0.5D, 0.75D and 1D, loaded at the

surface with a circular load pad. Experiment setup and procedures were similar to those to be described in Chapter 3 of this thesis. Internal pressure in these tests was either 0% or 60% of the specified minimum yield stress. Surface loads and pad displacements, ovalization, and hoop and axial strain were measured. The pipe models were machined to size from 2.5" Schedule 80 API 5L X52 pipe. The yield strength of the machined pipe was on average 454 MPa.

They observed that the pipe response increased with decreasing pipe diameter, which can be related to pipe ring stiffness and mechanical rigidity of the pipe. The tests also confirmed that the as the internal pressure was increased so was the pipe soil system stiffness. Similar deformation mechanism were observed in this test series as were in the previous surface loading test programs at the C-CORE centrifuge, those detailed in this thesis, Chapters 3 and 5. Those similarities will be discussed in more detail in Chapter 6.

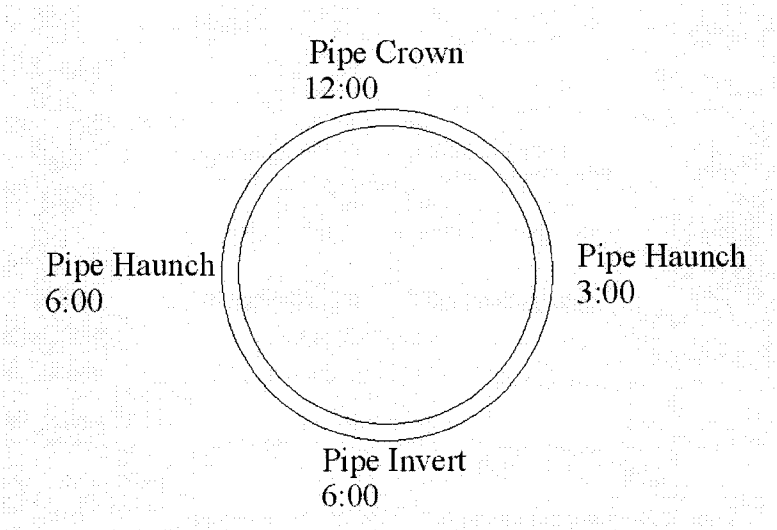

Figure 2-1: Pipe Location Names

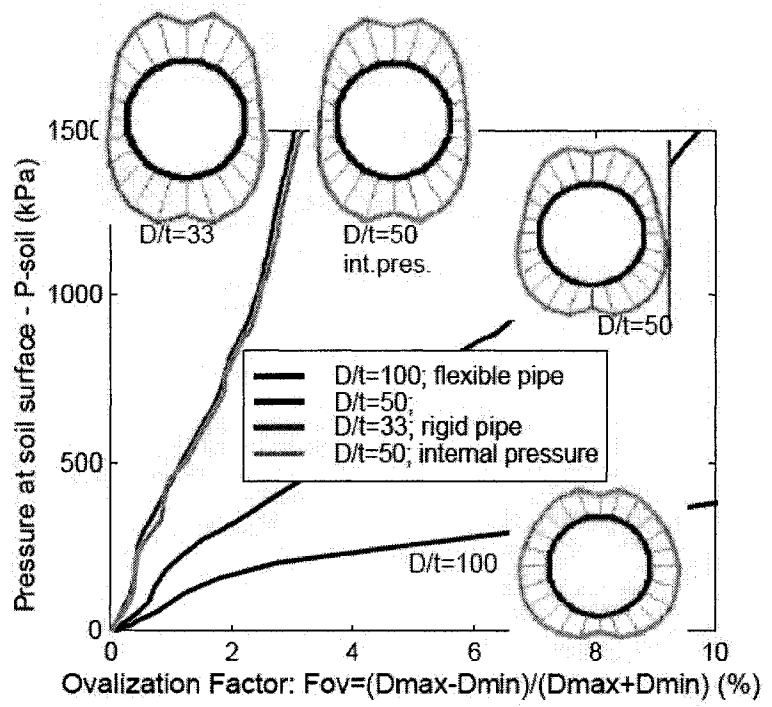

Figure 2-2: Soil Surface Pressure versus Ovalization for Varying Pipe Stiffness (Popescu *et al.*, 2002))

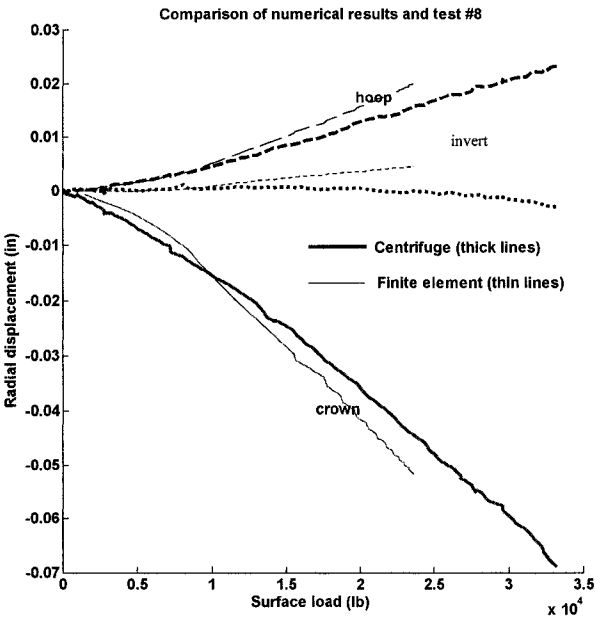

Figure 2-3: Ovalization Comparison, 36" Pipe (C-CORE, 2005)

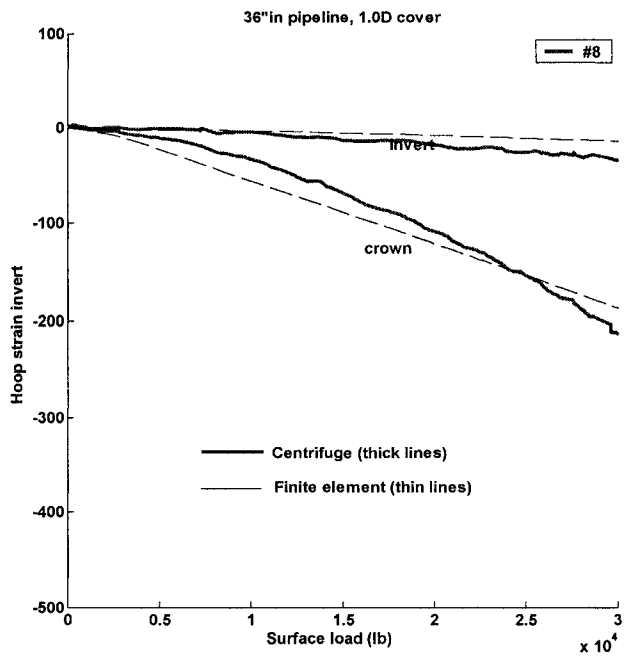

Figure 2-4, Hoop Strain Comparison, 36" Pipe (C-CORE, 2005)

3.0, Surface Loading of Pressurized Aluminum Pipes in the Centrifuge

3.1 Test Design

3.1.1 Overview

The objective of this test program was to compare data from surface loading tests in the centrifuge to data from the full-scale program of SwRI. Initial test parameters used in this investigation were based on the full-scale testing that took place at SwRI. A small instrumented model pipe was used for the centrifuge tests in order that multiple tests could be performed in each test bed. The strong box used for testing contained six pipes in each sand bed. Instrumentation for the tests included strain gages, ovalization sensors, a pressure sensor and an LVDT. Six pipes were instrumented to be used for the 24 pipe tests. Due to instrumentation malfunctions, several pipes could not be reused throughout the test program. For the last two test series, three pipes were reused in two test beds to test the six pipe configurations. The pipes were pressurized during testing using compressed air in the unmanned centrifuge containment chamber. Loading was accomplished using a 2-axis linear drive system and a load pad. The tests were carried out so as to vary cover depth, pressure level, loading condition and sand density. Table 3.1 shows details of the pipe and Table 3.2 shows the test condition details. Test sets T2 to T 6 are discussed in the sections to follow. Test set T1 was a proof test and the data set is incomplete and therefore is not discussed.

3.1.2 Pipe Model and Instrumentation

The SwRI prototype pipe to be modelled for these tests was an API X52 pipe with a 16" OD and a 0.375" wall. This pipe has a D/t, diameter divided by thickness, ratio of 42.7 and material properties including a SMYS of 360 MPa (52,000 psi) and an ultimate tensile strength of 455 MPa (66,000 psi). An aluminum 2024-T3 tube was found to be the best match in commercially available tube to scale to the pipe used at SwRI. The tube had a 1 1/8" outside diameter, a wall thickness of 0.028" and a D/t ratio equal to 40.2. Post test measurements of the model pipes found an average wall thickness of 0.030". This seamless tube is specified to have a yield strength of 345 MPa (50,000 psi) and an ultimate strength of 483 MPa (70,000 psi). Experimentation determined the yield strength of 310 MPa (45,000 psi) at 0.1% plastic strain, with a modulus of elasticity of 68GPa (9,860 ksi) for the model pipes. Tension testing of pipe specimens was carried out in the Materials Testing Lab of Memorial University of Newfoundland. The equipment used included an Instron TTDM 2215 uniaxial test frame, number 1123, MUN 3033, calibration check 2 April 2001, with an Instron GRM D30 load cell. Load and extension data were collected from this equipment. The tensile strength tests were conducted in accordance with ASTM A370 (1997). As shown in Figure 3.1, strain in the test specimen, calculated from extension records was plotted versus the stress, calculated from load records and area measurements. A test specimen is shown in Figure 3.2. Using this pipe dictated a g level of 14.2 gravities (16" OD / 1 1/8" OD). Table 3.1 summarizes the above data. The test package was designed using standard centrifuge scaling laws as described in section 2.5.

Instrumentation for this test program measured internal pipe pressure, internal pipe strain (axial and hoop), pipe ovalization, load pad penetration and surface load. A pressure sensor was used to measure the air pressure in the pipe network. This pressure sensor was an Omega PX212-3KGV, 3000psi transducer. Each pipe was internally strain gauged with 4 hoop and 4 axial strain gages. Strain gage layouts can be seen in Figure 3.3. Hoop and axial strain measurements were accomplished with the use of four uniaxial (Vishay CEA-06-062UW-120) and two biaxial strain gauges (Vishay EA-06-062TT-120). These 120Ω strain gages had gage lengths and grid widths of 1.57 and 3.05 mm respectively. For this measurement ¼ wheatstone bridge layouts were used with bridge completion taking place on an external circuit board. All strain gages were placed on the inner surface of the pipe along either the top or bottom centerline. Strain measurements were taken at the pipe mid-length (point of loading) and at 18 mm from the longitudinal midpoint, which represents 254 mm in the prototype test configuration. Strain gages were glued to the interior of the pipe using an inflatable bladder system. A template of clear plastic sheet was drawn and cut matching the inside dimensions of the pipe. This template included the locations of the strain gages. The strain gages were attached to the template on the gage locations with double sided tape and the template was then slid into the pipe and aligned axially and circumferentially. The bladder was then inserted into the pipe and inflated with compressed air, causing the plastic template to compress the gages, covered in slow dry glue, onto the inside wall of the pipe. Pressure remained on the bladder for 24 hours to allow sufficient time for the glue to dry. This attachment method proved to be adequate. After completion of the test program

the pipes were cut in half circumferentially to allow measurements of the strain gage locations. An average of 0.75mm in variation from strain gage target location to actual location was found. The gages were labeled S1 through to S8 with 3 suffixes on the end to indicate hoop or axial (H or A), crown or invert (C or I) and center or offset position on the pipe (C or O). A positive hoop strain reading indicates an increase in hoop strain, or a tensile strain. A positive axial strain reading indicates an increase in axial strain, or a tensile strain.

A central mandrel connected the pipe end caps and carried the end load generated by the air pressure. This mandrel eliminated axial stress in the pipe due to internal pressure and gave the illusion of an infinitely long pipe. This end cap condition was different than the SwRI tests where welded end caps caused tension to be carried in the pipe wall. The pressure seal was made on the end caps using an o-ring. Furthermore, the central mandrel supported the two ovalization transducers oriented 90° from each other. The end cap and ovalization transducers can be seen in Figure 3.4. Each transducer mounted at 12:00 and 3:00 monitored the pipe ovalization at the mid-length. Fabricated from spring steel, the cantilever type ovalization transducers are ¼ inch wide, 2 inches long and 0.028 inch thick. Two 90°-rosette strain gauges attached in a full-bridge were mounted on the top and bottom surfaces of each transducer near the fixed base. A positive reading from these transducers would indicate that they are bending inward or the pipe is deflecting inward. A hermetically sealed electrical bulkhead connector was used to pass signals from inside the pressurized pipe to the signal conditioning box. A schematic of the pipe assembly can be seen in Figure 3.5 and the assembled pipe can be seen in Figure 3.6.

The ovalization sensors were calibrated using a micrometer mounted within a calibration frame. The central mandrel was ½" drill rod with M12 threads on each end. The assembly was designed assuming an internal pressure of 1875 psi or 12.9 MPa. The end cap area is approximately 515mm^2 (found using the end cap inside diameter of 28.58 mm and diameter of the tapped hole for the mandrel, ½" or 12.7 mm and subtracting the areas found with those diameters). The force in the mandrel when the pipe was pressurized was approximately 6.7 kN resulting in a stress in the mandrel of 52 MPa or approximately a quarter of the yield strength of the steel (drill rod). The force the M12 threads were capable of holding was 45 kN well above the axial force of 6.7 kN in the mandrel.

The pressure level in the pipe was determined using the Barlow formula for hoop stress in a pipe:

$$\sigma_{hoop} = \frac{PD}{2t} \tag{3.1}$$

where σ_{hoop} is the hoop stress in pipe (Pa), P is the pressure in pipe (Pa), D is the inside diameter of pipe (m) and t is the wall thickness of pipe (m) (Mohitpour *et al.*, 2002). The target hoop stress at the start of the test was a percentage of it's SMYS, Specified Minimal Yield Strength. For this test series SMYS was taken as the pipe's actual yield strength, 310 MPa. At 80% SMYS with a 1 1/8" outside diameter, a 0.028" wall thickness and a hoop stress of 80% of 310 MPa the pipe was pressurized to 12.9 MPa.

Vertical displacement of the load pad was measured with two LVDT's (Linear Variable Displacement Transducers) (Intertechnology model number 0243-0000). The LVDT's

were mounted to measure displacement of the pad 180° apart. A ball bearing was used in the load pad assembly to avoid moment and side loading of the assembly. The load pad was driven by a vertical actuator with an in line load cell. See Figure 3.7 for the load pad and ball bearing assembly. A LVDT was also used to measure the sand settlement at one point on the soil sample. A custom built load cell was attached in line above the load pad with an M12 threaded rod. The vertical drive displacement was measured using a rotary potentiometer.

Calibration of the various sensors was carried out using standard practices of the centrifuge center at C-CORE. The load cell was calibrated in compression before the test program began. With the load cell was mounted in a loading frame, weights were added as transducer voltage and the value of the weights added were recorded. The LVDT's and the ovalization sensors were calibrated using a micrometer calibration jig. The hoop strain gages were calibrated using the data read from the pressure transducer during pressurization of the pipes. The hoop stress and strain were found using this pressure data and the pipe dimensions in section 3.1.2 and the equation below:

$$\sigma_{hoop} = E\varepsilon_{hoop} \tag{3.2}$$

where ε_{hoop} is the hoop strain and E is the modulus of elasticity (Pa) of the pipe. The axial gauges were also calibrated using the pressure up data considering the Poisson effect and this equation:

$$\nu = \frac{\varepsilon_{axial}}{\varepsilon_{hoop}} \tag{3.3}$$

where the axial strain and the hoop strain are related by Poisson's ratio. Using the pressurization data to calibrate the strain gages allowed a new calibration factor to be found for each test accounting for any work hardening during testing. The theoretical strain gage calibration factors were found using:

$$\frac{E_0}{E_s} = \frac{F\varepsilon 10^{-3}}{4 + F\varepsilon 10^{-6}} \tag{3.4}$$

where E_0 is the output voltage (mV), E_s is the bridge supply voltage (V), F is the gage factor of strain gages and ε is the actual strain (microstrain). The experimentally determined strain gage calibration factors were found to have a +/-7% difference from the theoretical strain gage calibration factor.

3.1.3 Test Parameters

SwRI used a 22.6" (574mm) diameter circular load pad and loaded to a maximum of 60,000 lbs (267kN). The test package was designed using standard centrifuge scaling laws as described in section 2.5. This resulted in a model load pad diameter of 1.59" or 40.4 mm (22.6"/14.2g). The maximum model load was estimated to be 297.6 lbs or 1.3kN (60,000lbs/14.2^2g).

Table 3.2 shows the tests carried out and the parameters used in each test including loading condition, soil cover, relative density and internal pressure. The test name is comprised of three components T-number-letter, T indicating test, the number indicating the test number and the letter indicating the pipe letter designation. The pipe letter designation was used to track the pipes, their locations for a test and their testing history. A letter occurring twice in one test series indicate that pipe was reused, buried and tested

in a second test bed, to complete that test series. The loading condition used was either symmetric or asymmetric. For symmetric loading the pipe was loaded midspan above the pipe centerline. For asymmetric loading the pipe was loaded at specified distances from the pipe centerline. Examples of the two loading conditions can be seen in Figure 3.8. The soil cover was also varied from 0.5 to 2 pipe diameters deep from the top of the pipe to the soil surface. The relative density of the sand was varied, using 40% and 80% relative density as the two target densities. The internal pressure used in the tests was either 5% or 80% of the SMYS. The minimum distance (center to center) between the pipes was 288 mm, and from the wall was 119 mm. The diameter of the pipes used in this test program was 28.5 mm. As the pipes are more than 4 diameters apart, there should be no influence on each other (Bulson, 1985).

3.1.4 Testing Equipment

Existing strong box, vertical actuator and a horizontal actuator were modified and used for this test program. The experiment package on the centrifuge arm can be seen in Figure 3.9. Top views of the package can be seen in Figure 3.10 and Figure 3.11. A side schematic of the setup is shown in Figure 3.12. The strong box was an aluminum box supporting the experiment head works and containing the soil sample and pipe network. The strong box was capable of holding 6 pipe models for one test. Loading of the pipe models was accomplished with a 2-axis linear drive system consisting of the linear and horizontal drive units as shown in Figure 3.13. The vertical actuator was used to load the pipe, while the horizontal actuator was used to position the vertical actuator above the pipe while in flight.

The 2-axis actuator system is assembled such that the vertical drive component sits on the horizontal component with no mechanical fastening therefore it is restricted in the force it can exert by its own self weight at a particular g level. The mass of the vertical drive is 25.23 kg and therefore at 14.6g it is capable of pushing with a force of 3.6 kN against its own self weight. For this test series the expected load of 50,000lbs or 222 kN full-scale was equal to 1.04kN at 14.6 g and can therefore could be resisted by the drive's self weight.

A scuba tank filled with compressed air was used to pressurize the pipes. It was connected to a system consisting of solenoid valves, a pressure regulator, pressure transducer and pipe manifold so as to pressurize three pipes simultaneously. In Figure 3.14 the pressure regulator is in the mid left hand side of the photo and in Figure 3.15 the gas system is shown in schematic form. The original design called for nitrogen to be used to pressurize the pipes and it was used in the initial proof test of the system. Nitrogen cylinders that were readily available could not provide the volume of gas needed to sufficiently pressurize a three pipe system. Fixed to each pipe was a flow reducing orifice to eliminate pressure shock on the pipe network from pressurizing and venting the pipe system. Other miscellaneous components include signal condition boxes for data acquisition and a string displacement potentiometer used to position the vertical drive.

3.1.5 Geotechnical Conditions

Alwhite medium-fine sand (#00), a readily available manufactured siliceous material with consistent properties, was selected for the modelling program. The prototype backfill material was red sand from Oak Island. The index properties of these two materials are compared in Table 3.3 based on Zhu (1998) who performed a series of triaxial tests on #00 Alwhite silica sand at 90% relative density. The grading curves are compared in Figure 3.16. Eleven drained triaxial compression tests were undertaken under confining stresses, p' of 100 to 250 kPa. The sands triaxial compression frictional properties are compared in Figure 3.17. Young's modulus, E is calculated by:

$$E = E_o \, p_a \left(\frac{p'}{p_a}\right)^{0.5} \tag{3.5}$$

for Alwhite sand secant normalized Young's modulus, E_o to 0.5% axial strain of 230 and 470 at initial relative densities of 50 and 90% respectively, where p_a is atmospheric pressure and p' is the soil pressure (Zhu, 1998).

Test beds were prepared by means of dry pluviation using a sand rainer, built by the author, as seen in Figure 3.18. The device uses a translating hopper to rain sand into a containment box in such a manner so as to achieve the desired relative densities. To achieve the quarter diameter bedding layer with a variety of cover depths stepped foundations were built inside the strong box. Sand was rained into the box to the spring line of the shallowest pipe. Trenches, shown in Figure 3.19, were then excavated by means of a vacuum system that was used to remove sand until a ¼ D deep sand bed remained under the pipe. This system was mounted on a beam that spanned across the strong box. This beam also acted as a known datum or reference to measure the trench

depth. The pipes lying in their trenches can be seen in Figure 3.20. Once the pipes were placed in the formed trenches the sand rainer was used to cover the pipes above the desired backfill level. The vacuum and skid mechanism were then used to vacuum the sand surface level to the correct pipe cover height. The completed buried pipe network with protruding gas and instrumentation lines is shown in Figure 3.21. Density cup were placed in the strong box before each test and removed and the sand density calculated after testing. Average measurements from these density cups can be seen in Table 3.4. Relative densities of 80 and 40% relative density were chosen to match to comparable test programs, by SwRI as detailed in Chapter 2. The percent relative densities (%RD) were calculated using equations 2.11 and 2.12.

3.2 Test Procedure

The test bed was prepared as described in section 3.1.5. With the pipes situated in the completed test bed the experiment head works were assembled and the test package was placed in the centrifuge basket. Three pipe models were remotely pressurized simultaneously prior to centrifuge spin up. During this time data were collected from the pipe instrumentation. The pipes were pressurized to either 5% or 80% of the experimentally determined yield stress of the tube which is referred to in this report as 5% or 80% SMYS. The centrifuge was brought to test speed, then decelerated to 10g and then brought back to test speed three times when a new test bed was tested. This was done to condition the sand bed to ensure consistent conditions for subsequent tests. The centrifuge was accelerated to 49.4 rpm giving 14.2g at a radius of 5.21m, the centerline of the pipe. With the centrifuge at test speed the vertical actuator was used to load the

pipe. The load was applied to each pipe section on its longitudinal and transverse lines of symmetry. Loading of the pipe was carried out using a displacement controlled system. Three test termination criteria were used to determine when to stop loading the pipe. A model vertical load of 1.3kN (60,000lbs) was used as one test termination criteria. Recording data from hoop strain gages and determining when the gage had reached 90% SMYS was the second termination criteria. Tests were also ended when the load pad LVDT reached its maximum measurable displacement. When three pipes were tested, the centrifuge was stopped and gas remotely vented. The package would then be rearranged to test the other three pipes.

3.3 Test Results

In this section centrifuge test results obtained on the aluminum pipe models will be described, discussing the effects of varying the test parameters. Comparison of these results to other centrifuge tests programs, full-scale tests and numerical results will be presented in Chapter 6.

The C-CORE report "Centrifuge Modeling of Pipeline Stress Due to Heavy Equipment Encroachment" is the contract report for the phase of the surface loading program described in this chapter, (C-CORE, 2002). Data analysis of the test results carried out for this thesis revealed several errors in that report. For many of the tests carried out the test labels were incorrectly transferred between the data collection and the data analysis steps, resulting in the data being labeled with incorrect names and therefore incorrect pipe burial depths. These errors were found through examining centrifuge flight records, log

books and data analysis code. Several conclusions made for the contact report were based on these incorrectly labeled data. This thesis should be considered an update to the results and interpretation in the contract report.

The data collected for each test was processed and presented in graphical form using MATLAB. Test T3C is used as an example in Figure 3.22 to show the sequence of events in a typical pipe test as recorded from the load pad load cell, data in this plot is shown in model units. These events are important in understanding how the data was analyzed. Event A shows the load cell for a period of time with no external load. Event A is the time, after data collection had begun and the pipes had already been remotely pressurized, when the centrifuge was being prepared for operation. Event B shows data where the load cell reading becomes negative indicating a tensile load. This tensile load occurred due to the self-weight of the suspended load pad increasing due to the acceleration of the centrifuge. Event C shows a cycling of the centrifuge g level to condition the sand bed. Event D is the application of the load on the sand surface or the initial loading of the pipe. To analyze the results from each test the load and load pad displacement readings were zeroed at this point of initial load application. This zeroing of the data has not been carried out for the data in the figure shown. Zeroing at this point subtracted the self weight of the load pad and also subtracted any movement of the load pad read by the displacement transducer prior to the load application. The time sequence that is spanned by event E is the data of interest to this study and therefore the time frame that the data presented in this thesis are taken from. The loading of the pipe is carried out using a displacement controlled actuator, this explains the saw tooth pattern in the data.

Event F is when the load is released and the load pad is lifted from the sand. Finally event G shows the deceleration of the centrifuge and therefore the self-weight of the load cell decreasing.

Test T3C is also used as an example to show the sequence of events in a typical pipe test as recorded from a strain gage, Figure 3.23. Events in this plot correspond to the previous plot of load verses time. Event A is the time, after data collection had begun, when the centrifuge was being prepared for operation. At this time the pipe has already been pressurized and the initial hoop strain (~230microstrain) induced in the pipe due to internal pressure (5%SMYS) is shown. Event B shows data where the strain increases slightly due to the increase in self-weight of the pipe and the increased soil load when the centrifuge accelerates. Event C shows a cycling of the centrifuge g level to condition the sand bed. Event D is the application of the load on the sand surface or the initial strain increases in the pipe. To analyze the results from each test the strains were zeroed at this point to show changes in strain due to the load application only and not due to internal pressure. Zeroing at this point subtracted the initial pressurization strains and the strains due to self weight of the pipe and soil under 14.6g. This zeroing of the data has not been carried out for the data in the figure shown. As previously stated the time sequence that is spanned by event E is the loading of the pipe, event F shows the load being released and event G shows the deceleration of the centrifuge.

The initial strain value in Figure 3.23 of about 230 microstrain corresponds to the pipe pressurized to 5% SMYS. Table 3.5 shows typical strains in the pipe after the pipe was

pressurized. The target pressure is the pressure that when applied would result in the target hoop strain. That target pressure and hoop strain was calculated using equations 3.1 and 3.2 and the percentage of the SMYS for the particular test (5% or 80%). Also shown is the pressure read from the pressure sensor. Strains, hoop and axial, were calculated from that pressure reading and are shown as calculated strains. In the table these strains can be compared to the strains actually measured with the strain gages, the measured strains. As shown the target, measured and calculated strains compare well in each of the tests. The percent difference between the calculated and target strains are in the table to demonstrate their close agreement.

The data presented in the remainder of this thesis are in equivalent prototype units. Model surface loads are multiplied by the scale factor squared and displacements by the scale factor, following centrifuge scaling laws as described in chapter 2. Figure 3.24 and Figure 3.25 show a typical strain verses surface load plots and a typical ovalization versus surface load plot respectively. The strain and ovalization response (transducer response) is very approximately linear with surface load. Straight lines were fitted through the strain and ovalization versus surface load data. The slopes of these lines (strain divided by the surface load or pipe ovalization divided by the surface load) are used and compared to examine trends in the data due to varying test parameters. These gradients or ratios are presented in both tabular form and in plot form in the forthcoming sections. The ratio units are microstrain / kN ($\mu\varepsilon$/kN) and mm/N x 10^{-1} for the strain and ovalization ratios respectively.

The Appendix A contains data plots for each pipe tested. The first is Load Pad Penetration vs. Surface Load, with several tests plotted on the same axis for comparison. The Pipe Response vs Surface Load figure for each test includes 3 plots, Hoop Strain vs. Surface Load, Axial Strain vs. Surface Load and Ovalization vs. Surface Load. The data are presented in prototype conditions in each plot. The top right corner of each plot contains the test code that will be used throughout this thesis with the parameters "Test Scale" "material" - "test number" - "pipe designation" - "soil cover" - "soil density" - "pipe pressure" - "loading condition". Test Scale indicates the test scale and is either Cent or Full indicating either a centrifuge or a full-scale test. The material is indicated by either Al or St indicating aluminum or steel. Test number or test series numerical designation is 2 through 6 as listed in Table 3.2. Pipe designation is the alphanumerical name of the pipe model used, either A, B, C, D, E, or F. The soil cover is either 0.5, 0.75, 1, 1.5 or 2 pipe diameters. The soil density used was 40% or 80% relative density sand. The pipe pressure that the model was pressurized to was either 0% (no pressure), 5% or 80% of the pipe materials SMYS. The loading condition was either symmetrical, "S", asymmetrical, "A", or square load pad, "S". The asymmetrical tests will show a number in brackets after the pipe letter, indicating the distance from pipe centerline to the center of the load pad application area. For example, A2(50) was the second time pipe A was tested and the load was applied 50 mm from centerline.

The ovalization data had to be adjusted to account for the sensors in several tests being wired with reverse polarity. This reverse polarity was discovered when in several tests the ovalization sensors did not follow the trends found in the majority of the tests.

Reversing the polarity (adding a negative sign before the data) in data analysis was justified by examining ovalization sensors data as the centrifuge was accelerated. Since the mandrel was a not as stiff as the pipe it deflected more when it was subjected to an increase in self weight due to the increased centrifugal g. Therefore all 12:00 ovalization sensors should read negative ovalization when an increased g is applied (the mandrel will deflect downward more than the pipe resulting in an apparent increase in ovalization). The 3:00 ovalization sensor should read positive as a result of an increased g being applied (the mandrel will deflect downward causing the 3:00 sensor to measure a smaller pipe radius or an apparent decrease in ovalization). These trends were observed in the majority of tests and in the tests where the opposite of that trend was recorded it was assumed that the sensor was installed with reverse polarity.

The two LVDT's on the load pad used to measure load pad penetration were also used to measure the load pad tilt. In the symmetrical tests the average load pad tilt was 2.7°. In test T6C the load pad tilted 7.3° accounting for variations from the data in this test from test T6E of comparable conditions. In the asymmetric loading tests the average load pad tilt was 4.3°. This increase in tilt was caused by the unsymmetrical loading arch created in the sand when the pad was positioned off center from the pipe.

3.3.1 Test Set-2

These pipe tests were conducted at 80% SMYS in a test bed at 40% relative density sand, which would be considered a 'poor installation' by Moser (2001). Three pipes were located at 0.75D (Test 2A (Test 2 pipe A)), 0.5D (Test 2B) and 1.0D (Test 2C) cover

depths. Hoop and axial strains and ovalization are measured with increases in surface load directly above the pipe (symmetric loading). In Figure 3.26 the hoop strain / surface load, axial strain / surface load and ovalization / surface load gradients are each plotted against pipe diameter for each of the transducers. These transducers include each of the strain gages shown in figure 3.3 and also the two ovalization sensors positioned at 12:00 and 3:00 at the center of the pipe..

Strain gauge S7ACO did not work in Test 2A. The initial hoop strain level was close to yield from the high internal pressure. Plastic strains were measured from several gages in these tests. In Test 2A in strain gage S1HCO a change of ~ 500 microstrain giving a total strain when the strain due to pressure is added of over 4100 microstrain. Similarly in strain gage S4ACC a change of 600 microstrain gives a total strain of over 1800 microstrain. These plastic strains are evident in Figure A2, showing a nonlinear strain response with load, above 60kN. Test 2C S4ACC saw a change due to loading of over 900 microstrain in the axial direction combining with pressurization strains of 1200 microstrain to total over 2100 microstrain. In Test 2A the ovalization sensor at 3:00 malfunctioned, as did strain gages S1HCO and S3HCC in test 2 C and the ovalization sensor at 3:00 in test 2B.

Two main modes of pipe deformation were identified under surface loading: ovalization of the pipe cross-section and bending in the long section. These 2 modes are associated with the hoop strain and axial strain response, as shown in Figure 3.26. The ovalization mode was not associated with an elliptical pipe shape. The pipe crown deflected

significantly, inward, with very small outward deformations of the pipe haunch. The crown deformation was confirmed by both the internal crown hoop strain gauges and the vertical ovalization sensor. The crown deformation decreased with increasing cover (~5.6mm at 0.5D to 2.8mm at 1D). The invert hoop strains and the horizontal pipe haunch deformations were negligible over most cover depths. Modest invert hoop tensile strains were measured under 0.5D cover as a result of significant pipe crown hoop strains.

Both hoop and axial strains decrease with cover depth as seen in Figure 3.26, Test 2 Gradient Comparisons. Strain gage S1HCO in T2B appears to be reading too low for this trend but this is because that for this 0.5D cover test the load pad penetration was considerably less than in the other tests and therefore the effective cover between the pad and pipe was larger than the other tests. This could also be as a result of soil arching over the pipe at the lower cover, a 1.69" load pad over a 1.125" pipe. The bending mode is represented by the axial tensile strains in the pipe invert. These bending strains decrease with increasing cover. The axial compressive strains in the pipe crown result from both the global bending of the pipe and from the Poisson effect associated with the pipe crown internal tensile hoop strains.

3.3.2 Test Set-3

These pipe tests were conducted at 5% SMYS in a test bed of 40% relative density sand. Three pipes were located at 0.75D (Test 3A), 0.5D (Test 3B) and 1.0D (Test 3C) cover depth. Hoop and axial strains and ovalization are measured with increase in surface load directly above the pipe (symmetric loading). In Figure 3.27, the hoop strain / surface

load, axial strain / surface load and ovalization / surface load gradients are each plotted against pipe diameter for each of the transducers.

Strain gage S7ACO and the 3:00 ovalization sensor did not work in tests 3A. Strain gages S7ACO, S4ACC and S5AIC in Test 3C and strain gage S3HCC in Test 3B also malfunctioned. Plastic strains were measured in strain gages S1HCO and S3HCC in Test 3A as the surface load increased. The depth of cover is shallow 0.5D in this test. The combined effect of cover depth, low internal pressure and low soil density possibly causes the crown of the pipe to plastically strain. Bulson (1984) described similar collapse mechanism under these conditions.

Two main modes of pipe deformation were again identified under surface loading: ovalization of the pipe cross section and bending in the long section. These 2 modes are associated with the hoop strain and axial strain response, as shown in Figure 3.27. The ovalization mode was not associated with an elliptical pipe shape. The pipe crown deflected significantly with lesser deformation of the pipe haunches. The crown deformation was confirmed by both the crown hoop strain gauges and the vertical ovalization sensor. The crown deformation and hoop strain decreased consistently with increasing cover. Smaller invert tensile hoop strains and horizontal pipe haunch diametral increases resulted from the significant pipe crown deformations. The bending mode is represented by the axial tensile strains in the pipe invert, as shown in Figure 3.27. These bending strains decrease slightly with increasing cover. The larger axial

compressive strains in the pipe crown result from the addition of global bending strain and the Poisson effect associated with the pipe crown tensile hoop strains.

3.3.3 Test Set-4

These pipe tests were conducted at 80% SMYS in a test bed of 80% relative density sand. Six pipes were located at 0.5D (Test 4B), 0.75D (Test 4E), 1.0D (Test T4D&F) 1.5D (Test T4A) and 2.0D (test T4C) cover depths. Hoop and axial strains and ovalization are measured with increase in surface load directly above the pipe (symmetric loading). In Figure 3.28 the hoop strain / surface load, axial strain / surface load and ovalization / surface load gradients are each plotted against pipe diameter for each of the transducers.

In Test 4D strain gages S4ACC, S6HIC, S7ACO and S8HIO and the 3:00 ovalization sensor did not work. In Test 4B strain gages S6HIC and S8HIO did not work. In Test 4F strain gages S2AIO, S3HCC, S4ACC, S5AIC and S7ACO and the 12:00 ovalization sensor did not work. Strain gauges S7ACO and S6HIC and the 3:00 ovalization sensor malfunctioned in Test 4A. The initial hoop strain level was close to yield from the high internal pressure. Plastic strains were measured in strain gauge S3HCC in Test 4D as the surface load increased. Two possible reasons are the pipe becomes plastic at this stress level, or there is buckling of the crown. Moser (2001) noted one way to identify the initiation of buckling is with the increase in surface load the crown of the pipe moves inward while the horizontal diameter along the spring line increases. If buckling occurs at the crown, the curvature changes at the crown and the spring line comes inward. From the horizontal ovalization data no such change was observed. Therefore, the sudden

increase in strain is considered to denote the onset of plasticity. Pipes D, E and F showed significant off sets in their un-pressurized post excavation strain gage readings indicating plastic deformation of the pipe. These pipes were therefore not used in the remainder of the test program.

Two main modes of pipe deformation were identified under surface loading: ovalization of the pipe cross section and bending in the long section. These 2 modes are associated with the hoop strain and axial strain response, as seen in Figure 3.28. The ovalization mode was not associated with an elliptical pipe shape. The pipe crown deflected significantly with smaller deformation of the pipe haunch. The crown deformation was confirmed by both the crown hoop strain gauges and the vertical deformation sensor. The crown deformation decreased with increasing cover with Test 4E, 0.75D cover, being the exception showing comparable deformation to the 1D test. The invert hoop strains and the horizontal pipe haunch deformations were negligible over the range of cover depths. The small invert hoop tensile strains possibly result from the Poisson effect from the invert axial tensile strains. The bending mode is inferred by the axial tensile strains in the pipe invert, as seen in Figure 3.28. Axial strains also decrease with cover as expected.

3.3.4 Test Set-5

These pipe tests were also conducted at 80% SMYS in a test bed of 80% relative density sand. Six pipes were located at 0.5D (test T5E1), 0.75D (test T5A3 & A4), 1.0D (test T5E2 & C2), 1.5D (test T5A1 & A2) and 2.0D (test T5C1) cover depth. Hoop and axial

strains and ovalization are measured with increasing surface load to the side of the pipe (asymmetric loading). In Figures 3.29 and Figure 3.30 the hoop strain / surface load, axial strain / surface load and ovalization / surface load gradients are each plotted against pipe diameter for each of the transducers, with the first figure being the 20mm offset tests and the second the 50mm offset tests. In this test series the strain gage S7ACO and the ovalization sensor at 3:00 did not work on pipe A. In test T5C2 the ovalization sensor at 12:00 malfunctioned. In test T5C1 strain gages S6HIC and S8HIO and the ovalization sensor at 12:00 did not work.

The hoop strains in the crown (S1HCO and S3HCC) but are much less than those obtained from the previous tests. In Test 4B, 0.5D cover hoop crown strains of 2500 and 3500 microstrain were reached with 130mm penetration while in Test 5E1, 0.5D cover and 50 mm load off centerline hoop crown strains of -55 and -45 microstrain were reached with 160mm penetration. This reduction in hoop strain was less when the load pad was moved closer to the centerline, 20 mm rather that 50 mm. In Test 4C, 2D cover hoop crown strains of 450 and 350 microstrain were reached with 300mm penetration while in Test 5C1, 2D cover and 20 mm load off centerline hoop crown strains of 230 and 270 microstrain were reached with 340 mm penetration. This reduction in hoop strains is because a significant portion of load is transferred to the soil. Similarly, axial strains are less in this test. For the 20mm offset tests slight reduction in strains with soil cover can be seen, but for 50mm tests the data is scattered and soil cover against pipe response does not show any trends. Pipe ovalization was minimal in the asymmetrical tests and as a result data discussion is limited. For the tests with the loading at a 50 mm

offset the hoop strains obtained from all the hoop strain gauges (S1HCO, S3HCC, S6HIC and S8HIO) are compressive (negative) unlike previous tests where hoop strains are tensile (positive) at the crown. A comparison between the first and second loading sequence shows that the strain is less for the second sequence of load. Firstly, the load at 20 mm offset significantly compresses the soil layer as the load pad is very close to the pipe. Secondly, the load at 50 mm offset is at a larger horizontal distance from the pipe.

3.3.5 Test Set-6

These pipe tests were conducted at 5% SMYS in a test bed of 80% relative density sand. Six pipes were located at 0.5D (test T6E1), 0.75D (test T6A2), 1.0D (test T6C2&E2), 1.5D (test T6A1) and 2.0D (test T6C1) cover depth. Hoop and axial strains and ovalization are measured with increase in surface load directly above the pipe (symmetric loading). In Figure 3.31 the hoop strain / surface load, axial strain / surface load and ovalization / surface load gradients are each plotted against pipe diameter for each of the transducers. In this test series strain gages S1HCO and S7ACO did not work on pipe A. Also strain gage S8HIO did not work on pipe C.

The two main modes of pipe deformation were identified under surface loading: ovalization of the pipe cross section and bending in the long section. These 2 modes are associated with the hoop strain and axial strain response, as shown in Figure 3.31. The ovalization mode was not associated with an elliptical pipe shape. The pipe crown deflected significantly with smaller deformations of the pipe haunch. The crown deformation was confirmed by both the crown hoop strain gauges and the vertical

deformation sensor. The crown deformation decreases with increasing cover with Test 6E2 as the exception. In this test very high strains are seen in the crown of the pipe and the larger ovalization could be explained by plasticity in the pipe. Hoop and axial strains in all tests show the trend of decreasing with cover depth. Tests E1, 0.5D cover and A2, 0.75D cover show smaller strain / load ratios than expected but this can be explained by low penetration depths. The bending mode is represented by the axial tensile strains in the pipe invert. The axial compressive strains in the pipe crown result from both the bending strain and the Poisson effect associated with the pipe crown compressive hoop strains.

3.4 Discussion

3.4.1 Overview

Four main parametric effects are considered from the model test study were soil cover, internal pipe pressure, soil relative density, and surface load position. The magnitude and relative stiffness of the pipe and the surrounding soil will control the deformation response of the pipe. The soil stiffness increases with increasing relative density. Soil stiffness effects on pipe response have been investigated by a number of researchers, for example Howard (1977). The pipe wall and the internal pressure that stiffens the pipe control the pipe stiffness. The relative stiffness between the pipe section and the soil can be considered using the denominator of the equation 2.8.

$$24\,S + p + 1.85\,E' \qquad (3.6)$$

The pipe sectional stiffness comprises the pipe structure, 24S and the internal pressure, p. The comparative soil stiffness is 1.85E'. The pipe structural stiffness, S (EI/D^3) was constant between tests. The pipe cross sectional moment of inertia is $I = t^3/12$ per unit length, the pipe young's modulus, E=68GPa and given the dimensions of the pipe, an OD of 28.6mm and a wall thickness of 0.71mm, a pipe structural stiffness of 0.09 MPa can be calculated. Internal pressures, p, of 0.8 and 13MPa were used to pressurize the pipe to hoop stresses of 5% and 80% SMYS respectively. The soil modulus is estimated from the Young's modulus measured from the triaxial compression tests at relative densities of 50 and 90%, Section 2.4. An average surface bearing pressure under the scaled 22.6" diameter load pad at 10,000 lbf is 170 kPa. A confining stress of 100 kPa is assumed to be representative in the vicinity of the buried pipe. The soil modulus, E' is then taken as 20 and 40 MPa at 40 and 80% relative density respectively. The stiffness of the pipe and soil are compared in Table 3.6. The pipe internal pressure has the most significant effect on the relative stiffness. The sand is more than 10 times stiffer than a low pressurized pipe with an initial 5% SMYS hoop stress. Soil arching can therefore be expected around the pipe. The sand and the high-pressurized pipe with an initial 80% SMYS hoop stress have quite similar stiffness.

Two main modes of pipe deformation were identified under surface loading: ovalization of the pipe cross-section and bending in the long section. These 2 modes are associated with the hoop strain and axial strain response. The hoop strain response was confirmed by the measured ovalization of the pipe crown and haunch. The ovalization mode was not associated with an elliptical pipe shape. The pipe crown deflected significantly with

little or no deformation of the pipe haunch. The use of the Iowa formula in this case is thus questionable, as it assumes the pipe deforms as an ellipse. The bending mode is represented by the axial tensile strains in the pipe invert. The axial compressive strains in the pipe crown result from both the bending strain and the Poisson effect associated with the pipe crown hoop strains.

3.4.2 Soil Cover

At the start of the tests, the sand layer compresses due to the increased self-weight due to the centrifugal force. This compression produces very small strain on the pipes. This is very similar to the test results of Trott *et al.*. (1984) where they found that the effect of soil compression due to centrifugal force is very small while the effect of field compaction is significant. This effect, as mentioned in section 3.3, is not seen in the presented data due to zeroing of the data at the time the load pad begins to load the soil.

The effect of soil cover was presented for each test set in Sections 3.3.1 to 3.3.5 as shown in Figures 3.25 to 3.30. Table 3.7, also compares the transducer gradient for varying soil cover. In this table the tests are arranged so that tests with three similar conditions (density, pressure and offset) are grouped together and the trends due to varying the soil cover can be observed. In this table it can be seen that when the offset was zero an increase in cover depth caused reductions of the gradients. For the tests where the pipe was loaded at an offset no trends could be observed in varying the cover depth. The hoop and axial strains decrease with increasing cover depth in all tests. The pipe ovalization is

negligible for the conditions tested with a cover greater than 1.5D. The longitudinal pipe bending strains do not reduce as quickly and persist beyond 1.5D cover.

3.4.3 Internal Pipe Pressure

Table 3.8 compares the transducer gradients for varying internal pressures. In this table the tests are arranged so that tests with three similar conditions (cover, density and offset) are grouped together and the trends due to varying the internal pressure can be observed.

Crown and invert (more so crown) hoop strains increase significantly with the decrease in pressure in 40% soil density tests and marginally in 80% soil density tests. This can be attributable to the more comparable stiffness ratios between the two conditions, Table 3.6. Crown axial strains show a slight increase in strain with a decrease in pressure. In 40% relative density tests, the surface load causes about twice the crown deformation but about half the longitudinal bending strains (axial invert) of the pipe at 5% SMYS than at 80% SMYS, this trend continues for the 80% relative density but is less prevalent. The ovalization mode is also different with changing internal pressure. At 80% SMYS there is less diametral deflection of the pipe invert or the pipe haunch. This is attributed to the similar stiffness of the pipe and underlying soil. At 5% SMYS there are small diametral inward deflections of the pipe invert and outward deflections of the pipe haunch. The haunch deflections are however about a fourth of those at the pipe crown, that is the pipe does not adopt an elliptical shape under these loading conditions. The difference with internal pressure is attributable to the distinct difference in stiffness ratios between the two conditions, Table 3.6.

3.4.4 Soil Relative Density

Table 3.9 compares the transducer gradients for varying soil relative densities. In this table the tests are arranged so that tests with three similar conditions (cover, internal pressure and load offset) are grouped together and the trends due to varying the soil relative density can be observed.

For 5% SMYS the soil density has little effect in the pipe strains and deflections. Decreases in axial strains are seen in the 80% SMYS tests when soil density in increased. These smaller bending strains can by up to 3 times smaller in the stiffer soil when the soil covers are small. Crown hoop strains tend to increase with soil density. Axial crown and invert hoop see little effects from the soil density variation.

3.4.5 Surface Load Position

The surface load position effect is identified by comparing test sets 4 and 5 that were loaded on the pipe center and off centre respectively. The other test conditions of cover, 80% of SMYS and 80% relative density are the same in both test sets. Table 3.10 compares the transducer gradients for varying load offsets. In this table the tests are arranged so that tests with three similar conditions (cover, density and pressure) are grouped together and the trends due to varying the load offset can be observed. In this table it can be seen that an increase in load offset results in a reduction of the gradient. In seven of the fifty cases only one transducer reading was available so no trend can be observed. In four of the fifty cases the gradient changes were so small or were erratic

and no trend could be accessed. Invert hoop strain gradients are negligible as discussed in section 3.4.2. Tests 4A, 5A1 and 5A2 with a 0.75D soil cover have a different crown hoop strain response. T4A has a tensile response, T5A1, 20 mm offset has a smaller tensile response while T5A2 is compressive. This phenomenon can be explained by the semi analytical results by Moore (1987), see chapter 6. Similar trends in crown hoop strains are seen in each of the soil covers. The axial strain from the longitudinal bending moment in the pipe decrease with increased load offset.

3.4.6 Repeated Tests

Of the twenty six tests carried out in this test program there were 2 that that had the same test parameters as others. Test T4D and test T4F were both carried out with 1D cover, at 80% SMYS pressure, 80% relative density soil and 0mm loading offset. For these two tests, one of the ten comparable transducer functioned in both tests. Therefore any comparison of test T4B to test T4F is not reasonable. Test T6C2 and test T6E2 were both carried out with 1D cover, at 5% SMYS pressure, 80% relative density soil and 0mm loading offset. For these tests nine of the ten transducers were able to be compared. This comparison shows that in most transducers there was a greater response during test T6E2. Investigation of the load pad penetration in these tests shows that for test T6E2 the load pad tilted by 1.1degrees and in Test T6C2 7.3degrees. The greater tilting of the load pad in test T6C2 would result in a load distribution in the soil that reduced the soil stress on the pipe. Figure 3.32 compares the crown hoop strain gages and the crown ovalization sensors from the two tests, showing the effect of the tilting load pad.

Table 3-1: Pipe Parameters

Property	C-CORE (14.2 g)	SwRI (full-scale)
Pipe Material	Aluminum 2024-T3	Steel API X52
Outside Diameter	1 1/8"	16"
Wall Thickness	0.028"	0.375"
D / t	40.2	42.7
Yield Strength	50,000psi	52,000psi
Ultimate Strength	70,000psi	66,000psi
Yield at 0.1% (determined experimentally)	45,000psi	Not known
Modulus of Elasticity (determined experimentally)	9860ksi	Not known
Load Pad Diameter	1.59" (22.6"/14.2g)	22.6"
Design Load for Experiment Setup	297lbs (60000lbs/14.2g^2)	60000lbs

Table 3-2: Centrifuge Test Parameters

Test Set	Test Name	Soil Cover (D)	Soil Density (%)	Pipe Pressure (% SMYS)	Loading condition
1	T1P	1	40	80	Symmetric
	T2A	0.75	40	80	Symmetric
2	T2B	0.5	40	80	Symmetric
	T2C	1	40	80	Symmetric
	T3A	0.75	40	5	Symmetric
3	T3B	0.5	40	5	Symmetric
	T3C	1	40	5	Symmetric
	T4A	1.5	80	80	Symmetric
	T4B	0.5	80	80	Symmetric
4	T4C	2	80	80	Symmetric
	T4D	1	80	80	Symmetric
	T4E	0.75	80	80	Symmetric
	T4F	1	80	80	Symmetric
	T5A1	1.5	80	80	Asymmetric, 20mm from center
	T5A2	0.75	80	80	Asymmetric, 50mm from center
5	T5C1	2	80	80	Asymmetric, 20mm from center
	T5E1	0.5	80	80	Asymmetric, 50mm from center
	T5A3	0.75	80	80	Asymmetric, 20mm from center
	T5A4	1	80	80	Asymmetric, 50mm from center
	T5C2	1	80	80	Asymmetric, 20mm from center
	T5E2	1	80	80	Asymmetric, 50mm from center
	T6A1	1.5	80	5	Symmetric
	T6C1	2	80	5	Symmetric
6	T6E1	0.5	80	5	Symmetric
	T6A2	0.75	80	5	Symmetric
	T6C2	1	80	5	Symmetric
	T6E2	1	80	5	Symmetric

Table 3-3: Prototype and Model Sand Comparison.

Parameter	Red Sand (Oak Island)	#00 Alwhite silica sand
Max. dry density, γ_{max} (kN/m^3)	17.1	15.8
Min. dry density, γ_{max} (kN/m^3)	12.9	12.7
Mean grain size, D_{50} (mm)	0.22	0.32
Internal angle of friction, ϕ	35.3° (D_r = 79%)	41° (D_r = 90%)

Table 3-4: Relative Density Measurements (Average Post Test)

Test 2	47.3%
Test 3	44.1%
Test 4	81.5%
Test 5	82.5%
Test 6	79.5%

Table 3-5: Pipe Pressurization Strains

Test	Target Pressure (MPa)	Target Hoop Strain (microstrain)	Measured Pressure (MPa)	Calculated Strain (microstrain)		Measured Strain (microstrain)		Percent Difference in Strain (Calculated to Measured)	
				Hoop	Axial	Hoop	Axial	Hoop	Axial
T2	13.00	3650	12.82	3600	-1188	3662	-1196	1.70%	0.67%
T3	0.81	228	0.84	235	-78	228	-75	-3.10%	-3.42%
T4	13.00	3650	12.95	3637	-1200	3612	-1212	-0.68%	0.99%
T5	13.00	3650	12.90	3615	-1193	3748	-1215	3.61%	1.85%
T6	0.81	228	0.84	235	-78	238	-81	1.12%	4.11%

Table 3-6: Comparative Pipe and Soil Stiffness

Sand Relative Density	5% SMYS (24S + p) + (1.85E')	80% SMYS (24S + p) + (1.85E')
40% RD	3 + 37	15 + 37
80% RD	3 + 74	15 + 74

Table 3-7: Transducer Gradients, Soil Cover

Test Name	Cover (D)	Soil Density %	Internal Pressure (%SMYS)	Offset (mm)	Ratios (με/kN for strain gages and mm/N X 10^{-1} for ovalization)									
					S1HCO	S2AIO	S3HCC	S4ACC	S5AIC	S6HIC	S7ACO	S8HIO	OV12	OV3
T2B	0.5	40	80	0	2.72	6.51	7.47	-6.14	7.59	0.41	-2.53	2.72	6.50	
T2A	0.75	40	80	0	4.69	4.71	3.55	-6.64	4.18	-0.37		-0.97	3.25	
T2C	1	40	80	0		3.48		-5.74	2.94	-0.41	-2.85	-0.85	1.69	-0.32
T3B	0.5	40	5	0	15.39	2.62		-6.40	2.62	5.98	-4.20	4.93	7.20	-2.09
T3A	0.75	40	5	0	14.90	2.75	10.00	-6.29	2.39	3.98		2.75	4.98	
T3C	1	40	5	0	5.96	1.86	2.08			3.61		2.90	3.31	-1.29
T4B	0.5	80	80	0	8.00	2.61	8.00	-5.00	2.61		-2.69		4.44	-0.80
T4E	0.75	80	80	0	3.16	3.37	5.42	-5.46	3.37	-0.45	-5.46	-0.45	5.45	-0.58
T4D	1	80	80	0	4.28	2.81	5.84		1.90				4.97	
T4F	1	80	80	0	5.16					-0.52		-0.52		-1.04
T4A	1.5	80	80	0	2.28	2.16	2.75	-2.87	2.16			-0.32	1.86	
T4C	2	80	80	0	1.25	1.87	1.57	-2.26	1.64	-0.08	-1.55	-0.33	0.76	-0.26
T5A3	0.75	80	80	20	-0.79	2.06	-1.08	-1.55	1.87	-0.79		-0.69	0.11	
T5C2	1	80	80	20	1.00	2.34	1.41	-2.27	1.84	-0.39	-0.51	-1.60		-0.51
T5A1	1.5	80	80	20	0.97	2.02	1.36	-2.43	2.02	-0.32		-0.45	0.98	
T5C1	2	80	80	20	0.95	1.29	1.02	-1.23	1.29		-1.23			-0.09
T5E1	0.5	80	80	50	-0.27	0.19	-0.32	0.19	0.33	-0.36	0.19	-0.23	-0.56	-0.98
T5A4	0.75	80	80	50	-0.29	0.43	-0.29	-0.25	0.43	-0.29		-0.29	0.82	
T5E2	1	80	80	50	-0.29	0.78	-0.73	-0.72	1.03	-0.84	-0.49	-0.65	-0.78	-2.29
T5A2	1.5	80	80	50	-0.34	0.74	-0.45	-0.61	0.64	-0.28		-0.28	0.21	
T6E1	0.5	80	5	0	9.63	2.41	9.01	-6.84	2.02	4.06	-6.84	3.71	6.32	-1.92
T6A2	0.75	80	5	0		2.69	8.87	-5.09	2.46	3.03		2.07	6.00	-1.08
T6C2	1	80	5	0	6.80	2.99	7.35	-6.07	2.70	1.32	-3.86		3.20	-1.12
T6E2	1	80	5	0	7.20	3.57	9.90	-6.56	3.18	2.31	-6.56	1.93	6.55	-1.22
T6A1	1.5	80	5	0		2.08	9.55	-4.05	1.79	2.72		1.73	3.80	-1.12
T6C1	2	80	5	0	3.79	1.70	3.05	-2.80	1.54	0.55	-1.80		1.25	-0.80

Table 3-8: Transducer Gradient Comparisons for Varying Internal Pressure

Test Name	Cover (D)	Soil Density %	Internal Pressure (%SMYS)	Offset (mm)	Ratios (με/kN for strain gages and mm/N X 10^{-1} for ovalization)									
					S1HCO	S2AIO	S3HCC	S4ACC	S5AIC	S6HIC	S7ACO	S8HIO	OV12	OV3
T3C	1	40	5	0	5.96	1.86	2.08			3.61		2.90	3.31	-1.29
T2C	1	40	80	0		3.48		-5.74	2.94	-0.41	-2.85	-0.85	1.69	-0.32
T3A	0.75	40	5	0	14.90	2.75	10.00	-6.29	2.39	3.98		2.75	4.98	
T2A	0.75	40	80	0	4.69	4.71	3.55	-6.64	4.18	-0.37		-0.97	3.25	
T3B	0.5	40	5	0	15.39	2.62		-6.40	2.62	5.98	-4.20	4.93	7.20	-2.09
T2B	0.5	40	80	0	2.72	6.51	7.47	-6.14	7.59	0.41	-2.53	2.72	6.50	
T6C1	2	80	5	0	3.79	1.70	3.05	-2.80	1.54	0.55	-1.80		1.25	-0.80
T4C	2	80	80	0	1.25	1.87	1.57	-2.26	1.64	-0.08	-1.55	-0.33	0.76	-0.26
T6A1	1.5	80	5	0		2.08	9.55	-4.05	1.79	2.72		1.73	3.80	-1.12
T4A	1.5	80	80	0	2.28	2.16	2.75	-2.87	2.16			-0.32	1.86	
T6C2	1	80	5	0	6.80	2.99	7.35	-6.07	2.70	1.32	-3.86		3.20	-1.12
T6E2	1	80	5	0	7.20	3.57	9.90	-6.56	3.18	2.31	-6.56	1.93	6.55	-1.22
T4D	1	80	80	0	4.28	2.81	5.84		1.90				4.97	
T4F	1	80	80	0	5.16					-0.52		-0.52		-1.04
T6A2	0.75	80	5	0		2.69	8.87	-5.09	2.46	3.03		2.07	6.00	-1.08
T4E	0.75	80	80	0	3.16	3.37	5.42	-5.46	3.37	-0.45	-5.46	-0.45	5.45	-0.58
T6E1	0.5	80	5	0	9.63	2.41	9.01	-6.84	2.02	4.06	-6.84	3.71	6.32	-1.92
T4B	0.5	80	80	0	8.00	2.61	8.00	-5.00	2.61		-2.69		4.44	-0.80

Table 3-9: Transducer Gradient Comparisons for Varying Soil Density

Test Name	Cover (D)	Soil Density %	Internal Pressure (%SMYS)	Offset (mm)	Ratios (με/kN for strain gages and mm/N X 10^{-1} for ovalization)									
					S1HCO	S2AIO	S3HCC	S4ACC	S5AIC	S6HIC	S7ACO	S8HIO	OV12	OV3
T3B	0.5	40	5	0	15.39	2.62		-6.40	2.62	5.98	-4.20	4.93	7.20	-2.09
T6E1	0.5	80	5	0	9.63	2.41	9.01	-6.84	2.02	4.06	-6.84	3.71	6.32	-1.92
T3A	0.75	40	5	0	14.90	2.75	10.00	-6.29	2.39	3.98		2.75	4.98	
T6A2	0.75	80	5	0		2.69	8.87	-5.09	2.46	3.03		2.07	6.00	-1.08
T3C	1	40	5	0	5.96	1.86	2.08			3.61		2.90	3.31	-1.29
T6C2	1	80	5	0	6.80	2.99	7.35	-6.07	2.70	1.32	-3.86		3.20	-1.12
T6E2	1	80	5	0	7.20	3.57	9.90	-6.56	3.18	2.31	-6.56	1.93	6.55	-1.22
T2B	0.5	40	80	0	2.72	6.51	7.47	-6.14	7.59	0.41	-2.53	2.72	6.50	
T4B	0.5	80	80	0	8.00	2.61	8.00	-5.00	2.61		-2.69		4.44	-0.80
T2A	0.75	40	80	0	4.69	4.71	3.55	-6.64	4.18	-0.37		-0.97	3.25	
T4E	0.75	80	80	0	3.16	3.37	5.42	-5.46	3.37	-0.45	-5.46	-0.45	5.45	-0.58
T2C	1	40	80	0		3.48		-5.74	2.94	-0.41	-2.85	-0.85	1.69	-0.32
T4D	1	80	80	0	4.28	2.81	5.84		1.90				4.97	
T4F	1	80	80	0	5.16					-0.52	0.00	-0.52		-1.04

Table 3-10: Transducer Gradient Comparisons for Varying Load Offset

Test Name	Cover (D)	Soil Density %	Internal Pressure (%SMYS)	Offset (mm)	Ratios (με/kN for strain gages and mm/N X 10^{-1} for ovalization)									
					S1HCO	S2AIO	S3HCC	S4ACC	S5AIC	S6HIC	S7ACO	S8HIO	OV12	OV3
T4B	0.5	80	80	0	8.00	2.61	8.00	-5.00	2.61		-2.69		4.44	-0.80
T5E1	0.5	80	80	50	-0.27	0.19	-0.32	0.19	0.33	-0.36	0.19	-0.23	-0.56	-0.98
T4E	0.75	80	80	0	3.16	3.37	5.42	-5.46	3.37	-0.45	-5.46	-0.45	5.45	-0.58
T5A3	0.75	80	80	20	-0.79	2.06	-1.08	-1.55	1.87	-0.79		-0.69	0.11	
T5A4	0.75	80	80	50	-0.29	0.43	-0.29	-0.25	0.43	-0.29		-0.29	0.82	
T4D	1	80	80	0	4.28	2.81	5.84		1.90				4.97	
T4F	1	80	80	0	5.16					-0.52		-0.52		-1.04
T5C2	1	80	80	20	1.00	2.34	1.41	-2.27	1.84	-0.39	-0.51	-1.60		-0.51
T5E2	1	80	80	50	-0.29	0.78	-0.73	-0.72	1.03	-0.84	-0.49	-0.65	-0.78	-2.29
T4A	1.5	80	80	0	2.28	2.16	2.75	-2.87	2.16			-0.32	1.86	
T5A1	1.5	80	80	20	0.97	2.02	1.36	-2.43	2.02	-0.32		-0.45	0.98	
T5A2	1.5	80	80	50	-0.34	0.74	-0.45	-0.61	0.64	-0.28		-0.28	0.21	
T4C	2	80	5	0	1.25	1.87	1.57	-2.26	1.64	-0.08	-1.55	-0.33	0.76	-0.26
T5C1	2	80	5	20	0.95	1.29	1.02	-1.23	1.29		-1.23			-0.09

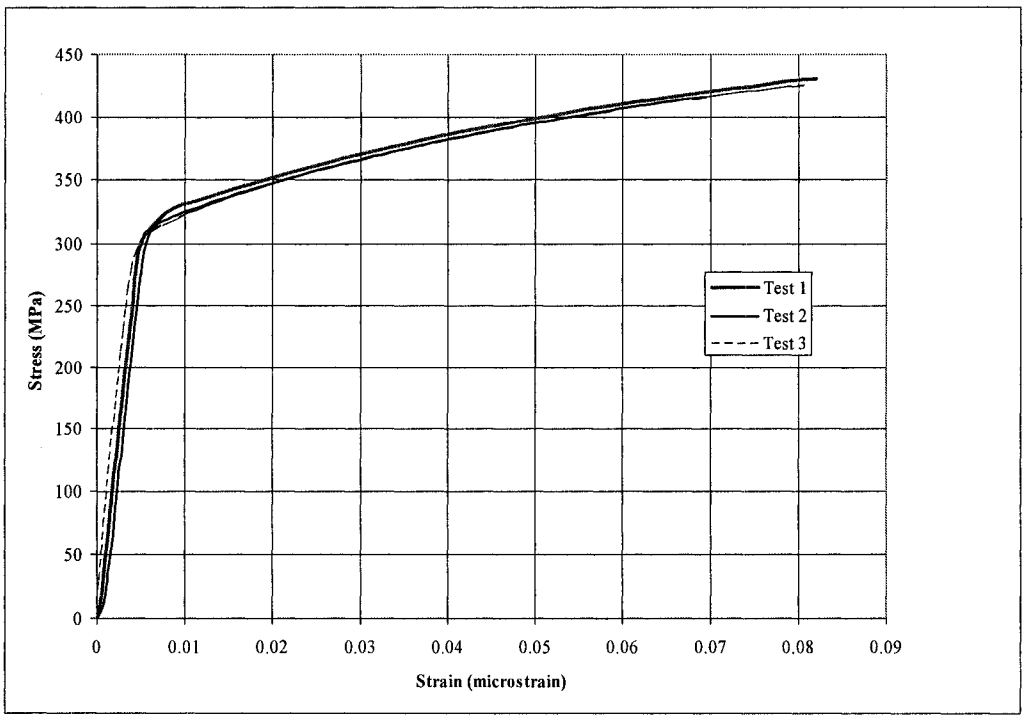

Figure 3-1: Stress Strain Plots for Aluminum Test Specimens

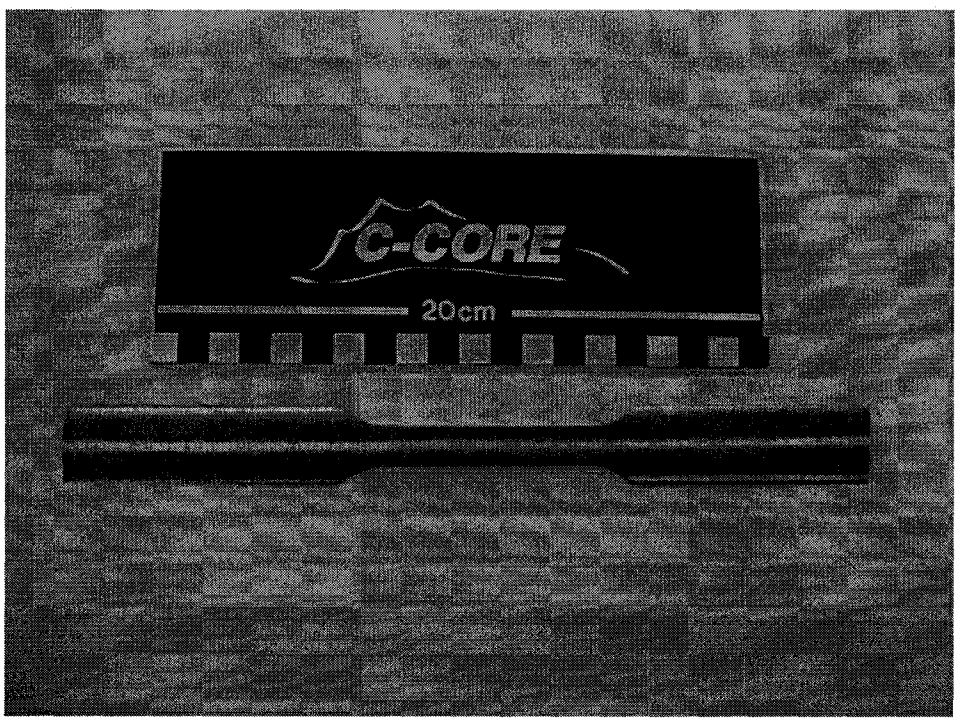

Figure 3-2: Tensile Test Specimen

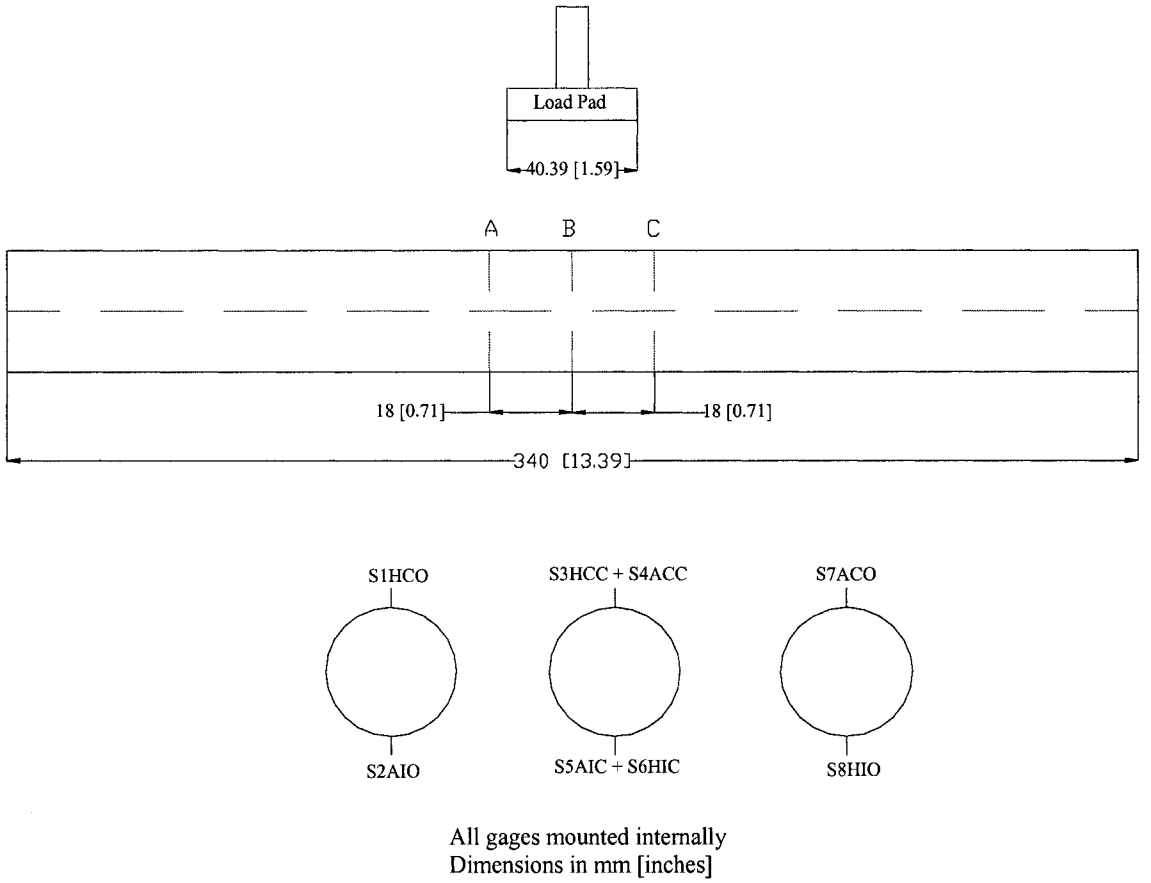

Figure 3-3: Strain Gage Layout

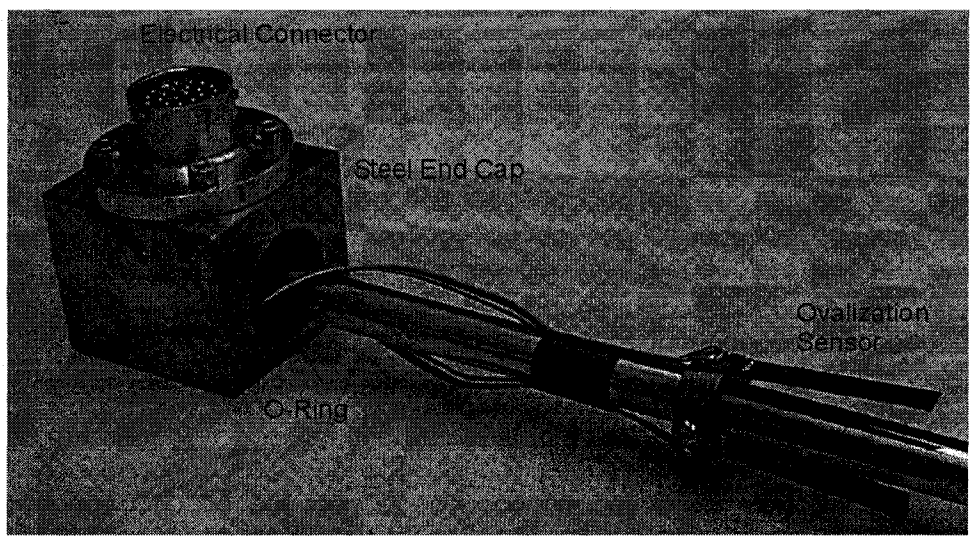

Figure 3-4: End Cap and Ovalization Transducers

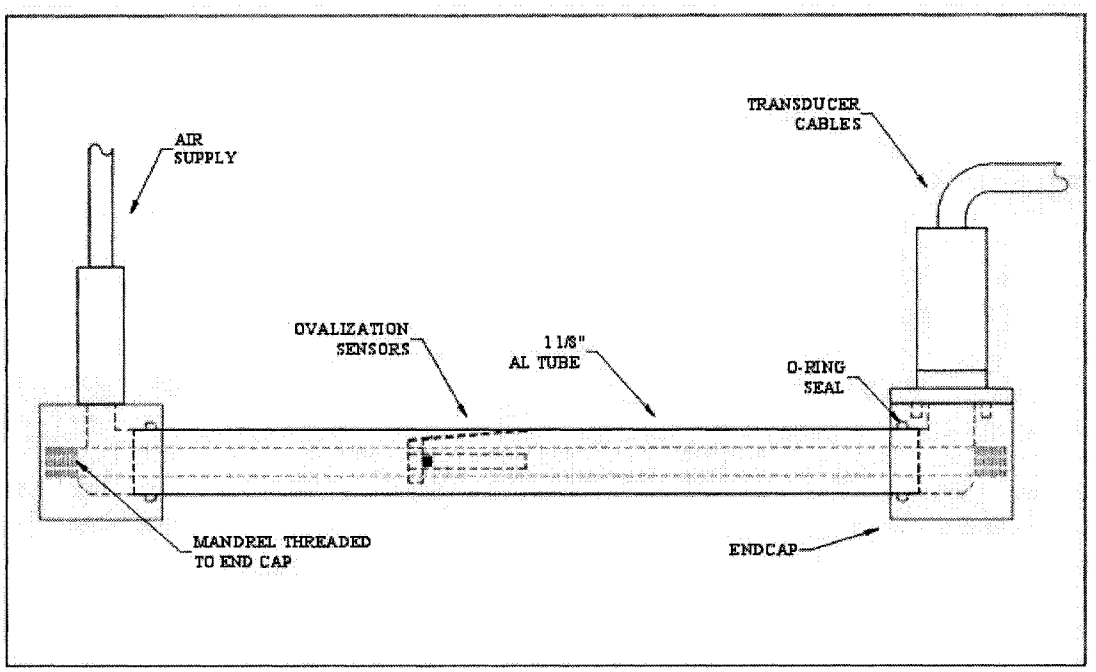

Figure 3-5: Schematic of the Pipe Assembly

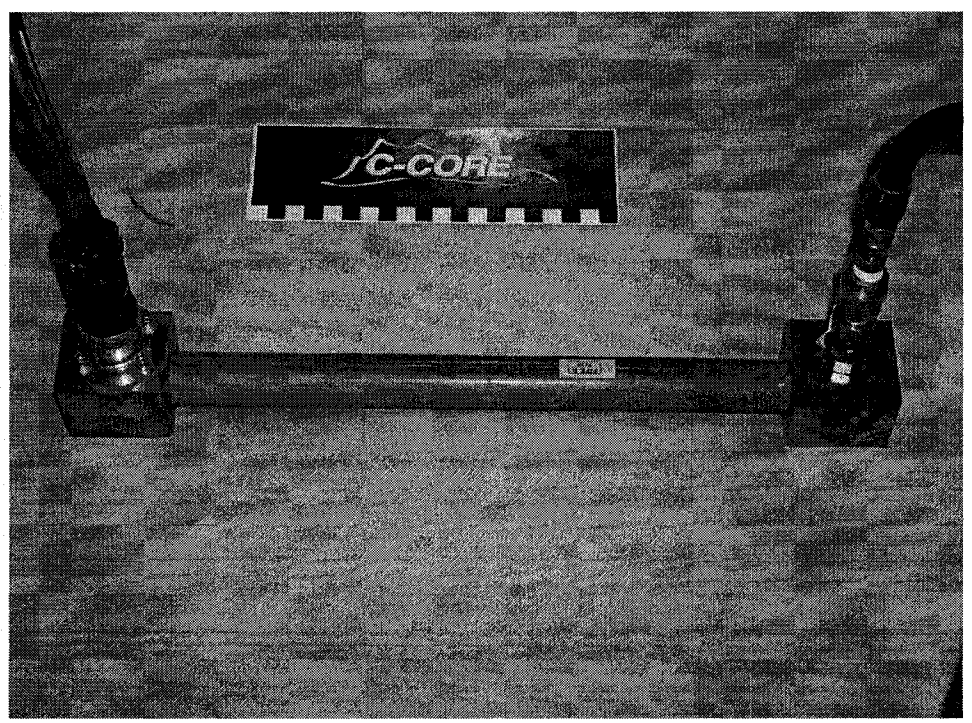

Figure 3-6: Assembled Pipe

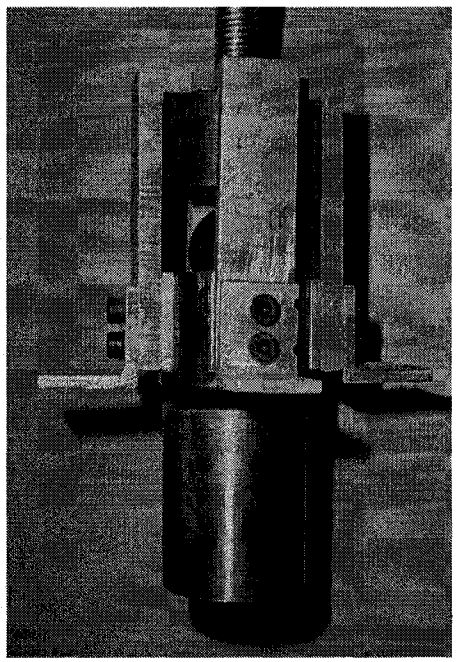

Figure 3-7: Load Pad

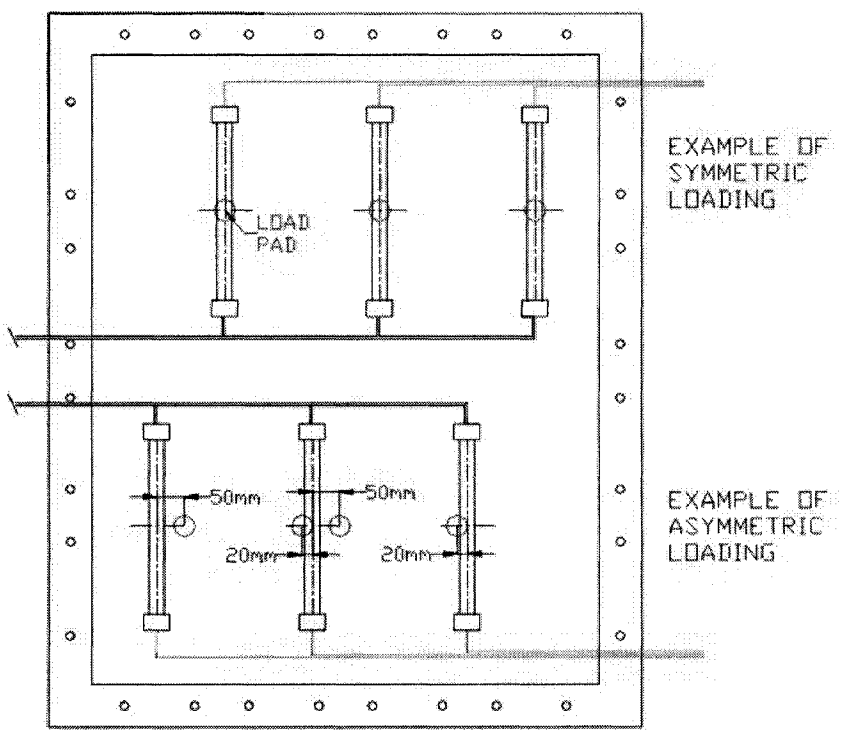

Figure 3-8: Loading Configurations

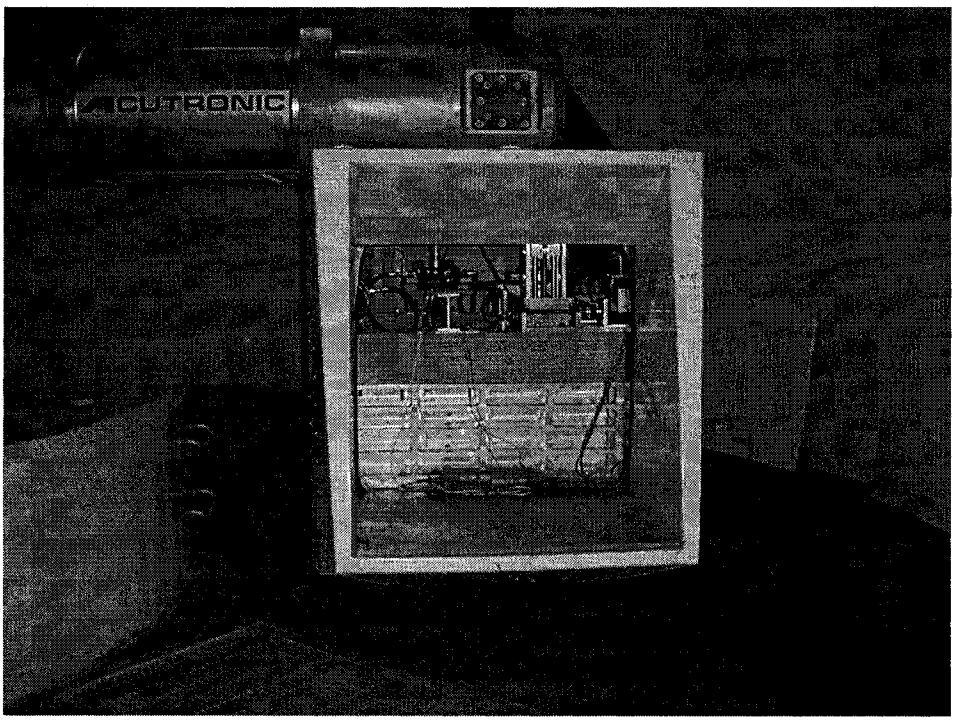

Figure 3-9: The Experiment Package on the Centrifuge Arm

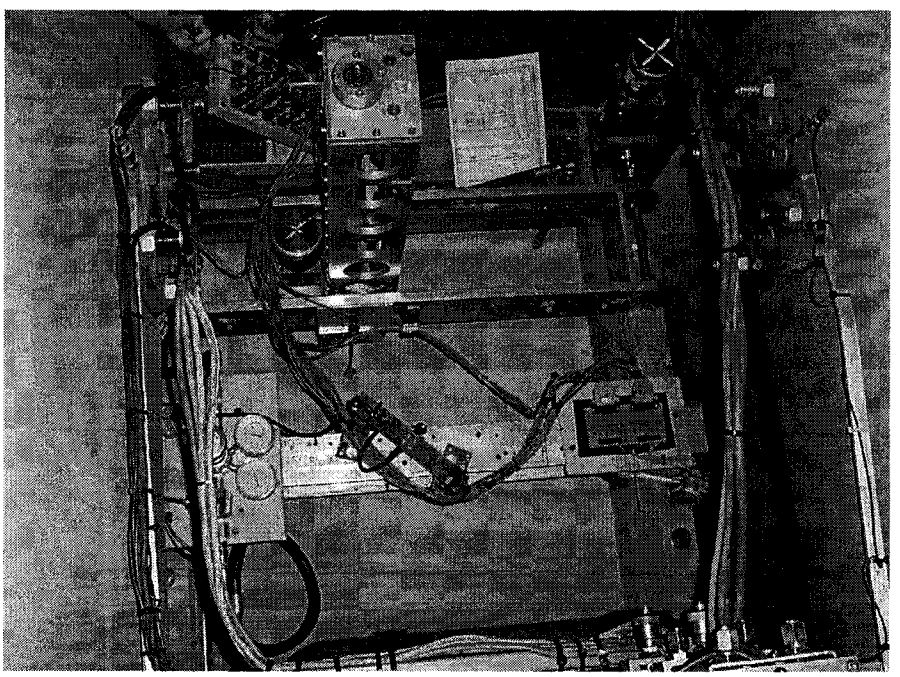

Figure 3-10: Plan View of the Package on the Centrifuge Arm

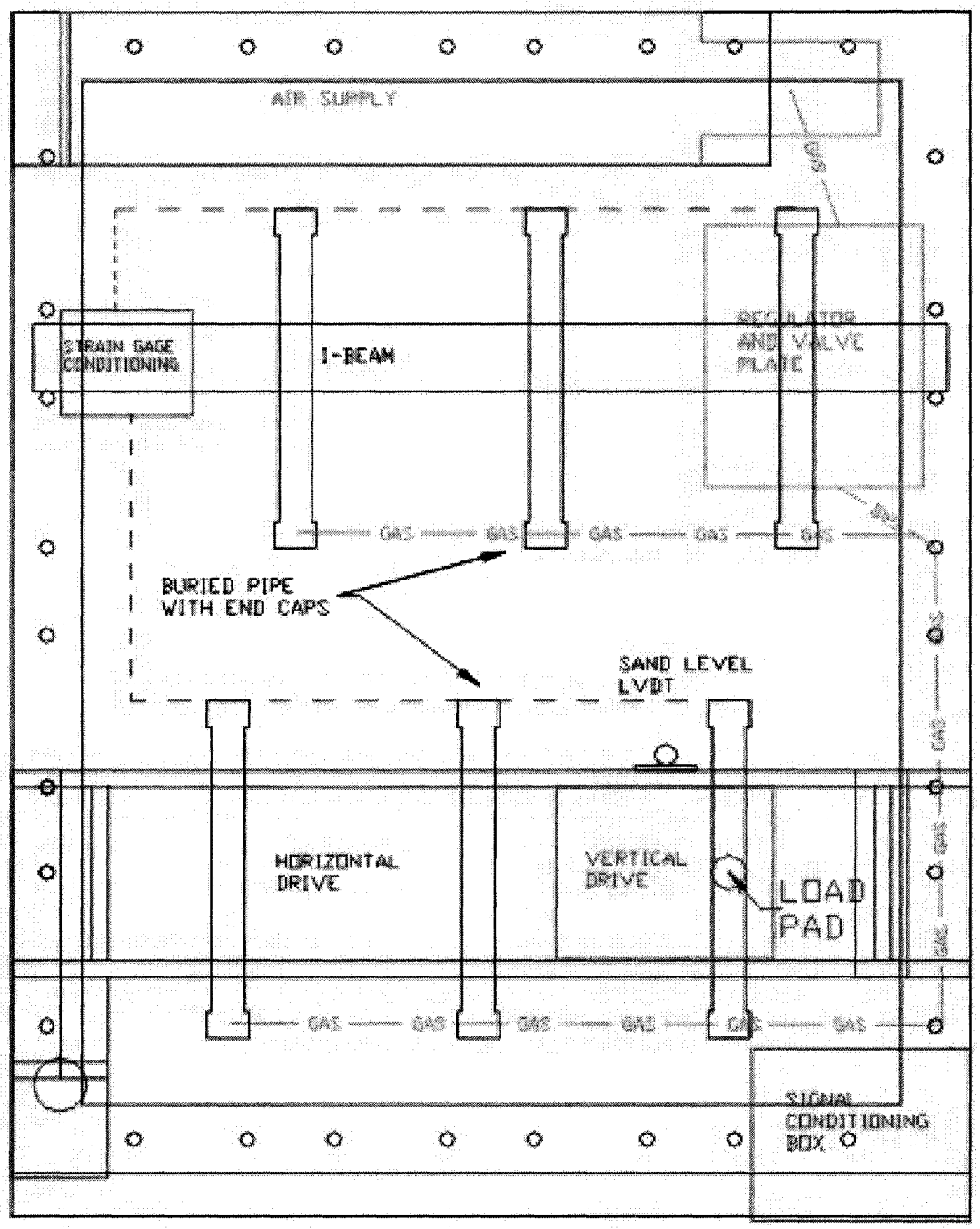

Figure 3-11: Schematic Plan View of the Package

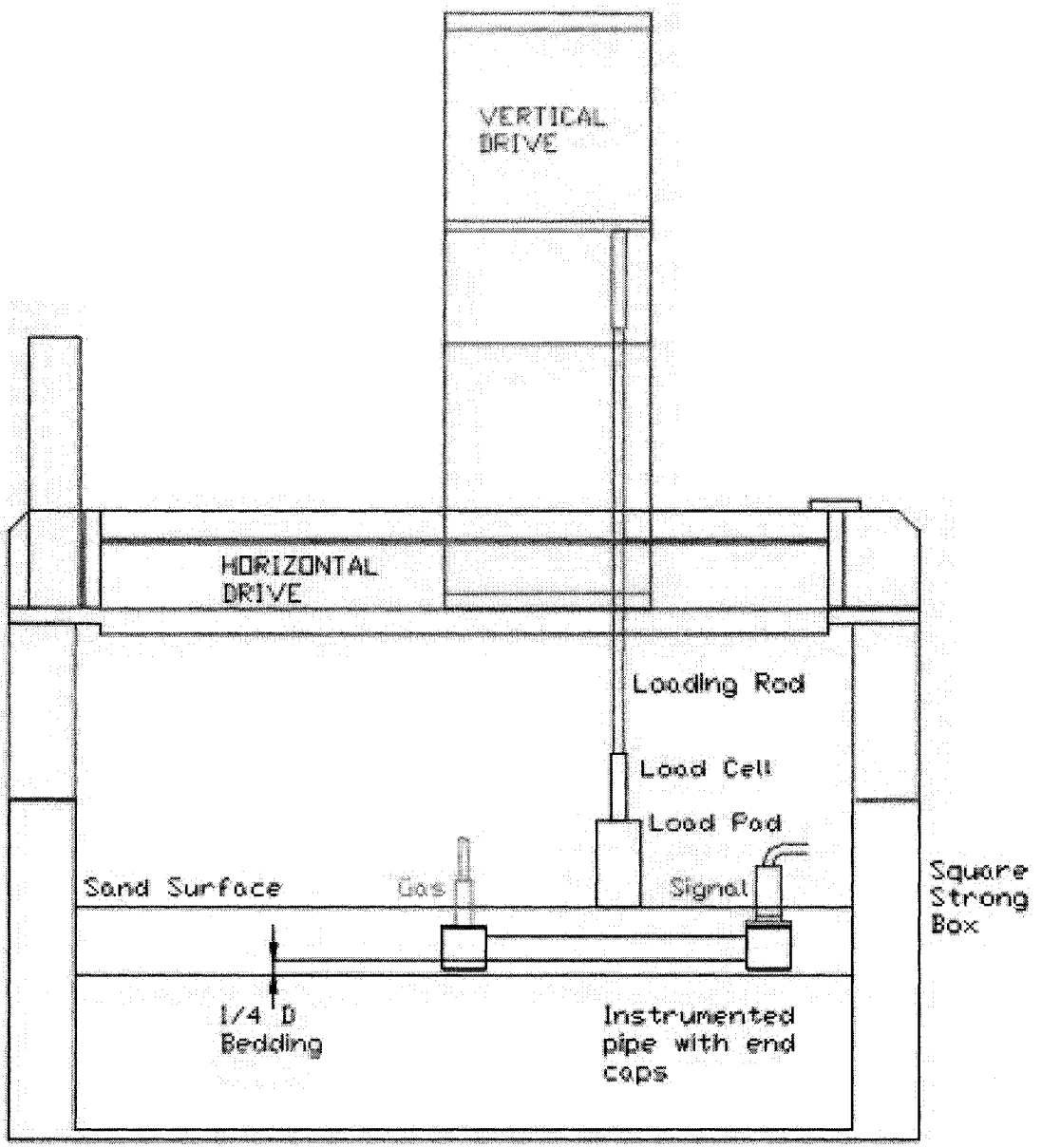

Figure 3-12: Schematic Side View of the Package

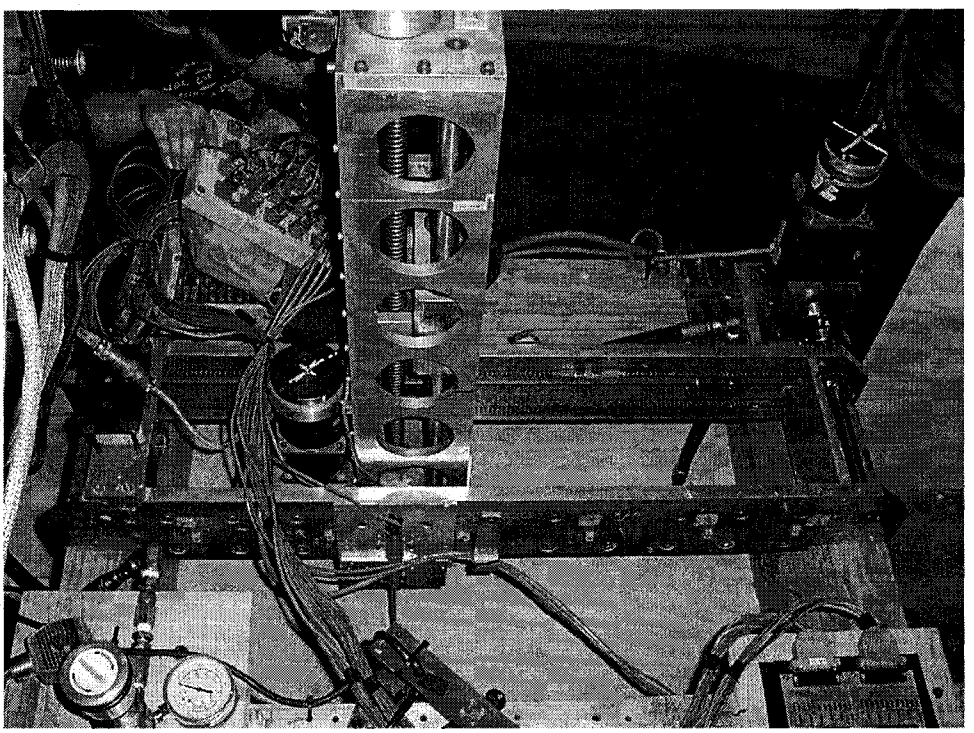

Figure 3-13: 2-axis Linear Drive, Linear and Horizontal Drive Units

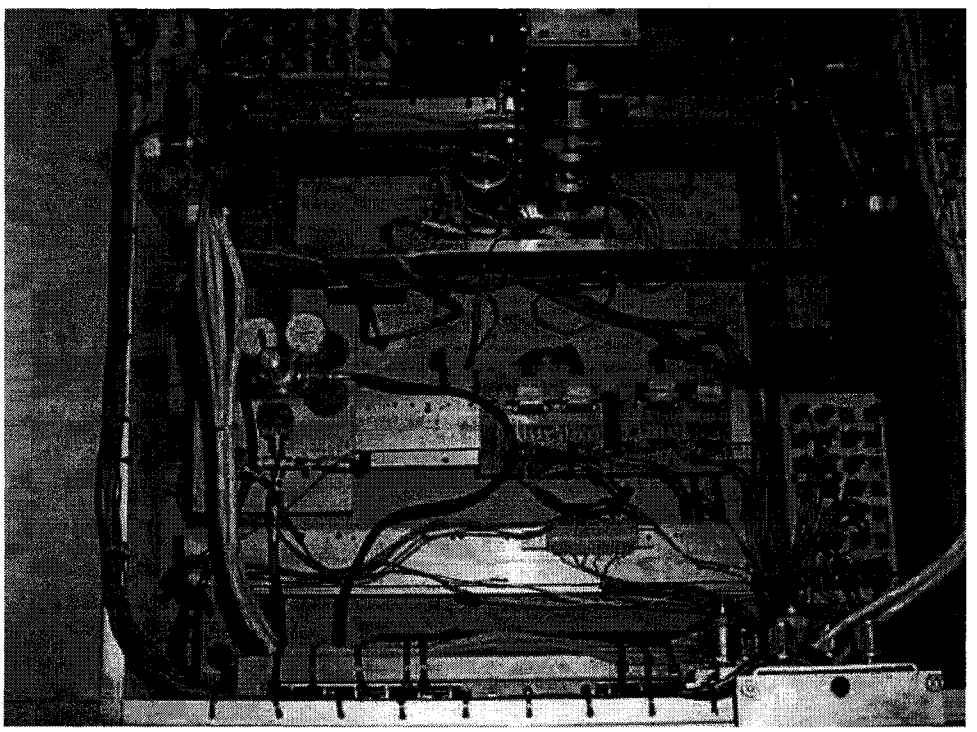

Figure 3-14: Top View of Package

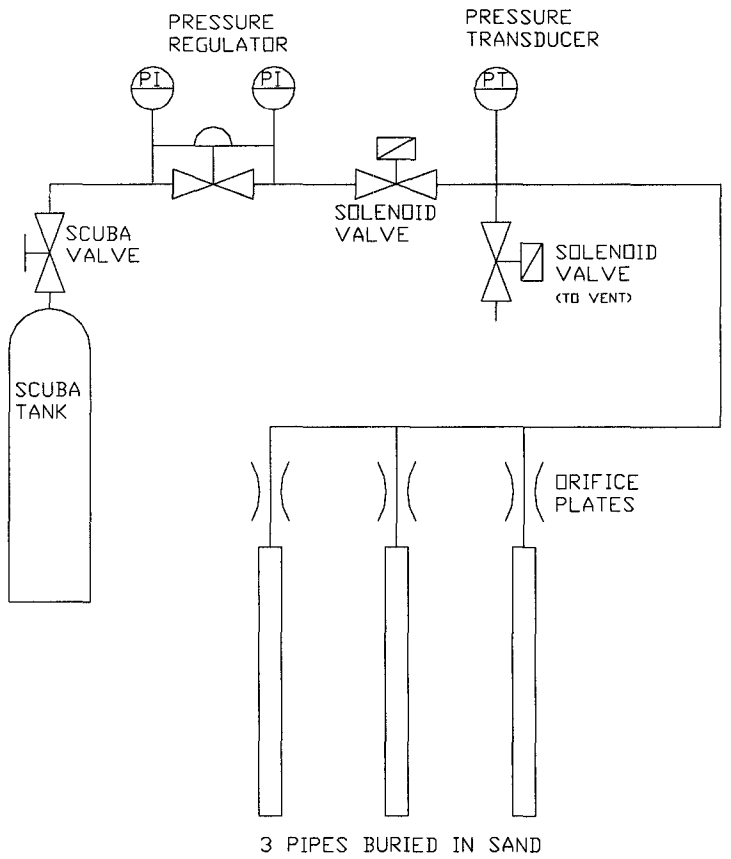

Figure 3-15: Gas System Schematic

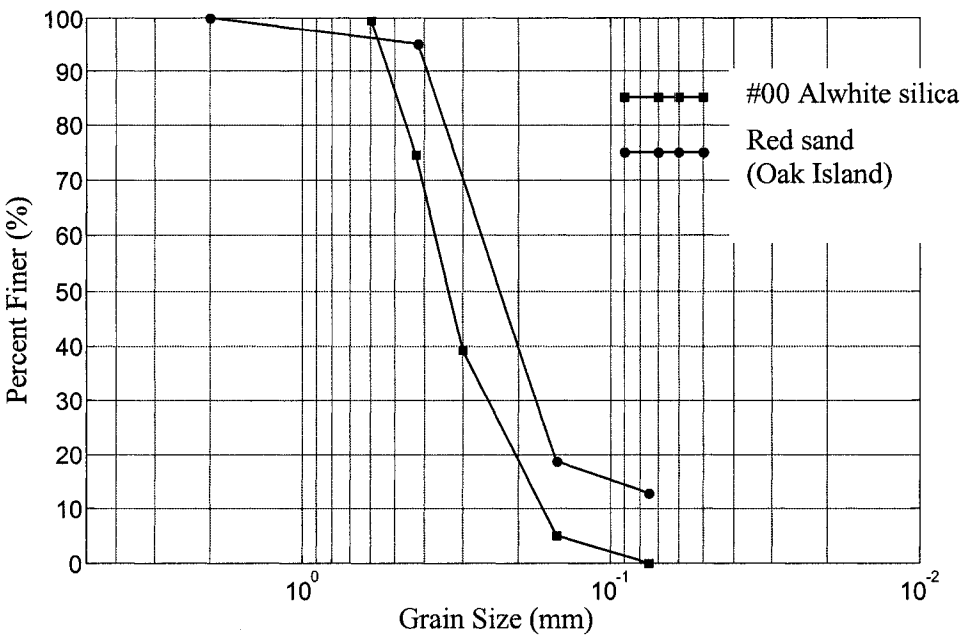

Figure 3-16: Sand Grading Curves

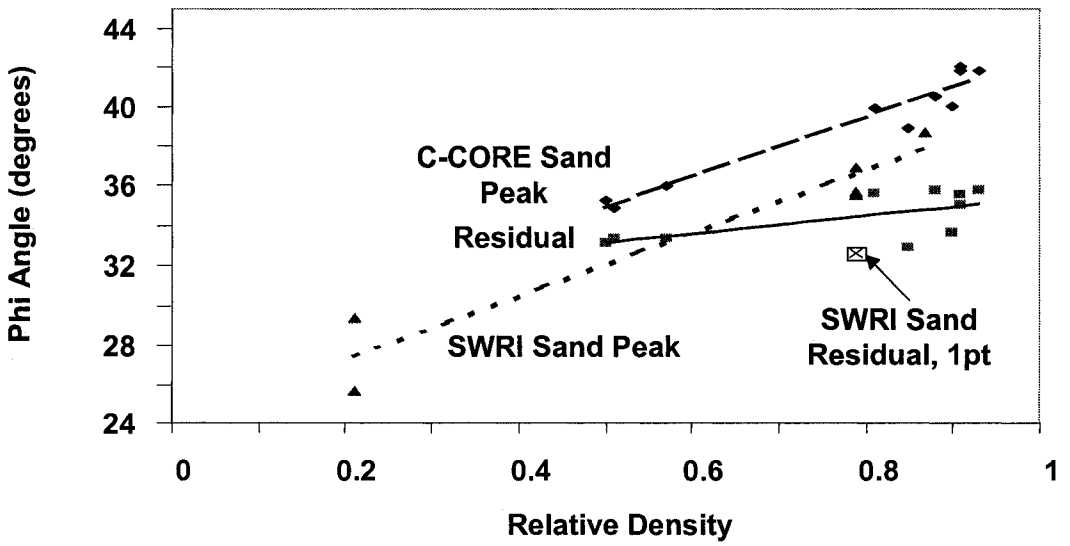

Figure 3-17: Sand Triaxial Compression Frictional Properties

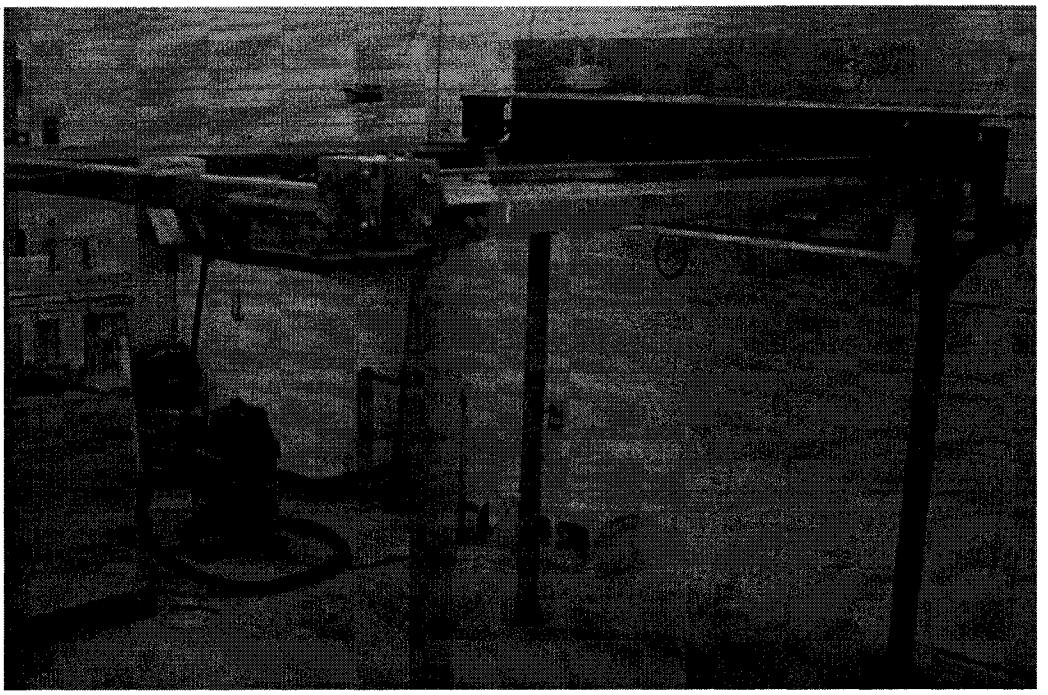

Figure 3-18: Sand Rainer

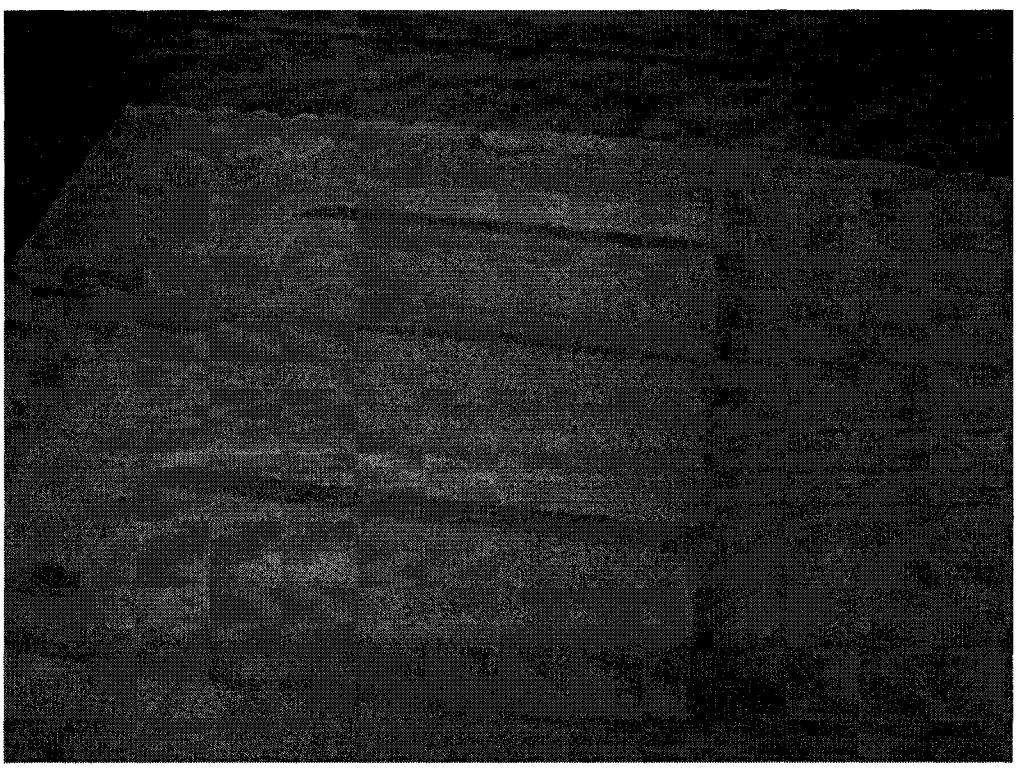

Figure 3-19: Vacuumed Trenches

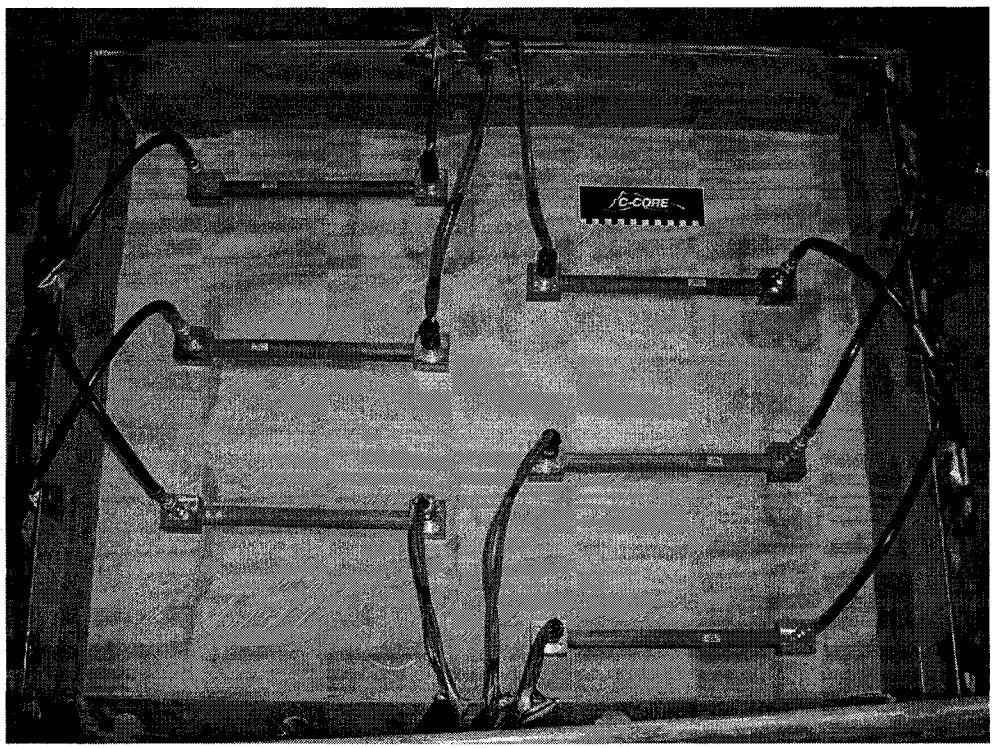

Figure 3-20: Pipes Lying in their Trenches

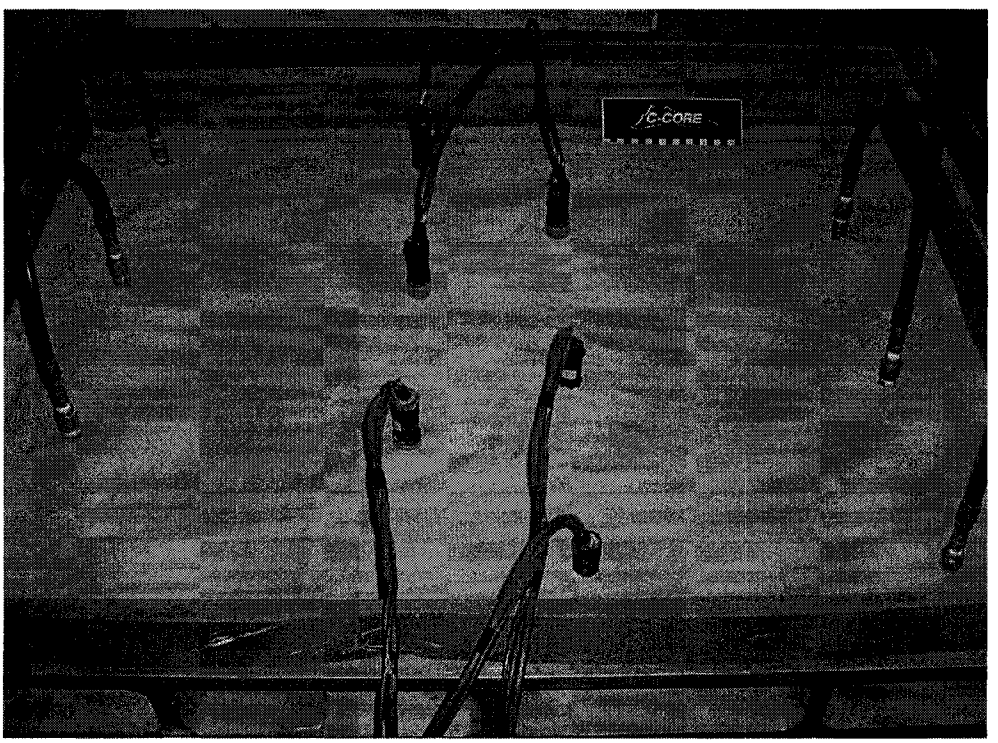

Figure 3-21: Buried Pipes

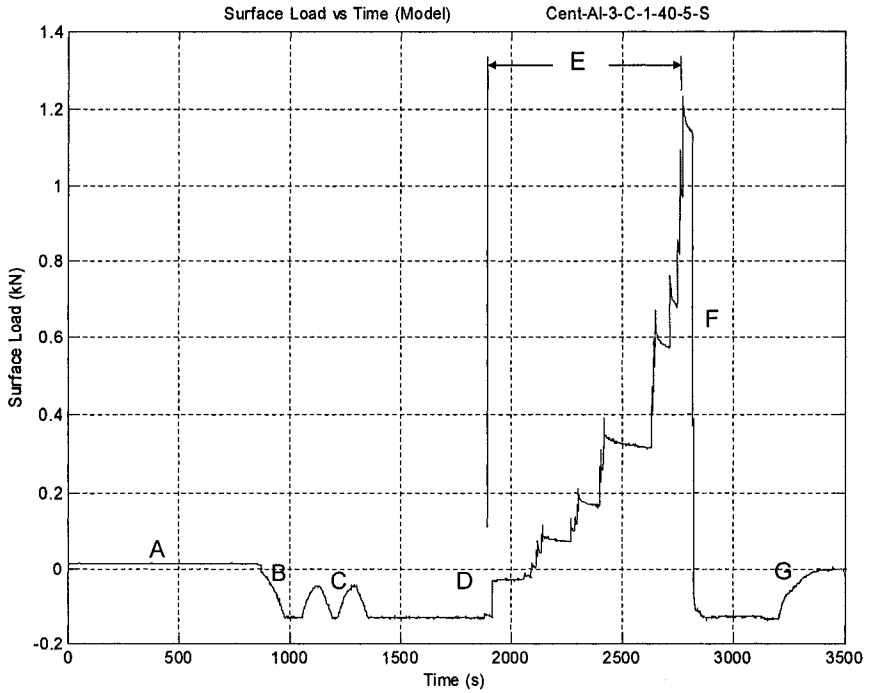

Figure 3-22: Loading Sequence, Surface Load versus Time

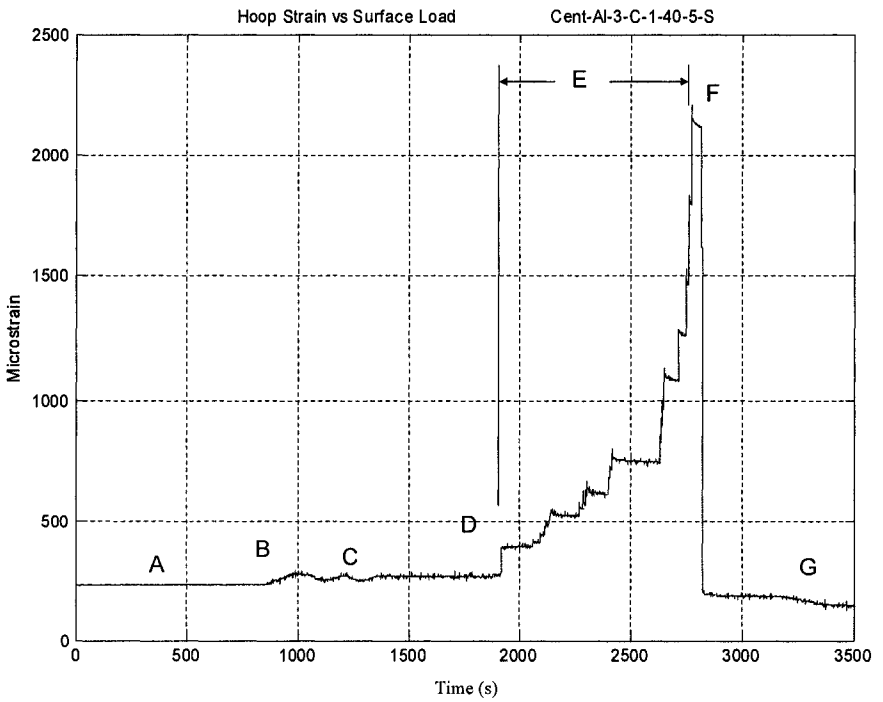

Figure 3-23: Loading Sequence, Strain versus Time

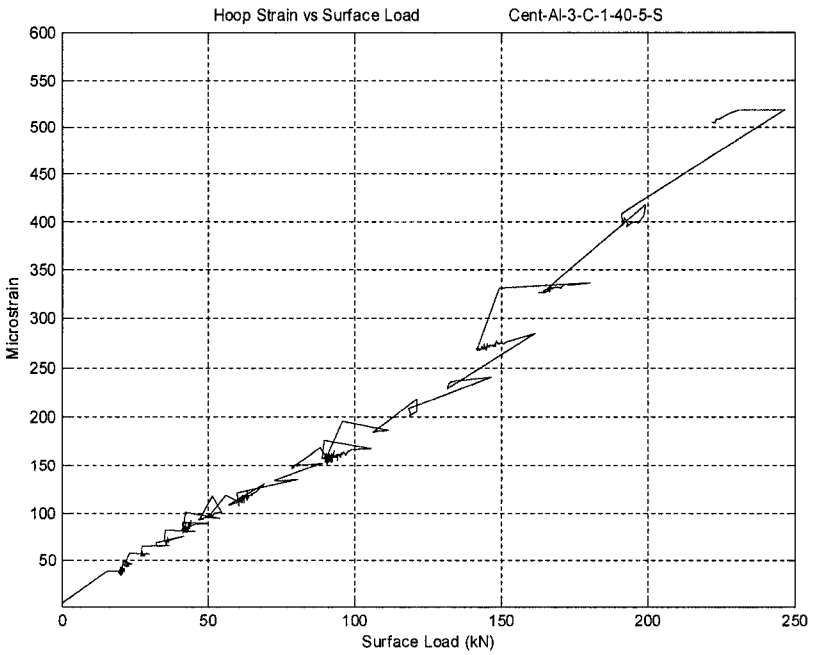

Figure 3-24: Typical Strain versus Surface Load Plot

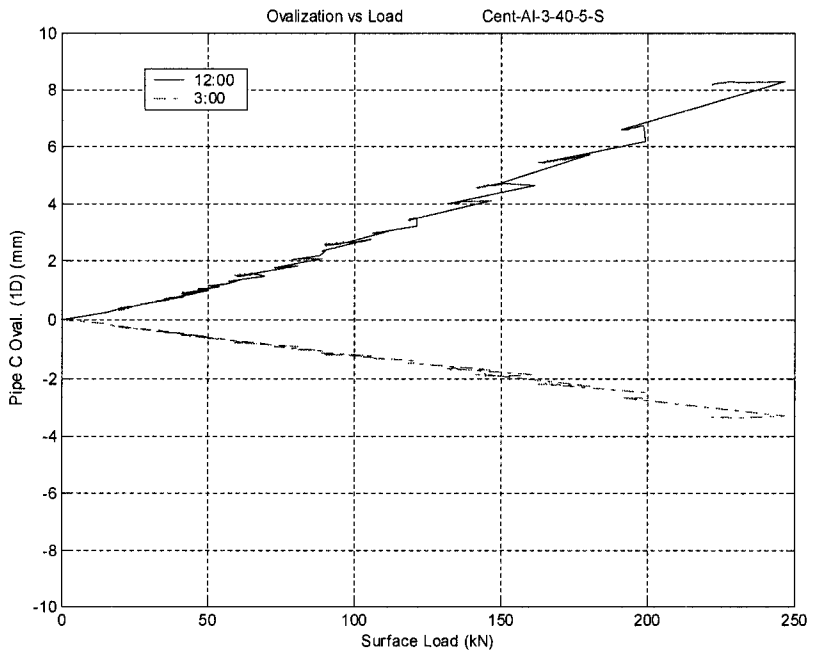

Figure 3-25: Typical Ovalization versus Surface Load Plot

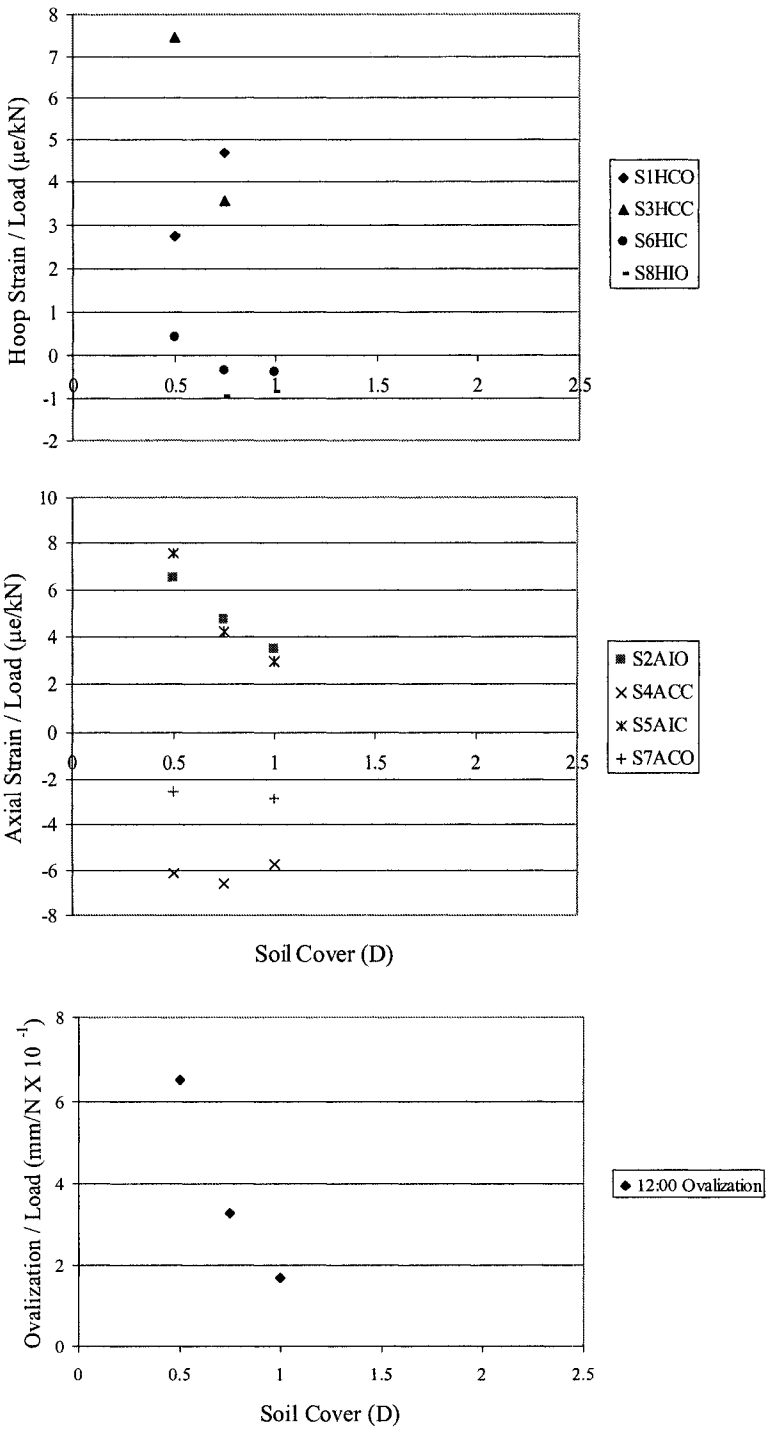

Figure 3-26: Test 2 Transducer Gradients with Varying Soil Cover

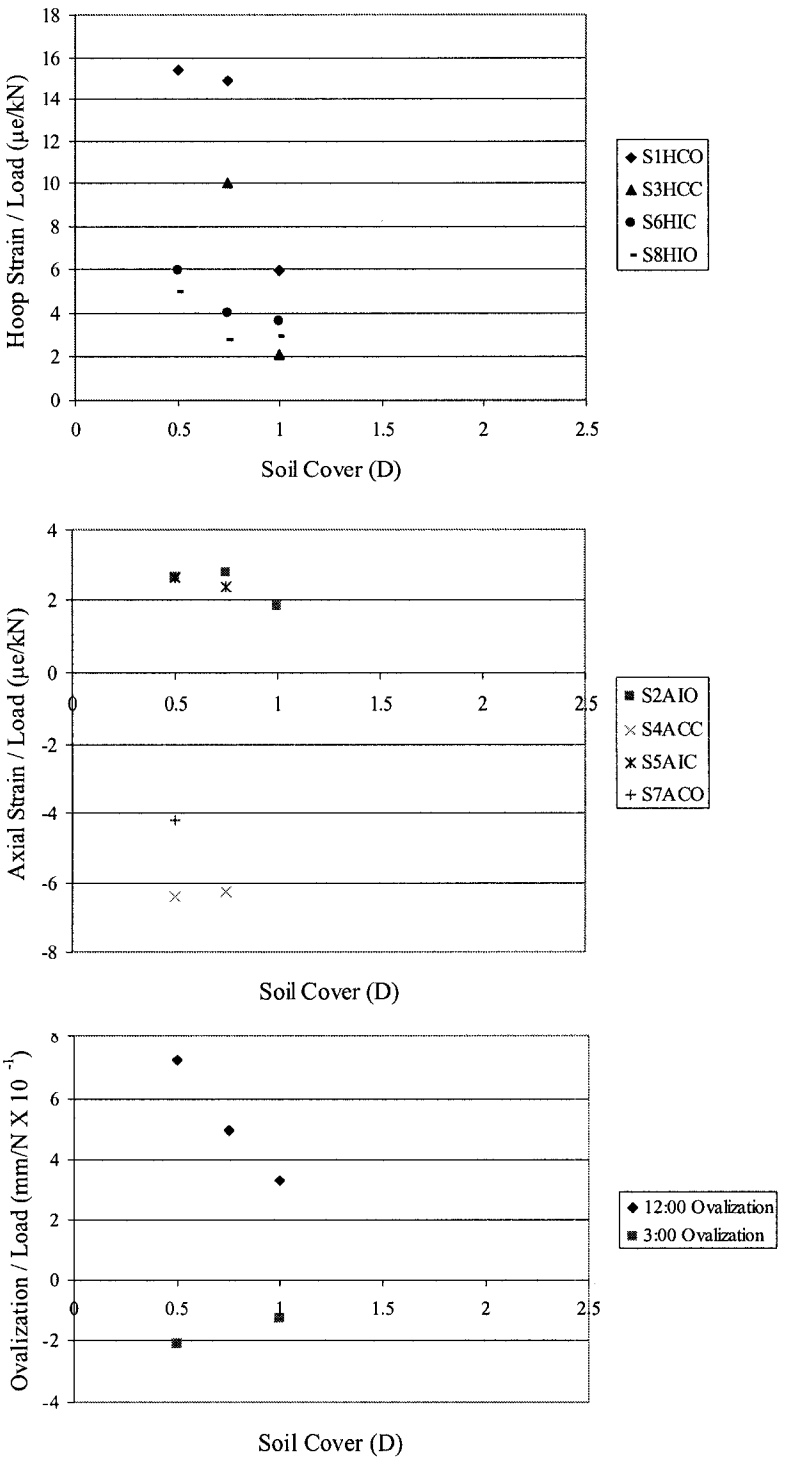

Figure 3-27: Test 3 Transducer Gradients with Varying Soil Cover

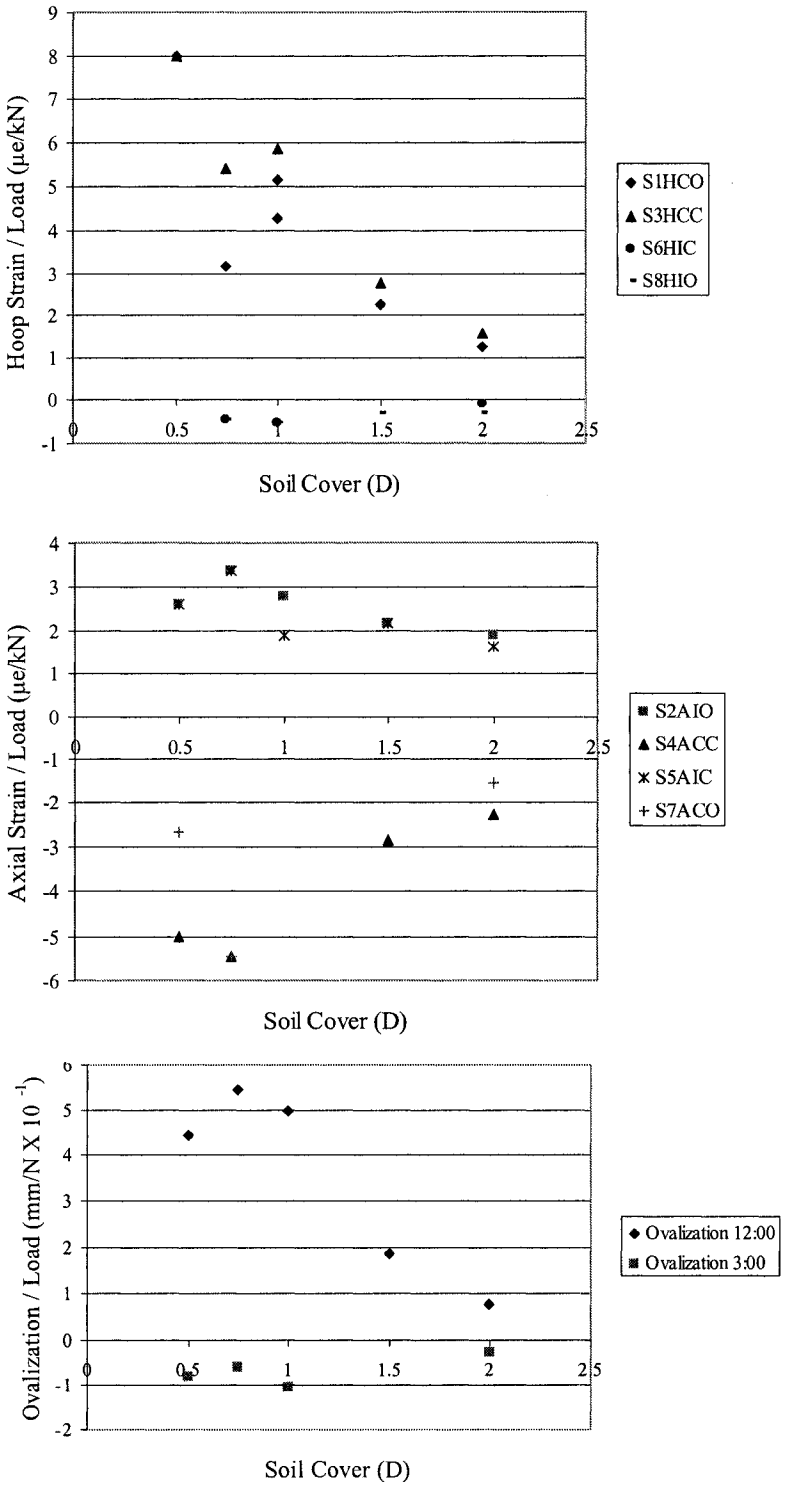

Figure 3-28: Test 4 Transducer Gradients with Varying Soil Cover

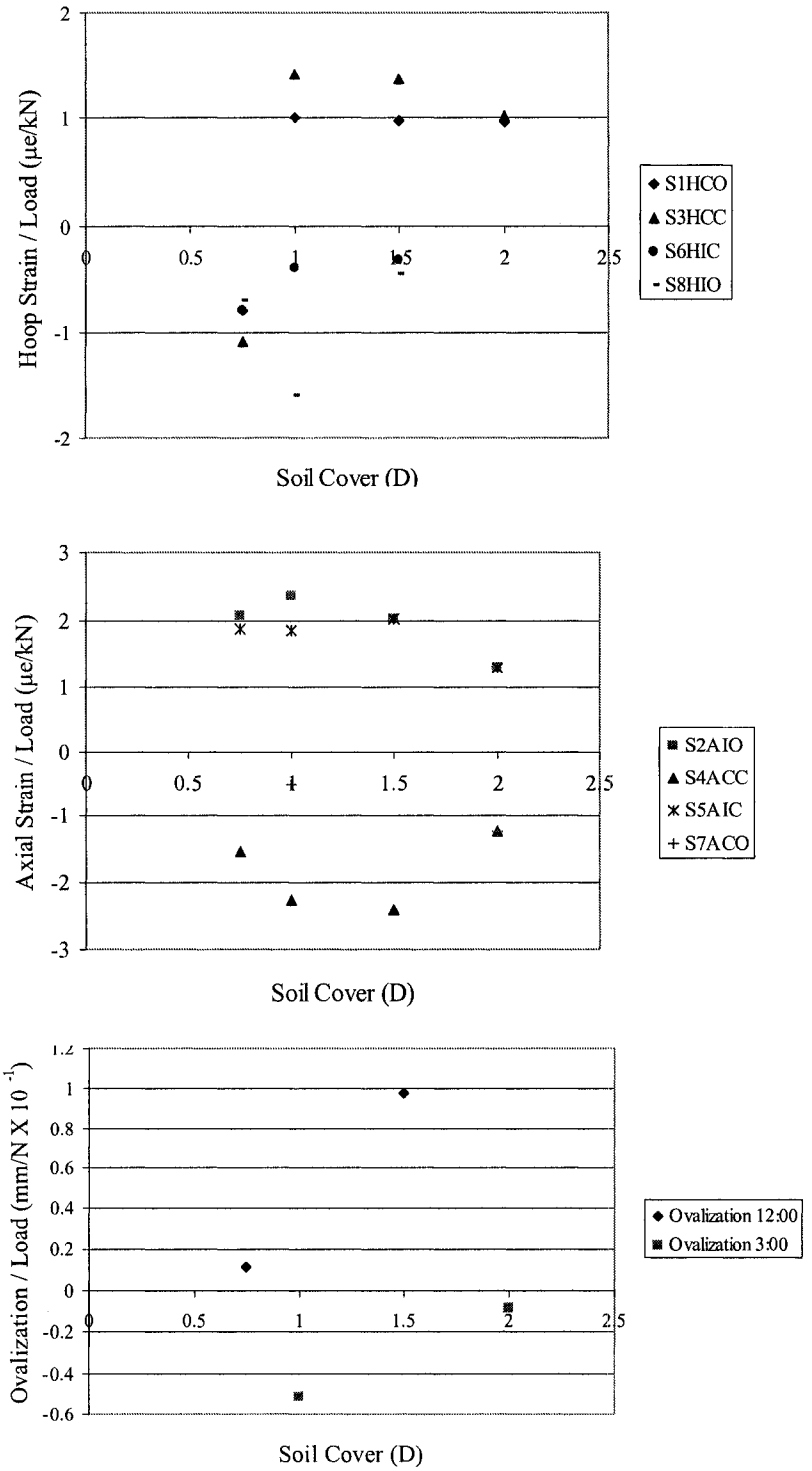

Figure 3-29: Test 5 Transducer Gradients with Varying Soil Cover, 20mm Offset

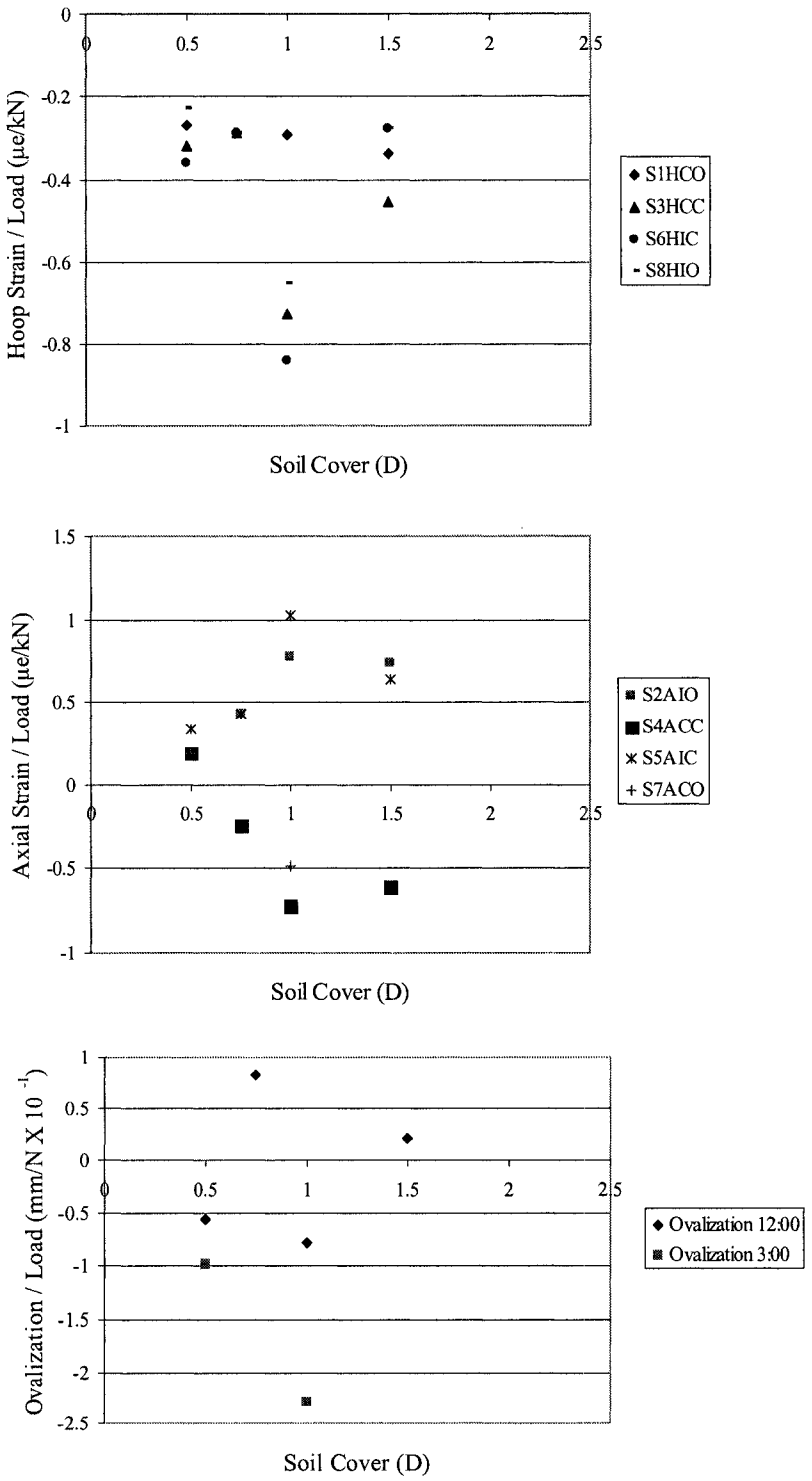

Figure 3-30: Test 5 Transducer Gradients with Varying Soil Cover, 50mm Offset

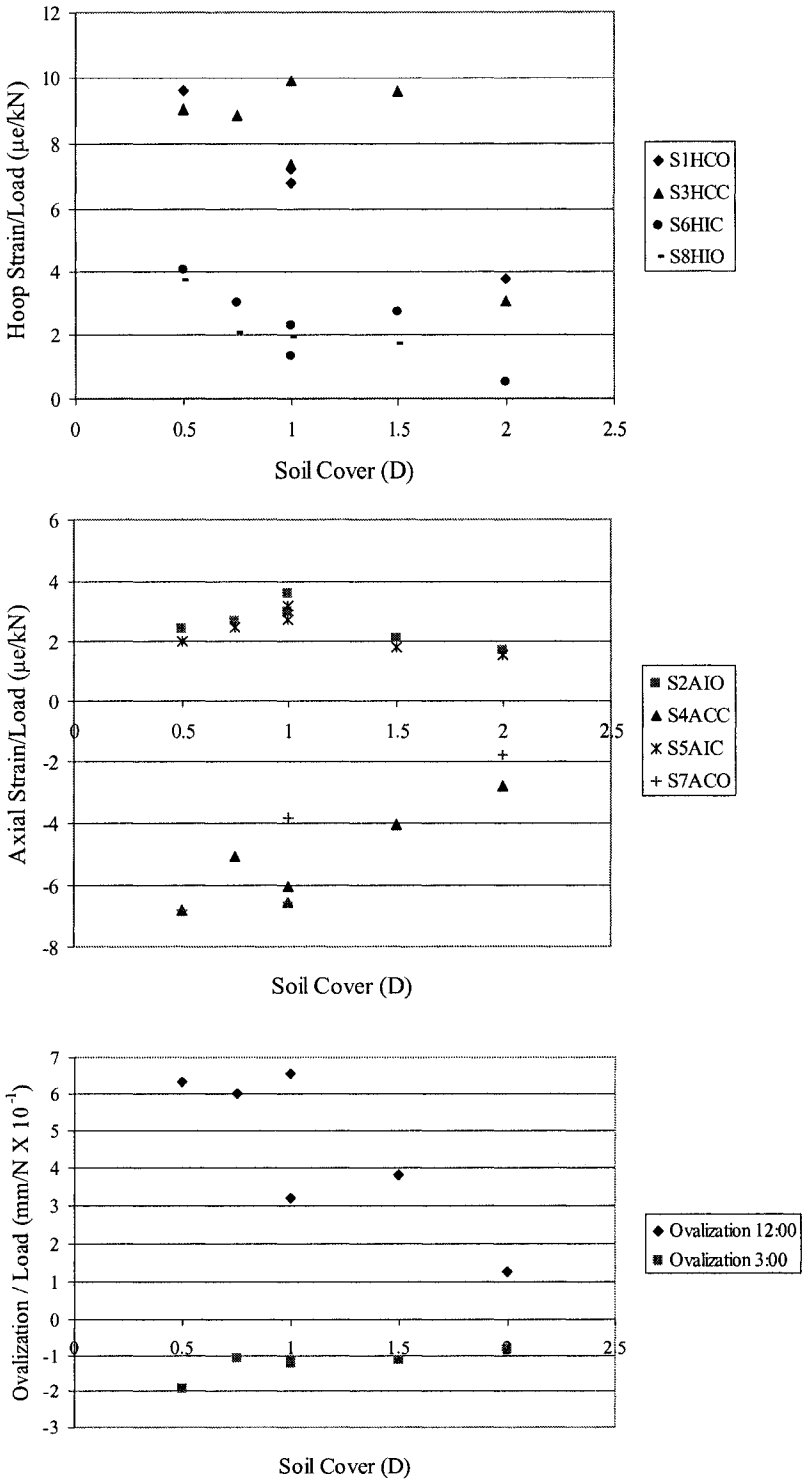

Figure 3-31: Test 6 Transducer Gradients with Varying Soil Cover

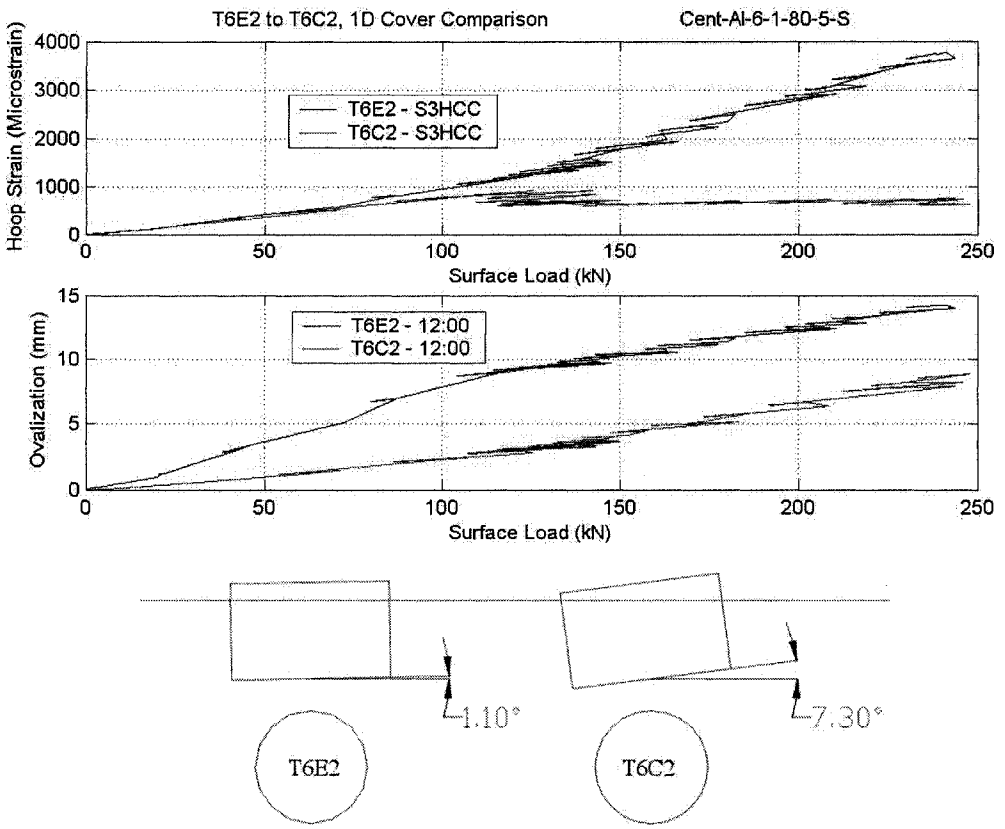

Figure 3-32: Repeated Test Comparison, Tilting Effect

4.0, Surface Loading of Steel Pipes at Full-Scale

4.1 Test Design

4.1.1 Overview

Phase II of the surface loading program at C-CORE consisted of a series of full-scale and reduced scale centrifuge tests on buried steel pipe sections (C-CORE, 2003b). The investigated parameters, physical test conditions, and experimental procedure were selected, where feasible, to enable a consistent and fair comparison between the full-scale prototype to centrifuge model. This chapter will detail the full-scale tests on the un-pressurized steel pipes and Chapter 5 will detail the centrifuge program that complemented these full-scale tests.

The full-scale experiments consisted of three surface loading tests on the same pipe section, a 16" outside diameter (406mm) steel pipe, at three burial depths. Cover depths were 0.5D, 1.0D and 1.5D, where D is the pipe outside diameter. The soil beds were prepared with 1D sand bedding for each test. The surface load was applied to the soil surface using a circular load pad instrumented with a load cell and displacement transducers. The pipes were instrumented to measure hoop and longitudinal strain and pipe ovalization. A summary of the tests carried out are shown in Table 4.1.

4.1.2 Pipe Model and Instrumentation

For these tests a 16" outside diameter (406mm) steel pipe with a wall thickness of 0.375" (9.53mm) was used. With a D/t ratio of 42.7 and a length of 4.648m (183") this pipe section is comparable to the model pipe sections used for the tests described in Chapter 5. The pipe material was steel A106B with a factory specified yield strength of 240MPa (35ksi) and tensile strength of 414MPa (60ksi). The yield strength of the pipe was determined by carrying out tension testing of pipe specimens in the Materials Testing Lab of Memorial University of Newfoundland. The equipment and methods used to carry out these tests and the analysis methods were the same as for the tests in section 3.1.2. Stress strain plots from these tests can be seen in Figure 4.1. The yield strength and modulus of elasticity were experimentally determined to be 345 MPa (50ksi) and 225 GPa (32,600ksi) respectively. A summary of the pipe characteristics and test conditions are shown in Table 4.2.

The pipe was positioned in the center of the test tank giving a distance from the pipe to the tank side walls of 1.288m and to the tank end walls was 0.81m. This distance of 1.288m or 3.2D is sufficient to assume the tank walls had no influence on the loading. The same section of 16" pipe was tested at three burial depths. Figure 4.2 shows a schematic of the pipe positioned in the test tank

Instrumentation for this test program included external strain gages (axial and hoop), pipe ovalization (displacement measuring laser transducers), load pad penetration and surface

load. The full-scale pipe was instrumented with 14 external strain gauge bridges and 4 ovalization (diametral displacement) laser transducers. Strain gage layouts can be seen in Figure 4.3. Hoop and axial strain measurements were accomplished with the use of ten uniaxial and two biaxial strain gauges. For this measurement ¼ Wheatstone bridge layouts are used with bridge completion taking place on an external circuit board. Strain measurements are taken at the pipe mid-length (point of loading) and at 256 mm (10.1") from the longitudinal midpoint. The biaxial strain gauges were used at the pipe centerline at the crown and invert to allow both hoop and axial strains to be measured at this same location. Shunt calibrations were carried out on each of the gages using a 120kΩ resistor simulating 500 microstrain and a 60kΩ resistor simulating 1000 microstrain. The strain gage was shunted directly at the gage location. The shunt calibrations were on average 7.5% difference from the theoretical strain gage calibrations. The shunt calibrations varied from their average by a maximum of 2.5%. Figure 4.4 shows the loading frame with the instrumented pipe in place in the tank before being backfilled.

Displacement laser transducers were used for ovalization or diametrical deflection measurement. Figure 4.5 shows a schematic of the laser / ovalization transducer layout. The four lasers were mounted on a carriage that was capable of traveling along a central mandrel inside the 16" pipe. The lasers were mounted on the carriage, to give 12:00, 3:00, 6:00 and 9:00 measurements to the pipe. The carriage on its mandrel can be seen in schematic form in Figure 4.6 and in a photograph in Figure 4.7. The carriage was

manufactured of 5" aluminum square tubing, fitted with rollers, two cable attachment points and a displacement potentiometer attachment point. A laser was mounted on each of the four faces of the carriage measuring distance from the carriage to the inside wall of the pipe. A string potentiometer was mounted on the mandrel, with the string attached to the carriage, tracking the carriage location in the pipe. The carriage via the rollers could ride along the mandrel, a section of 4" aluminum square tubing. The carriage was also guided by ball bearings on the side and bottom interfaces between it and the mandrel. These ball bearings forced the carriage to ride a straight and consistent path on the mandrel. The tubing was chosen so as to be stiff enough to carry the load of the carriage and minimize deflection along its 4.6m length. The mandrel was supported at each pipe end by plywood end caps fitted with o-rings, Figure 4.8. During pipe loading the carriage was positioned at the center of the pipe and periodically traversed along the mandrel to measure pipe ovalization each side of the pipe longitudinal center line. Moving of the laser carriage was accomplished by using a hand crank and pulley system, as depicted in Figure 4.6 and pictured in Figure 4.9. Pulleys 1, 2 and 4 carried a 1/8" diameter stainless steel cable wound around a hand crank drum. Turning the hand crank either clockwise or counterclockwise allowed the carriage to be moved in either of two directions along the mandrel. Pulley 3 was used to "pay out" and "pay in" the laser transducer cables as the carriage moved along the mandrel. As shown in Figure 4.10 a plastic pipe on the outside of the end cap housed three of the pulleys and incorporated two snorkels that passed the cables to the sand surface.

The applied load and vertical displacement of the loading plate was measured with a load cell and three string potentiometers respectively. To prevent moment and side loading of the assembly, the load cell had a rounded tip that acted as a ball bearing. In Figure 4.11 the load pad with load cell and string pots are shown positioned under the load frame on a test bed.

4.1.3 Test Facility

Full-scale Testing was carried out in the C-CORE full-scale test facility which was described in section 1.3.2. The existing facility underwent a refit to accommodate the surface loading program. The overhead gantry and crane used to move heavy loads in the facility was moved to provide space for the new load frame. Existing machine screw actuators were assembled with a new load frame to accomplish the loading of the pipe. A photograph in Figure 4.4 and a schematic in Figure 4.12 show the test tank with the load frame situated above the unburied pipe and the filled test tank with a partially embedded load pad under the load frame. Other miscellaneous components used in the program included a load cell and string pots to measure the pad load and movement, laser transducers and strain gages used to measure the pipe response, signal condition boxes and mobile data acquisition system.

4.1.4 Load Frame Design

A load frame was designed and constructed to apply a surface load to the sand surface above the pipe using two existing machine screw actuators. Figure 4.12 and Figure 4.13

show schematics of the loading frame on which the various parts of the frame can be seen and identified by their labels. The actuators, Figure 4.14, consisted of a Duff Norton worm gear capable of 6" (152mm) of stroke, driven by a Bauer gear motor powered from A Wood's E-TRAC AC inverter. The stationary sides of these actuators were bolted to two steel I-beams, the main beams, which spanned the test tank. The 12"X6" steel I-beams have a flange thickness of 0.44" and a web thickness of 0.26". The ends of the main beams were bolted to the concrete floor via four I beam legs. The moving ends of the two machine screw actuators were attached to the ends of another I-Beam, the loading beam, and driving the actuators simultaneously moved the loading beam downward, into the test tank. Bolted to the bottom center of the loading beam was an Intertechnology load cell, model number CSP1-D3-100K-3CP5, rated to 100,000lb. This load cell's rounded end was used to apply load to the load pad, placing a point load on the pad and preventing any moments from being transfer into the load frame. The loading frame was positioned over the tank such that this load cell transferred the load from the actuators into the center of a load pad. A 22.6" diameter steel load pad was placed on the sand surface above the longitudinal and transverse line of symmetry of the buried pipe. Figure 4.11 is a photograph of the load pad during Test 1.

Locations of the actuators on the main beams and the length of the loading beam were determined so as to minimize the stresses and deflections in the three beams. Bending stresses and deflections were calculated as detailed in Appendix B, Load Frame Calculations. Calculations showed that maximum stresses of 80 and 85 MPa would

occur in the main beams and loading beams respectively when a load of 222kN was applied to the sand. These stresses were within the yield limits of the steel beams. Stress calculations were also carried out on all bolted connections, as also detailed in the Appendix B. Imperial Grade 8 bolts, ½" and ¾" diameter, were used to bolt the actuators to the beams and beams to legs. Stress calculations for the tensile load in these blots and in the I-beam flange showed stresses within acceptable limits.

Red Head, HSLG-N 20/60, concrete anchors were used to fasten the frame legs to the concrete floor. These fasteners were rated to 7310 lbs, or 32.5kN working load and to 113kN ultimate load in 4000psi (27MPa) concrete. Calculations showed that during a surface load test each leg could be subjected to 55.6 KN. Initially the frame was tested with one anchor per leg, assuming the anchor would be sufficient considering the ultimate load rating was two times the design load. During this proof testing one of the anchors loosened. For the second proof test a second anchor was added to each leg. Two anchors in each leg effectively secured the frame for full-test loads. Appendix B contains calculations carried out for these anchors and for the concrete floor.

The maximum full-scale load that could be applied using this load frame was 50,000 lbs, corresponding to the maximum load of the preexisting actuators. To obtain the maximum load rating from the actuators the inverters were programmed to run the motors at a translation rate of 10mm/hour.

4.1.5 Geotechnical Conditions

Alwhite medium-fine sand (#00), a readily available manufactured siliceous material with consistent properties, was used in the full-scale program. Full-scale density measurements were accomplished using density pans that were excavated after preparing each 4" sand lift. Density data was also collected post-test using the water replacement method for sand density measurement. Test bed preparation and density measurement are described in detail in section 4.2. A summary of the full-scale density data is presented in Table 4.3. The average sand density found using the water replacement method was approximately 1% higher than the densities found from the density pans. Densities in the three tests varied by less than 1% from an overall average of 1554 kg/m^3, or a relative density of 82.2%.

4.2 Test Procedure

The test bed was prepared by first shoveling the sand from storage bags into an aluminum hopper. The filled hopper was raised over the tank wall and into the tank by an overhead crane. Then sand was then dumped into the tank until a 4" (101.4mm) layer was formed over the tank plan area. The sand was raked level and if needed, more sand was added for the layer. A 4' x 8' sheet of ¾" plywood was then placed on the sand bed and a vibrating tamper, Vibco Patchman PM-1012, was used to densify the layer. Four passes were made over the plywood surface with the vibrating tamper, ensuring that the whole surface was passed over completely and uniformly. The plywood would then be moved throughout the test bed until the entire surface was uniformly tamped. This procedure

was repeated for each layer until the test bed depth was achieved. This preparation method was practiced prior to test bed preparation in a smaller test tank. The dimensions of this smaller tank were precisely taken, masses of sand used were recorded and densities calculated to insure that this tamping method would result in the desired relative density.

After placing the initial bedding layer of 16" (406.4mm)(1 pipe diameter) a further 4" layer was placed in the tank and a trench, as seen in Figure 4.15, in the shape of the pipe was formed for placement of the instrumented pipe. The pipe was then positioned in the tank in such a location that the load frame could be correctly positioned above it. The soil preparation procedure was repeated covering the pipe and achieving the desired cover depth. The filled tank is shown in Figure 4.11. During test-bed preparation density pans were placed throughout the test bed. After completion of the test the density pans were excavated and weighed to allow calculation of the soil density.

Densities were also checked post-test using the water replacement method. A flat level area of dimension of approximately 0.6m x 0.6m was vacuumed on the soil surface. A vacuum equipped with a vacuum trap (to hold any sand collected by the vacuum) was used to vacuum a conical shaped hole in the middle of this area. Collecting the sand in the trap allowed the mass of the sand in this area to be determined. A thin plastic sheet was then placed in the hole and water was poured into the hole until it was level with the top of the hole. Care was taken not to disturb the shape of the cone and to add a volume

of water that matched the volume of sand removed. Using the mass of this water and the mass of sand removed the soil density for that cone was calculated. Approximately twenty of these measurements were taken in each test bed at varying elevations to find an average test bed density. The densities calculated with this method agree with the densities calculated from the density pans, as shown in Table 4.3. Photographs showing the water replacement method of density measurement are shown in Figures 4.16 to 4.19.

With the instrumented pipe buried to the desired cover depth the data acquisition system was connected to the pipe and the load pad and the load frame were placed above the pipe. The loading mechanism was a displacement-controlled system capable of 10mm/hour. Test ending criteria was either when it was deemed that appreciable data was collected for a fair comparison to centrifuge tests or when the load pad had tilted to such a degree that the loading system could no longer function. Loading of the pipe took place over several hours or days during which data was collected from strain gages, load pad string potentiometers, laser ovalization sensors and the load cell. The carriage was periodically (approximately once every hour) traversed along the mandrel to measure ovalization along the pipe length at increasing pad penetration depths and loads (one profiling session taking three to four minutes). When it was not being traversed along the mandrel the carriage was parked at the pipe centerline. For Test 1 and 2 the carriage covered a length of ~ 0.9m each side of the pipe center and in Test 3 it traversed 0.6m to one side of center and 1.2m to the other. For Test 3 the laser transducer at 9:00 malfunctioned and data could not be collected.

Penetrating into the sand with a pinned load pad without tilting was difficult in all three tests. This was initially caused by the manner in which the loading actuators were aligned. With realignment of the actuators, vertical loading could be achieved. Perfect alignment of actuators, beams, anchor legs, pipe and sand surface at a large scale is difficult and near impossible. Preparing a sand bed such that the sand below a load pad is of a consistent density is also near impossible. These two factors are why loading the pipe without tilting could not be achieved. The data will show several loading and unloading lines where modifications were made to the actuators to reduce tilting of the pad. Some reloading lines were also carried out to evaluate the elastic behavior of the pipe soil system.

4.3 Test Results and Discussion

4.3.1 Overview

In this section results from three full-scale surface loading tests carried out will be described. All three full-scale tests used 16" steel pipes with a D/t = 42.67. The three pipes were buried in sand with an average relative density of 82%. Tests 1 to 3 had soil cover of 1.0D, 1.5D and 0.5D, respectively. The three full-scale tests carried out are detailed in Table 4.1. Pipe ovalization from the laser displacement transducers and axial and hoop strains from strain gages were measured with increasing surface loads. The data collected was processed and presented in graphical form using MATLAB. Data will

be presented that was collected from strain gages and lasers, during pipe loading with the laser carriage parked at the center of the pipe longitudinal centerline. Also plots of ovalization versus position on the mandrel are presented from test runs of the laser carriage along the pipe longitudinal centerline. These carriage runs took place approximately once per hour during pipe loading at increasing load pad loads and penetrations. All data are filtered to reduce signal errors.

As in Chapters 3 strain gradients and ovalization gradients were calculated for each of the transducers. While there is a nonlinear nature to the pipe response to load these gradients aid in data comparison Any nonlinearity to the data is not severe enough to make the observations invalid. Approximate lines are fitted to data to obtain the gradients of strains and ovalization, microstrain/kN and mm/N X 10^{-1}.

Locations of strain gages and lasers are shown in Figure 4.3 and Figure 4.5. In the figures to follow the strain gages and ovalization sensors are identified in the plot legend by two codes. The first code is T# #D, which indicates the test of a particular number corresponding to table 4.1, followed by the burial depth (D). The second code is S#, indicating the strain gage number, followed by either a H or an A indicating either a hoop or axial gage, 12:00, 3:00, 6:00 or 9:00 indicating the location of the gage circumferentially on the pipe, and finally either an O or a C indicating the gage is either on the longitudinal center line (C) or off the centerline (O) The ovalization sensors are

indicated simply with the test number, cover depth and either a 12:00 for crown or a 3:00 for haunch.

4.3.2 Load Pad Penetration

For each test plots of surface load versus load pad penetration are shown in Figures 4.20, 4.21 and 4.22. In these plots the load pad penetration is an average of the three pad displacement transducers. Unloading cycles occurred during the tests for different reasons including adjustment of load pad rotation and adjustment of testing facilities. The plots initially show a steady increase of load with penetration, then the surface load remains constant while load pad penetration increases because of the soil failure beneath the pad (when the load reaches the bearing capacity of the pad). In all tests but particularly evident in Test 2 after several unloading cycles and considerable pad penetration, the maximum load slightly increases. This may have happened due to presence of the underlying pipe and position of load pad after penetration into the soil.

Figures 4.23, 4.24 and 4.25 show surface load versus load pad penetration and load pad penetration versus load pad rotation for each of the full-scale tests. In these surface load versus load pad penetration plots each of the displacement transducers are each plotted against load showing how the pad penetrated at an angle. These three displacement transducers were attached to the load pad in a triangular pattern so as to capture any rotation of the pad. The second in each pair of plots, is the load pad penetration versus load pad rotation. The rotations are the angles calculated between each of the points of

penetration measurement on the pad. For example Plane 1-2 is the rotation of a line drawn between displacement transducers (string pots) 1 and 2. The experimental setup was designed to vertically load the pad, however, the load pad rotated during increased pad penetration due to some asymmetric elements in both the load frame and the soil response. To minimize the effects of the load pad rotation on the experimental results, the loading was stopped several times during each test to adjust the actuator to help correct the rotation of the load pad. This correction was done by modifying the actuator position and it did not disturb the pad or the soil sample. A photograph showing the pad rotation can be seen in Figure 4.26. In tests 1, 2 and 3 the load pad rotation maximums were 3.5°, 2.5° and 2.5° respectively. This rotation does not affect the experimental results.

4.3.3 Transducer Response to Surface Load

The transducer response to surface load includes the response of the laser transducers (ovalization) and the strain gages (hoop and axial) to the load applied to the surface of the pipe. Figure 4.27, shows two typical strain versus surface load plots. These plots contain data from the three full-scale tests, each at a different cover depth, showing the decrease in strain with an increase in cover depth. Similar plots showing the same soil cover effect for the other transducers, strain gages and displacement lasers, can be found Appendix C. This Appendix includes two sets of plots one set that only shows the initial loading line for the test and a second set of plots that show all the loading lines or cycles within one test. The plots showing the initial loading line are shown to more visually demonstrate

the strain reduction with cover. In the second set of plots the cycle lines tend to be offset from each other, have the same gradient, and show the elastic behavior of the pipe. These lines, hysteresis loops, also show the plastic accumulation of stress in the soil, exerting stress on the pipe after the surface load is removed.

Figures 4.28, 4.29, 4.30 and 4.31 show gradients of hoop strains, axial strains and ovalizations for the three tests. These plots confirm the decrease in transducer response with increasing cover and also serve to demonstrate some of the other observations mentioned below. The two main modes of pipe deformation identified in these full-scale tests were ovalization of the pipe cross-section and bending in the long section. These two modes are associated with the hoop strain and axial strain response. The ovalization mode was not associated with an elliptical pipe shape. The pipe crown deflected significantly inward with small outward deformation of the pipe haunches and very little change in the invert. For the largest cover, 1.5D, the deformation of the pipe invert and haunches were considerable relative to that of pipe crown. However, the deformation mode was not elliptical. The crown deformation was confirmed by both the crown hoop strain gauges and laser readings. The crown and haunch deformations decreased with increasing cover.

Compressive axial strain was recorded both in Sections A & B at the crown. As expected these compressive strains decreased with increasing cover depth. Small tensile axial strains were recorded at the invert and changed little with cover. These axial strains

result from the bending strains and the Poisson's effect associated with the pipe crown and invert compressive hoop strains. The hoop strains decrease with an increase of cover depth. Hoop strains are negative (compression) at crown and invert and positive (tension) at haunches. Hoop strains at the crown are significantly larger particularly in Section B, the mid section of the pipe.

4.3.4 Ovalization along the Pipe Length

Ovalization along the pipe length was measured by the translation of the laser carriage along the mandrel. In each test the carriage was translated along a portion of the mandrel at increasing loads and displacements. Reported here are only carriage ovalization data from one load for each test (approximately the maximum test load).

The elastic nature of the pipe response can be seen in Figure 4.32. This is a plot of laser readings along the mandrel before the test began subtracted from the laser readings along the mandrel after test completion versus laser carriage location for Test 1. It implies that that the pipe permanently ovalized up to 0.2mm. But the laser transducer has a resolution of 0.06mm and a linearity error of 0.2mm meaning the pre and post test readings are essentially equal and the pipe has not deformed.

Figure 4.33 show traces of pipe ovalization versus carriage location for the laser carriage run at the maximum load applied in Test 1. Similar plots are included in the Appendix

for the Tests 2 and 3. The spikes in the data for the 6:00 laser are index markers (steel blocks) placed inside the pipe that are being recognized by the laser transducer.

The mid section (Section B in Figure 4.3) of the pipe is not exactly located in the middle of the plot due to positioning of the laser carriage pulleys. The symmetric behavior of the pipe to surface load can be seen in the plot with the maximum ovalization occurring at about the 950mm location on the mandrel corresponding the center of the load pad. The ovalization in the pipe tends to diminish toward the sides. As with the centerline measurements the dominant deformation occurred at the crown and ovalization values are relatively small in other directions. For Test 3 the laser transducer located at 9:00, L4 failed and no data could be recorded. Also for Test 3, data was artificially shifted to place the pipe centerline in line with the centerline in tests 1 and 2 to aid in making comparisons.

Table 4-1: Test List

Test	Cover Depth	Bedding Depth	Load Pad Geometry
Full-Scale 01 (pipe A)	1.0D	1.0D	Circular
Full-Scale 02 (pipe A)	1.5D	1.0D	Circular
Full-Scale 03 (pipe A)	0.5D	1.0D	Circular

Table 4-2: Experimental Parameters

Pipe Parameter:	Steel Pipe:
Outside Diameter	406mm (16″)
Wall Thickness	9.53mm (0.375″)
D/t Ratio	42.6
Material	A106B
Yield Strength (factory specified)	240MPa (35ksi)
Yield Strength (experimentally determined)	345MPa (50ksi)
Tensile Strength (factory specified)	414MPa (60ksi)
Modulus of Elasticity (experimentally determined)	225GPa (32,600ksi)
Soil Type	Dense Sand (80% relative density)
Load Pad Diameter	574mm (22.6″)

Table 4-3: Density Measurements of Full-Scale Test Beds

Experimental Program	Density Measurement Method	Density (kg/m^3)	% Relative Density
Full-Scale Test 1	Density Pans	1551	83.0
	Water Replacement	1563	86.3
	Global Density	1547	81.8
Full-Scale Test 2	Density Pans	1536	78.5
	Water Replacement	1550	82.5
Full-Scale Test 3	Density Pans	1553	83.5
	Water Replacement	1570	79.4

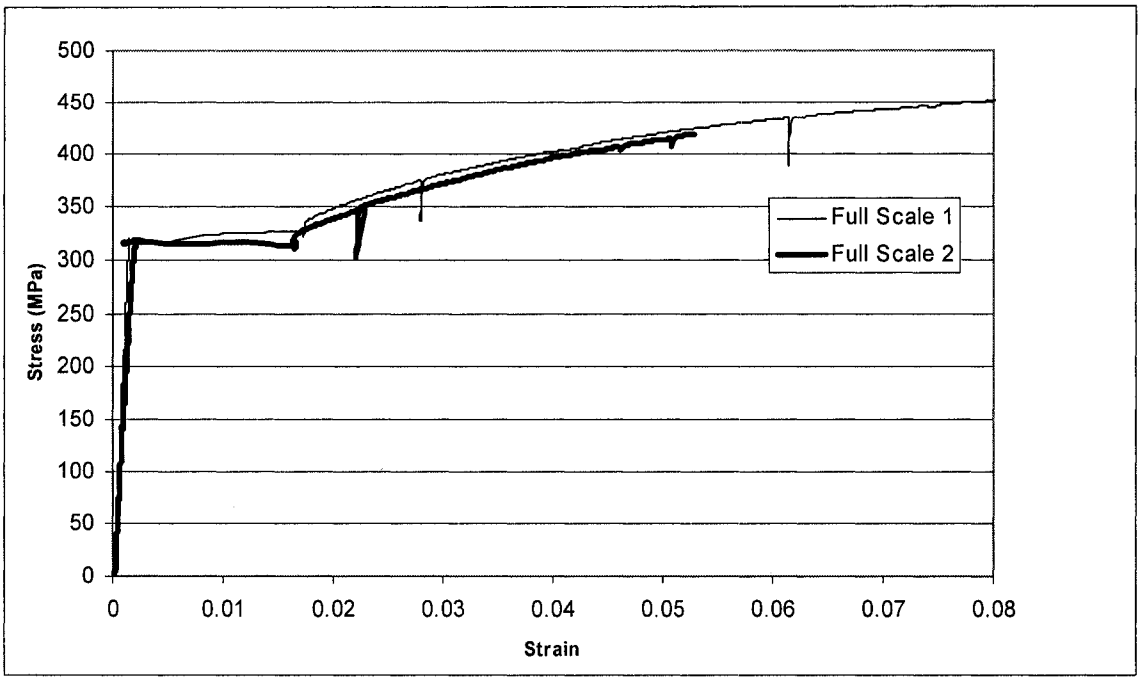

Figure 4-1: Stress Strain Plot for Steel Pipe Tensile Specimen

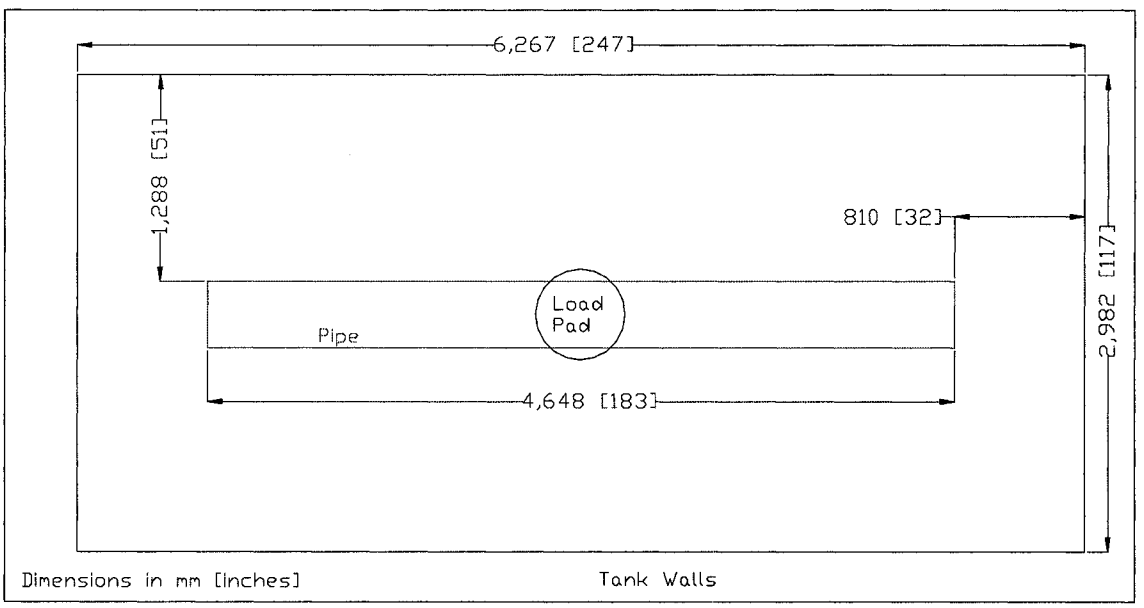

Figure 4-2: Schematic of Pipe Positioned in the Test Tank

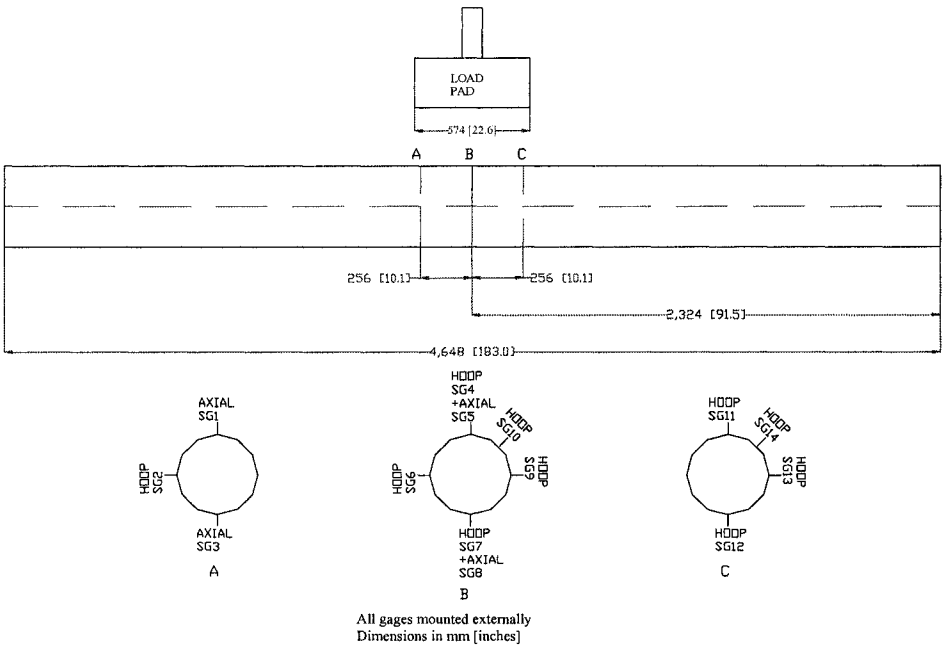

Figure 4-3: Strain Gage Layout for Full-Scale Testing

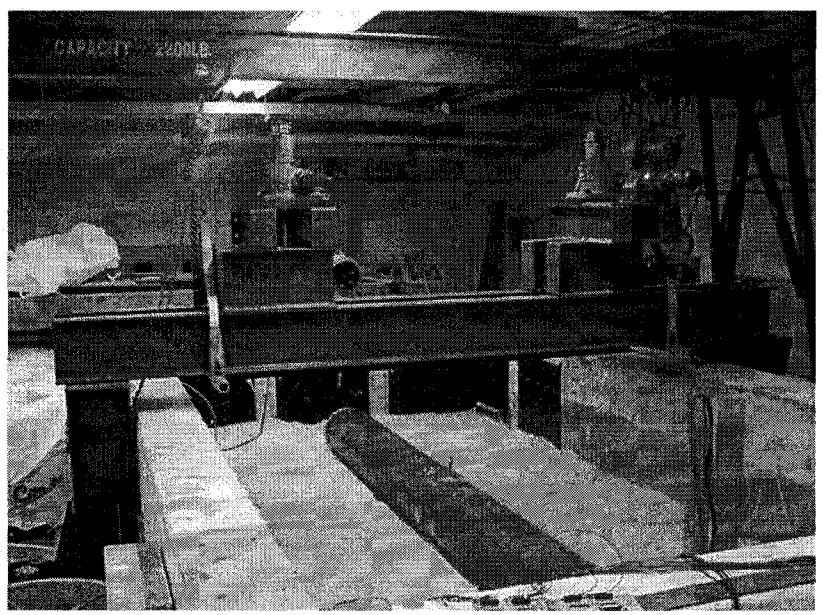

Figure 4-4: Test Tank with Pipe and Load Frame

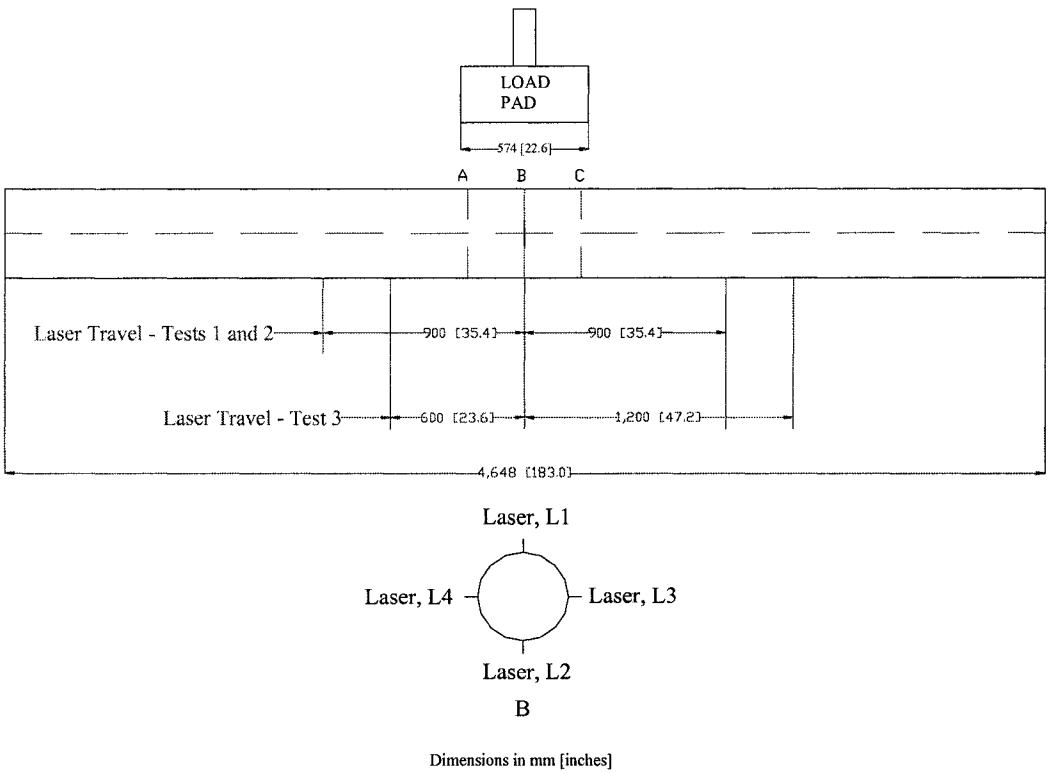

Figure 4-5: Laser / Ovalization Transducer Schematic

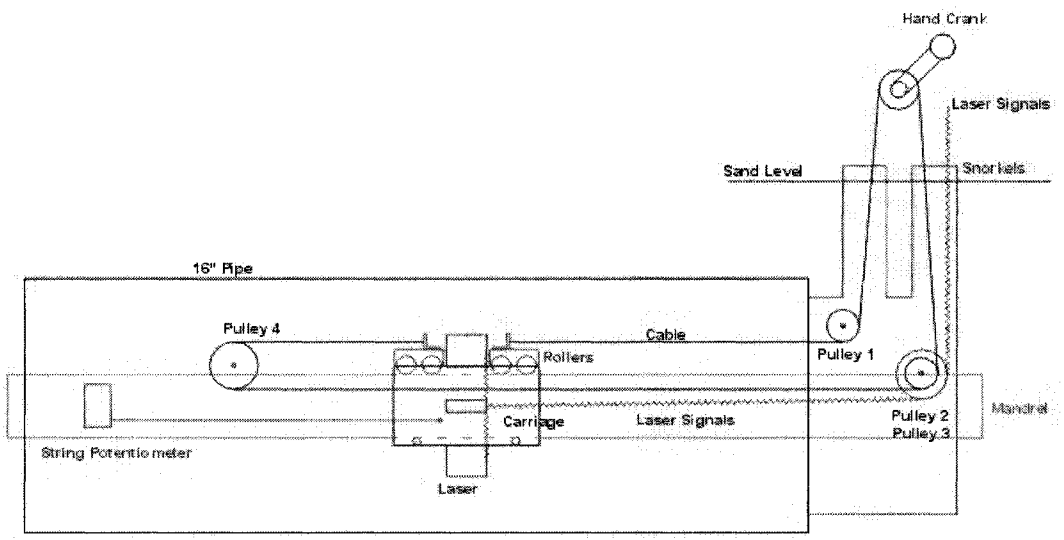

Figure 4-6: Laser Carriage Schematic

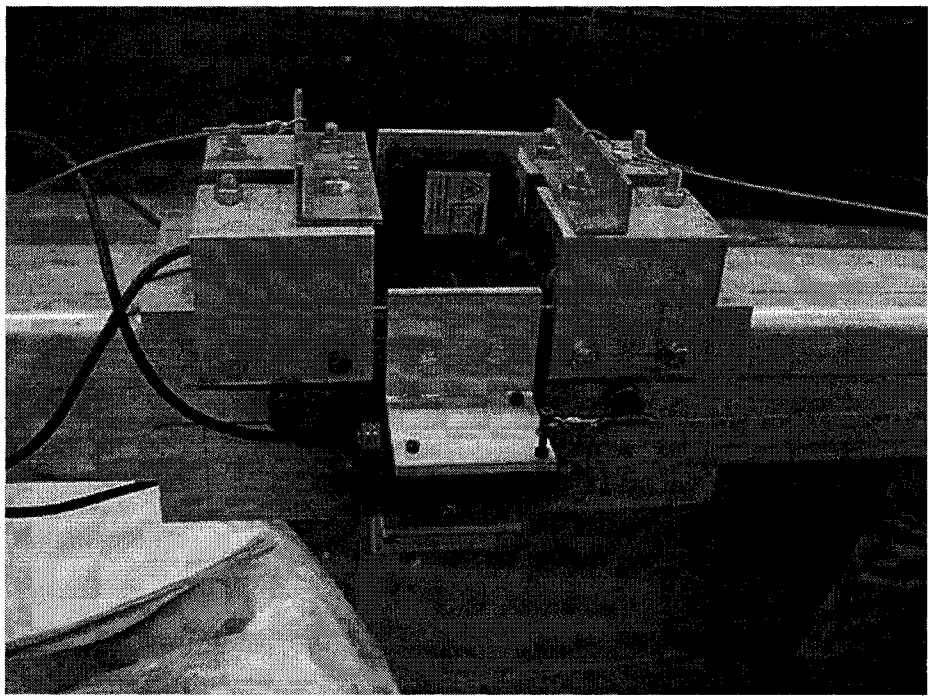

Figure 4-7: Laser Carriage for Ovalization Profiling

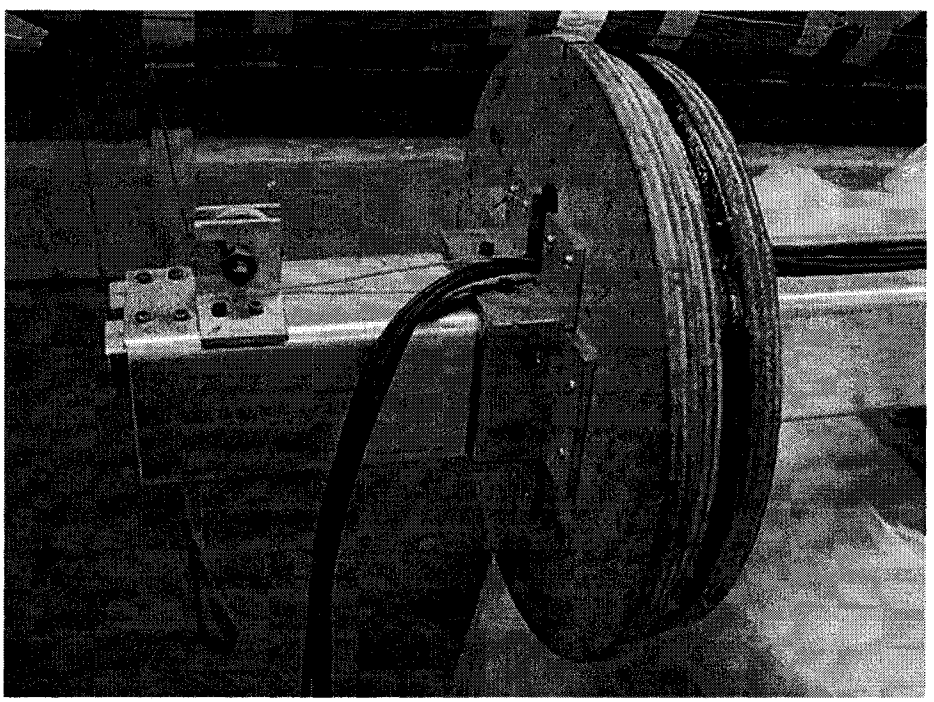

Figure 4-8: End Cap Holding Central Mandrel

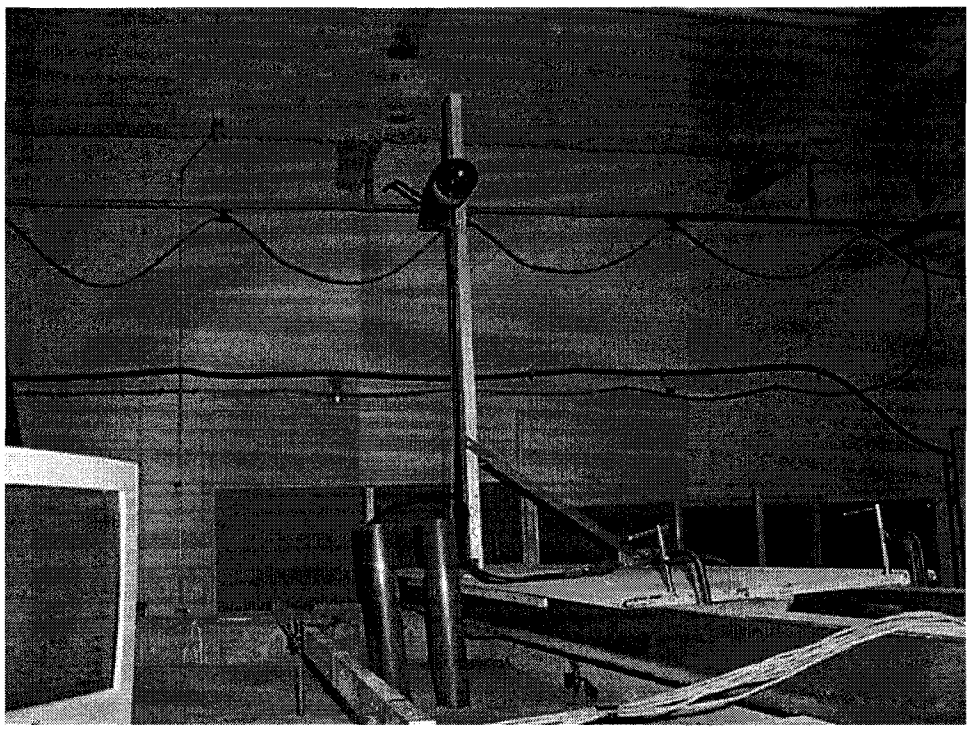

Figure 4-9: Hand Crank for Laser Carriage

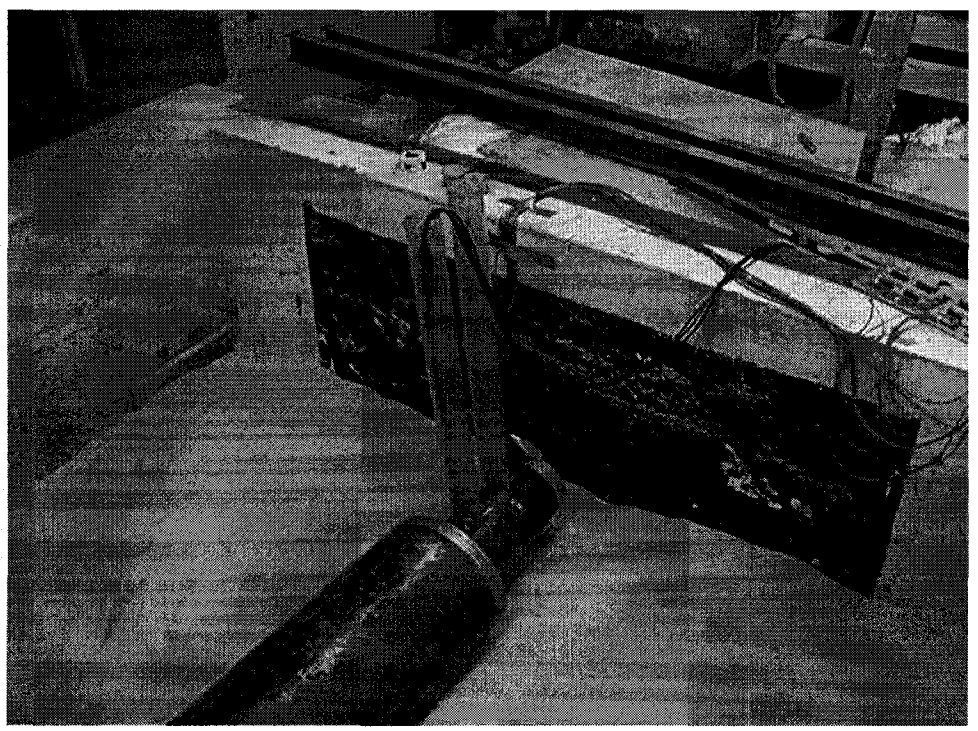

Figure 4-10: Snorkel

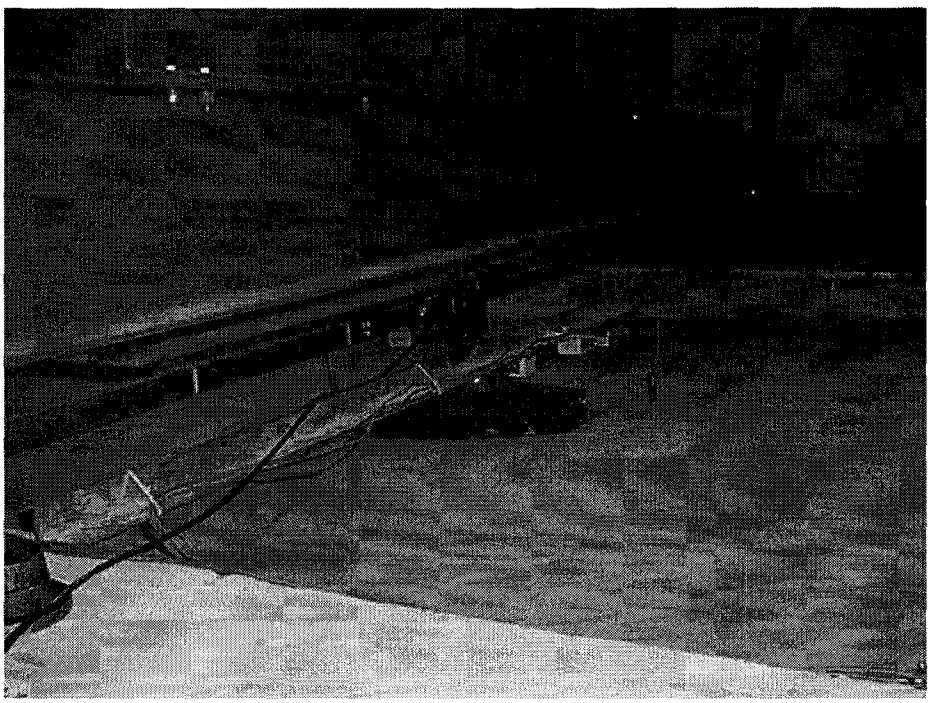

Figure 4-11: Partially Embedded Load Pad under Load Frame

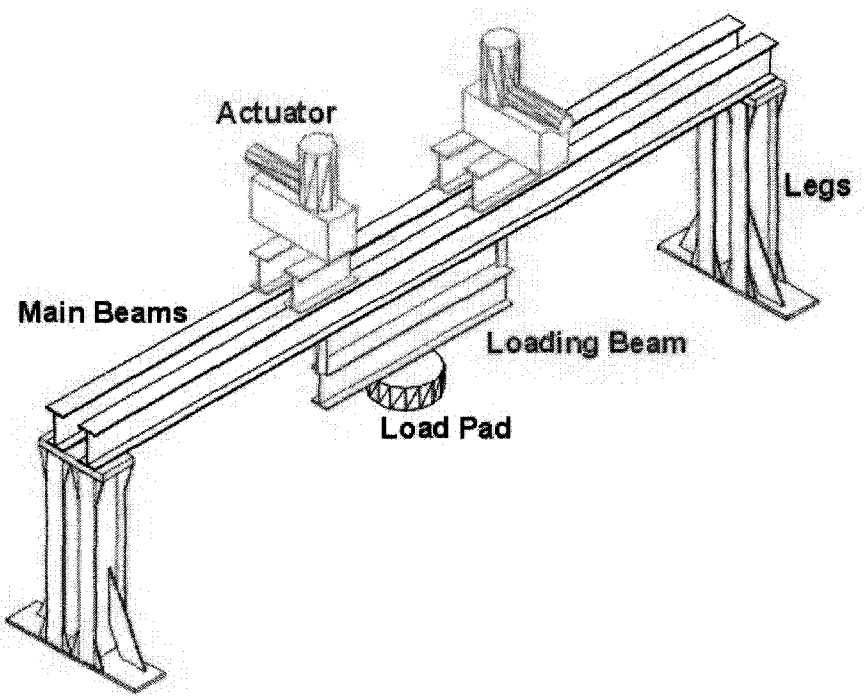

Figure 4-12: Load Frame Schematic 1

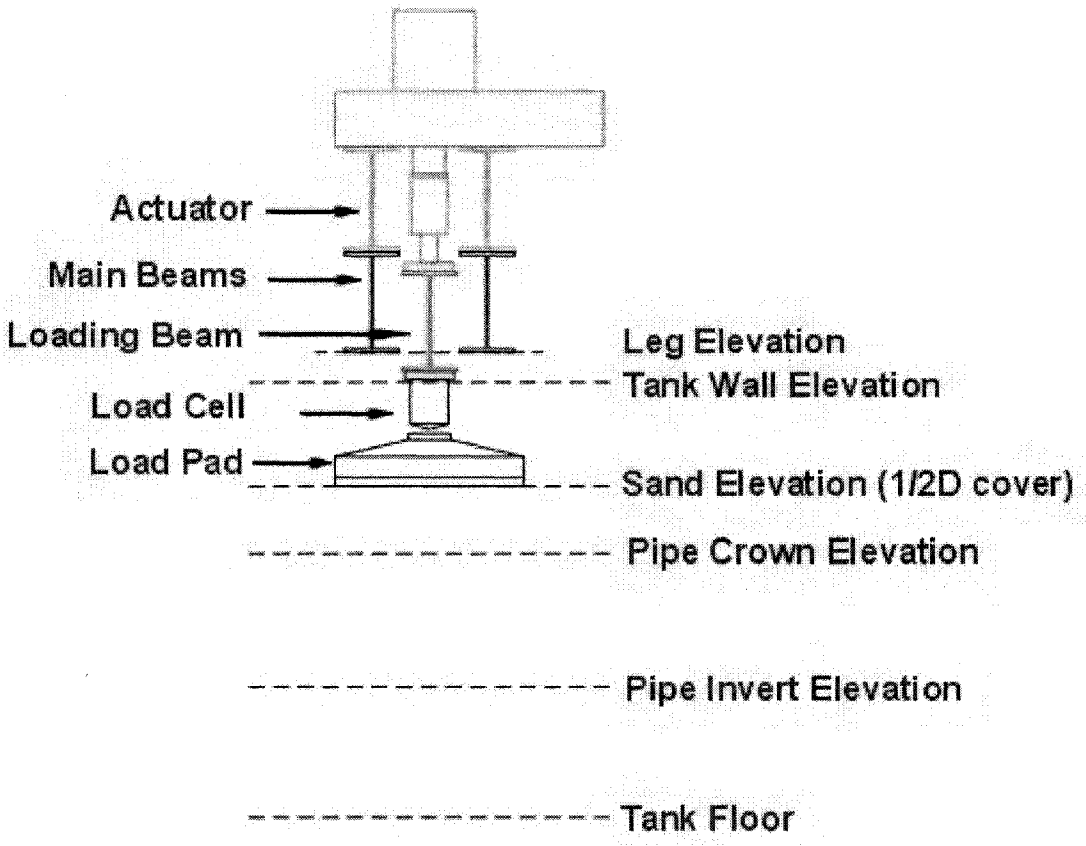

Figure 4-13: Load Frame Schematic 2

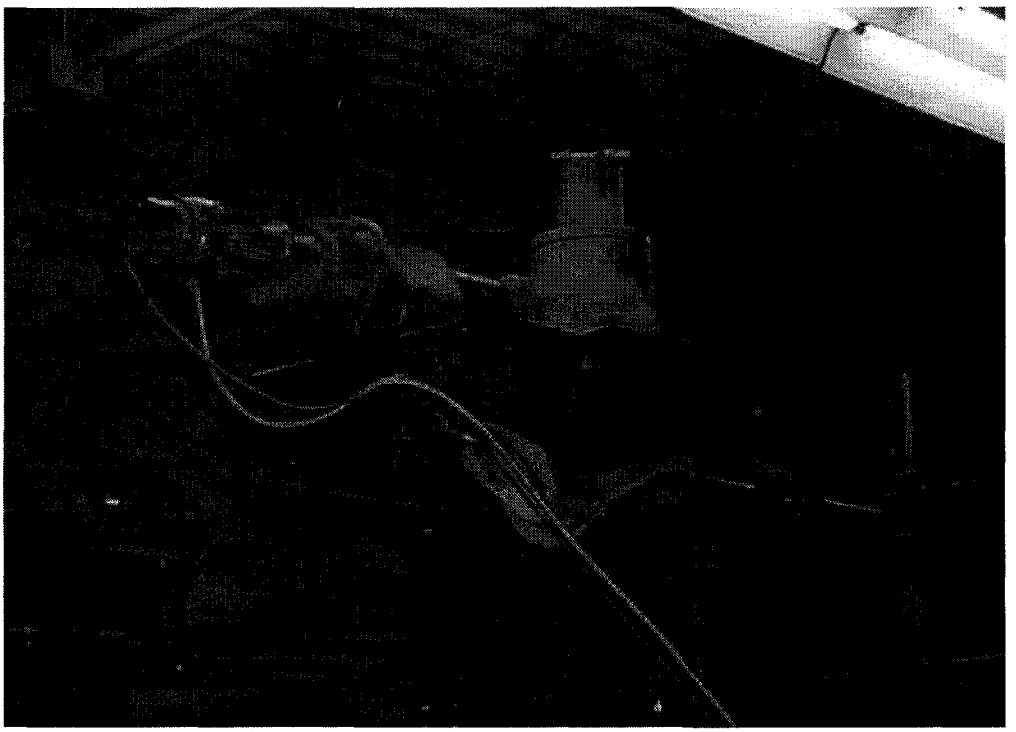

Figure 4-14: Actuator

Figure 4-15: Full-Scale Trench

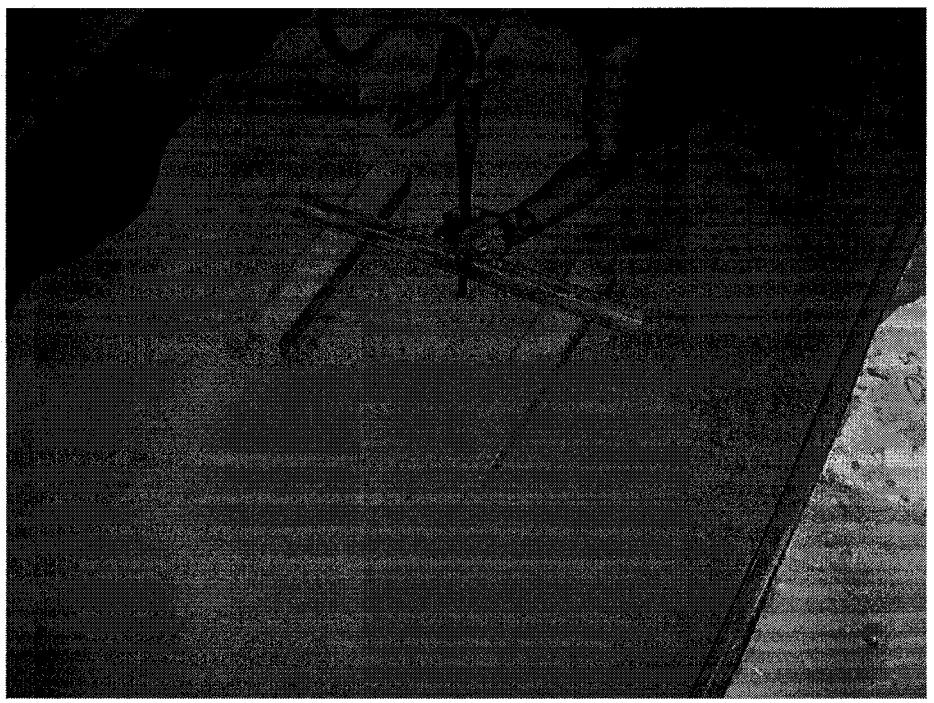

Figure 4-16: Sand Surface being Vacuumed Level for Density Measurement

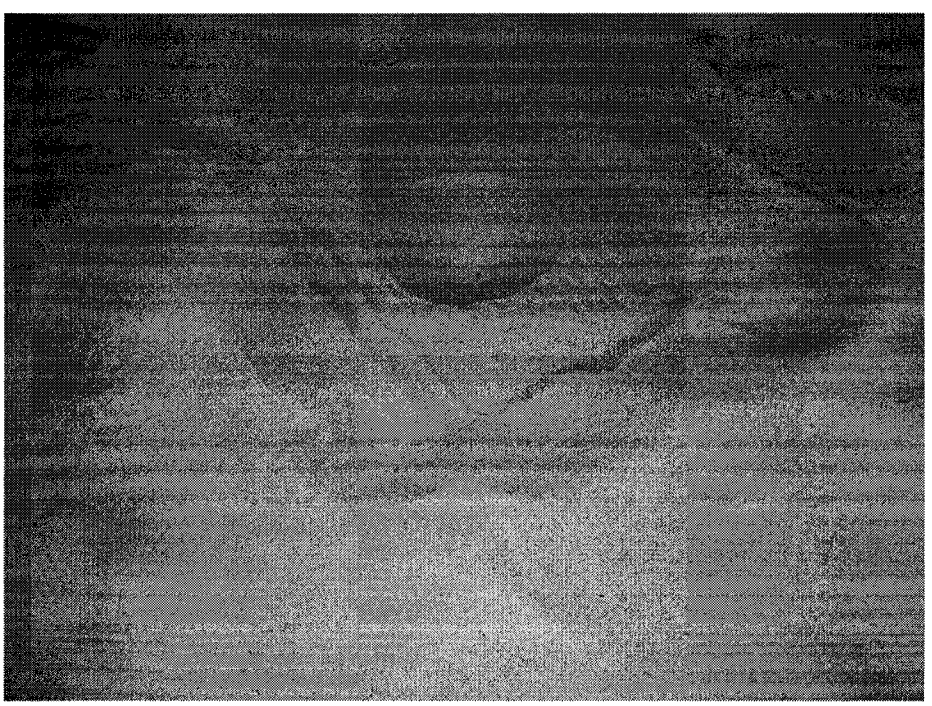

Figure 4-17: Cone Shaped Hole Vacuumed in Sand

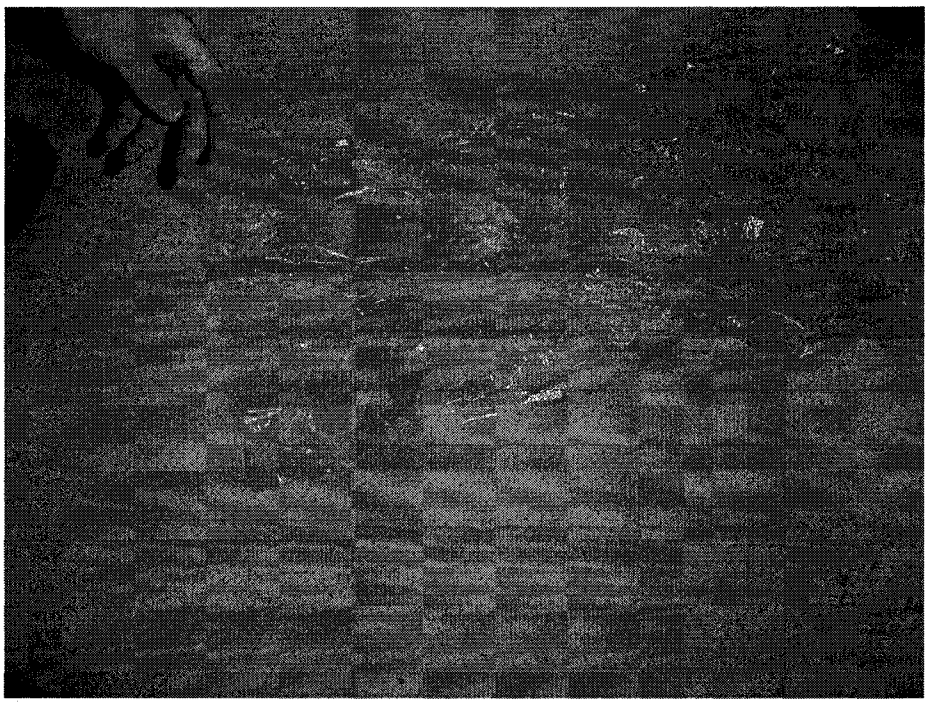

Figure 4-18: Water in Hole with Plastic Sheet

Figure 4-19: Weighing the Sand in the Vacuum Trap

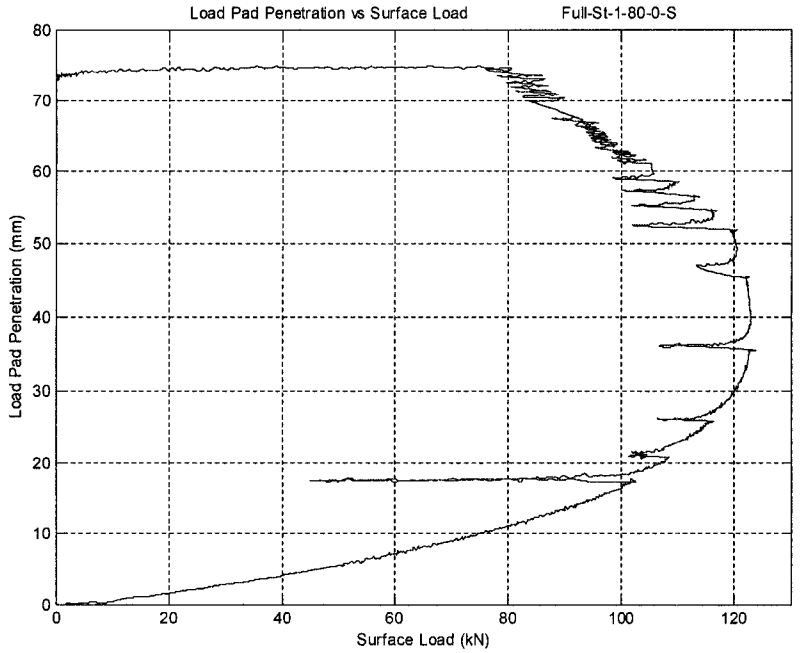

Figure 4-20: Load Pad Penetration versus Surface Load for Full-Scale Test 1

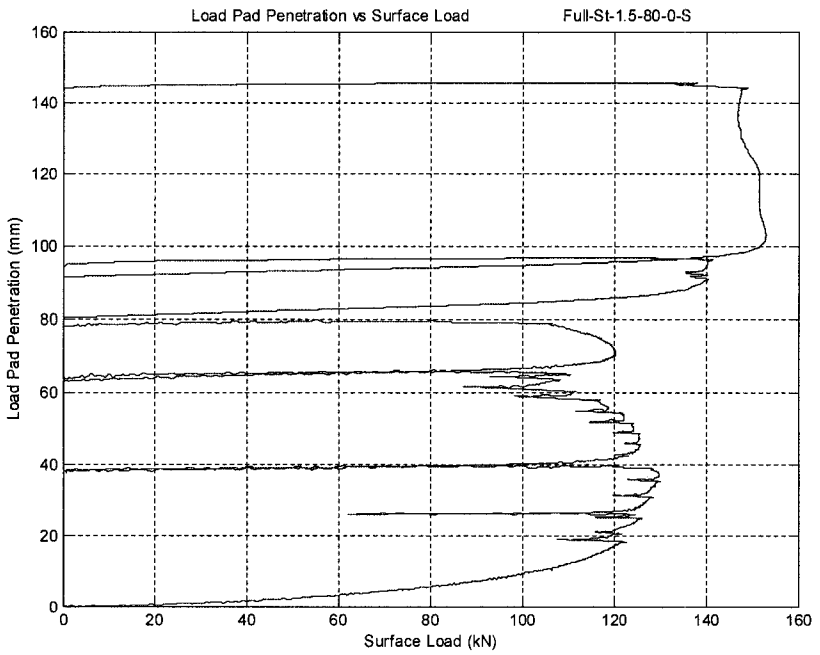

Figure 4-21: Load Pad Penetration versus Surface Load for Full-Scale Test 2

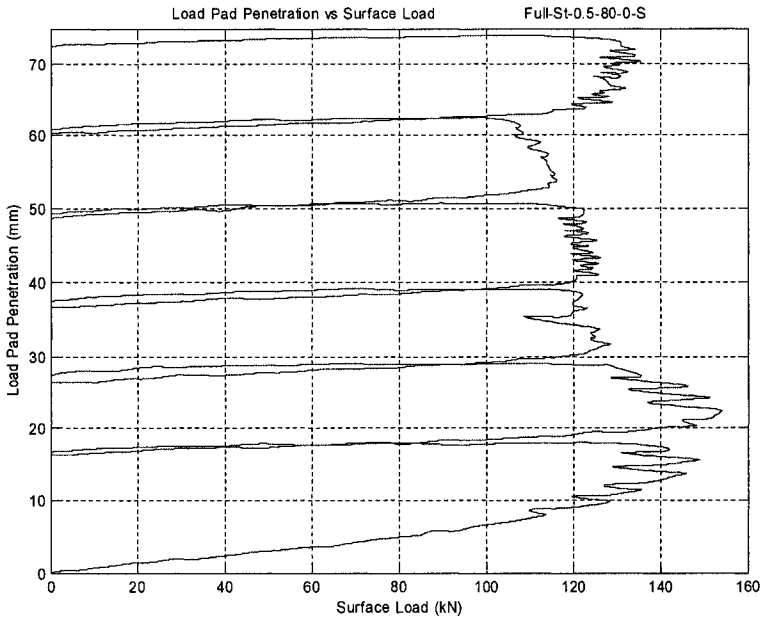

Figure 4-22: Load Pad Penetration versus Surface Load for Full-Scale Test 3

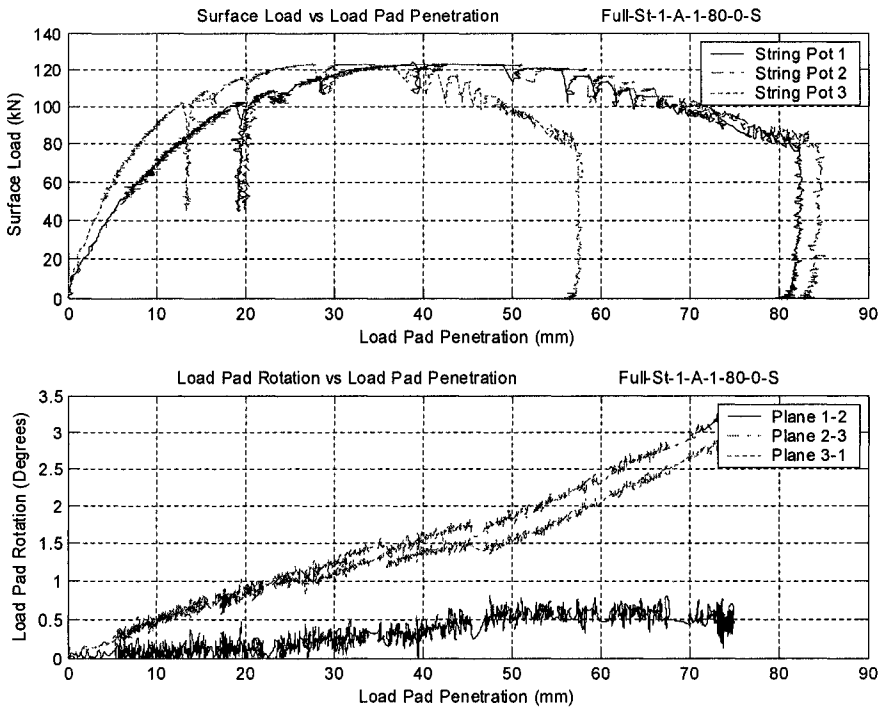

Figure 4-23: Load Pad Rotation versus Surface Load for Full-Scale Test 1

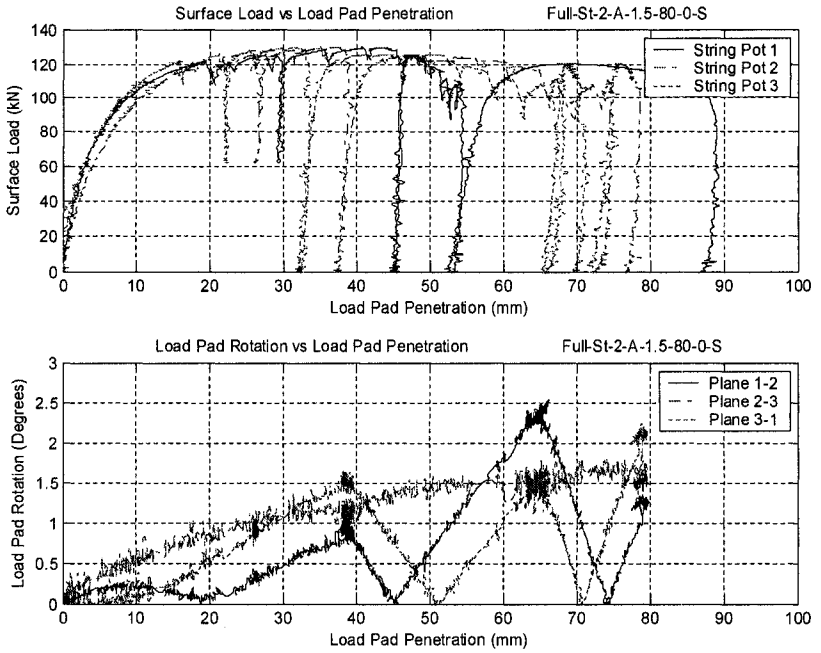

Figure 4-24: Load Pad Rotation versus Surface Load for Full-Scale Test 2

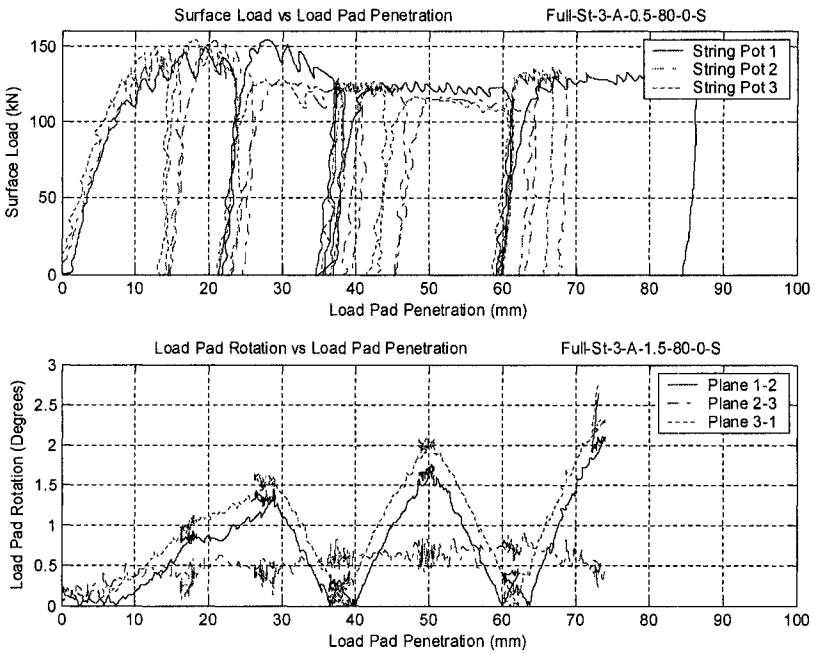

Figure 4-25: Load Pad Rotation versus Surface Load for Full-Scale Test 3

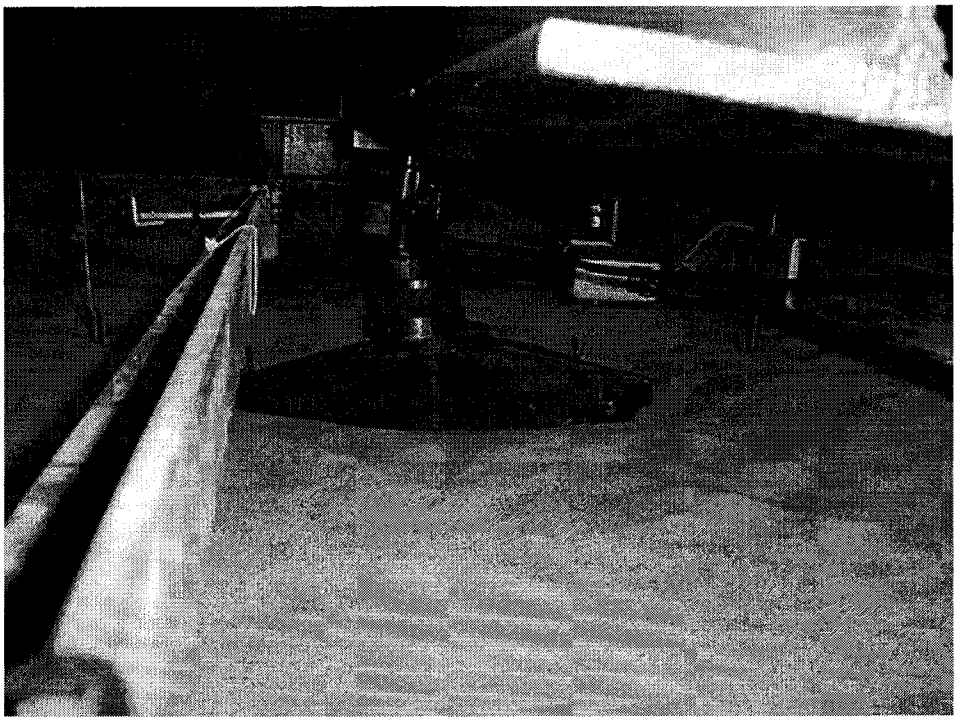

Figure 4-26: Load Pad Rotation

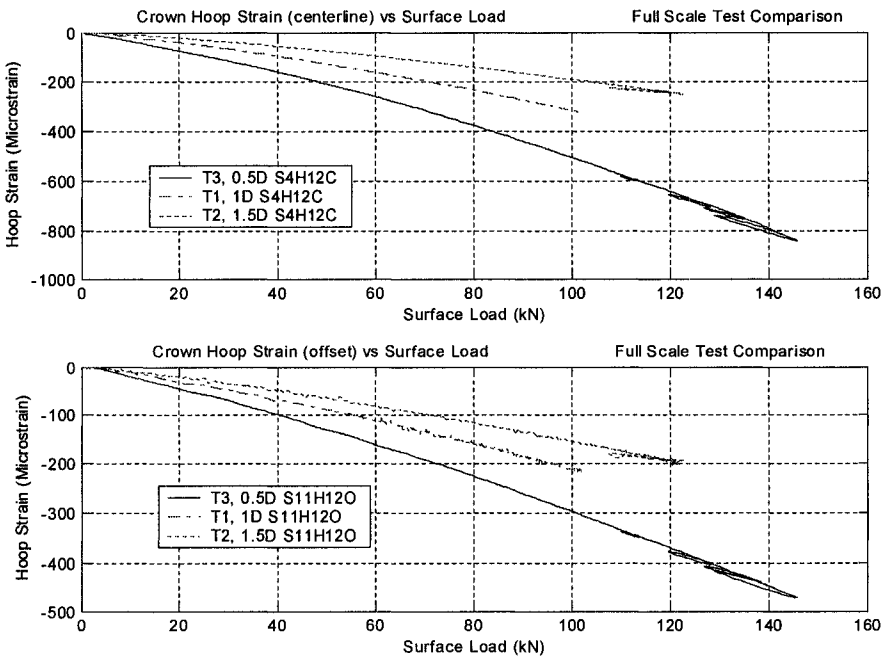

Figure 4-27: Typical Strain versus Surface Load Plots

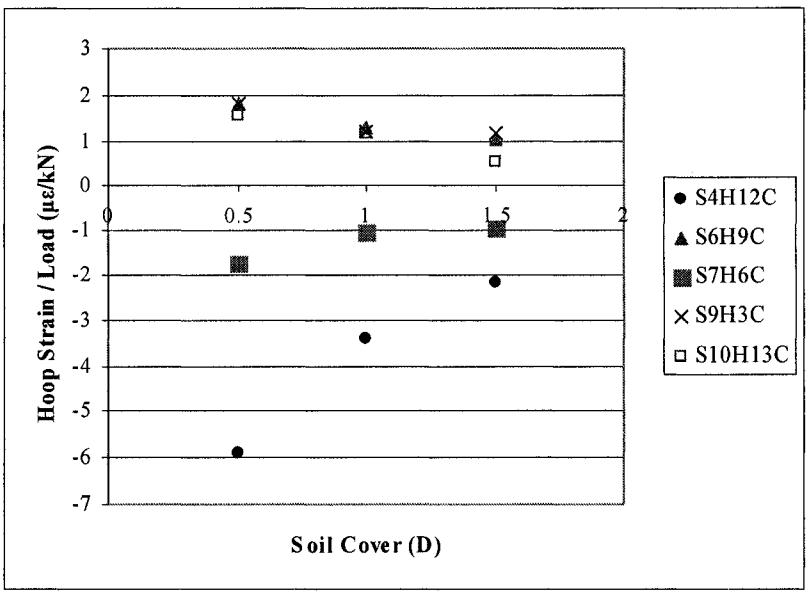

Figure 4-28: Hoop Strain Gradients at Pipe Centerline

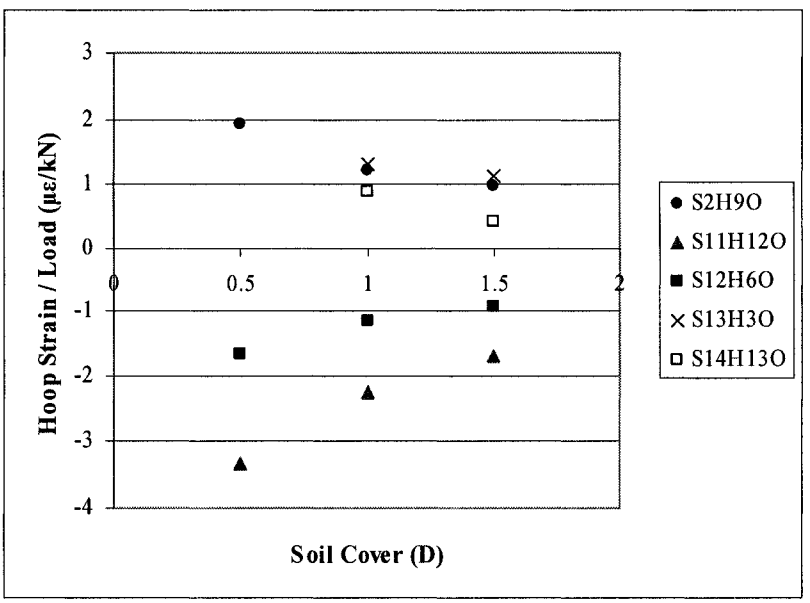

Figure 4-29: Hoop Strain Gradients Offset from Pipe Centerline

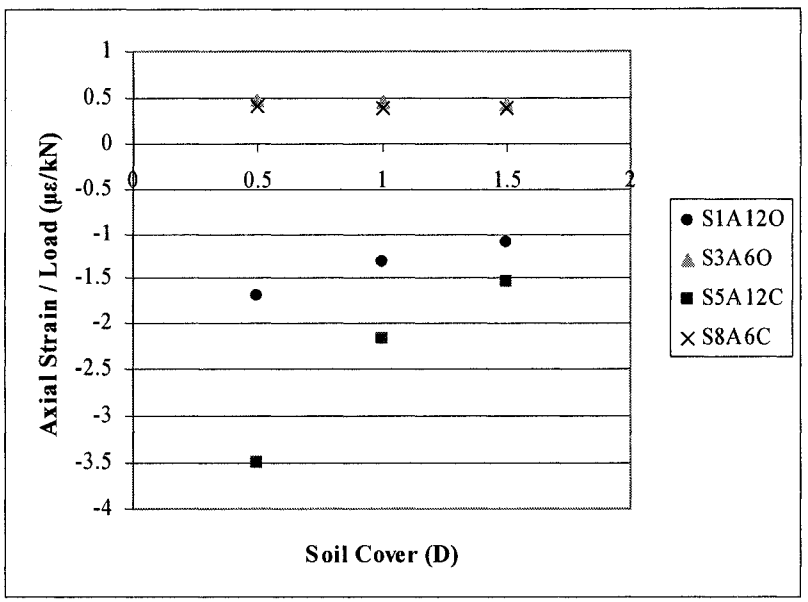

Figure 4-30: Axial Strain Gradients

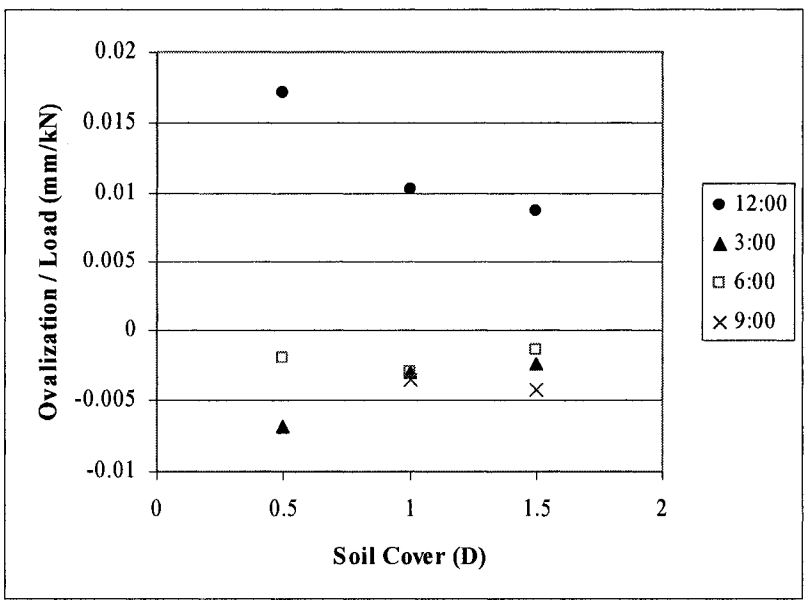

Figure 4-31: Ovalization Laser Transducer Gradients

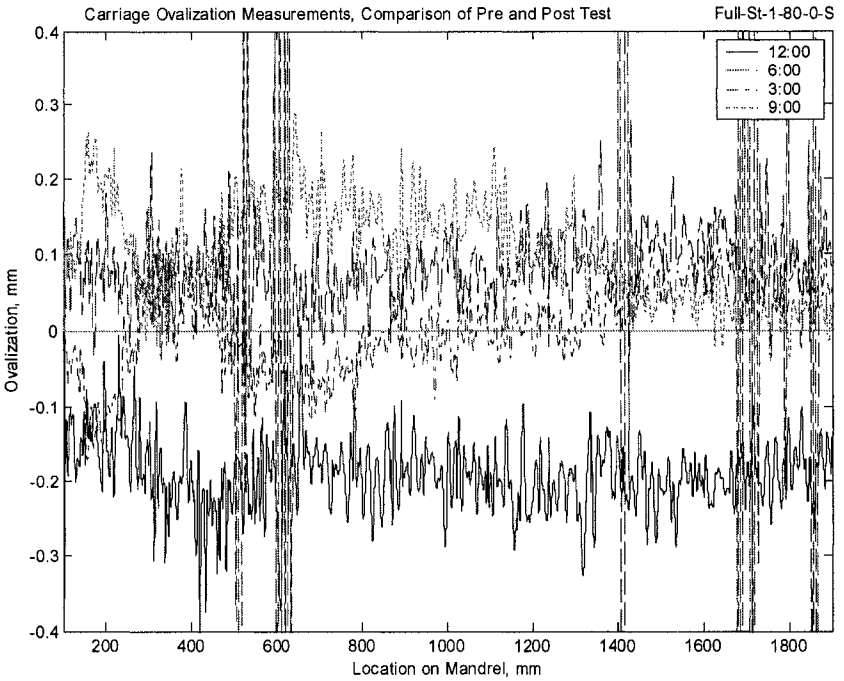

Figure 4-32: Linear pipe Behavior, Test 1

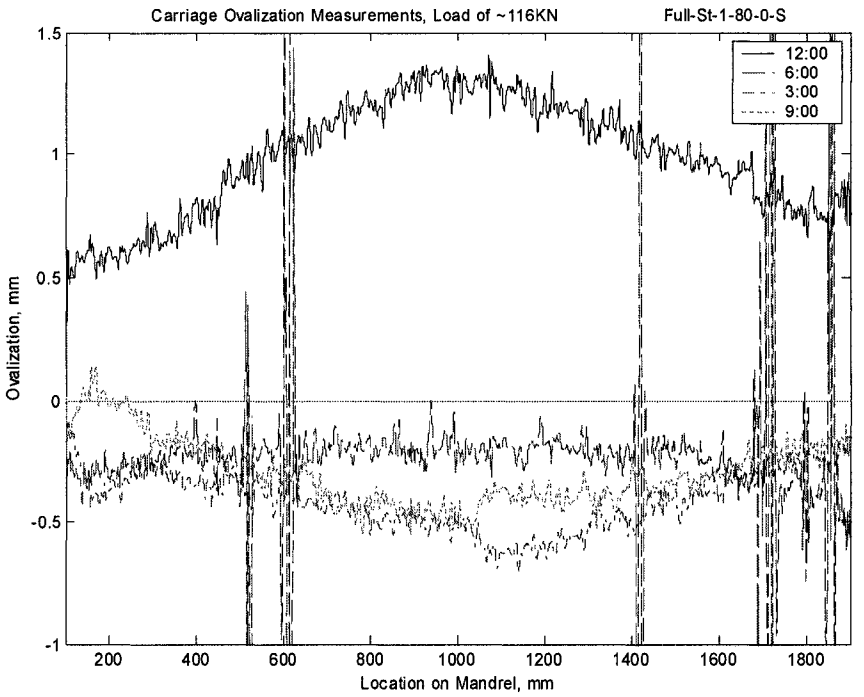

Figure 4-33: Pipe Ovalization versus Laser Carriage Location, Test 1

5.0, Surface Loading of Steel Pipes in the Centrifuge

5.1 Test Design

5.1.1 Overview

Phase II of the surface loading program at C-CORE consisted of a series of full-scale and reduced scale centrifuge tests on buried steel pipes. The investigated parameters, physical test conditions, and experimental procedure were selected, where feasible, to ensure a consistent and fair comparison from full-scale prototype to centrifuge model. This chapter will detail the centrifuge tests on three un-pressurized steel pipes with 0.5, 1.0 and 1.5D cover that are directly comparable to the full-scale tests of chapter 4. The chapter will also detail three additional tests investigating the effects of cover depth, bedding conditions and footing geometry. The six individual model pipe sections, with a diameter of 43mm (1.69"), were tested in a single centrifuge test bed. The pipes were instrumented to measure hoop and axial strain and pipe ovalization. Load and displacement of the load pad were measured with a load cell and LVDT's respectively. A summary of the test carried out and the test parameters are shown in Table 5.1.

5.1.2 Model Pipe and Instrumentation

The full-scale prototype pipe to be modelled for these tests was a 16" outside diameter (406mm) A106B steel pipe with a wall thickness of 0.375" (9.53mm), as detailed in section 4.1.4. The model pipe was manufactured from an A333 Gr6 steel pipe, machined to an outside diameter of 43mm (1.69″) resulting in a 1mm (0.04″) wall thickness. This

pipe has a D/t ratio of 42.3, a SMYS of 240MPa (35ksi) and an ultimate yield strength of 414MPa (60ksi). Experimentation determined the yield strength of 317MPa (46ksi) at 0.1% plastic strain, with a modulus of elasticity of 204MPa (29.6ksi). Tension testing of the pipe specimens was carried out as previously specified in section 3.1.2. As shown in Figure 5.1, strain in the test specimen, calculated from extension records was plotted versus stress, calculated from load records. Table 5.2 summarizes the above data. The test package was designed using standard centrifuge scaling laws as described in section 2.5. Using this pipe dictated a g level of 9.47 gravities (406mm / 43mm).

Instrumentation for this test program included external pipe strain gages (axial and hoop), pipe ovalization, loading pad penetration, sand surface displacements and surface load. The scaled pipe was instrumented with 12 external strain gauge bridges and 2 ovalization (diametral displacement) transducers. Strain gage layouts can be seen in Figure 5.2. Hoop and axial strain measurements were accomplished with the use of eight uniaxial and two biaxial strain gauges. For this measurement ¼ Wheatstone bridge layouts are used with bridge completion taking place on an external circuit board. Strain measurements are taken at the pipe mid-length (point of loading) and at ~27mm from the longitudinal midpoint for centrifuge tests, which represents 255.9mm in the prototype test configuration. The strain gages were calibrated using a shunt calibration method. The shunt strain gage calibration factors used in the data analysis were found to be on average 3.2% different from their average and 7% different from the theoretical strain gage calibration factor.

The centrifuge pipes were instrumented with ovalization transducers in the form of a strain gaged beams as described in section 3.1.2. In this test series the ovalization sensor was attached to a central mandrel that acted only as a transducer beam. The central mandrel also served as a tie rod for the end caps of the pressurized pipes in chapter 3.

5.1.3 Testing Equipment

The C-CORE centrifuge, as described in chapter 1, was used for this test program. For these tests a centrifuge rectangular strong box was used to contain the test bed and a 2-axis linear drive system was used for loading, as in the first phase of the testing program described in chapter 3. For more details on this equipment and the associated equipment such as the loading actuator and signal conditioning system see section 3.1.4. As in the previous centrifuge test program a ball bearing was used in the load pad assembly to avoid moment and side loading of the assembly. For this test series a 60.6mm (2.39") diameter load pad was driven by a vertical actuator with an in line load cell and LVDT's to measure displacement, Figure 5.3. This load pad diameter corresponds to the full-scale load pad diameter of 574mm (22.6") at a g level of 9.47g (574mm/9.47g=60.6mm). For two centrifuge tests a rectangular load pad as shown in Figure 5.4 was used. This load pad was sized to have an area equal to the circular load pad (2884mm^2) (70mm x 41mm).

5.1.4 Geotechnical Conditions

The sand used for these tests was medium-fine sand (#00 Alwhite silica sand) as used in the full-scale test program of Chapter 4, more details of the sand and relative density calculations can be found in section 4.1.5. For centrifuge testing test beds were prepared by means of dry pluviation using a sand rainer. Details of the sand rainer and raining procedure can be seen in section 3.1.5. A photograph of the pipe trenches is shown in Figure 5.5 and of the pipes lying in their trenches in Figure 5.6. The same procedure, as detailed in chapter 3, was used to create the sand bed with the sand rainer and vacuum mechanism. The only difference was the preparation of a 1D bedding layer for these tests rather than the ¼ D bedding used for the aluminum pressurized pipes. Density cup were placed in the strong box before each test, then removed and the sand density calculated after testing. Global and density cup measurements of 72 and 73% relative density respectively were calculated for the centrifuge test bed, as can be seen Table 5.3.

5.2 Test Procedure

With the pipes buried in the completed test bed the experiment head works were assembled and the test package was placed in the centrifuge basket. With the centrifuge at test speed the vertical actuator was used to load the pipe. The surface load was applied to each pipe on its longitudinal and transverse lines of symmetry. Loading of the pipe is carried out using a displacement controlled system. Two test termination criteria were used to determine when to stop loading the pipe. A model vertical load of 1.323kN (60,000lbs) was used as one test termination criteria. Recording data from hoop strain

gages and determining when the gage had reached appreciable strain levels to compare to full-scale and to each other was the second termination criteria.

5.3 Test Results and Discussion

5.3.1 Overview

For this test program one centrifuge test was carried out that included surface loading of six different buried pipe sections, these tests are detailed in Table 5.1. The data collected for each pipe was processed and presented in graphical form using MATLAB. As in Chapters 3 and 4 strain gradients and ovalization gradients were calculated for each of the transducers. The transducer response with surface load was assumed linear and the response was divided by the load to find the slope and provide a means of comparing the tests. Locations of strain gages are shown in Figure 5.2. Ovalization was measured at the pipe longitudinal centerline at 12:00 and 3:00.

In the figures to follow the strain gages and ovalization sensors are identified in the plot legend by two codes. The first code is CT# #D, which indicates a centrifuge test of a particular number corresponding to Table 5.1, followed by the burial depth (D). The second code is SG#, indicating the strain gage number, followed by either a H or an A indicating either a hoop or axial gage, 12:00, 3:00, 6:00 or 9:00 indicating the location of the gage circumferentially on the pipe, and finally either an O or a C indicating the gage is either on the longitudinal center line (C) or off the centerline (O) The ovalization

sensors are indicated simply with the test number, cover depth and either a 12:00 for the crown or a 3:00 for the haunch.

5.3.2 Load Pad Penetration

Figure 5.7 shows the load pad penetration response from the four tests with a circular load pad. Figure 5.8 shows the load pad penetration response for the rectangular load pad at two cover depths and a circular pad of comparable cover for comparison. For each test the plots of surface load versus load pad penetration (average of the three displacement transducers) are shown individually in Appendix D. During testing unloading cycles were carried out to allow for comparison to full-scale tests. These plots commonly show a steady increase of load with penetration, then the surface load remains constant while load pad penetration increases because of soil failure beneath the pad (when the load reaches the bearing capacity of the pad).

Figures 5.9 show surface load versus load pad penetration and load pad penetration versus load pad rotation for the 1.5D cover, test CT2, pipe E. Similar plots for the other tests can be found in Appendix D. In these surface load versus load pad penetration plots each of the displacement transducers are each plotted against load showing how the pad penetrated at an angle. These three displacement transducers were attached to the load pad in a triangular pattern so as to capture any rotation of the pad. The second in the plot pair, the load pad penetration versus load pad rotation, plot the angles between each of

the points of penetration. This rotation angle varied in the tests from 2.5° to 8° from the horizontal. As previously this rotation does not affect the experimental results.

5.3.3 Transducer Response to Surface Load

The transducer response to surface load includes the response of the bender elements (ovalization transducers) and the strain gages (hoop and axial) to the load applied to the surface of the pipe. Results are discussed and plots are presented to accompany the discussion in the following sections while a complete set of test plots are included in Appendix D.

5.3.4 Circular Pad Load Tests

Figures 5.10, 5.11 and 5.12 show the strain versus surface load plots comparing the four centrifuge tests where cover depth was varied and a circular load pad was used to load the pipe. Figure 5.13, shows the ovalization response at 12:00 and 3:00. These plots show the decrease in strain and ovalization with an increase in cover depth. The cycles shown in the pad penetration versus surface load plots can also be seen in these plots. The cycle lines tend to be offset from each other but have the same gradient, showing an elastic behavior of the pipe. These lines, hysteresis loops, also show the plastic accumulation of stress in the soil, exerting stress on the pipe after the surface load is removed. The strain and ovalization response to surface load is very approximately linear with surface load. Approximate lines are fitted to data to obtain the gradients of strains and ovalization, microstrain/kN and mm/N X 10^{-1}. Figure 5.14, 5.15, 5.16 and 5.17 show gradients of

hoop strains, axial strains and ovalizations for the four tests. Locations of the strain gages can be seen in figure 5.2. The soil cover for the pipe in these plots range from 0.5D to 2.0D. Most of the gradients decrease with increase in soil cover. The exception being several of the transducers gradients in the 2D cover tests are approximately equal or in some cases slightly larger than its corresponding 1.5D test transducer gradients. This discrepancy can be explained by experimental error and the low influence of the load on the pipe over 1.5D cover.

The two main modes of pipe deformation identified in these tests were ovalization of the pipe cross-section and bending in the long section. These two modes are associated with the hoop strain and axial strain response. The ovalization mode was not associated with an elliptical pipe shape. The crown of the pipe significantly deformed inward while there was a small outward deformation at the haunch. The crown deformation was confirmed by both the crown hoop strain gauges and laser readings. The crown and haunch deformations decreased with increasing cover.

Compressive axial strain was recorded both in Sections A & B at the crown. As expected these compressive strains decreased with increasing cover depth. Small tensile axial strains were recorded at the invert and changed little with cover. These axial strains result from the bending strains and the Poisson's effect associated with the pipe crown and invert compressive hoop strains. The hoop strains decrease with increase of cover depth. Hoop strains are negative (compression) at crown and invert and positive

(tension) at haunches. Hoop strains at the crown are significantly larger particularly for Section B, the mid section of the pipe.

5.3.5 Rectangular Load Pad Tests

Figures 5.18 and 5.19 compare strain and ovalization response to load for two tests with a rectangular pad and two with a circular pad. Plots for the remaining transducers, showing similar trends can be found in Appendix D. Strain and ovalization trends are similar to those described in section 5.3.4. With an increase in cover depth the transducer response, strains and ovalizations, are reduced. Comparison of the 0.5D rectangular load pad and circular load pad response show that the pipe response was greater for the circular load pad. The rectangular load pad has dimensions of 70mm by 41 mm, sized to have the same area as the circular pad (~2800mm^2). The length of the pad was perpendicular to the pipe length. The load exerted by the rectangular pad, with a length across the pipe of 70mm, was bridging the pipe more than the 60.6mm diameter circular pad. The crown hoop stresses for the circular pad were as much as 1.5 times that of the rectangular pad. This trend although less prevalent continues in axial strain gages and ovalization sensors. Comparing the 1.5D cover rectangular load pad test and circular pad strain response show that while the response in the rectangular pad tests is always less the magnitudes of the two are very similar. The ovalization response for the rectangular load pad test is substantially lower than the circular pad test. For the 0.5D cover rectangular load pad test the bedding depth was 1.5D. This deeper cover depth may have influenced the

results. Lack of tests with varied bedding depths prevent conclusions from being drawn on bedding influence.

The load pad displacement data is not reliable for applied load levels greater than 125kN for test CT4, pipe "b" and test CT2, pipe "e". The g level imposed self weight of the vertical drive was not sufficient to hold the drive down and at high surface loads the drive tilting on its base. The 2-axis actuator system was initially assembled such that the vertical drive component sat on the horizontal drive component with no mechanical fastening. In this configuration it was restricted in the force it can exert by its own self weight at a particular g level. The mass of the vertical drive is 25.23 kg and therefore at 9.43g it has a self weight of 2.33 kN (model scale). The driving axis of the vertical drive is 86 mm offset from its center of mass. Summing the moments about the end of the drive furthest from the load pad (force of drive self weight X distance from the center of the drive to the end of the drive = the force into the drive from the applied surface load X the distance between the end of the drive and the loading rod location) it is found that at 9.47g the drive can exert 125kN, prototype scale (1.4kN model scale) before the moments are equal and the drive will tilt. After tests CT4 and CT2 the drive was secured to its base allowing it to re-act the forces applied in the last four tests.

Table 5-1: Centrifuge Tests and Parameters

Test	Pipeline Designation	Cover Depth	Bedding Depth	% Relative Density	Load Pad Geometry
Centrifuge 01	F	2.0D	1.0D	80	Circular
Centrifuge 02	E	1.5D	1.0D	80	Circular
Centrifuge 03	A	0.5D	1.0D	80	Circular
Centrifuge 04	B	1.5D	1.0D	80	Rectangular
Centrifuge 05	C	0.5D	1.5D	80	Rectangular
Centrifuge 06	D	1.0D	1.0D	80	Circular

Table 5-2: Pipe Parameters

Pipeline Parameter:	Steel Pipe:
Outside Diameter	43mm (1.69″)
Wall Thickness	1mm (0.04″)
D/t Ratio	42.3
Material	A333 Gr6
Yield Strength (factory specified)	240MPa (35ksi)
Yield Strength (experimentally determined)	317MPa (46ksi)
Tensile Strength (factory specified)	414MPa (60ksi)
Modulus of Elasticity (experimentally determined)	204MPa (29.6ksi)

Table 5-3: Density Measurements for Centrifuge Test Bed

Density Measurement Method	Density	% Relative Density
Density Cups	1518	73
Global Density	1515	72

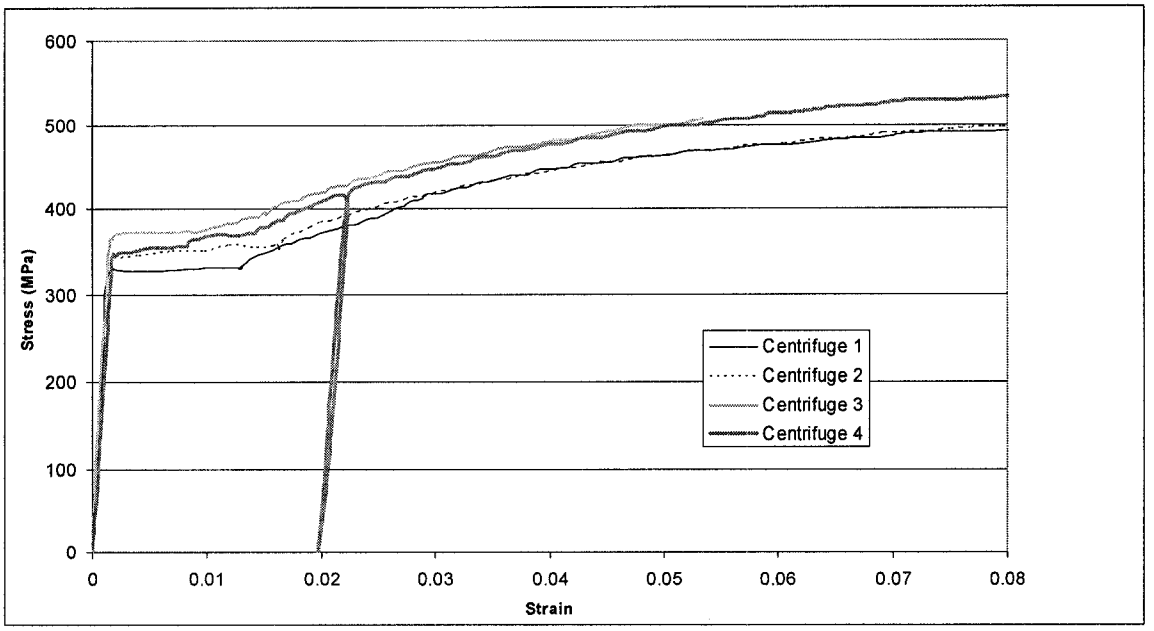

Figure 5-1: Stress Strain Plots for Steel Test Specimens

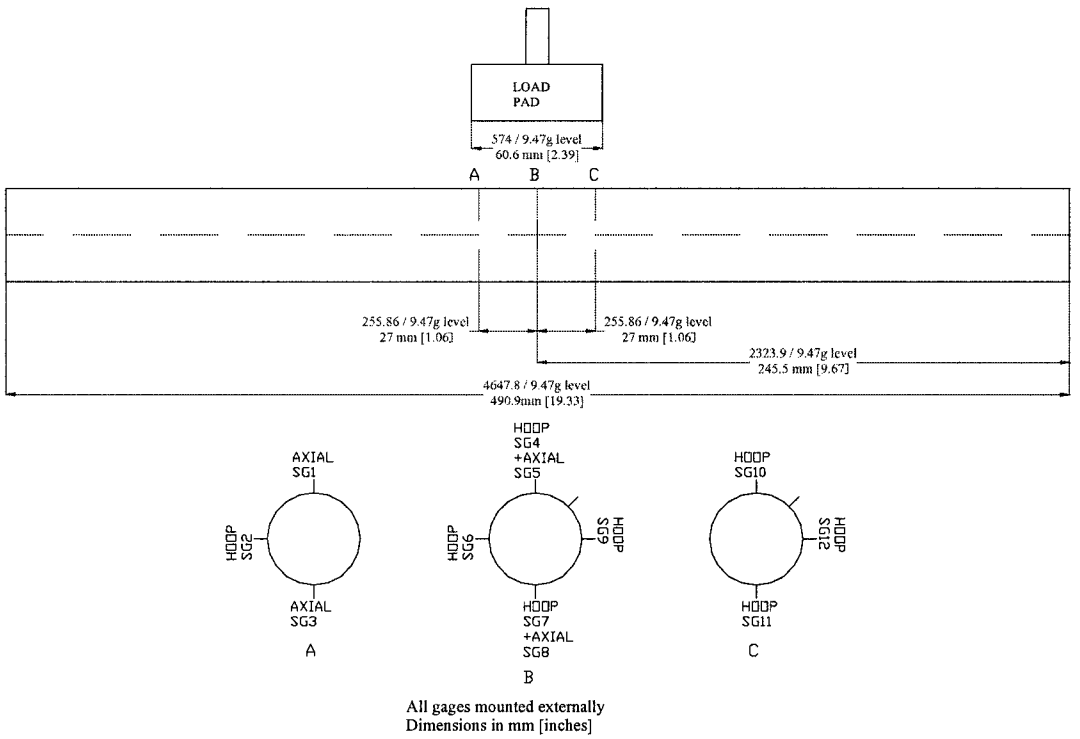

Figure 5-2: Strain Gage Layout for Centrifuge Testing

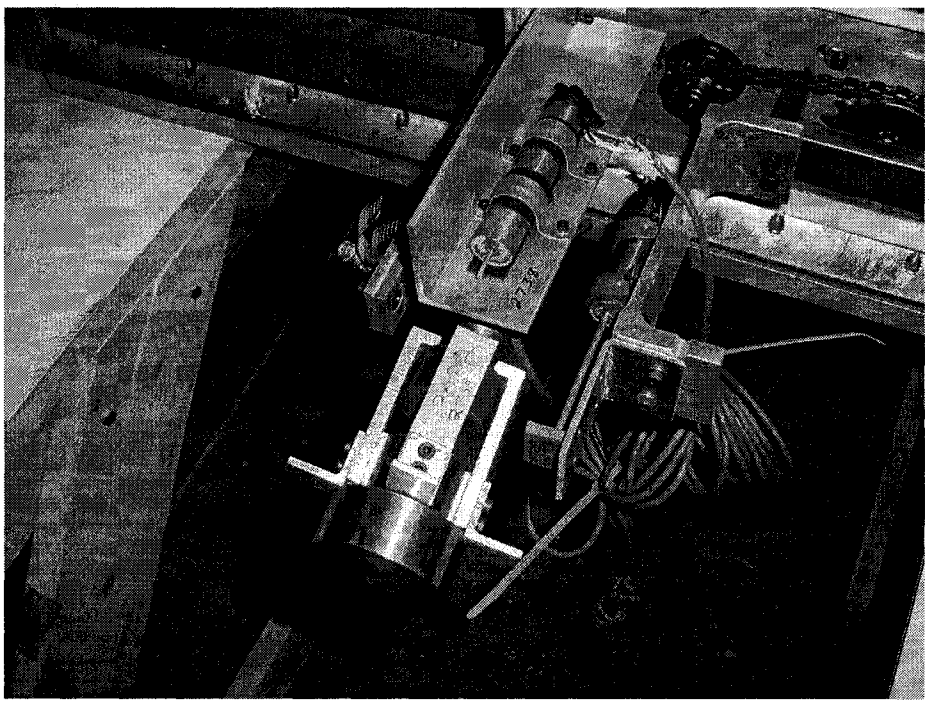

Figure 5-3: Centrifuge Circular Load Pad with LVDT's

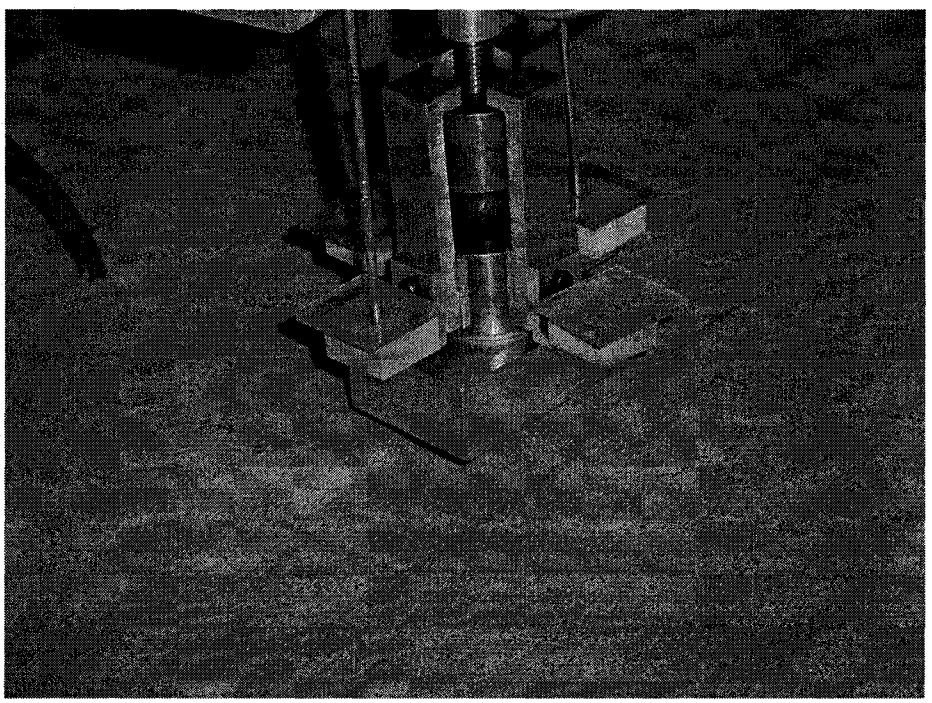

Figure 5-4: Rectangular Load Pad

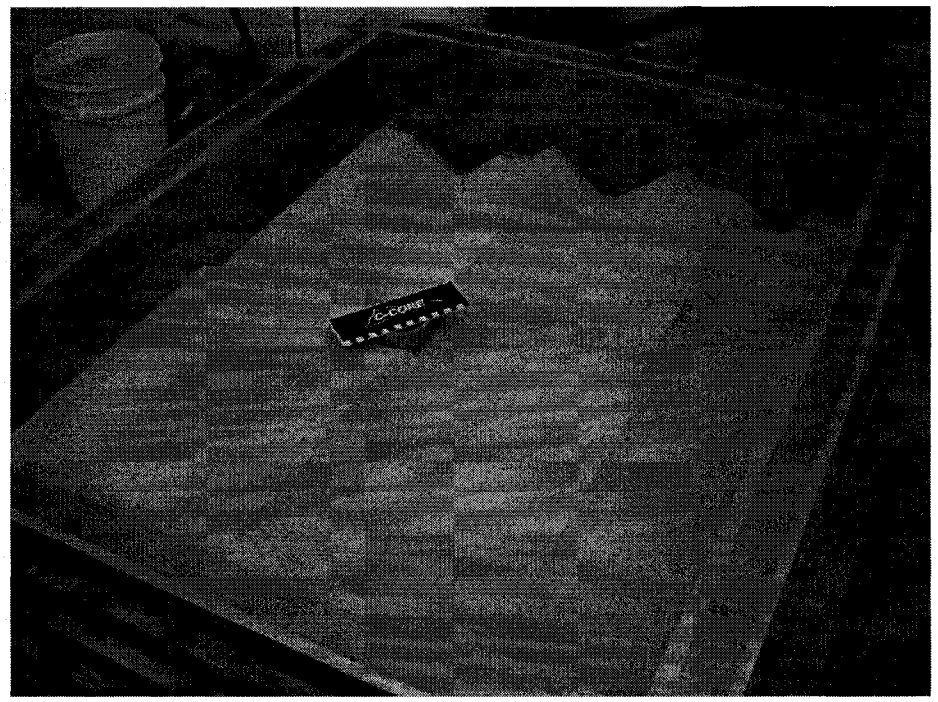

Figure 5-5: Centrifuge Pipe Trenches

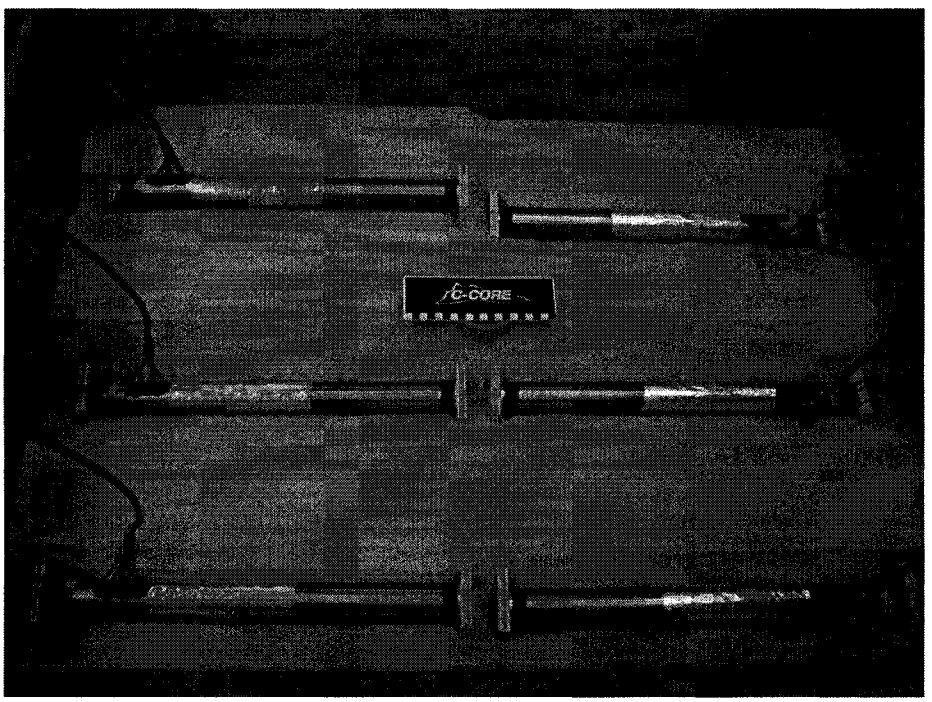

Figure 5-6: Centrifuge Pipes in their Trenches

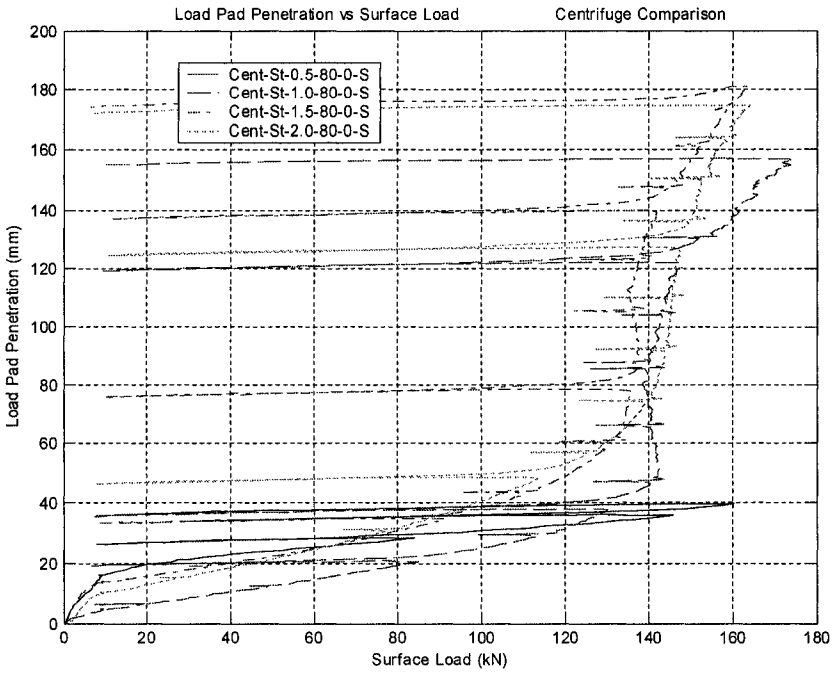

Figure 5-7: Penetration Response Comparison for Circular Pad, Varying Cover

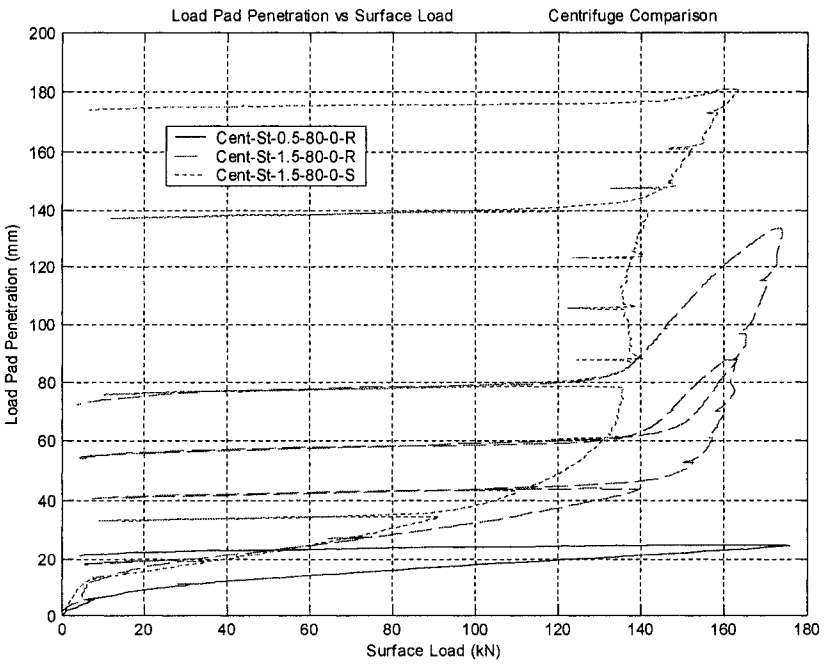

Figure 5-8: Penetration Response Comparison for Rectangular and Circular Pad

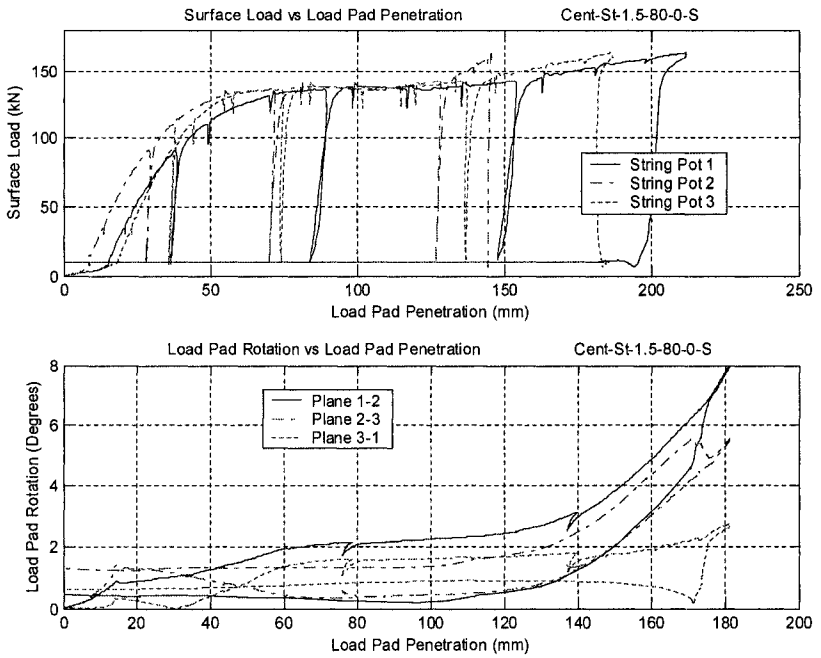

Figure 5-9: Pad Rotation, 1.5D Cover

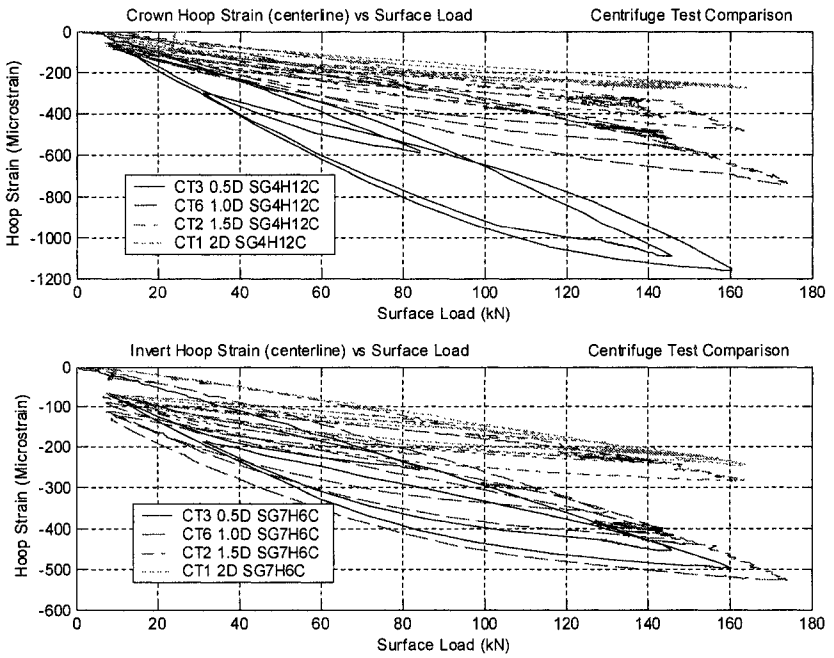

Figure 5-10: Crown and Invert Hoop Strain Comparison (Circular Load Pad)

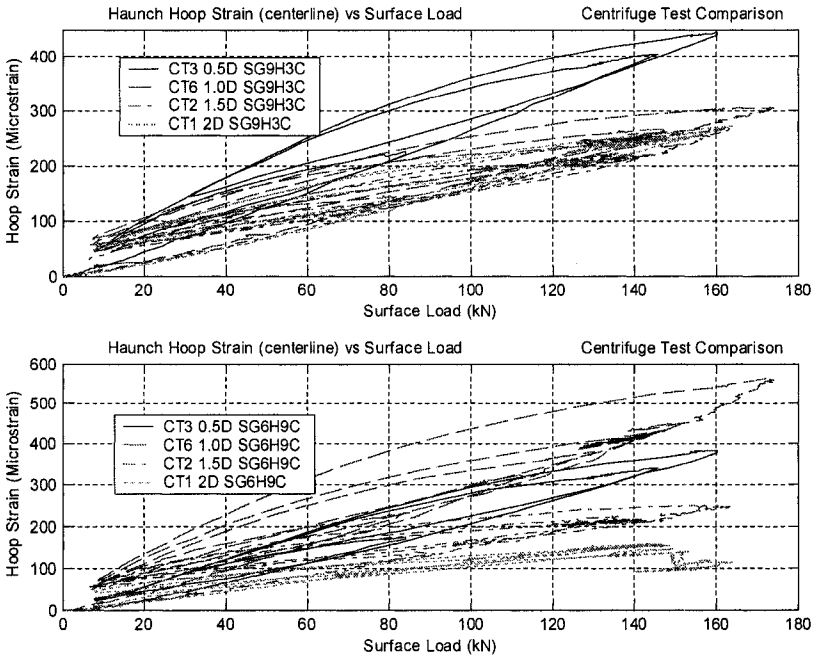

Figure 5-11: Haunch Hoop Strain Comparison (Circular Load Pad)

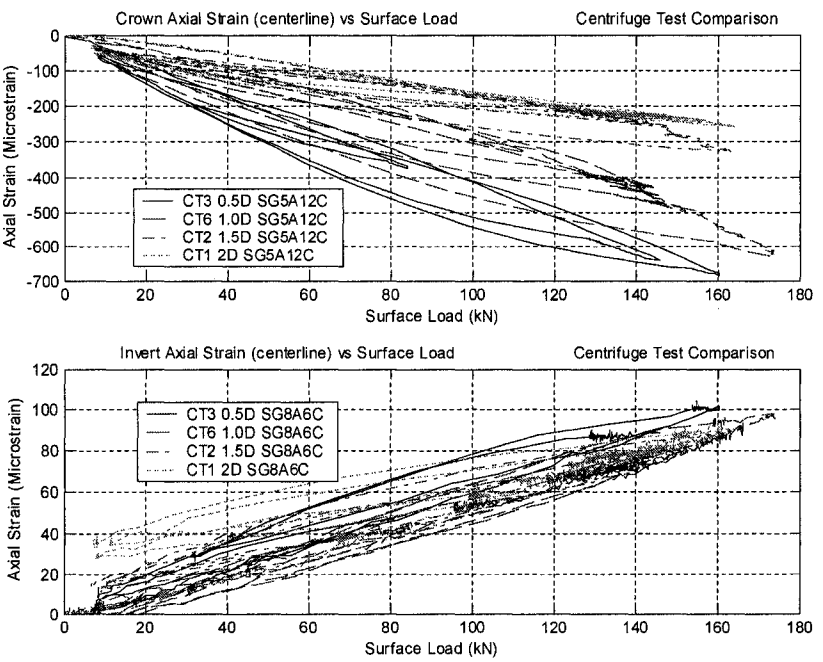

Figure 5-12: Crown and Invert Axial Strain Comparison (Circular Load Pad)

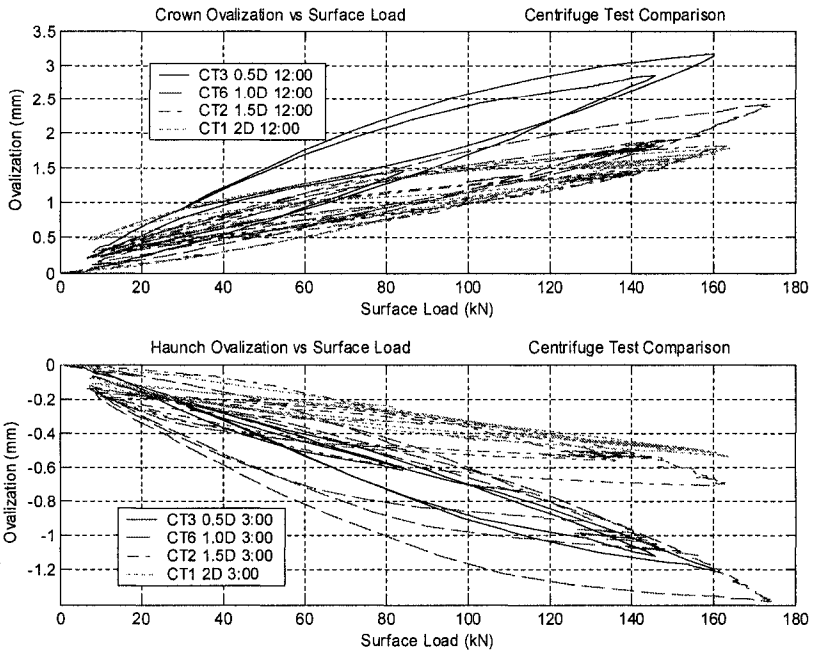

Figure 5-13: Ovalization Comparison (Circular Load Pad)

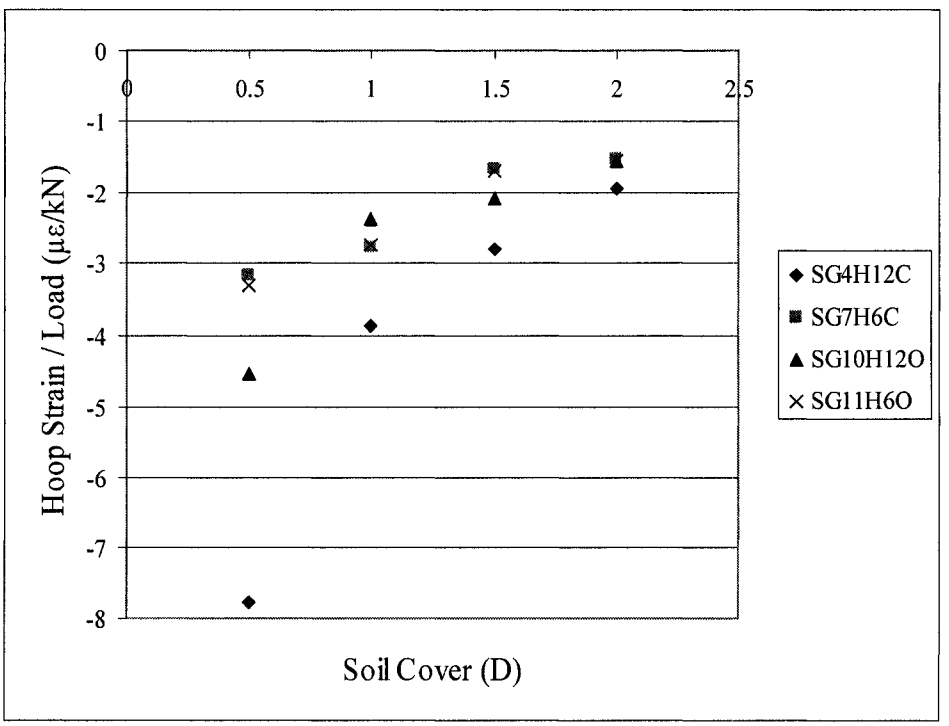

Figure 5-14: Hoop Strain, Crown and Invert Strain Gradient Comparison

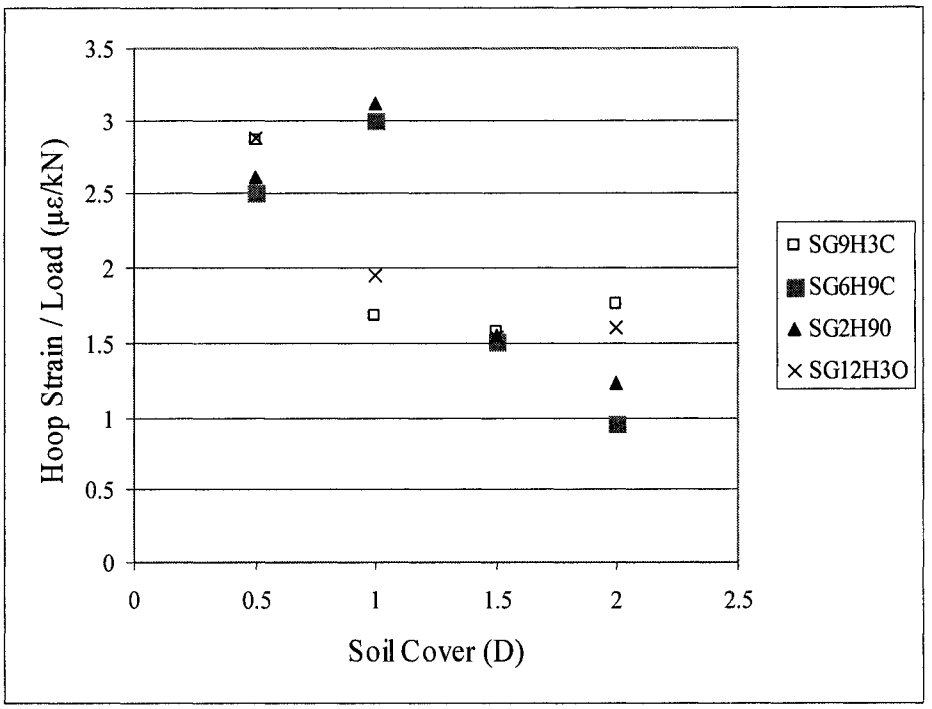

Figure 5-15: Hoop Strain, Haunches Gradient Comparison

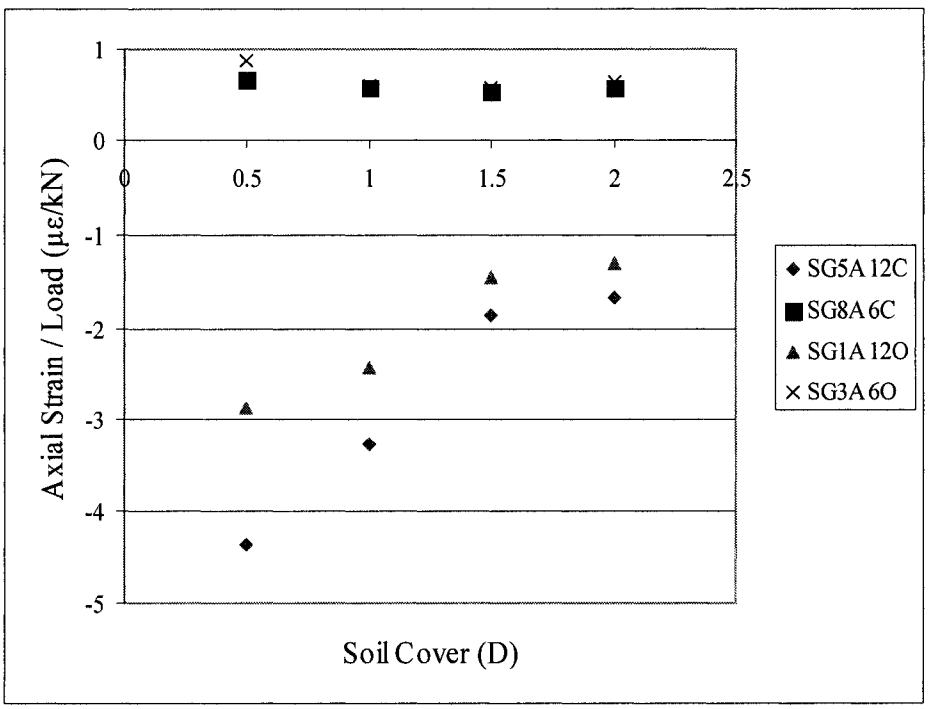

Figure 5-16: Axial Strain, Haunches Gradient Comparison

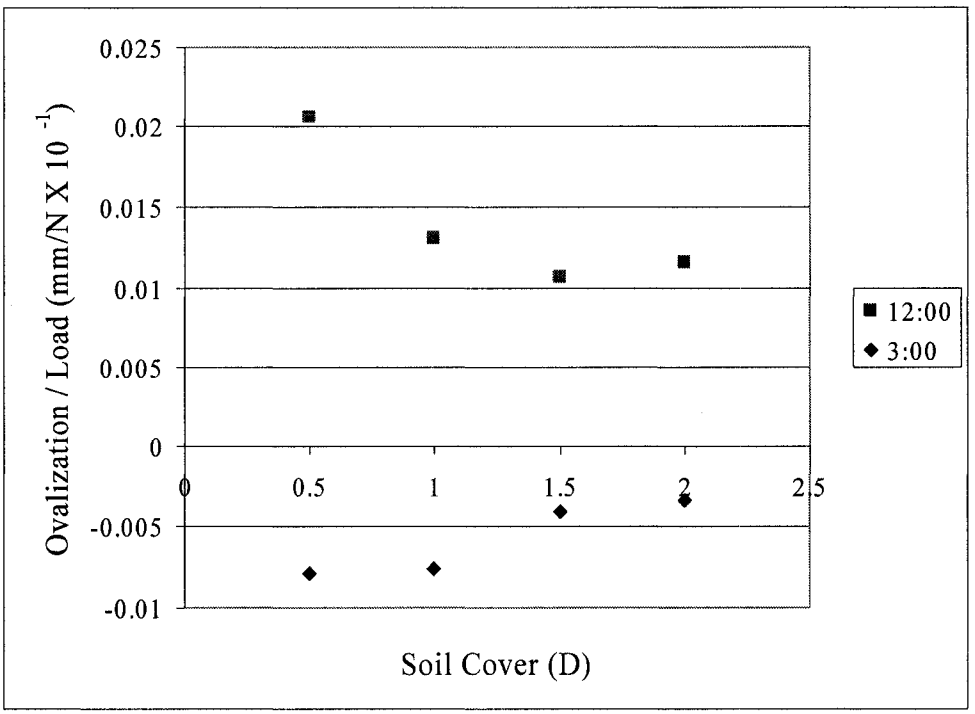

Figure 5-17: Ovalization, Crown and Haunch Gradient Comparison

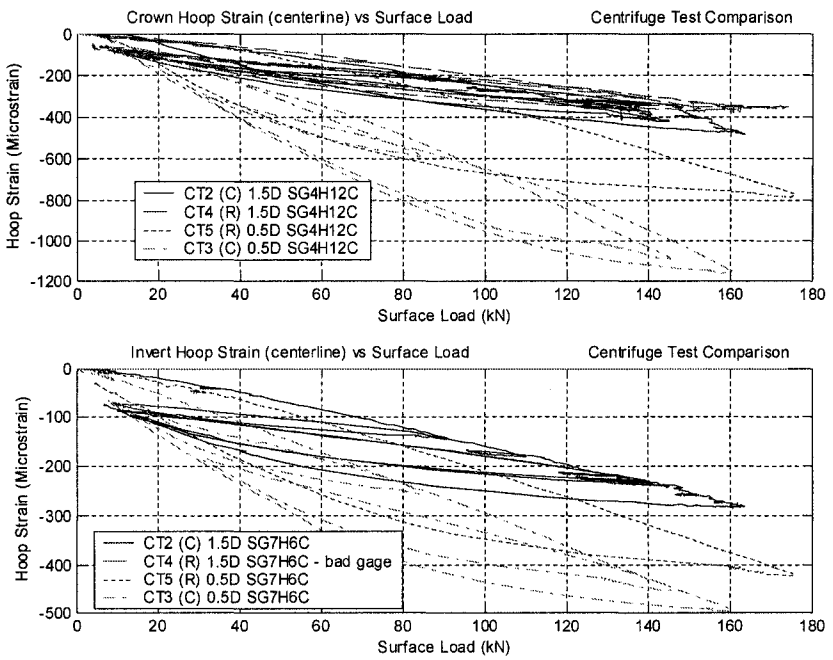

Figure 5-18: Crown and Invert Hoop Strain Comparison (Rectangular to Circular)

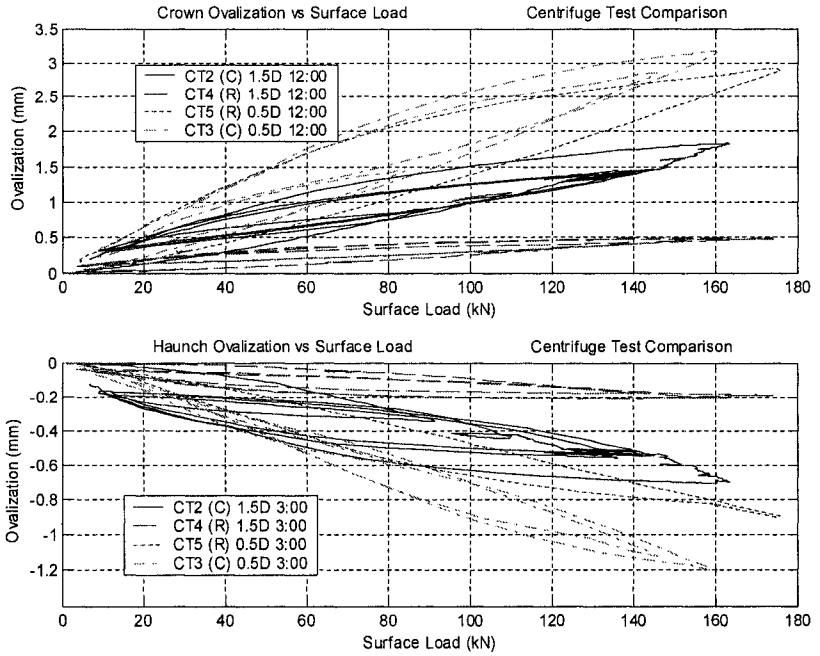

Figure 5-19: Ovalization Comparison (Rectangular to Circular)

6.0, Comparison of Test Programs

6.1 Comparisons to other Test Programs

6.1.1 SwRI Full-Scale Test Comparisons

The intention of the first surface loading program conducted at C-CORE, as described in Chapter 3, was to be an assessment of the applicability of centrifuge modeling to the studying of surface loading on buried pipes. This applicability was to be determined by a comparison of centrifuge results on a model pipe to the results of tests carried out during SwRI's full-scale program. Very limited data were made available from SwRI for comparison with the model tests. SwRI had reported to have carried out tests on 16" and 36" pipe with varying cover depths and internal pressures in Phase I and planned to extend their test parameters in Phase II. The report, Waldhart *et al.* (2001), referenced in this thesis includes some of the initial testing carried out on a 16" pipe in weak sand with some limited references to the other tests. This was the only data available for comparison in this thesis. Other data collected was kept confidential to SwRI and PRCI.

The Waldhart paper was used to formulate many of the test conditions and parameters used in the test program, described in Chapter 3, on buried aluminum pipes in the centrifuge. Waldhart used a 16" OD API X52 steel pipe, with a D/t of 43. This study used an aluminum 2024-T3 tube, with a 1 1/8" outside diameter (a prototype diameter of 15.98") and a D/t ratio equal to 40.2. The material properties compared well with the

SwRI pipe having a yield strength of 360 MPa and the aluminum model pipe having factory specified and experimentally determined yield strengths of 345 MPa and 310 MPa respectively (a difference of 4 and 15 % respectively). The aluminum pipe has a Young's Modulus of 68GPa in comparison with 205GPa for the steel pipe. Based on Spangler's solution, stress in pipe can be calculated from the following equation (American Water Works Association, 1989):

$$\sigma = 3v\frac{D}{t}(\frac{D}{t}-1)\left[K_b - \frac{K_x}{\frac{8E}{E'(\frac{D}{t}-1)^3}+0.732}\right] \approx 3v(\frac{D}{t})^2\left[K_b - \frac{K_x}{\frac{8Et^3}{E'D^3}+0.732}\right] \qquad (6.1)$$

where K_b is the bending coefficient, K_x is the is the deflection coefficient, E is the pipe elastic stiffness, E' is the soil elastic stiffness, D/t is the pipe diameter to wall thickness ratio and v is the loading pressure on the pipe. Based on this equation the stress induced by surface loading will be smaller for the aluminum pipe than steel pipe. The elastic strains will be larger for the aluminum pipe due to Hooke's law, $\varepsilon = \sigma$ / E. The relative mechanical stress or strain response ratios between the steel and aluminum pipe will not be constant. At higher load levels, the modulus of soil reaction (E') will be reduced due to soil shear deformation and increase due to higher confining pressure. Given the possible variations in E' and given the sensitivity of this equation to the E' value it is difficult to quantify the difference in stress and strain for the aluminum versus the steel pipe. It is estimated that the stress level experienced by the aluminum pipe could be approximately 0.65 to 1.0 times the stress levels in the steel pipe and the strains in the

aluminum pipe should be 2 to 3 times that of the measured strains in the steel pipe. Consequently, a one-to-one correspondence of the recorded values of aluminum and steel pipe response curves is not expected. For general trends however these pipes of different materials can be compared. For comparison purposes the strain data for the aluminum pipe were divided by 3 to plot them on the same axis as the steel pipe data and draw conclusions.

The C-CORE internal pressure levels of 5 and 80% SMYS were chosen based on the SwRI internal pressures of 5, 40 and 80% SMYS. The SwRI tests had a ¼ D bedding layer of the backfill material placed in the trench under the pipe, the centrifuge tests also used a ¼ D bedding layer in the centrifuge strong box. C-CORE also attempted to follow the SwRI test termination criteria of 60,000 lbs load in the load pad and a pressure level that was equivalent to 90% SMYS. The centrifuge program matched the 22.6" full-scale circular load pad with a properly scaled 1.59" load pad. As discussed in section 2.4, SwRI's reference to 70 and 80% relative density sand was found to be in inaccurate, therefore 40% and 80% relative density sands were prepared for the centrifuge tests to allow for better comparisons.

A notable difference in the test conditions were the pipe end conditions. The C-CORE pipes had a central mandrel connecting the two end caps with an o-ring sealing the pipe to the end cap. This pipe setup simulates an infinitely long pipe with no axial tensile strain induced in pipe wall from internal pressure. SwRI capped the end of their pipes

with axial tensile strain induced in pipe wall from internal pressure. Another difference was for the centrifuge testing one test was carried out per pipe burial. The pipe was excavated and buried in a new test bed before another condition, i.e. a different internal pressure, was tested. Waldhart explains SwRI's method of testing three pressures on one pipe in the same test bed, varying the pressure as the pipe is loaded and fitting lines to the data, post test, to generate plots for several tests conditions from one pipe test. Waldhart also states that between some tests only the area adjacent to the load pad, not the entire pipe, was excavated. While SwRI stated that the test results show that these two practices have minimal effect on the results it was decided that for the centrifuge tests it was necessary and prudent to only test one condition per pipe per test bed.

The Waldhart report presents strain versus surface load plots for the longitudinal centerline crown hoop and axial strain gages for the 16" pipe with 8" and 16" cover in weak sand at 5% and 80% internal pressure. Given these data sets eight C-CORE tests were chosen to compare to this data. Waldhart only reported strains from the crown hoop and axial gages at the longitudinal centerline, judging these to be the most critical. Therefore only those two gages can be compared to the centrifuge data. The tests to be used in the comparisons are presented in tabular form in Table 6.1. As detailed below, considering the differences in the pipe, sand properties, test configurations and uncertainty about the SwRI soil density the comparisons are very good.

Tests on aluminum pipes in the centrifuge, T3B and T3C, 0.5D and 1.0D covers, in 40% relative density sand with 5% SMYS pipe pressure were compared to SwRI data in Figure 6.1. As discussed above to convert to a scale comparable to steel prototypes, model strains for the aluminum pipes were divided by 3 to account for this difference in moduli. Comparing the hoop strains at 1D cover show the centrifuge strains seven times smaller than the full-scale strains. For the axial direction, with a 0.5D cover, a very good comparison is shown with the trend matching and the magnitude differing by only 30%. The axial gage was not available for 1D test and the hoop gage was not available for 0.5D test.

Tests on aluminum pipes in the centrifuge, tests T2B and T2C, 0.5D and 1.0D covers, in 40% relative density sand with 80% SMYS pipe pressure were also compared to SwRI data, as shown in Figure 6.2. Hoop strains at 0.5D cover show similar trends with a 30% difference at maximum load. In the axial direction, for a 0.5D and a 1.0 D cover, centrifuge pipe strains differ from SwRI strains from 60 to 90%. The hoop gage was not available for 1D test.

The centrifuge tests on steel pipes are compared to SwRI data in Figure 6.3. Despite these tests having different conditions, 0% SMYS pressure for full-scale and 5% SMYS pressure for SwRI, , 80% RD for full-scale and 40% RD for SwRI, these tests show good comparison. In the hoop direction the centrifuge steel readings vary from SwRI readings by 7 and 24% for 0.5 and 1 D covers respectively. Axial strains in the centrifuge steel

tests vary from SwRI tests by 20 and 40% for 0.5 and 1 D covers respectively. The full-scale tests on steel pipe are compared to SwRI data in Figure 6.4. Similar to the centrifuge steel tests the full-scale data had different conditions but does show good comparison. In the hoop direction the centrifuge steel pipe strains vary from SwRI readings by 27 and 37% for 0.5 and 1 D covers respectively. These lower hoop measurements for the C-CORE tests could be explained by the denser soil carrying more load than the looser soil in the SwRI test bed. Axial strains in the centrifuge steel tests vary from SwRI tests by 4 and 14% for 0.5 and 1D covers respectively. The centrifuge steel pipes showing a better comparison to SwRI than the full-scale tests can be explained by the density of the centrifuge sand (72%RD) being closer to the SwRI condition, a less stiff soil structure support. Given the differences in conditions for the tests the important factor in this comparison is not the magnitudes as detailed above but that the trends match. The trends do match between the two sets of tests very well.

Waldhart notes that as the internal pressure is increased the hoop strains caused by surfacing loading decreases, showing the pipe stiffening due to internal pressure. He also observes that axial strain is not as sensitive to internal pressure differences as hoop strain. These trends are also seen in the centrifuge aluminum tests when pressure is varied, as detailed in section 3.4.3. Strains in the four SwRI tests shown decreases with increasing cover depth. This trend is also seen in all the tests carried out at C-CORE, detailed in section 3.4.2, section 4.3 and section 5.3.

In concluding the paper Waldhart remarks that 10 to 20% error seen in the measurements (crown hoop strain only) is acceptable in full-scale testing. While he reports an 11% difference in the crown centerline hoop strain, examination of the data shows over 18% difference in axial centerline strains. These differences of 10 to 20% are seen in tests carried out in a bed prepared by the same methods on the same pipe section. While the C-CORE centrifuge to full-scale tests saw differences of up to 75% in comparing haunch hoop strains, the crown hoop strains, seen as most critical by Waldhart, differed by only 20%.

6.1.2 Other Full-Scale Test Comparisons

J.C. Potter (1985) carried out field tests measuring the effects of vehicle loads on buried high pressure pipe. He found that the internal pressure of the pipe has a significant effect of reducing vertical load on the deflected pipe. Similar results can be shown in the series of tests in this thesis. Examination of Table 3.7 shows that an increase in internal pressure reduced the strain and ovalization gradients. For example, the pipe crown hoop strain decreased by a factor of 1.6 from T6A2 to T4E, tests with similar conditions except an increase in internal pressure from 5% to 80%. Potter observed deformations decreased as the cover depth increased, with the deformation below 30" cover decreasing minimally. This can be seen in Chapter 5 where the crown hoop strains decreased by a factor of 2 from 0.5D cover to 1D cover but only by a factor of 1.4 from 1.5D to 2D cover.

6.1.3 Centrifuge Test Comparisons

Valsangkar and Britto (1979) reported carrying out centrifuge modelling of pipe sections subjected to surface loading. One of their conclusions was that because of arching, changing the stiffness had significant influence in reducing the load to the pipe. This was also seen in the test programs detailed in this thesis. In chapter 3 it is detailed how an increase in soil stiffness and or an increase in pipe stiffness, by way of increasing internal pipe pressure, causes the pipe response to reduce. A reduction in pipe response shows a reduction in load seen by the pipe because of arching through stiffer soil or through a stiffer structure.

Trott *et al.* (1984) compared results obtained using 1 m diameter prototype with a centrifuge model tested at an acceleration of approximately 10 g. They found pipe strains and deflections measured in the centrifuge model subjected to the same loading conditions (appropriately scaled) compared very well to the prototype. As in the C-CORE studies high strains in the crown were measured while the strains in the invert were very small. In the Trott study the prototype and model had similar load deflection responses but the prototype had a stiffer response, similar to the C-CORE program. The studies presented in Chapters 2, 3 and 4 of this thesis all show ovalization where there was a slight outward movement at the spring line and significant inward deflection of the crown, as also observed by Trott. Comparison of Trott's full-scale and centrifuge pipe response shows from 5 to 60% difference in strains and deflections. These differences

are comparable to the full-scale to centrifuge comparison detailed in section 6.2, where differences of 75% in haunch hoop strains but only 20% in the crown hoop strains.

As a continuation of the work presented in this thesis a series of tests on steel pipes were carried out in the C-CORE centrifuge as detailed in C-CORE (2005) . They modeled 36" and 48" diameter pipe with a D/t of 95 under similar conditions as the tests presented in this thesis. The pad displacement versus pad load behavior in each of that program and those presented in Chapters 3, 4 and 5, was non linear, all showing similar trends. In each of these programs pipe response increased with increasing load pad penetration and also with decreasing cover depth. The C-CORE, (2005) tests also confirmed that as the internal pressure was increased so was the system stiffness, i.e. pipe response lessens.

For the tests they carried out on pipes with no internal pressure the C-CORE, (2005) program resulted in several conclusions. The pipe deformation is not the classical elliptical mode shape. The response is characterized by primarily radial outward displacement at the pipeline haunches and radial inward displacement response at the pipeline invert indicating hoop compression. These conclusions confirm those from the tests carried out for this thesis, where small inward ovalizations were seen at the invert, larger outward deflections at the haunches and the largest pipe deformations took place at the crown where inward ovalization was measured. C-CORE, (2005) also noted that the longitudinal membrane response associated with the pipeline crown infers local flexural membrane action at the pipeline crown. This was first seen in the tests detailed in this

thesis, where compressive axial strains at the crown and tensile compressive strains in the invert, suggesting a longitudinal flexural membrane response.

6.1.4 FEA Comparisons

Fernando *et al* (1998) carried out a FEA study on buried pipe sections. Similar to this thesis, Potter at full-scale and Trott and Symons in the centrifuge, they found that greater increases above certain cover depths results in negligible pipe response decreases. Similar to the studies discussed in Chapters 3, 4 and 5 Fernando found maximum hoop stresses at the hoop and minimal at the invert. As an example, in Chapter 4, at 0.5D cover the hoop crown strain gradients were 5.9 and 3.3, hoop haunch strain gradients were 1.8 and 1.82 and hoop invert strain gradients were 1.7 and 1.6. For non-symmetric loading, Fernando simulated a load as a distance of one pipe radius from the pipe center, and found that the hoop stresses were less than for symmetrical loading. Section 3.4.5, details the reduction in pipe response when loads are applied at an offset from the pipe.

Sharp *et al.* (1985) carried out a study where they compared their FEA results to soil box tests carried out by Knight and Moser in the Buried Structures Laboratory at Utah State University. The authors state that while there is good correlation between the FEA and the soil box tests the deformation response of the pipe varied from FEA model to soil box test from 20 to 70%. Pipe hoop and axial strains varied from FEA model to soil box test from 5 to 80%. Although on fiber reinforced plastic pipes this program shows the variation between test methods, be it full-scale, centrifuge or finite element can have

some measurement locations with substantial percent differences but still be judged a good comparison.

As a continuation of the work presented in this thesis C-CORE, (2005) carried out centrifuge tests and FEA work on buried steel pipe subjected to surface loads. They were able to achieve good comparisons between FEA and experimental results for the modeled 36" pipe. They also carried out limited FEA on a 16" pipe to allow a comparison to the data presented in Chapter 4 and 5 of this thesis. Figure 6.5 and Figure 6.6 show comparisons of the FEA results to the experimental data from the full-scale and centrifuge programs. As seen in the figures trends are very similar and magnitudes are also fair.

Moore (1987) developed closed-form solutions predicting pipe response to surface loads with both symmetric and asymmetric loading. He found hoop forces that were compressive in asymmetric loading, hoop force producing compressive strains at the hoop and invert. The asymmetric tests, Test series 5, in chapter 3, showed compressive strains in the hoop crown. These compressive strains reduced as the distance from the pipe was reduced and in the symmetric loading tests the hoop crown strains were tensile. Although the conditions used in the semi analytical solutions of Moore are not exactly the same as the test conditions used in present study, it provides a suitable explanation of the pipe response for asymmetric load.

6.2 Comparison of the Three Programs

6.2.1 Overview

Three test programs were detailed in this thesis, surface loading of buried aluminum pipes in the centrifuge, chapter 3, surface loading of buried steel pipes at full-scale, chapter 4, and surface loading of buried steel pipes in the centrifuge, chapter 5. This section will compare these three test programs that have been extensively described and their results commented on in their respective chapters. For the Chapter 3 tests the objective of the test program was to compare data from surface loading tests in the centrifuge to data from the full-scale program of SwRI. Initial test parameters used in this investigation were based on the full-scale testing that took place at SwRI as described in section 2.4. The test conditions for the steel pipes, both chapters 4 and 5, were based on the aluminum tests but with the greater effort aimed towards matching the parameters of the two steel programs to make an accurate assessment of the centrifuge as a tool for this work. While the difference in material properties between the aluminum and steel will hinder a quantitative comparison, the results of the aluminum tests will still be compared to the steel tests observing trends in the data sets. Only aluminum tests from test series 6 will be compared as that test series has the most comparable conditions to the steel tests, 80%RD soil and 5%SMYS internal pressure.

Both centrifuge programs were carried out at the C-CORE centrifuge center using much of the same equipment, strong boxes, actuators and instrumentation. The C-CORE full-

scale facility, where the steel pipes at full-scale were tested, is situated in the building that adjoins the centrifuge facility. As a result much of the equipment is shared, displacement transducers, similar data acquisition systems, similar strain gaging techniques and so on. Calibration of the various sensors, in all the programs was carried out using standard practices of the C-CORE centrifuge center.

In the three test series instrumentation included strain gages, ovalization sensors, load cells and displacement transducers. The pipes were strain gaged so that in prototype conditions the gage locations in each test series were comparable. Strain measurements are taken at the pipe mid-length (point of loading) and at 256 mm (10.1") from the longitudinal midpoint. The aluminum 2024-T3 tube used in the first program had a 1 1/8" outside diameter (15.98" full-scale) and a D/t ratio equal to 40.2. The full-scale steel pipe was a 16" outside diameter and a D/t ratio of 42.7. The steel model pipe had an outside diameter of 1.69" (16" full-scale) and a D/t of 42.3. The pipes in the three test programs had experimentally determined yield strengths of 310 MPa for the aluminum pipe, 345 MPa for the full-scale steel A106B pipe and 317MPa for the centrifuge A333 Gr6 steel pipe. Figure 6.7 shows the stress strain curves for the steel pipes used in the centrifuge and full-scale tests. The common cover depths tested from the three programs were 0.5D, 1.0D and 1.5D. The centrifuge aluminum pipes had ¼ D bedding while the other two programs used 1D sand bedding. Alwhite medium-fine sand (#00), was used in the three programs, the sand and the sand preparation procedure is described in each respective chapter. Sand densities were comparable in the three programs with averages

of 81%RD for the centrifuge aluminum program, 82%RD for the full-scale program and 73%RD for the centrifuge steel program. This minor discrepancy in producing exact geotechnical conditions (82% versus 73%) does not have a significant effect on the experimental program success.

6.2.2 Comparison of Load Pad Penetrations

See Figure 6.8 and Figure 6.9, for plots of the load pad penetration and displacements for the three tests. These plots commonly show a steady increase of load with penetration, then the surface load remains constant while load pad penetration increases because of soil failure beneath the pad (when the load reaches the bearing capacity of the pad). The consistent load displacement response, most notable in the centrifuge and full-scale steel tests, demonstrates that soil conditions in various tests were well controlled. There is a difference in initial loading showing a stiffer response from the full-scale sand, consistent with it being slightly denser. In tests full-scale tests 1, 2 and 3 the load pad rotation maximums were 3.5°, 2.5° and 2.5° respectively. While in the steel centrifuge tests the rotation angles were from 2.5° to 8° from the horizontal. As previously stated this rotation does not affect the experimental results and was reasonably similar in each test.

6.2.3 Comparison of Transducer Response

The transducer response to surface load will be discussed for the three test programs, specifically the tests and transducers that are common to all. See Figure 6.10, Figure 6.11 and Figure 6.12 for plots of the hoop strain gradients (centerline), the hoop strain

gradients (off centerline) and the ovalization gradients versus cover depths. The legend in these plots contains the labels CT-Al for the centrifuge aluminum tests, FS-St for the full-scale steel and CT-St for the centrifuge steel tests. As discussed previously although the pipe response to surface load is not perfectly linear, fitting lines to the data and generating these gradients provides an effective method to compare the data from multiple tests. Such plots for the other pipe transducers are included in Appendix E. As can be seen in the figures there is good agreement in the transducer response in each of the test programs in terms of magnitude and trend. Crown hoop strains show excellent agreement as do haunch hoop and ovalization. The axial strain gages at the invert show the greatest error.

Also included in Appendix E is a series of plots each showing the response of a different transducer at the three soil covers in the centrifuge and full-scale tests. These plots serve as second method (to the gradients) to compare the data from the full-scale and centrifuge steel pipe tests. Two of these plots are shown in Figure 6.13 and Figure 6.14 for the hoop crown centerline strains and the crown ovalization. Examination of these plots show that the centrifuge strain and ovalization response to load is always larger than it is in the full-scale tests. This means that the response of the pipe at full-scale is stiffer than at the centrifuge scale. This can be explained by bedding differences, denser therefore stiffer sand in the full-scale bed, differences in the deflection lag factor (time effects) and slight differences in cover depth.

As discussed in Chapters 4 and 5 the transducer response (strains and ovalizations) versus load plots for each of the tests contain hysteresis loops. These loops are a result of the plastic accumulation of stress in the soil, exerting stress on the pipe after the surface load is removed. This can be seen when the strain in the pipe does not return to zero when the load is removed, the next load cycle (loop) starts at an offset from zero. This offset shows that the soil behaves inelastically, since the pipe strain remain in the steel's elastic range. The strain offsets when the load is removed from the soil are similar in both the full-scale and centrifuge tests.

Percent difference calculations of the full-scale response to the centrifuge response show several trends. The percent difference is highest at low loads and when this pipe is at the highest load levels the comparison shows the least percent difference. Also the location of transducer effects the percent difference. The axial strain gages have an average of approximately 30% and 75% difference in the invert and crown respectively. The hoop strain gages have an average of approximately 45%, 20% and 75% difference in the invert, crown and haunch respectively. The ovalizations have an average of approximately 20% and 33% difference in the crown and haunch respectively. As presented in Chapter 2 differences between results of experimental programs of similar conditions are common and accepted. The pipe response in magnitude and in trends showed good comparison throughout this study. The trends in each test program and their differences and commonality will be discussed further in Chapter 7.

Table 6-1: SwRI Test Comparisons

	Soil Cover (D)	Soil Density (% relative density)	Pipe Pressure (%SMYS)	Comparison to:
SwRI 1	0.5	40	5	
SwRI 2	1.0	40	5	
SwRI 3	0.5	40	80	
SwRI 4	1.0	40	80	
T3B	0.5	40	5	SwRI 1 in Fig. 6.1
T3C	1.0	40	5	SwRI 2 in Fig. 6.1
T2B	0.5	40	80	SwRI 3 in Fig. 6.2
T2C	1.0	40	80	SwRI 4 in Fig. 6.2
CT03A	0.5	80	0	SwRI 1 in Fig. 6.3
CT06D	1.0	80	0	SwRI 2 in Fig. 6.3
FS01	0.5	80	0	SwRI 1 in Fig. 6.4
FS03	1.0	80	0	SwRI 2 in Fig. 6.4

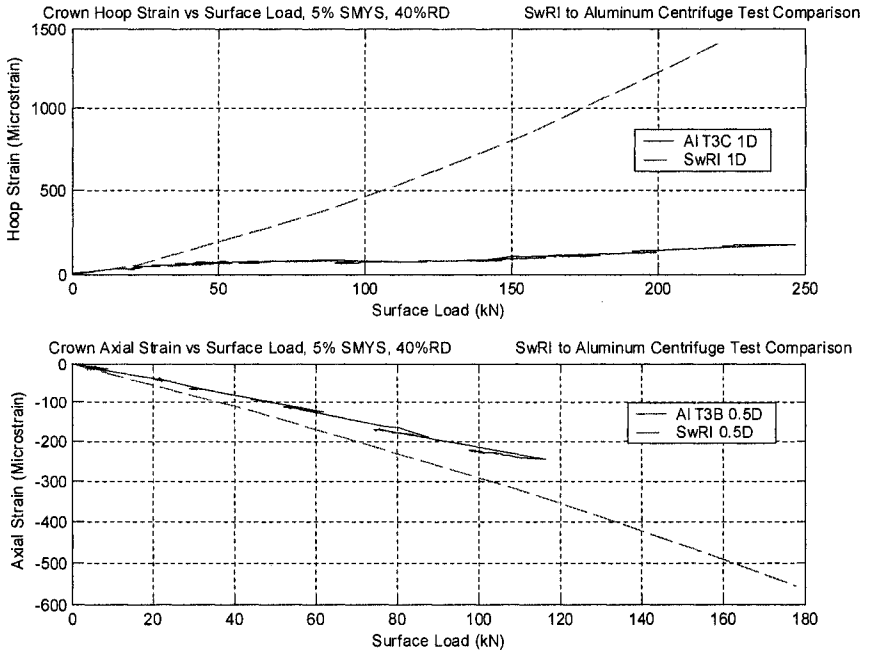

Figure 6-1: SwRI Comparison to Centrifuge Aluminum T3 Data

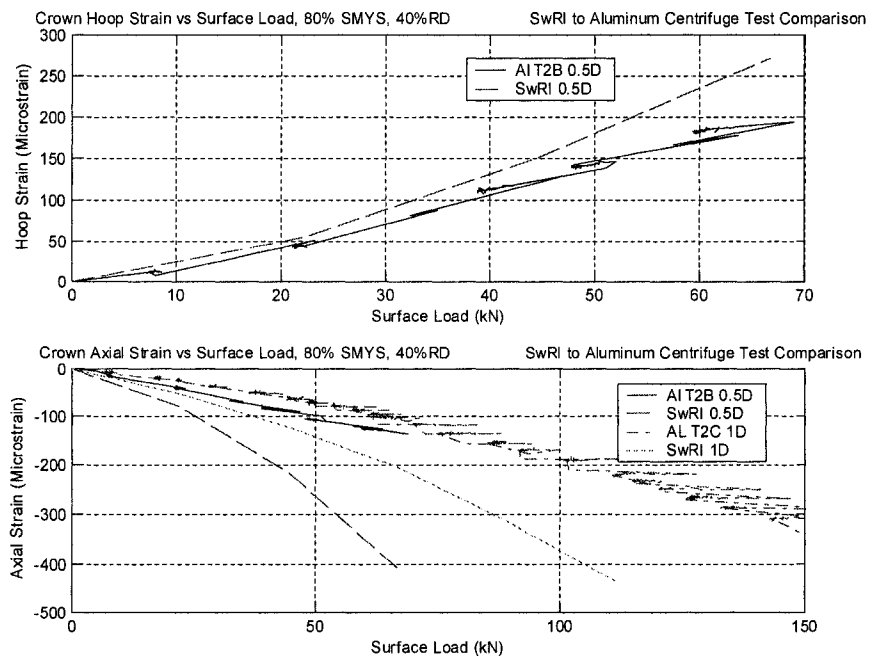

Figure 6-2: SwRI Comparison to Centrifuge Aluminum T2 Data

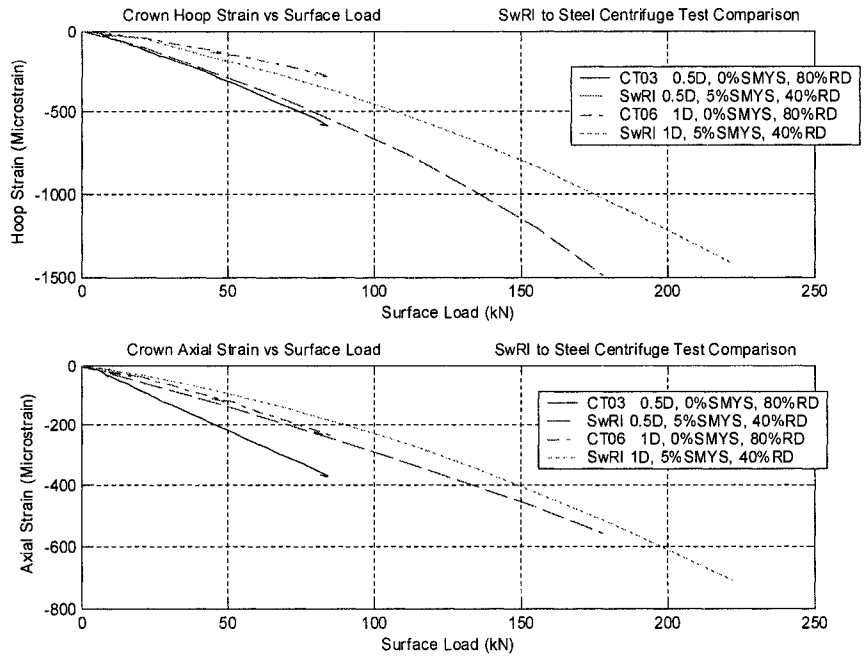

Figure 6-3: SwRI Comparison to Centrifuge CT03 and CT06 Data

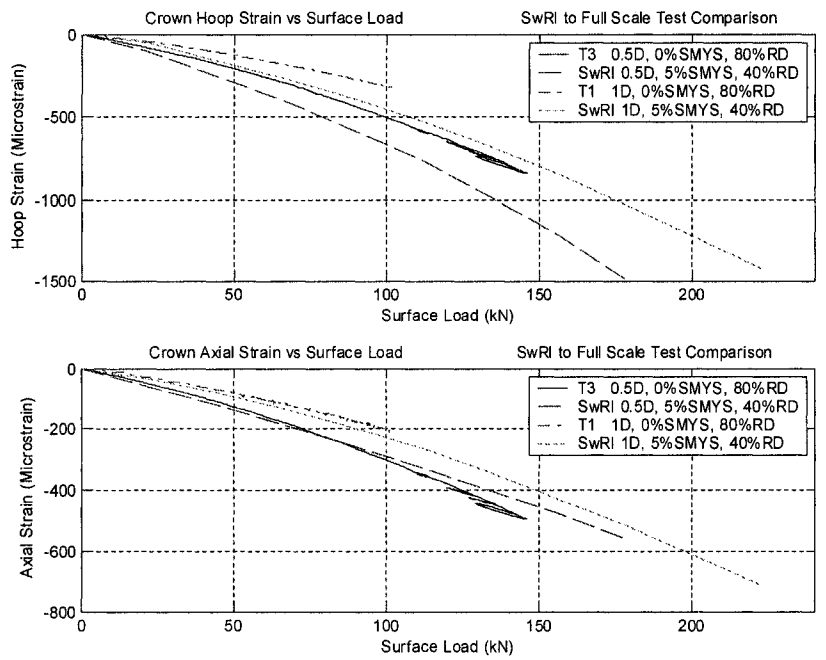

Figure 6-4: SwRI Comparison to Full-Scale T1 and T3 Data

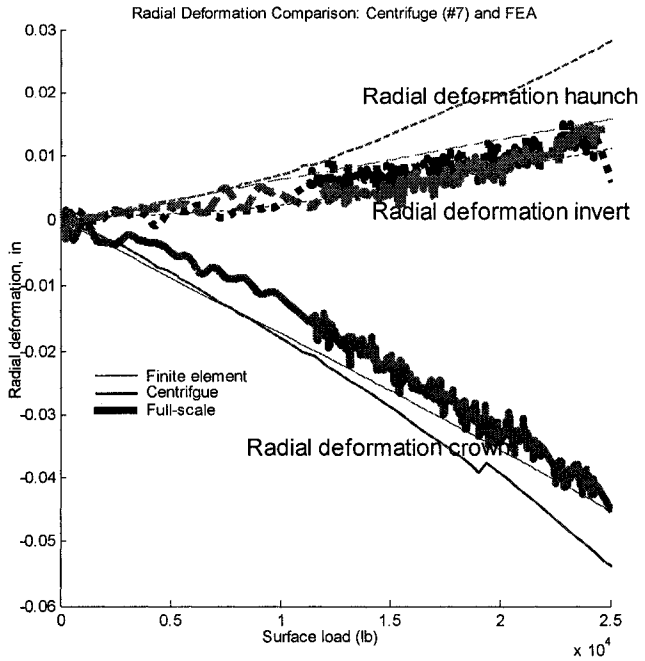

Figure 6-5: Full-Scale, Centrifuge and FEA Ovalization Comparison (C-CORE, (2005))

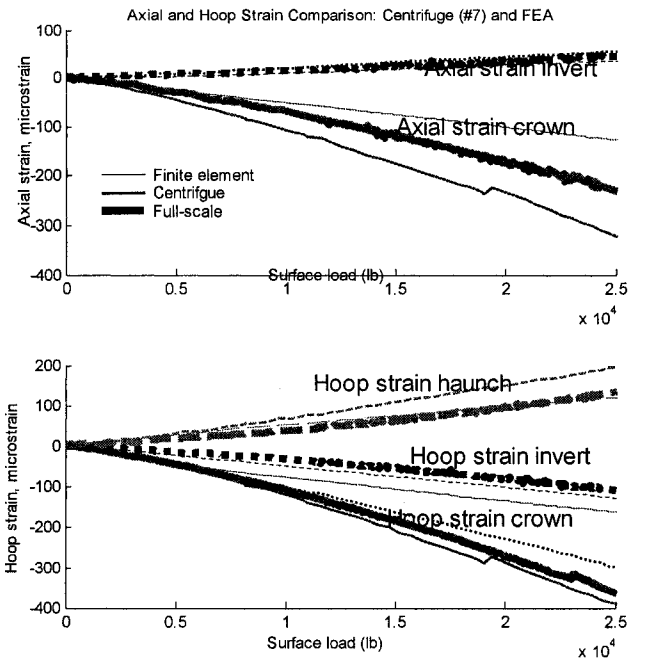

Figure 6-6: Full-Scale, Centrifuge and FEA Strain Comparison (C-CORE, 2005)

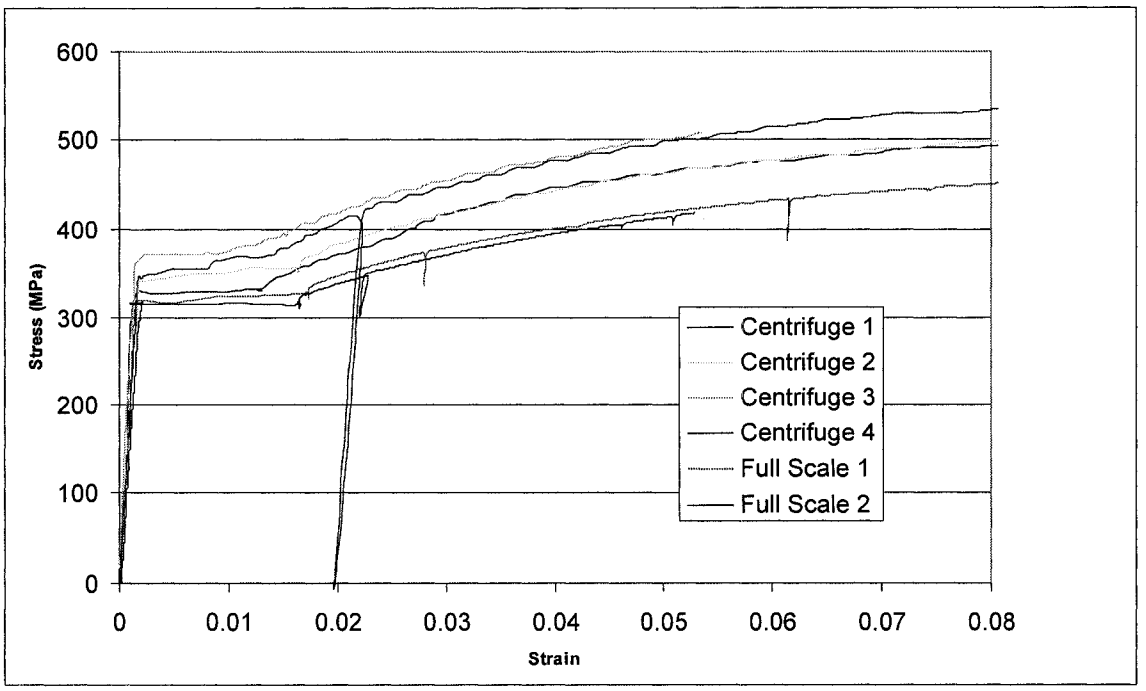

Figure 6-7: Steel Pipe Material

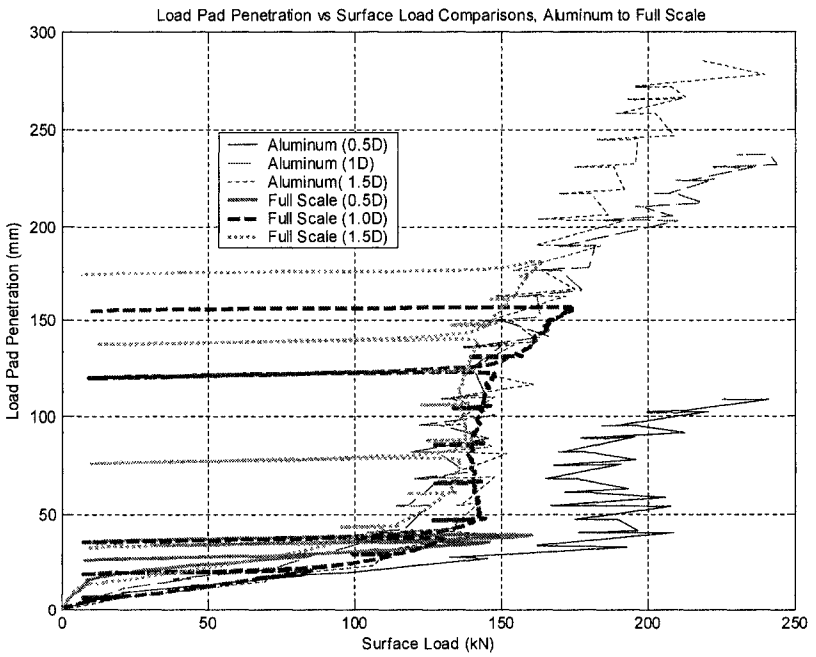

Figure 6-8: Pad Penetration vs. Surface Load Comparisons, Aluminum to Full-Scale

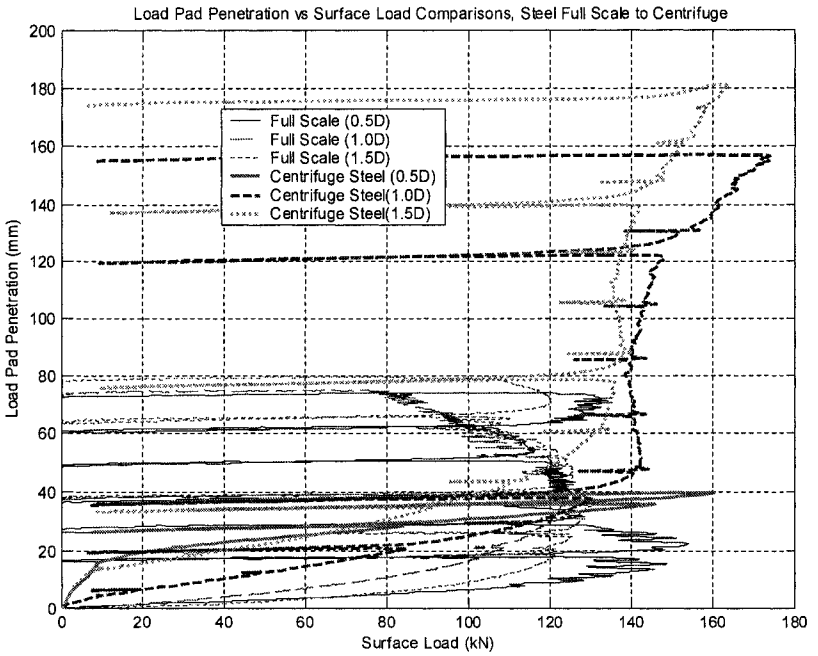

Figure 6-9: Pad Penetration vs. Surface Load Comparisons, Steel Full-Scale to Centrifuge

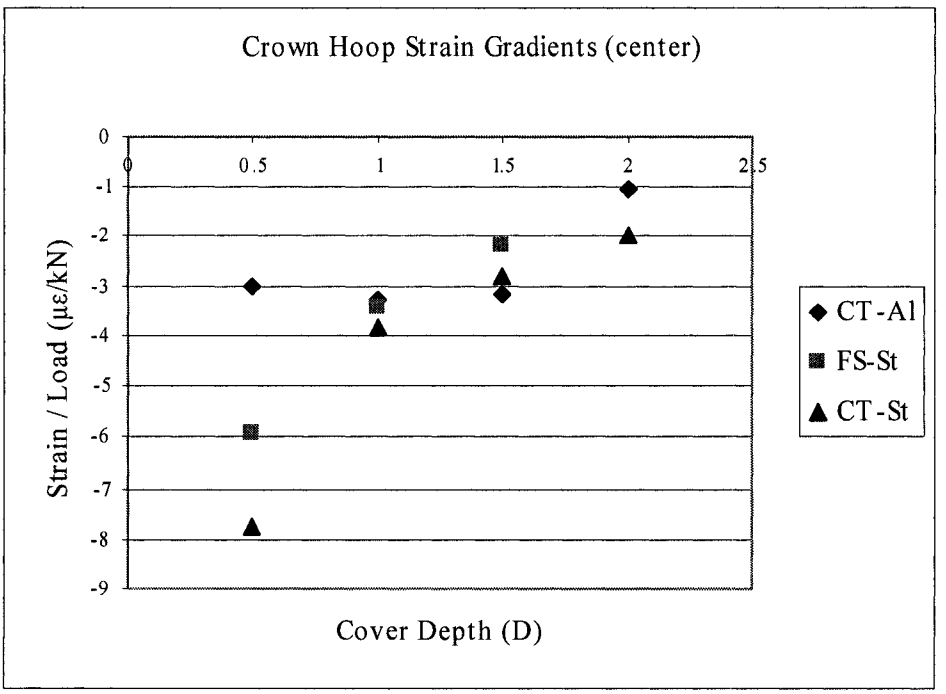

Figure 6-10: Crown Hoop Strain Gradients

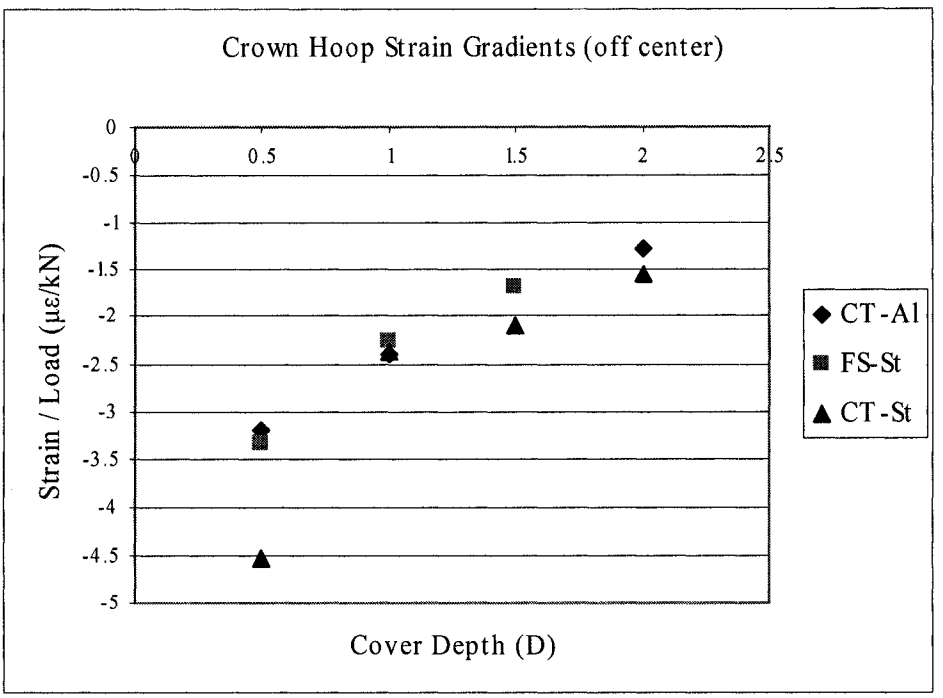

Figure 6-11: Crown Hoop Strain Gradients (Offset)

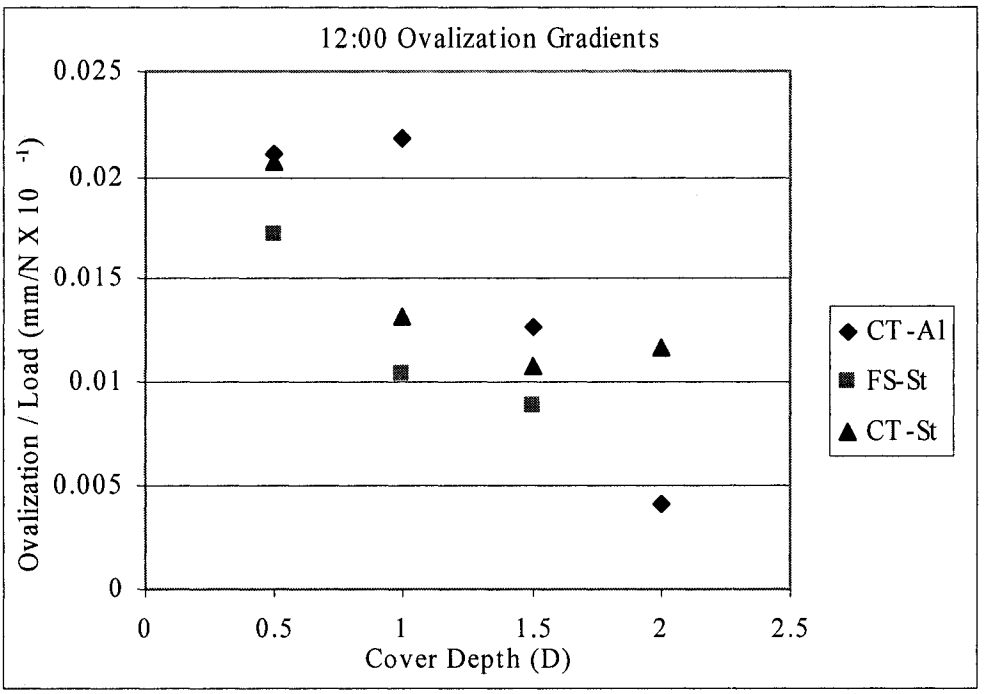

Figure 6-12: Ovalization Gradients

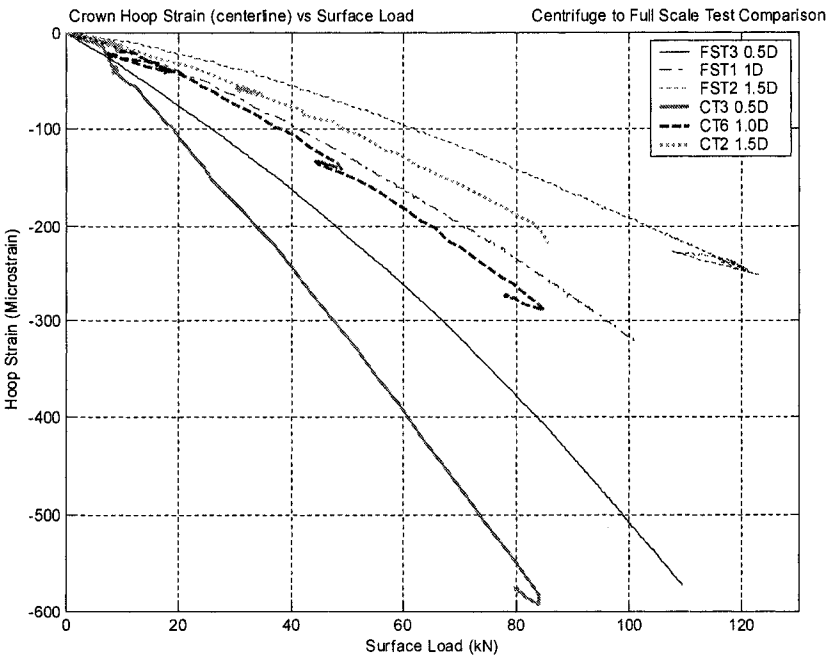

Figure 6-13: Crown Hoop Strain (Centerline) Comparison, Full-Scale to Centrifuge

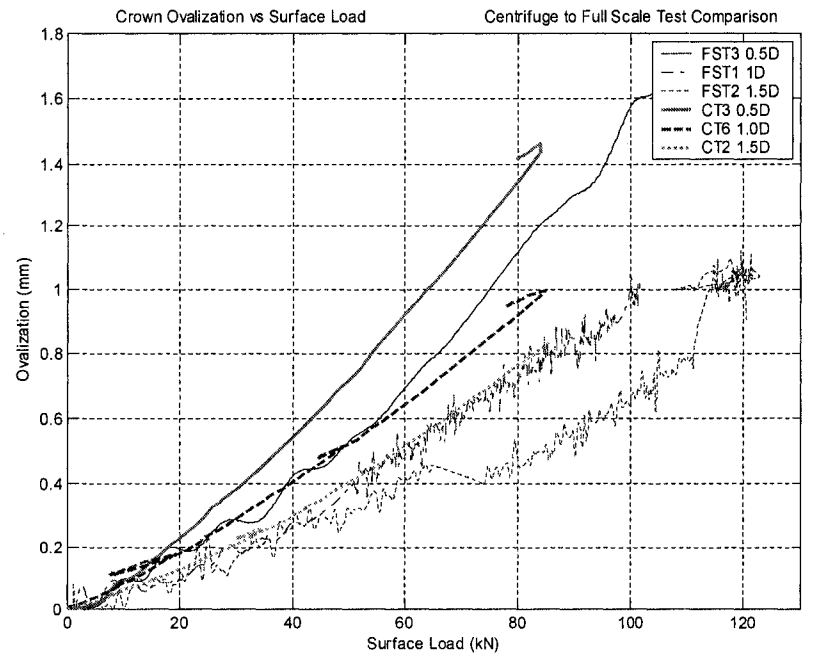

Figure 6-14: Crown Ovalization Comparison, Full-Scale to Centrifuge

7.0, Conclusions

The three test programs described in this thesis combined with the descriptions of similar work has validated centrifuge model testing as an effective method to evaluate the mechanical response of a buried steel pipe subject to non-typical surface loads. The work has shown that centrifuge modeling can be used as a replacement for or ideally in combination with full-scale and finite element analysis to study the effect of heavy equipment encroachment on buried pressurized pipes.

Comparisons of the test data to other full-scale, centrifuge and finite element analysis studies showed the consistency and quality of the data sets. The three test programs exhibited consistent trends, across the range of parameters for comparable test conditions, in terms of soil deformation mechanisms, surface pad load displacement behavior, and pipeline mechanical response. Any differences seen in the data sets, full-scale when compared to centrifuge, are typical to any study where several variables have an effect on the results. The study of the effect of surface loads on buried pipes is a soil/structure interaction problem. Any such problem is statically indeterminate, such that it must be recognized that when the pressure of the soil on the structure produces deflections in the structure, the structure in turn determines that soil pressure. Small variations in soil properties, pipe properties and dimensions, loading configurations, pipe bedding and cover can effect this soil/structure interaction and produce variations in the results.

Other than the applicability of centrifuge modeling to this type of study several conclusions can be drawn from this work.

The pipeline response is elastic based on the strain gage and ovalization transducer measurements. In all symmetrical loading tests, ovalization, hoop and axial strains decrease with an increase of cover depth except for the axial strain at the invert. Invert axial strains tended to be small and varied little with changing cover. One possible cause for this trend is that the soil failure in a similar manner in all tests, inducing similar bending in the pipe.

The soil behavior can be defined as nonlinear based on the relationship between the applied surface load and load pad displacement. There was some discrepancy between the full-scale and centrifuge tests for the load penetration response during the initial phases of loading event. This could be explained by slight differences in density or some unseen event in the initial bedding of the pad in the centrifuge. The unloading and reloading cycles carried out later in the tests show the soil behavior is consistent.

In general, an increase in soil density reduces or maintains the pipe strains and ovalizations. For 5% SMYS the soil density had little effect in the pipe strains and deflections. Decreases in axial strains are seen in the 80% SMYS tests when soil density in increased. Crown hoop strains tend to increase with soil density. Axial crown and invert hoop see little effects from the soil density variation.

The pipe internal pressure significantly increases the pipe stiffness. The ovalization mode changes with internal pressure. At 80% SMYS there is negligible diametral deflection of the pipe while at 5% SMYS there are small inward deflections of the pipe crown and outward deflections of the pipe haunch. Crown and invert (more so crown) hoop strains increase significantly with the decrease in pressure in 40% soil density tests and marginally in 80% soil density tests. In 40% relative density test bending strains (axial invert) reduce significantly with pressure increases but in 80% relative density sand these reductions are less prevalent. These observations can be attributable to the pipe and soil stiffness ratios in each case.

An increase in load offset, asymmetric loading, results in a reduction of strains and ovalizations. Invert hoop strain gradients are negligible. The axial strain from the longitudinal bending moment in the pipe decreases with increasing load offset. The crown hoop strain response becomes compressive with asymmetric loading, versus the typical tensile response during symmetric loading in the aluminum test program (internal gaging).

For symmetric loading, steel tests, hoop strains are negative (compression) at crown and invert and positive (tension) at haunches. These strains are larger in the mid section of the pipe. Axial strains are compressive at the crown and tensile at the invert. Two main modes of pipe deformation were identified under surface loading, ovalization of the pipe cross-section and bending in the long section. The ovalization mode was not associated

with the traditional elliptical pipe shape. The pipe crown deflected significantly with smaller deformations of the pipe haunch. The haunches, 3:00 and 9:00 pipe positions, deflected outward, indicating tension, under surface loads. At the pipe crown deflections were opposite in sign, inward deflections (hoop compression) and much larger in magnitude to the haunch. In the tests where the invert ovalization was measured deformations were small. The axial strain response is dominated by longitudinal deformation at the pipeline crown (compressive) with a limited axial strain response to load at the pipeline invert (tensile). These axial strains result from the bending strains and the Poisson's effect associated with the pipe crown and invert compressive hoop strains. This longitudinal deformation appears to be governed by longitudinal bending action that is local to the pipeline crown with a limited global bending response.

8.0, Recommendations

The three studies presented in this thesis prove the centrifuge as a valid tool in the study of the mechanical response of buried pipes to surface loads. This work leads to several recommendations for future studies.

The FEA work by C-CORE, (2005) compared well to the full-scale and centrifuge data sets. Using such an analysis procedure a parametric sensitivity analysis could be carried out, determining a list of the most critical parameters to be varied and studied. The parameters varied could include pipe diameter, D/t ratios, pipe material properties, internal pressure, pipe cover depth, geotechnical properties of native and backfill soil conditions for frictional and cohesive material, and load configuration. Load configuration variation could include pad geometry (i.e. tracked vehicles), load distribution, load magnitude and position relative to the pipe (asymmetric loading).

Added instrumentation in the pipes would be useful to study the effect of asymmetric loads and also in understanding the haunch deformation under symmetric loads. Strain gages and ovalization sensors at the 1:30 position would be a beneficial addition.

The parametric sensitivity analysis could aid in the formulation of a test matrix of tests to be carried out in the centrifuge varying several of the parameters above and expanding the knowledge base of the mechanical response of buried pipes to surface loads.

9.0, References

American Water Works Association Manual of Water Supply Practice, Steel Pipe a Guide for Design and Installation, (1989). 3rd Edition.

API 1102 (1993). "Steel Pipelines Crossing Railroads and Highways."

ASTMA 370 (1997). Standard Test Methods and Definition for Mechanical Testing of Steel Products. March 1997.

Bulson, P. S. (1985). "Buried structures: static and dynamic strength". London; New York: Chapman and Hall.

C-CORE (1999). Finite Element Analysis of Pipe/Soil Interaction Phase 1 – Two-Dimensional Plane Strain Analyses – Final Report. Report for, Geological Survey of Canada, C-CORE Report Number 99-C23, June 1999.

C-CORE (2001). Modeling Long-Term Pipe/Soil Interaction – Phase I. Report for Geological Survey of Canada, Snam S.p.A, Tokyo Gas Co. Ltd., Trans Canada PipeLines Ltd., Westcoast Energy Inc., C-CORE Report Number 00-C32, March 2001.

C-CORE (2002). Centrifuge Modeling of Pipeline Stress Due to Heavy Equipment Encroachment. Report for, Gas Research Institute (GRI), GRI Contract Number 8442, C-CORE Report Number R-02-018-609, November 2002.

C-CORE (2003). Extended Model for Pipe Soil Interaction. Prepared by C-CORE and D.G. Honegger Consulting. Report for, Design, Construction & Operations Technical Committee, Pipeline Research Council International, Contract PR-271-0184, Catalog Number L51990, August 2003.

C-CORE (2003b). Centrifuge and Full-Scale Modelling Comparison for Pipeline Stress Due to Heavy Equipment Encroachment, Prepared for GRI. C-CORE Publication R-03-065-219, December 2003.

C-CORE (2005). Additional Experimental Modeling of Pipeline Stress Below Heavy Equipment Encroachment Over Pipeline Right of Ways, C-CORE, Contract PR-271-0184, Pipeline Research Council, International, Inc.

Chambers, R. F., McGrath, T. J., and Heger, F. J. (1980). ''Plastic pipe for subsurface drainage of transportation facilities.'' National Corporative Highway Research Program, Transportation Research Board Rep. No. 225, 122–140.

Faragher, E., Rogers, C.D. and Fleming, P.R. (1998). "Laboratory Determination of Soil Stiffness Data for Buried Plastic Pipes", Transportation Research Record 1624, 231-236.

Fernando, N.S.M. and Carter, J.P. (1998). "Elastic analysis of buried pipes under surface patch loading". ASCE Journal of Geotechnical and Geoenvironmental Engineering, 124(8), pp 720-728.

Fourie, A.B. and Beer, G. (1988). "The importance of the failure criterion in the analysis of buried pipelines". St. Lucia, Qld.: Department of Civil Engineering, University of Queensland.

Gerbault, Marcel (1995). A Soil Structure Interactive Model, Second International Conference Advances in Underground Pipeline Engineering, Bellevue Washington, Published American Society of Civil Engineers New York, 42-53.

Gumbel J.E. and Wilson, J. (1981). "Interactive design of buried flexible pipes- a fresh approach from basic principles". Ground Engineering, 36-40. London: IPC Business Press.

Hartley, D. and Duncan, J.M. (1987). "E' and its variation with depth". Journal of Transportation Engineering, 113(5), 538-553.

Howard, A.K. (1977). "Modulus of soil reaction values for buried flexible pipe". Journal of Geotechnical Engineering. Division. ASCE, 103(1), 33-43.

Howard, A.K. (1981). "The USBR Equation for Predicting Flexible Pipe Deflection". International Conference on Underground Plastic Pipe, Pipeline Division of the American Society of Civil Engineers, Schrock, B. Jay, Editor.

Jaramillo, P. A. (1989). ''Review of field deflections of plastic pipes under soil loads.'' MS thesis, Univ. of Wisconsin, Madison, Wis.

Jeyapalan, J.K. and Abdel-Magid, A.M. (1984). "Importance of pipe soil stiffness ratio in plastic pipe design." ASCE Convention, San Francisco, CA.

Jeyapalan, J. K., and Jaramillo, P. A. (1994). ''New modulus of soil reaction—E' values for buried thermoplastic pipe design.'' Proc., ASCE Conf. on Hydraulics of Pipelines, American Society of Civil Engineers, New York, 239–260.

Jeyapalan, J.K. and Watkins, R. (2004) "Modulus of Soil Reaction (E') Values for Pipeline Design". Journal of Transportation Engineering Volume 130, No 1, January 1, 2004, 43-48.

Kawabata, T. and Mohri, Y. (1995). "Behaviour of buried large thin wall flexible pipes – Field Test and Numerical Analysis considered with Stage of Construction of Buried Pipe". Second International Conference Advances in Underground Pipeline Engineering, Bellevue Washington, Published American Society of Civil Engineers New York, 13-24.

Konuk, I., Phillips, R., Hurley, S. and Paulin, M.J. (1999). "Preliminary ovalisation measurements of buried pipelines subject to lateral loading". 18th International Conference on Offshore Mechanics & Arctic Engineering, St. John's, July 1999, paper 99-5023.

Leonards, G.A., Juang, C.H., Wu, T.H. and Stetkar, R.E. (1985). "Predicting Performance of Buried Metal Conduits". Transportation Research Record 1008, 42-52.

Masada, T. (2000). "Modified Iowa formula for vertical deflection of buried flexible pipe." Journal of Transportation Engineering, ASCE, 126(5), 440-446.

Mohitpour, M., Golshan, H. and Murray, A, (2002). Pipeline Design and Construction, A Practical Approach, Second Edition, ASME Press.

Moore, I.D. (1987). "Response of buried cylinders to surface loads". ASCE Journal of Geotechnical Engineering, 113(7), pp.758-773.

Moser, A.P. (2001). "Buried pipe design". Second edition. New York; Toronto: McGraw-Hill.

Nobahar, A., Popescu, R., and Konuk, I. (2000). "Estimating progressive mobilization of soil strength." 53rd Canadian Geotechnical Conference, pp.1311-1317.

Popescu R., Phillips R., Konuk I., Guo, P. and Nobahar, A. (2002). Pipe-Soil Interaction: Large Scale Tests and Numerical Modelling. Proceedings of the International Conference on Physical Modelling in Geotechnics, St. John's, Newfoundland, Canada, July 2002, in ICPMG '02, editors R. Phillips, P. Guo and R. Popescu, Balkema, 917-922.

Potter, J.C. (1985). "Effects of vehicles on buried, high-pressure pipe." ASCE Journal of Transportation Engineering, 111(3), pp.224-236.

Prevost R.C. and Kinew, K.K. (1994). "Basics of flexible pipe structural design." Journal of Transportation Engineering, 120(4), pp.653-671.

Rajani, B. and Kuraoka, S. (1995). "Field Performance of PVC Water Mains Buried in Different Backfills". Second International Conference Advances in Underground Pipeline Engineering, Bellevue Washington, Published American Society of Civil Engineers New York, 138-149.

Rogers, C.D.F. (1985). "Some Observations on Flexible Pipe Response to Load". Transportation Research Record 1191.

Schluter, J.C., and Capossela, T.A. (1998). The suitability of Spangler's Iowa formula for predicting deflection in all flexible pipes. American Society of Civil Engineers, Pipeline Division Conference, San Diego, California, pp 14-27.

Schofield, A.N., (1980). "Cambridge geotechnical centrifuge operations". Geotechnique 30(3): 227-268.

Shafer, G. E. (1948). ''Discussion: Underground conduits - An appraisal of modern research.'' Trans. Am. Soc. Civ. Eng., 113, 354–363.

Sharp, K., Anderson, L.R., Moser, A.P. and Bishop, R.R. (1985). "Finite Element Analysis Applied to the Response of Buried FRP Pipe under Installation Conditions". Transport Research Record 1008.

Shmulevich, I., Galili, N., and Foux, A. (1986). "Soil stress distribution around buried pipes." ASCE Journal of Transportation Engineering, 112(5), pp.481-494.

Spangler, M.G., (1941). The Structural Design of Flexible Pipe Culverts, Iowa Engineering Experiment Station, Bulletin 153.

Spangler, M.G. and Handy, R.L. (1894). "Soil engineering". New York: Harper & Row.

Stone, K.J.L and Newson, T.A. (2002). "Arching Effects in Soil-Structure Interaction". Physical Modelling in Geotechnics, ICPMG '02, editors R. Phillips, P. Guo and R. Popescu, Balkema, 935-939.

Taylor, R.N. (Editor), (1995). Geotechnical Centrifuge Technology, First Edition Chapman & Hall, New York, 91-117.

Trott, J.J. and Gaunt, J. (1972). "Experimental work on large steel pipeline at Kirtling". Crowthorne, Berkshire: Transport and Road Research Laboratory, Department of the Environment, TRRL laboratory report.

Trott, J.J., Taylor, R.N. and Symons, I.F. (1984). "Tests to validate centrifuge modeling of flexible pipelines." The Application of Centrifuge Modeling to Geotechnical Design, W.H. Craig (ed.). Manchester, UK, pp.226-254.

Valsangkar, A.J. and Britto, A.M. (1979). "Centrifuge tests of flexible circular pipes subjected to surface loading". Crowthorne, Berkshire: Tunnels and Underground Pipes Division, Structures Dept., Transport and Road Research Laboratory.

Waldhart, C.J., Smith, M.Q. and Gailing, R.W. (2001). "Effects of surface loading conditions on buried pipelines." Pipeline Research, Paper Number 29. New Orleans, LA, USA.

Watkins, R.K., Reeve, R.R. and Goddard, J.B. (1983). "Effect of Heavy Loads on Buried Corrugated Polyethylene Pipe". Transportation Research Record 903, 99-108.

Watkins, R.K., and Spangler, M.G. (1958). "Some characteristics of the modulus of passive resistance of soil: A study in similitude". Proceedings Highway Research Record, Cincinnati, 576-583.

Young, O. C. and Trott, J.J. (1984). "Buried rigid pipes: structural design of pipelines". London: Elsevier.

Zhu, F., (1998). Centrifuge modelling and numerical analysis of bearing capacity of ring foundations on sand. Ph.D. thesis, Memorial University of Newfoundland.

Appendix A
Chapter 3 Plots
Surface Loading of Pressurized Aluminum Pipes in the Centrifuge

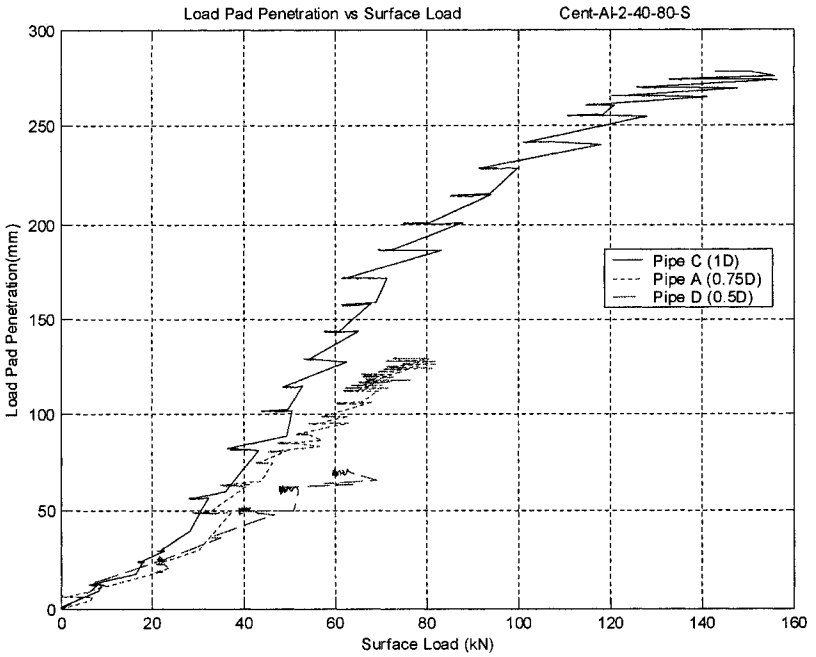

Figure A1: Load Pad Penetration versus Surface Load, Test 2

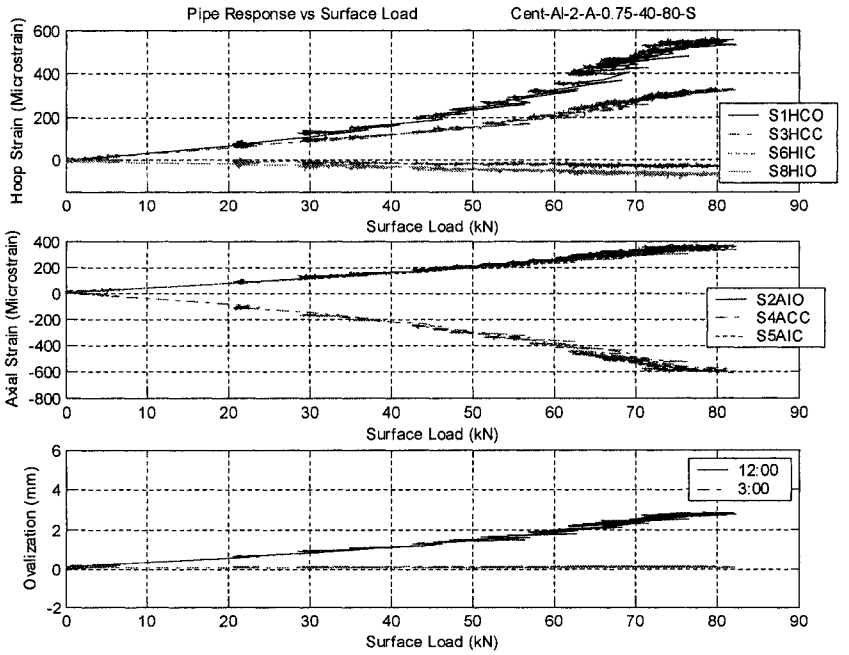

Figure A2: Pipe Response versus Surface Load, Test 2A

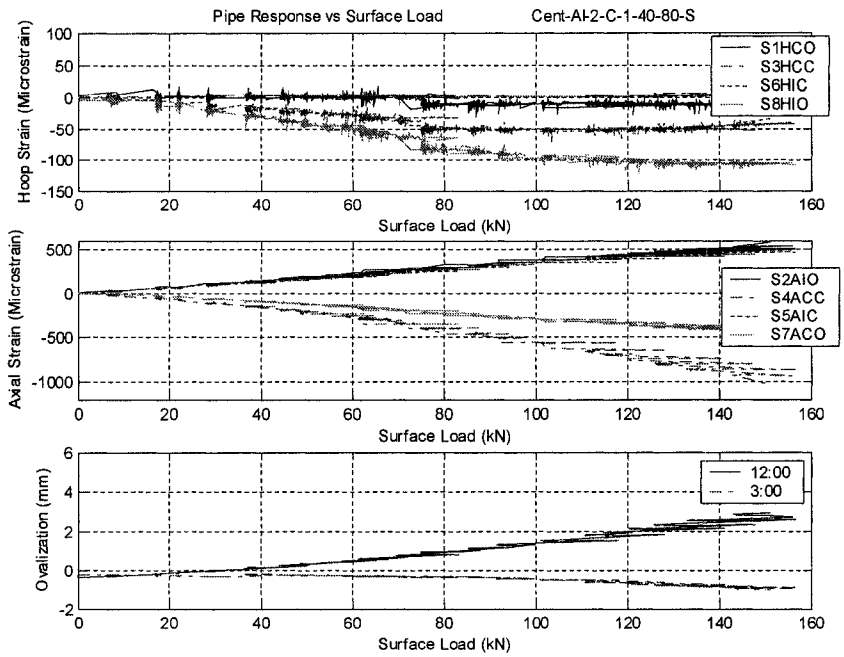

Figure A3: Pipe Response versus Surface Load, Test 2C

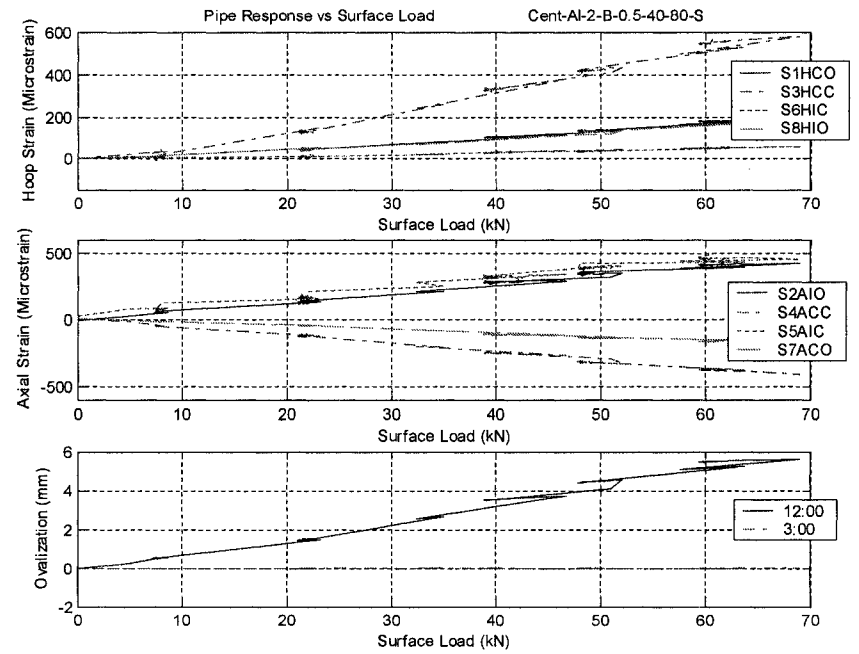

Figure A4: Pipe Response versus Surface Load, Test 2B

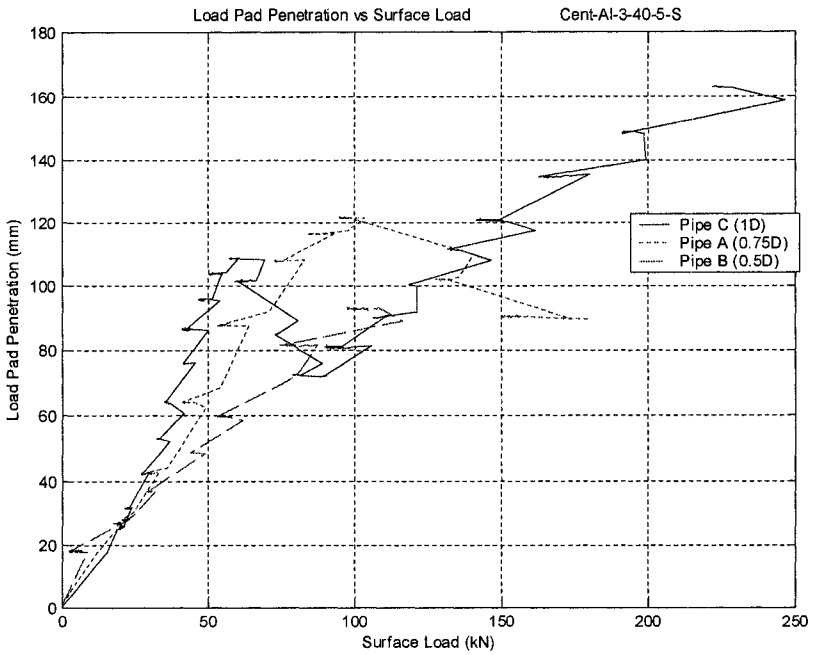

Figure A5: Load Pad Penetration versus Surface Load, Test 3

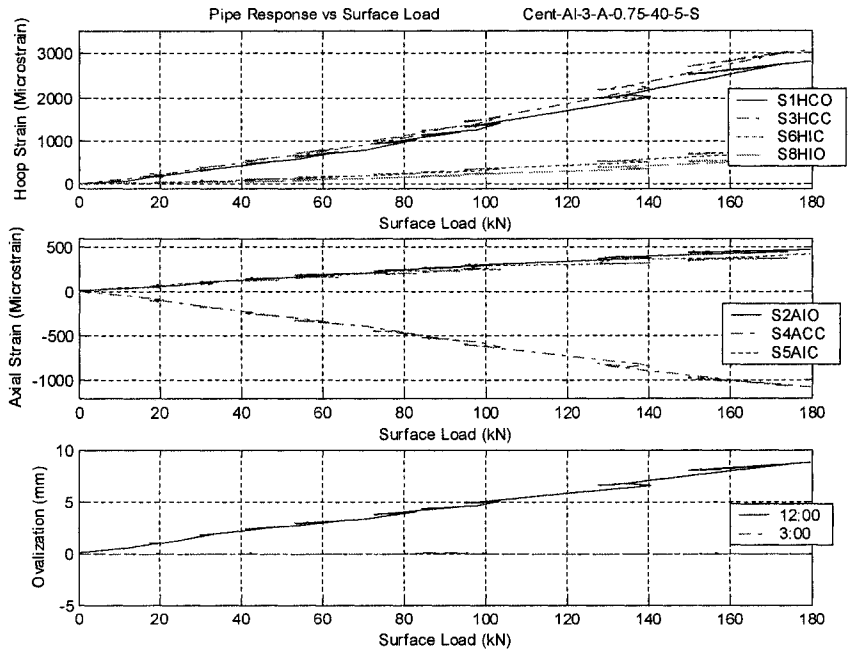

Figure A6: Pipe Response versus Surface Load, Test 3A

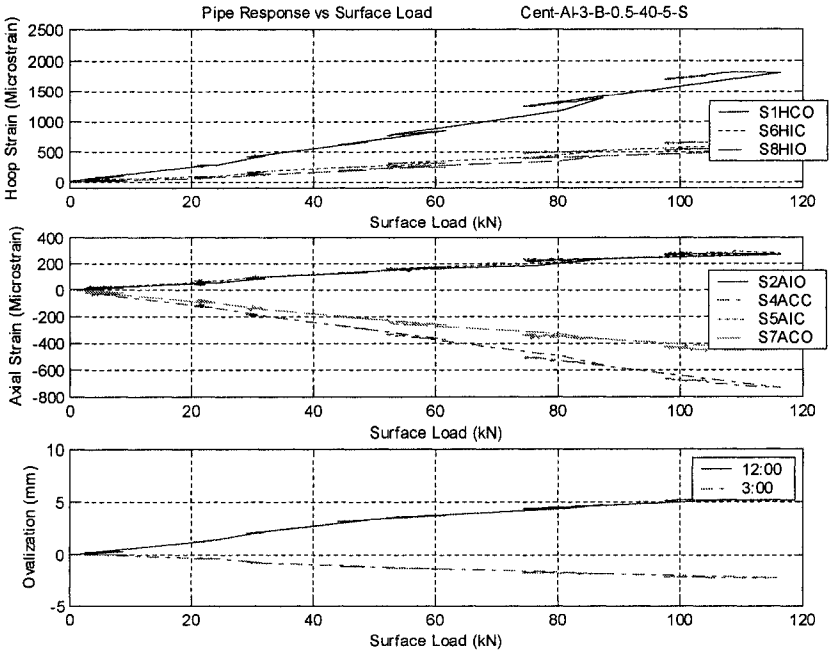

Figure A7: Pipe Response versus Surface Load, Test 3B

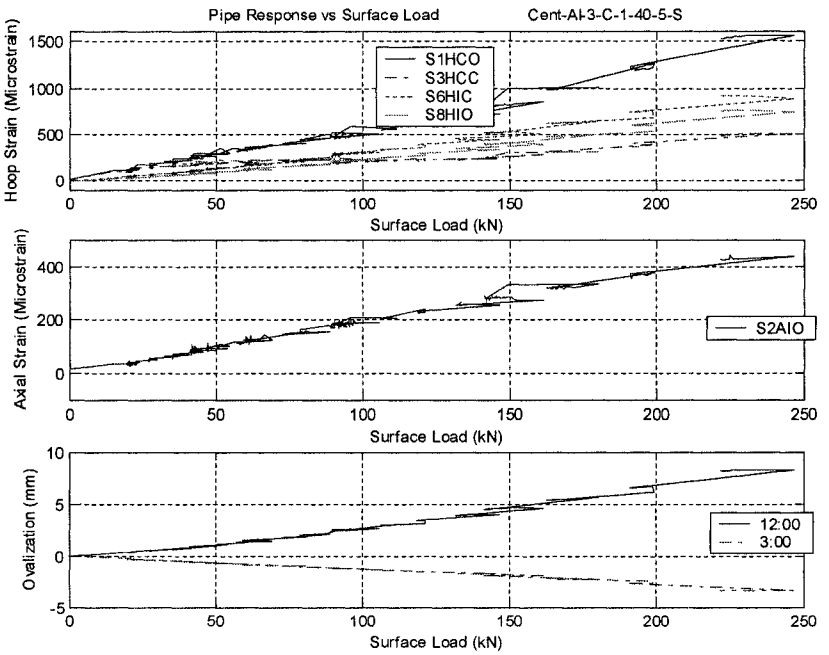

Figure A8: Pipe Response versus Surface Load, Test 3C

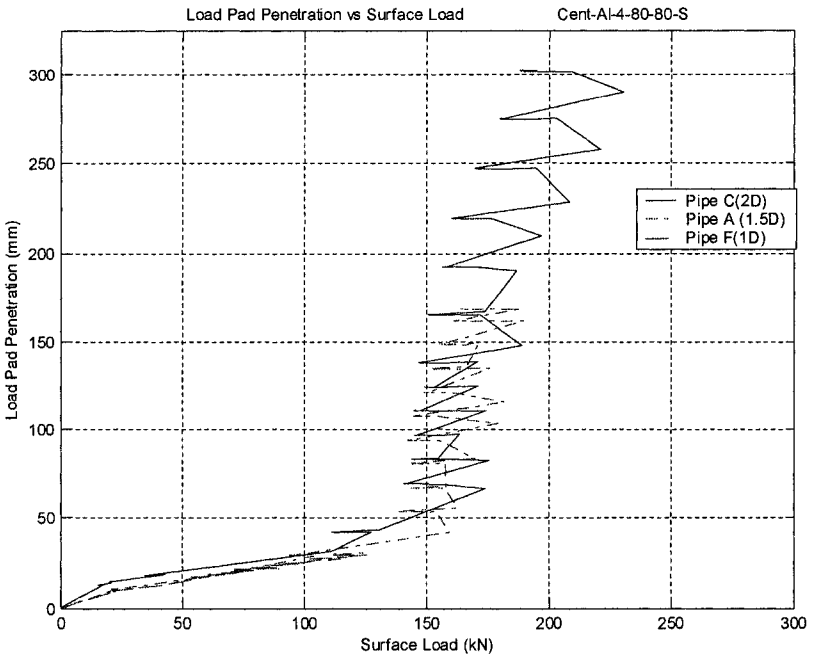

Figure A9: Load Pad Penetration versus Surface Load, Test 4, D, A, F

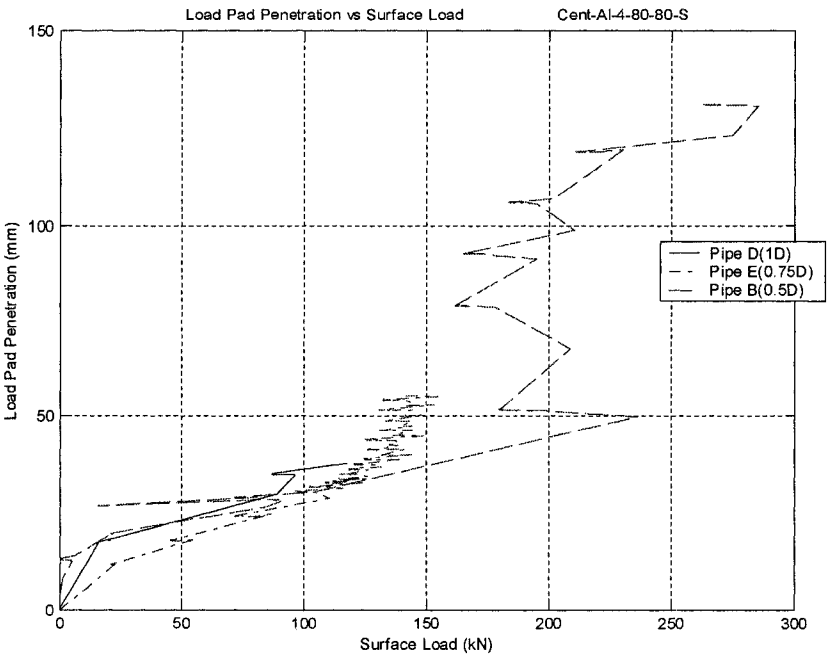

Figure A10: Load Pad Penetration versus Surface Load, Test 4, D, E, F

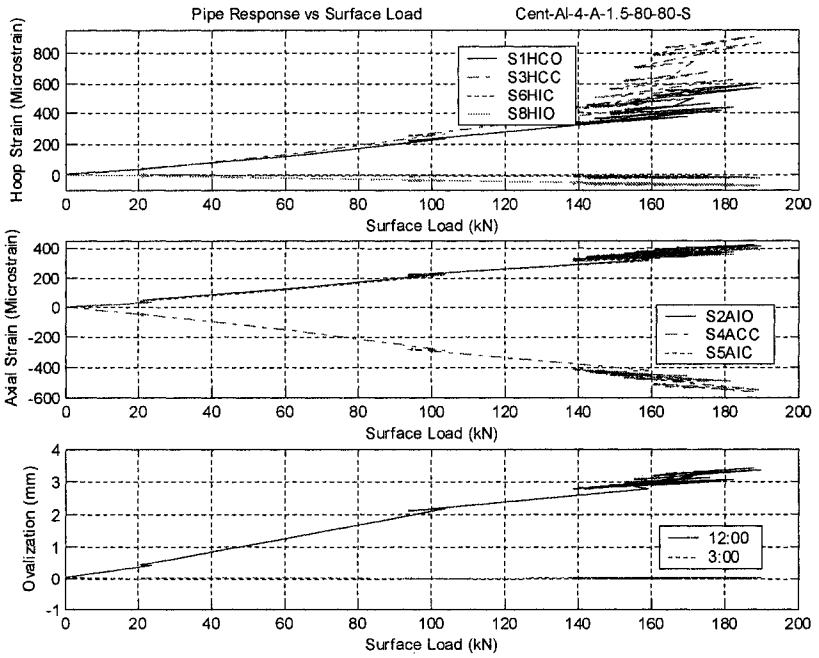

Figure A11: Pipe Response versus Surface Load, Test 4A

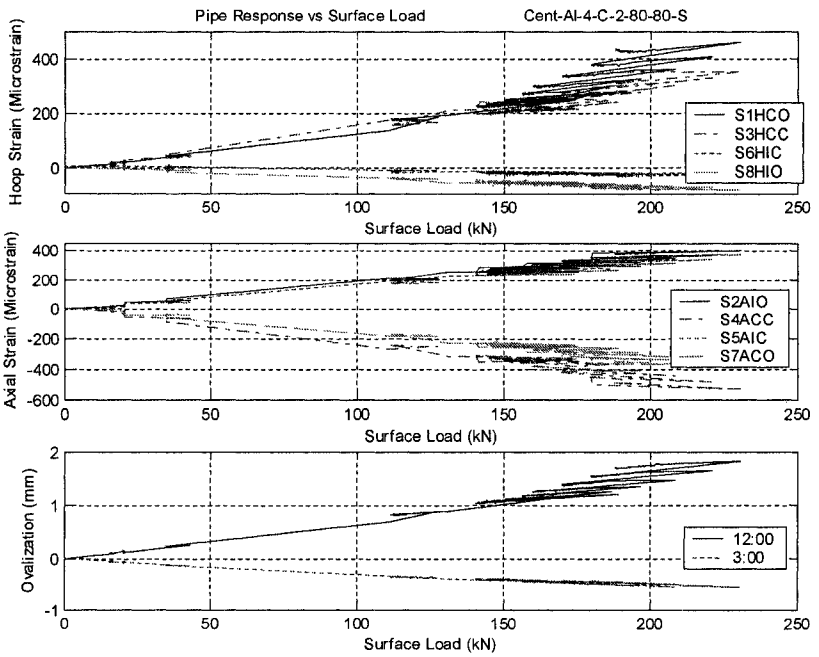

Figure A12: Pipe Response versus Surface Load, Test 4C

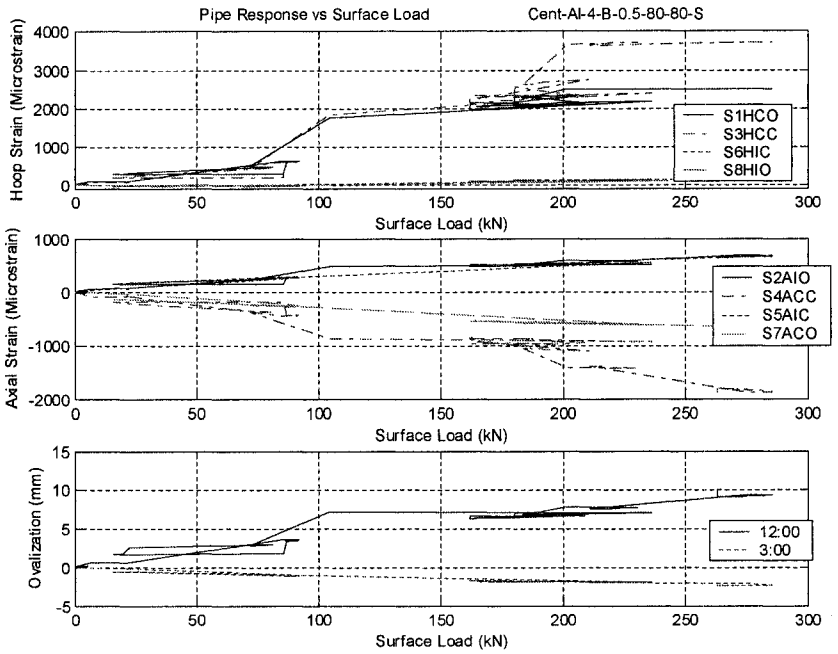

Figure A13: Pipe Response versus Surface Load, Test 4B

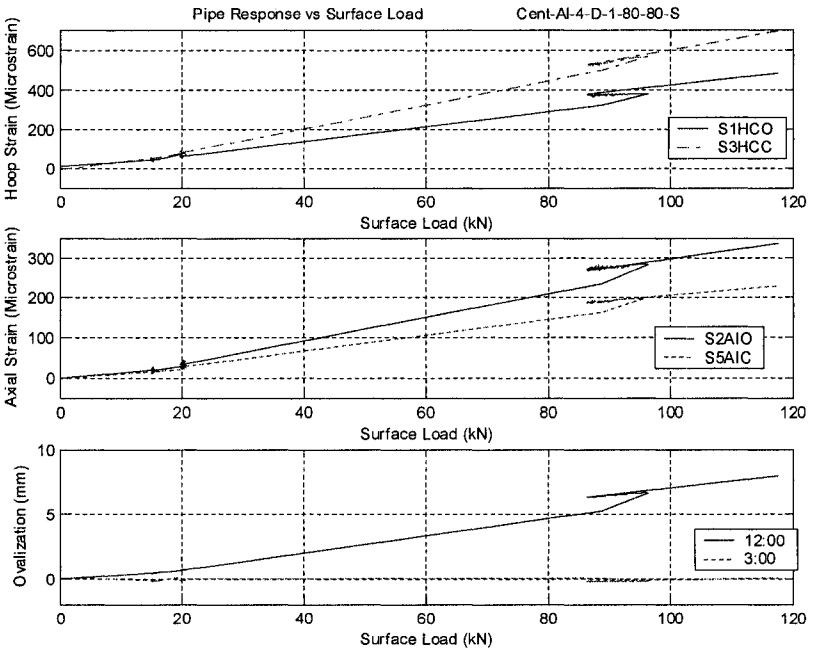

Figure A14: Pipe Response versus Surface Load, Test 4D

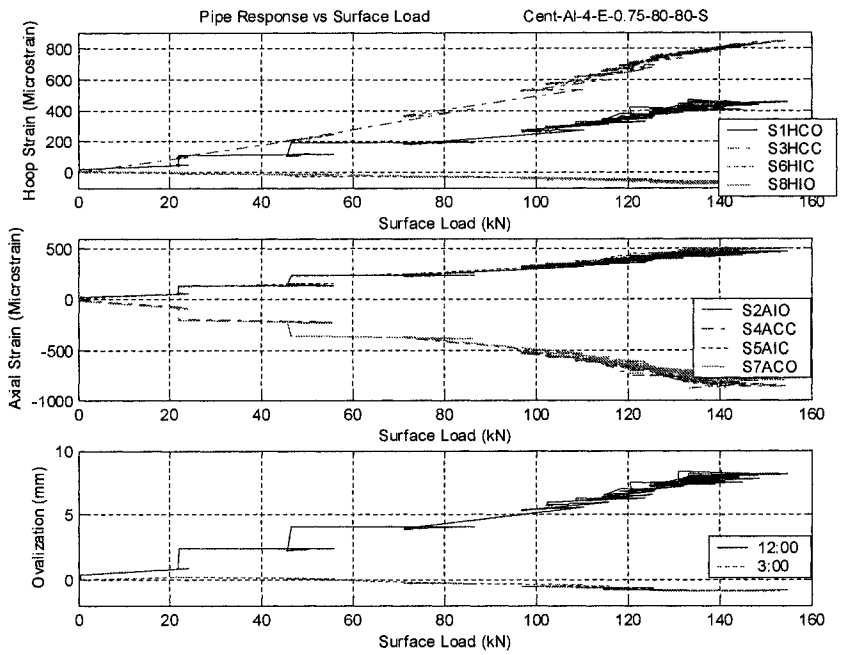

Figure A15: Pipe Response versus Surface Load, Test 4E

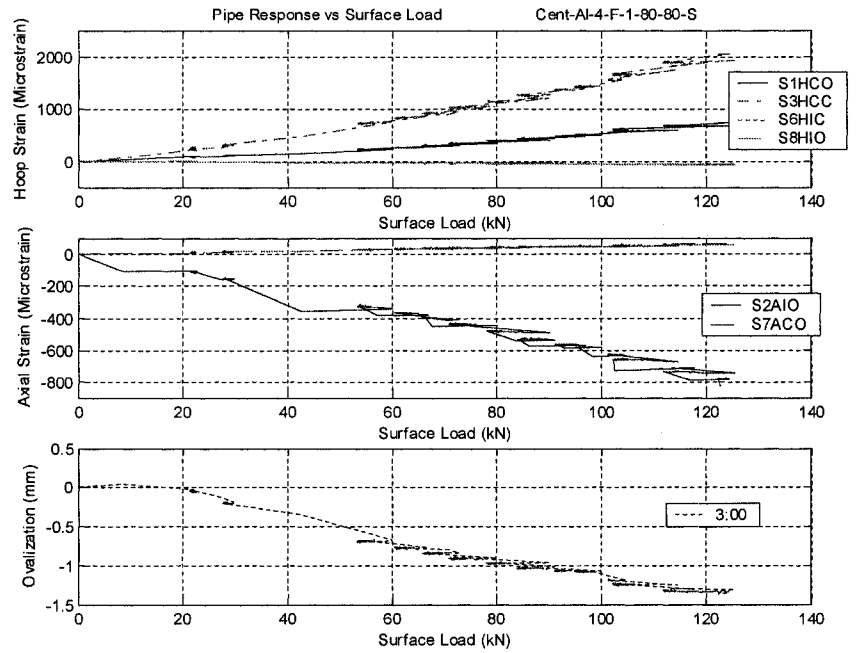

Figure A16: Pipe Response versus Surface Load, Test 4F

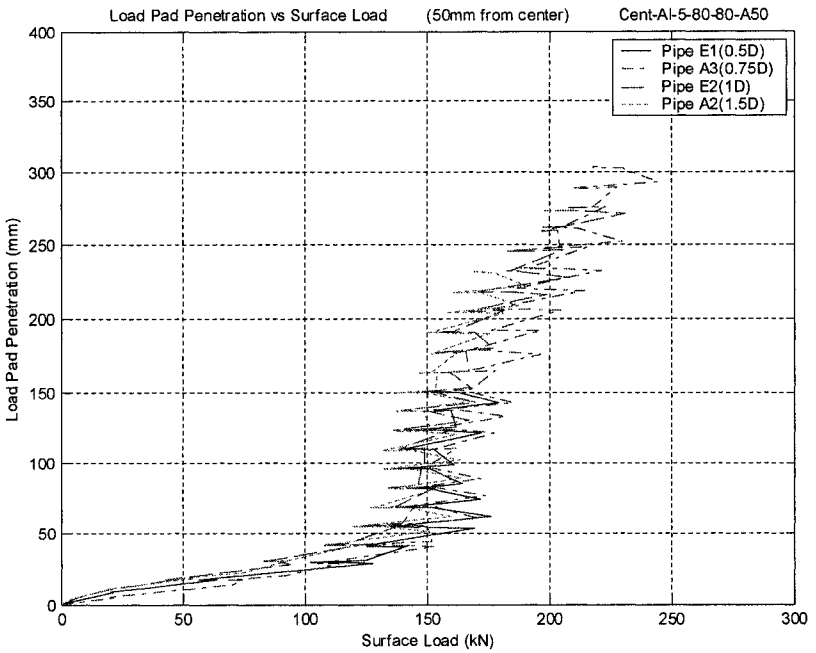

Figure A17: Load Pad Penetration versus Surface Load, Test 5, 50mm offset

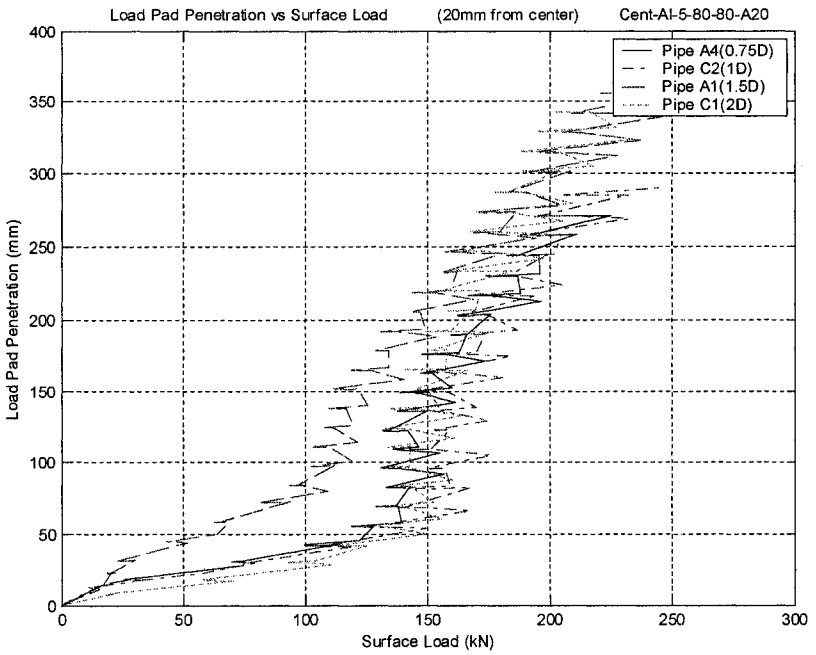

Figure A18: Load Pad Penetration versus Surface Load, Test 5, 20mm offset

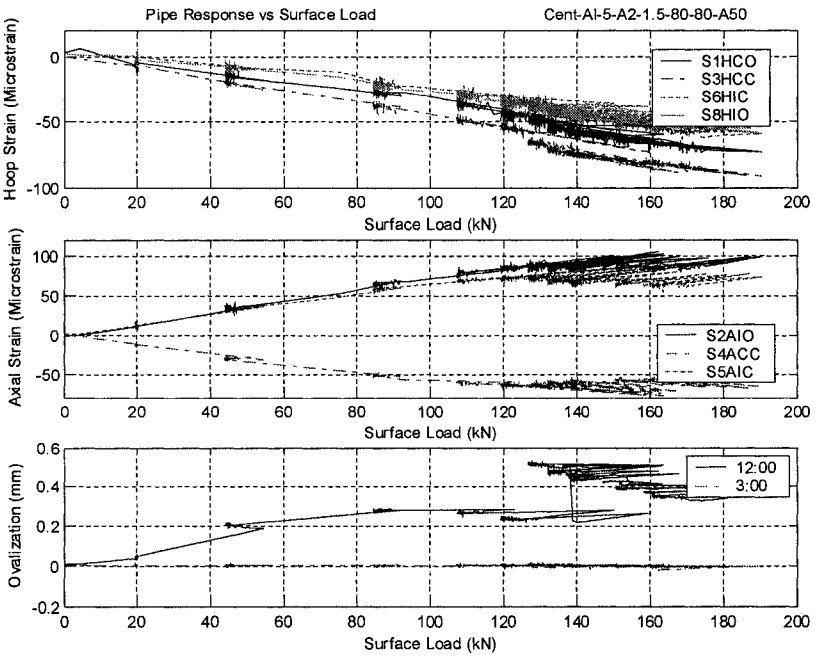

Figure A19: Pipe Response versus Surface Load, Test 5A2

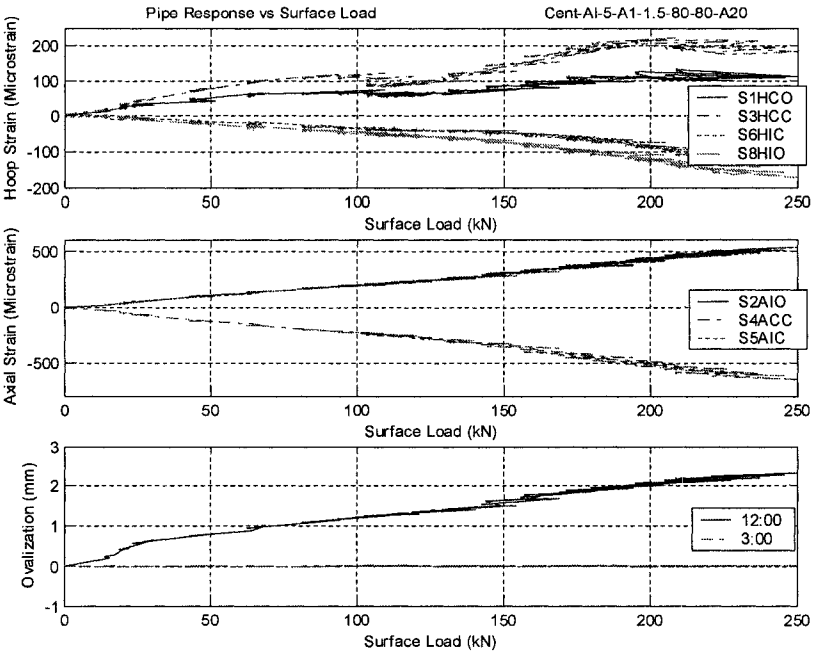

Figure A20: Pipe Response versus Surface Load, Test 5A1

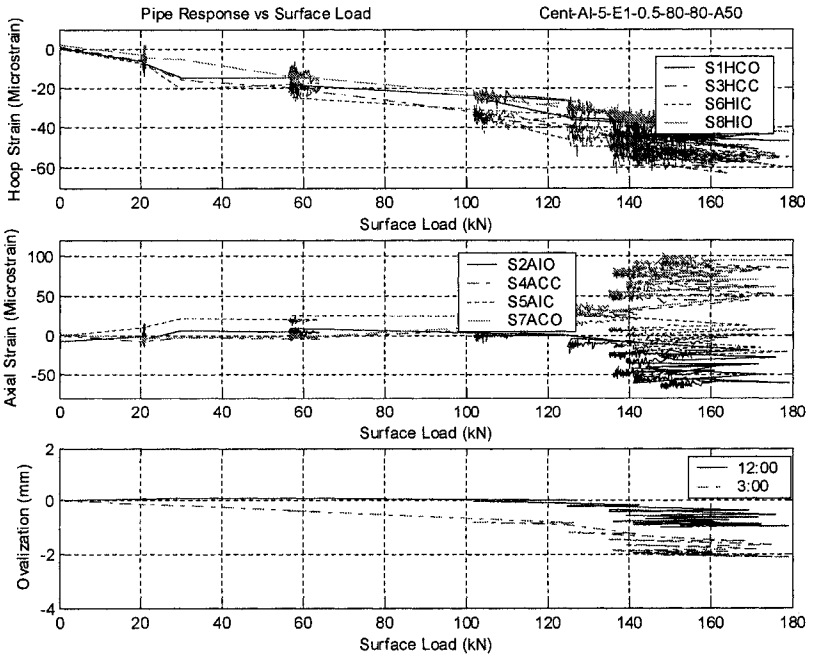

Figure A21: Pipe Response versus Surface Load, Test 5E1

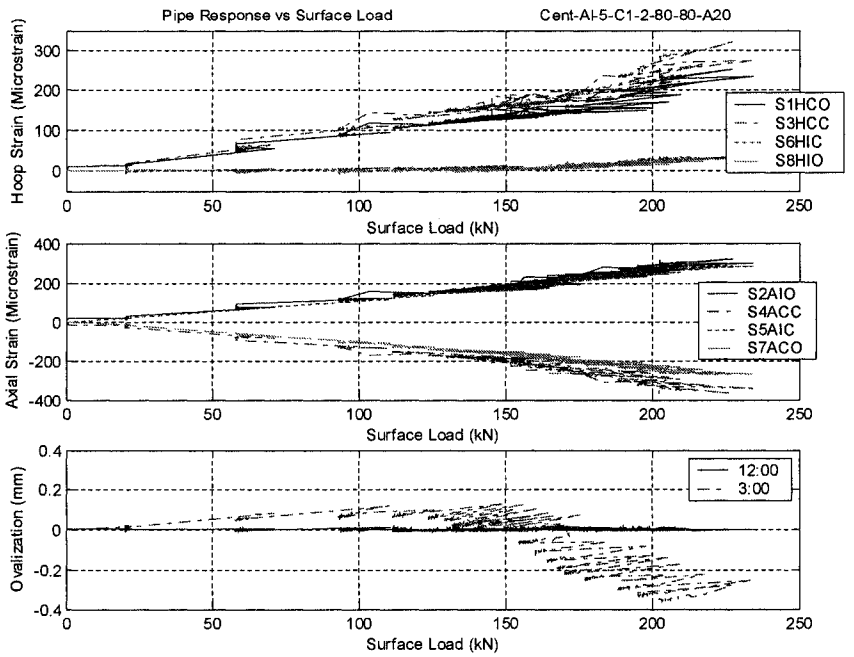

Figure A22: Pipe Response versus Surface Load, Test 5C1

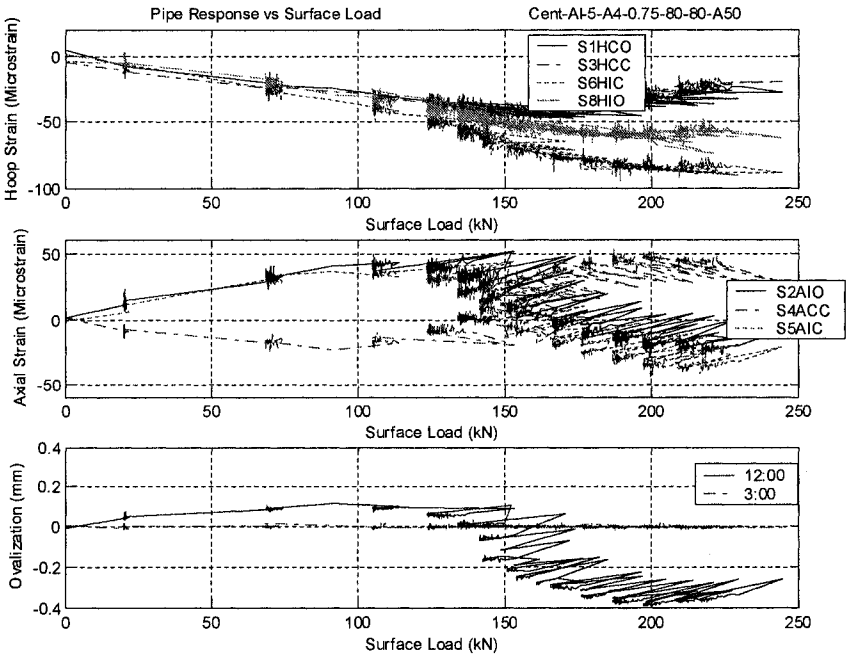

Figure A23: Pipe Response versus Surface Load, Test 5A4

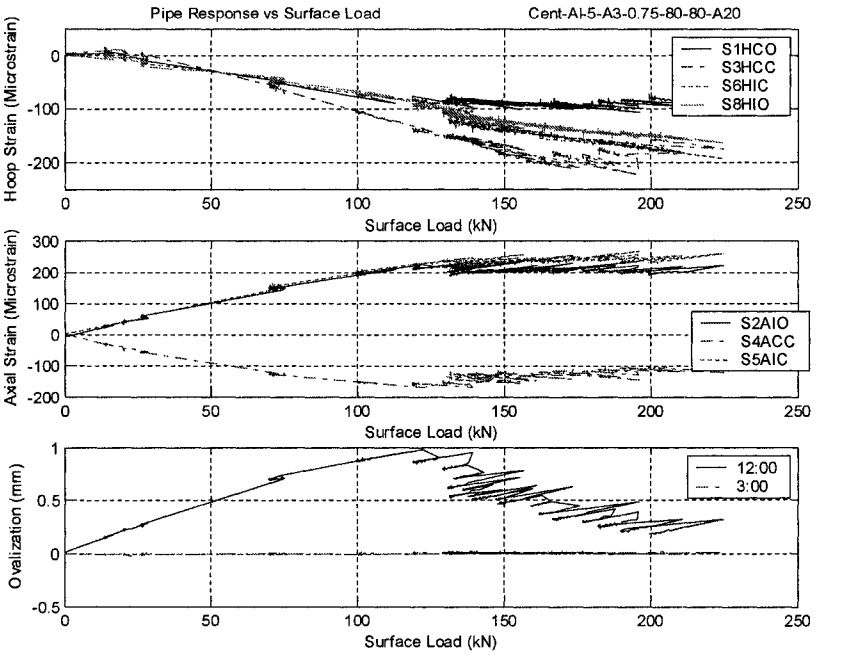

Figure A24: Pipe Response versus Surface Load, Test 5A3

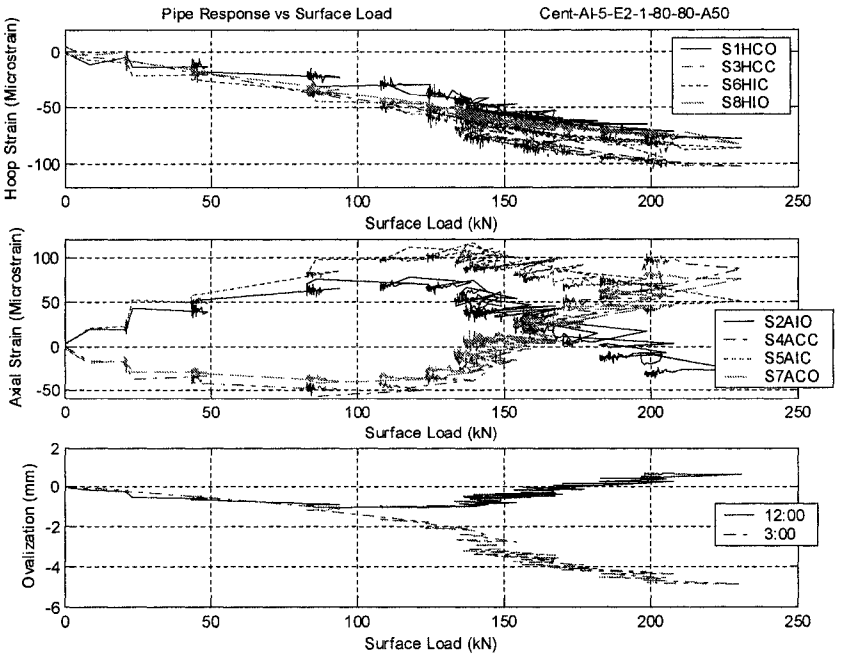

Figure A25: Pipe Response versus Surface Load, Test 5E2

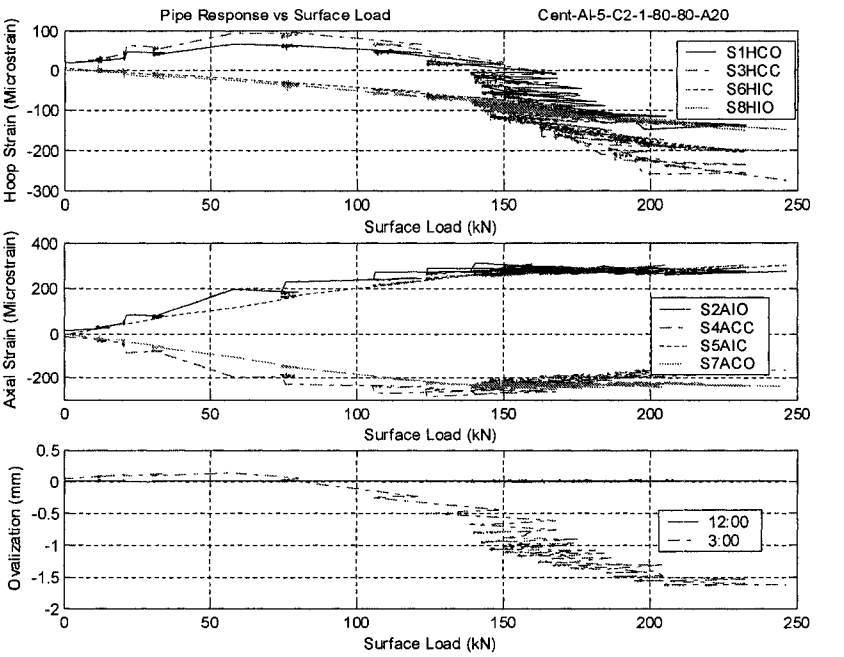

Figure A26: Pipe Response versus Surface Load, Test 5C2

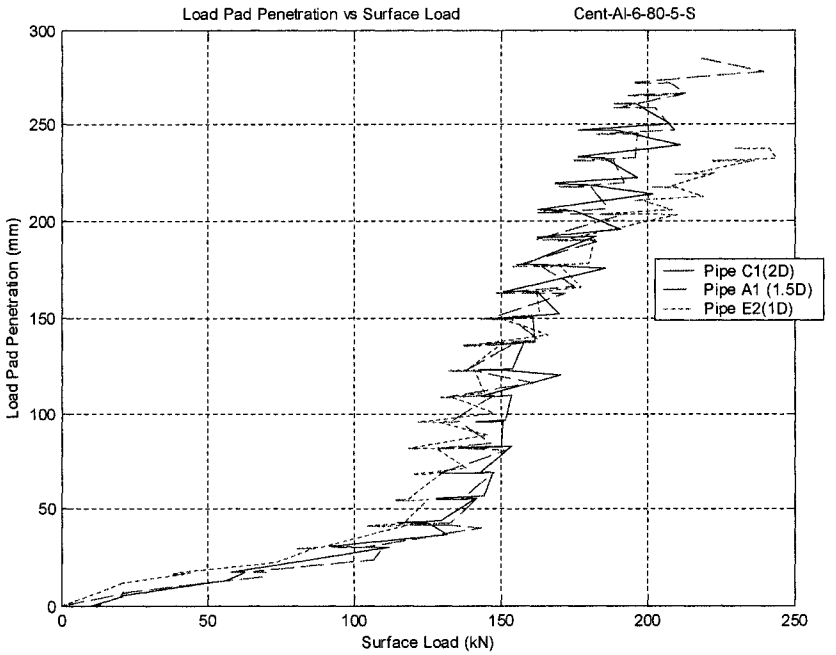

Figure A27: Load Pad Penetration versus Surface Load, Test 6, C1, A1, E2

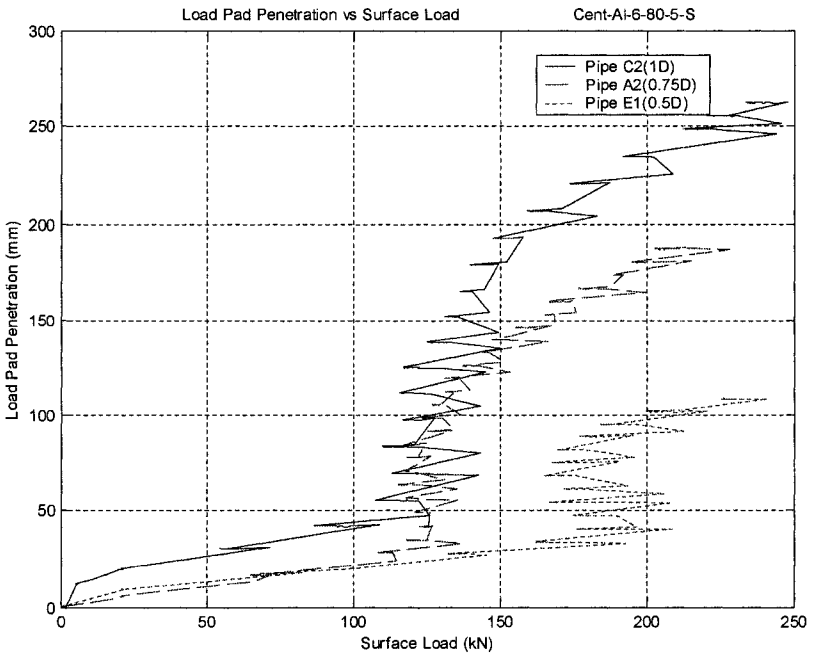

Figure A28: Load Pad Penetration versus Surface Load, Test 6, C2, A2, E1

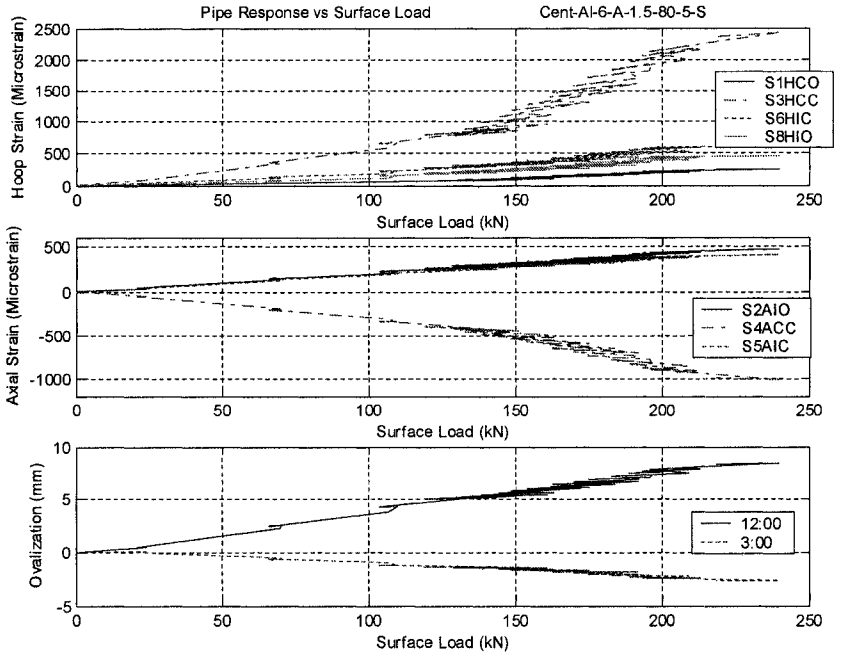

Figure A29: Pipe Response versus Surface Load, Test 6A-1.5

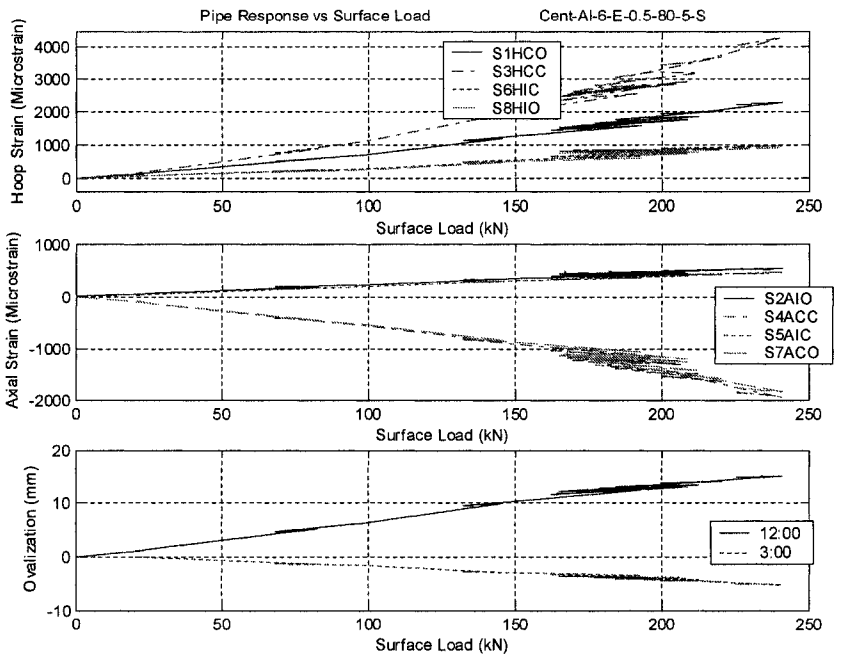

Figure A30: Pipe Response versus Surface Load, Test 6E-0.5

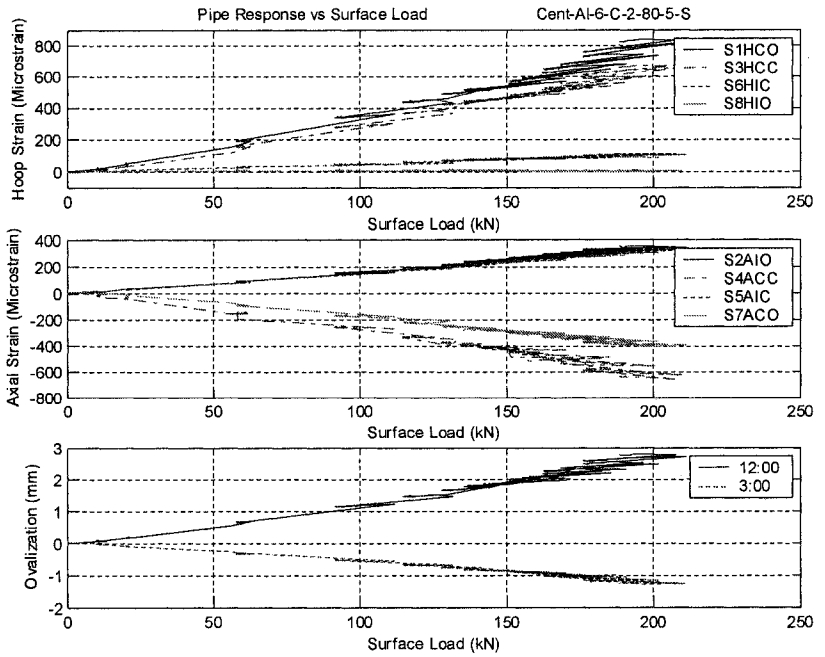

Figure A31: Pipe Response versus Surface Load, Test 6C-2

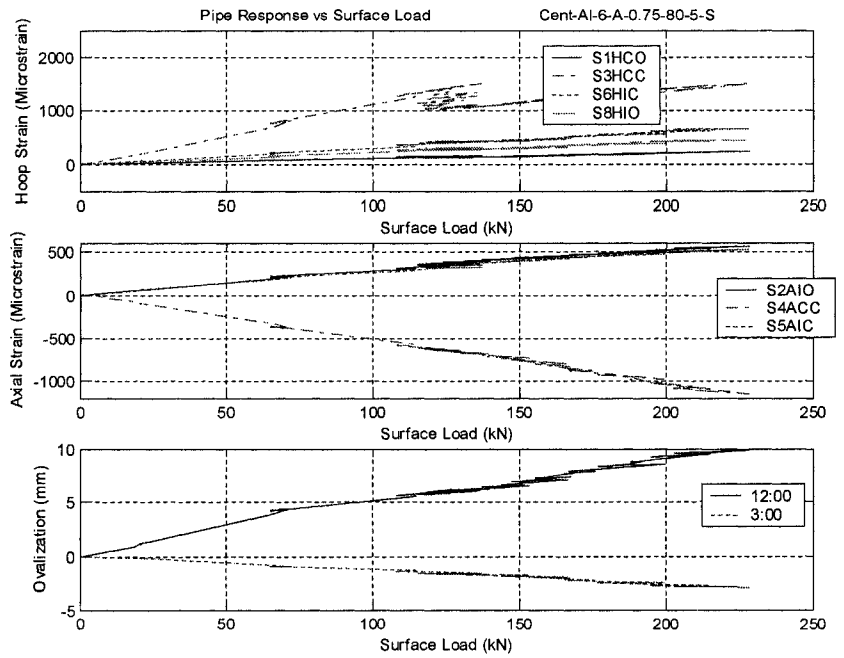

Figure A32: Pipe Response versus Surface Load, Test 6A-0.75

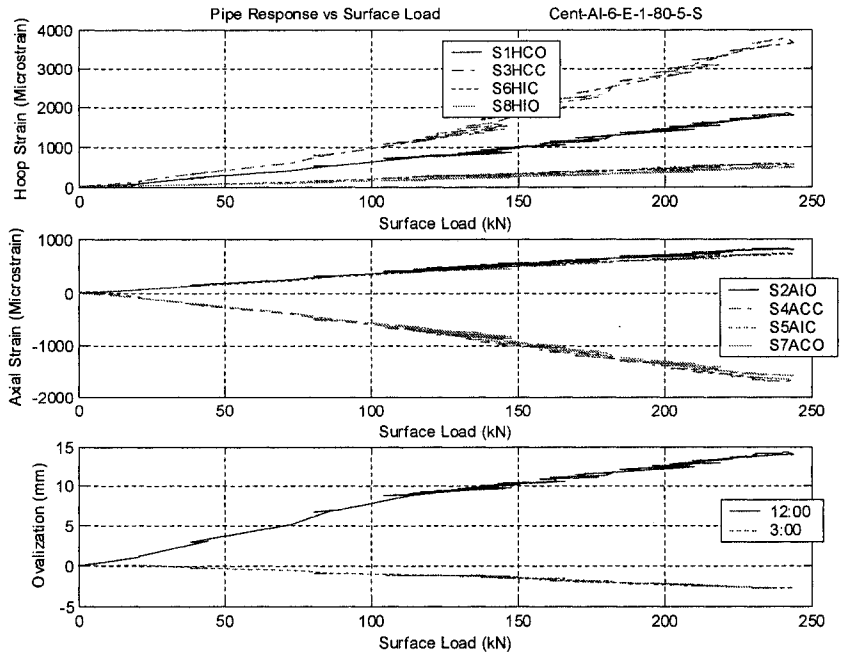

Figure A33: Pipe Response versus Surface Load, Test 6E-1

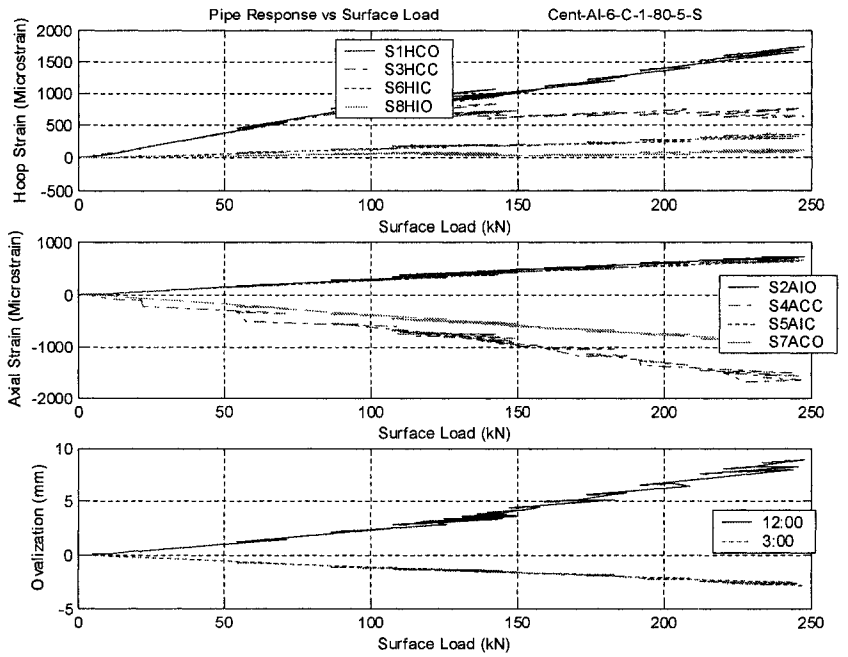

Figure A34: Pipe Response versus Surface Load, Test 6C-1

Appendix B
Load Frame Design Calculations

Beam Layout Diagram

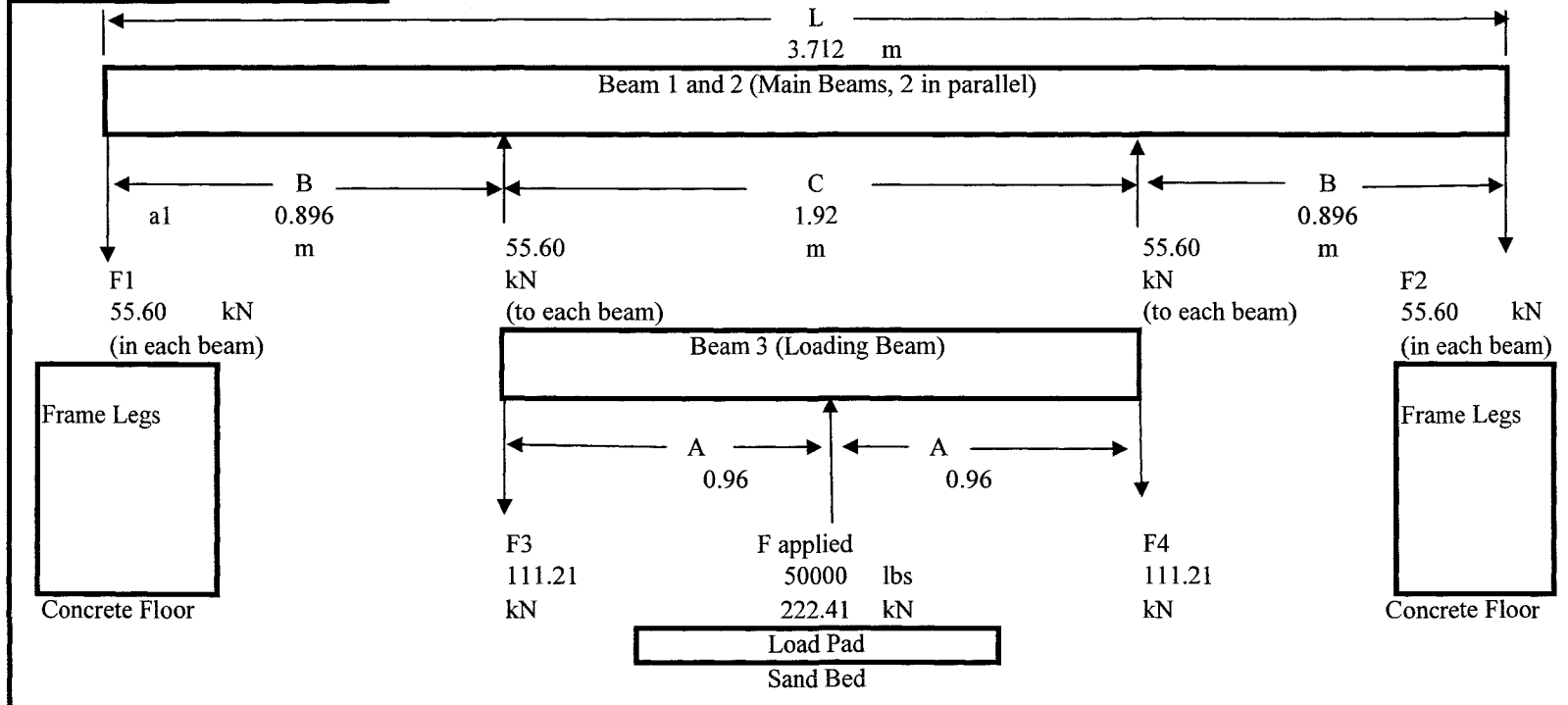

Fapplied = F actuators X 2 =	25000 lbs X 2 =	222.41 kN
F1 = F2 = Fapplied / 4 =	55.60 kN	
F3 = F4 = Fapplied / 2 =	111.21 kN	

Beam Cross Section

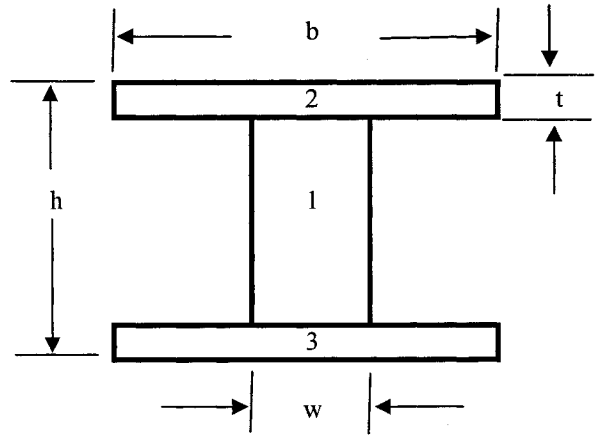

Steel Beam
E = 207 GPa
For Design assume:
σ_{yield} steel = 200 MPa

I Section Dimensions and Moment of Inertia

Width (b)	165.61 mm	Web Thickness (w)	6.60 mm
Height (h)	313.44 mm	Flange Thickness (t)	11.18 mm
Width	6.52 inches	Web Thickness	0.26 inches
Height	12.34 inches	Flange Thickness	0.44 inches

Item	h	b	Area	y	y*A
1	291.08	6.60	1922.32	156.72	301261.9
2	11.18	165.61	1850.84	307.85	569775.9
3	11.18	165.61	1850.84	5.59	10342.47
			5623.99		881380.3

Y = 156.72 mm

I_{xx} = Sum (1/12 * b * h^3 + A * d)

	1/12	b	h	A	d	I_{xx}
1	0.083333	6.60	291.08	1922.32	0.00	13573155
2	0.083333	165.61	11.18	1850.84	151.13	42292849
3	0.083333	165.61	11.18	1850.84	151.13	42292849

I beam

I_{xx} = 98158853 mm^4
I_{xx} = 9.816E-05 m^4

Analysis of Main Beams (2 in parallel) (Beam 1 or 2)			
Moment and Stress:			
Beam Load = F = Fapplied / 4 =	55.60 kN		
Point of load application = B =	0.896 m		
Using formulas for a supported beam with two symmetrical loads:			
Maximum Bending Moment in Beam 1 = M = F x B =		49.82 kN m	
Stress in Beam 1 = M y / I =		79.54 MPa	< σ_{yield} steel, Therefore connection ok.
Deflection:			
Using formulas for a supported beam with two symmetrical loads:			
Maximum deflection in Beam 1 = defl = F B (3 L^2-4B^2) / 24 E I =		3.90 mm	Connection ok.
Analysis of Loading Beam (Beam 3)			
Moment and Stress:			
Beam Load = F = Fapplied / 2 =	111.21 kN		
Point of load application = A =	0.96 m		
Using formulas for a supported beam with a point load in the middle:			
Maximum Bending Moment in Beam 3 = M = F L / 4 =		53.38 kN m	
Stress in Beam 3 = M y / I =		85.22 MPa	< σ_{yield} steel, Therefore connection ok.
Deflection:			
Using formulas for a supported beam with a point load in the middle:			
Maximum deflection in Beam 1 = defl = F L^3 / 48 E I =		5.83 mm	Connection ok.

Bolted Connection Strength

Bolt used include:				Washer outside diameter	
1/2 " bolt, At =	0.1419 inches^2	=	9.155E-05 m^2	1.062 " =	26.97 mm
3/4 " bolt, At =	0.334 inches^2	=	0.0002155 m^2	1.469 " =	37.31 mm
20 mm bolt, At =			0.00024 m^2		49.00 mm

Imperial bolts used were Grade 8	Proof Strength = S_p =	120	ksi and a Yield Strength = S_y =	130	ksi
	S_p =	827.4	MPa	S_y =	896.35 MPa
Metric bolts used were Grade 12.9	Proof Strength = S_p =	970	MPa and a Yield Strength = S_y =	1100	MPa

Bolts connecting actuators to main beams

0.5 inch diameter bolts, 8 bolts connect one actuator to the main beam, F = 111.21 kN exerted by one actuator

Check tensile stress in bolt: Tensile Stress in bolt = F / (A_t * number of bolts)

$\sigma_{tensile}$ bolt = 151.84 MPa per bolt < S_p ~ 830 MPa Therefore connection ok.

Check punching stress in I-Beam flange:

Diameter of washer = 26.97 mm flange thickness = 11.18 mm

A = circumfrence of washer * flange thickness = 0.000947 m^2

Punching Stress = F / (A_t * number of bolts)

$\sigma_{punching}$ steel = 14.68 MPa per bolt < σ_{yield} steel ~ 200 MPa Therefore connection ok.

Bolts connecting main beams to frame legs

0.75 inch diameter bolts, 4 bolts connect one actuator to the main beam, F = 55.60 kN into each leg

Check tensile stress in bolt: Tensile Stress in bolt = F / (A_t * number of bolts)

$\sigma_{tensile}$ bolt = 64.51 MPa per bolt < S_p ~ 830 MPa Therefore connection ok.

Alternate check of tensile stress in bolt, using the force due to the moment in the beam:

F_m = 438.11 KN $\sigma_{tensile}$ bolt = F_m / (At * number of bolts)

$\sigma_{tensile}$ bolt = 508.29 MPa per bolt < S_p ~ 830 MPa Therefore connection ok.

Check punching stress in I-Beam flange:

Diameter of washer = 37.31 mm flange thickness = 11.18 mm

A = circumfrence of washer * flange thickness = 0.00131 m^2

Punching Stress = F / (A_t * number of bolts)

$\sigma_{punching}$ steel = 10.61 MPa per bolt < σ_{yield} steel ~ 200 MPa Therefore connection ok.

Legs to Concrete Floor Anchors

Concrete Anchors used were Red Head HSLG-N 20/60							
(HSL = Heavy Duty Expansion Anchor, G = stud, N = slotted, 20 = diameter (mm), 60 = bolted plate thickness (mm)							
Minimum Recommended Embedment		130 mm	(assumes 4000psi concrete)				
Allowable Working Loads	Tension	7310 lbs =	32.52 kN	Shear	12905 lbs	57.40 kN	
Average Ultimate Loads	Tension	25500 lbs	113.43 kN	Shear	45020 lbs	200.26 kN	

Check tensile stress in bolt: Tensile Stress in bolt = F / (A_t * number of bolts)

20 mm dia bolt, 2 connecting plate to floor, F = 55.60 kN into each leg

$\sigma_{tensile}$ bolt = 115.84 MPa per bolt < S_p ~ 970 MPa Therefore connection ok.

Check punching stress plate welded to bottom of legs

Diameter of washer = 49.00 mm plate thickness = 12.70 mm

A = circumfrence of washer * flange thickness = 0.001955 m^2

Punching Stress = F / (A_t * number of bolts)

$\sigma_{punching}$ steel = 14.22 MPa per bolt < σ_{yield} steel ~ 200 MPa Therefore connection ok.

Check anchor rating against design:

20 mm Concrete Anchors are rated to 32.52 kN (working)

Assume only tension in: 2 bolts per leg, concrete bolt capacity = 65.03 KN (working)

In 1 leg 55.60 kN < 65 lN Therefore bolts ok.

Check bolts individually:

Summing Forces and Moments find: d1/d3 0.17

d2/d3 0.5

Gives F2 = 0.6 * F1

F2 = 33.36 kN ~ 33 kN (working load of bolts)

and < 113 kN (ultimate load) Therefore bolts ok.

F3 = 22.24 kN < 33 kN Therefore bolts ok.

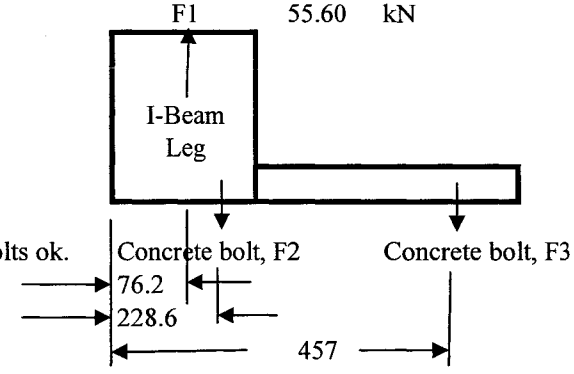

Concrete Stresses from bolts

Assume cone shaped concrete failure mode (45·)

r =	130.00	mm			
l =	183.85	mm			
Area = PI r (r^2 + l^2)^.5	0.09196	m^2			
Assume Force =	55.60	kN			
Stress = Force / Area	0.60	MPa <	13.79	MPa	Therefore concrete ok.

Assuming Concrete with:
Shear strength = 2000psi = 13.79 MPa

I-Beam weld stress calcs

Assume welding along w X 2 and h x 2

Length of weld ~	958.09	mm		
Leg of weld ~	5	mm		
Weld Area =	0.003386841	m^2		
F = Force =	55.60	kN		
St = F / Area =	16.42	MPa	< σ_{yield} steel ~ 200 MPa	Therefore connection ok.

Appendix C
Chapter 4 Plots
Surface Loading of Steel Pipes at Full-Scale

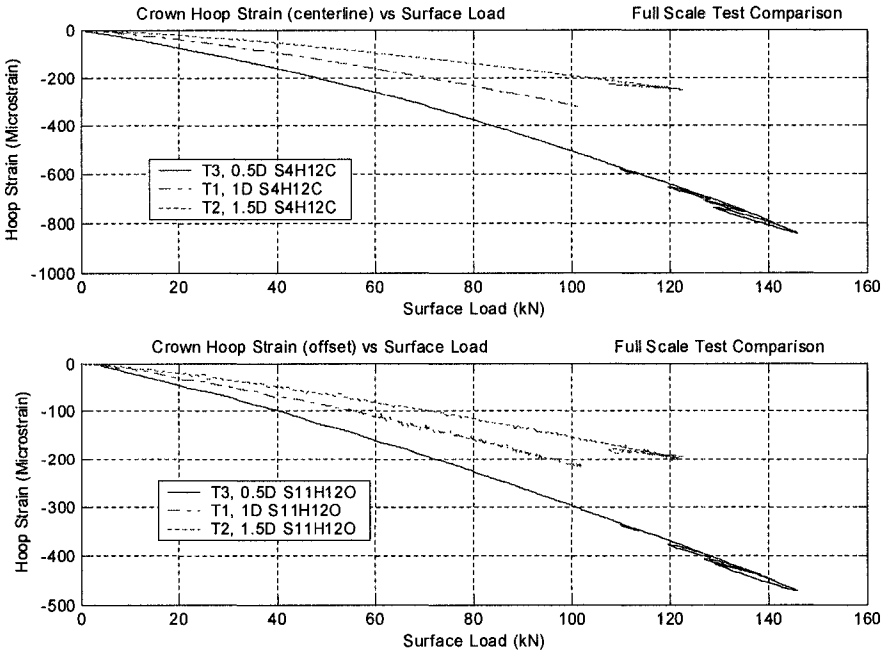

Figure C1: Crown Hoop Strain versus Surface Load

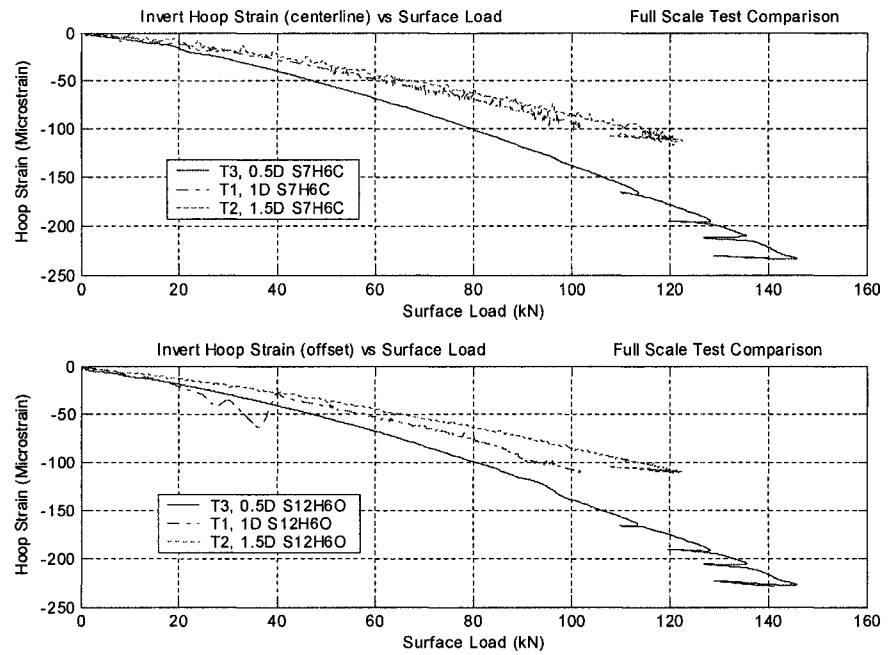

Figure C2: Invert Hoop Strain versus Surface Load

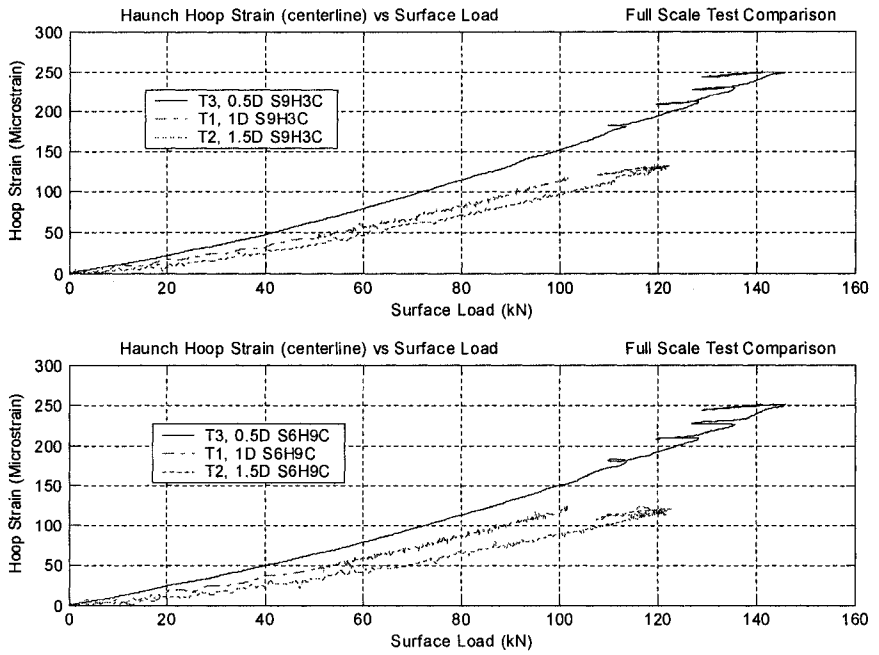

Figure C3: Haunch Hoop Strain versus Surface Load

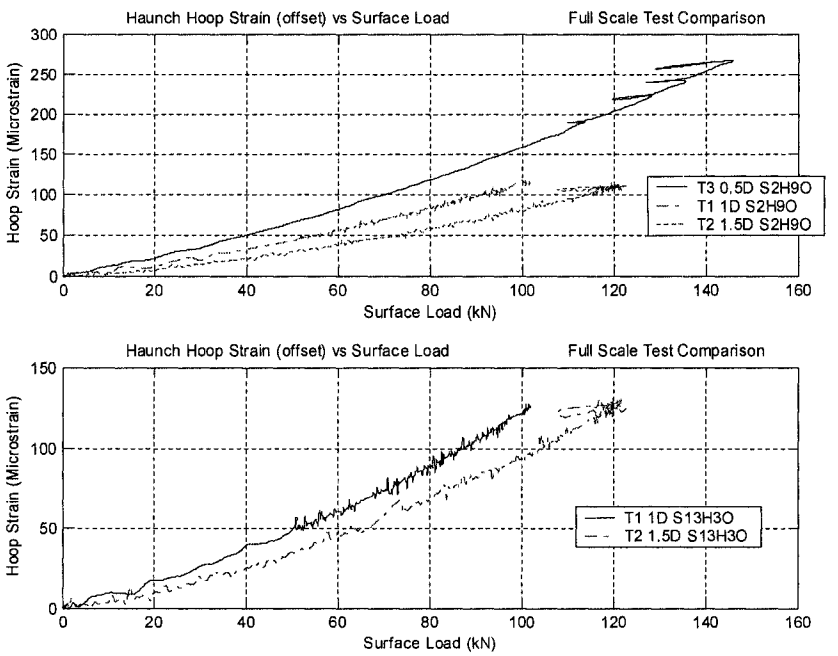

Figure C4: Haunch Hoop Strain versus Surface Load

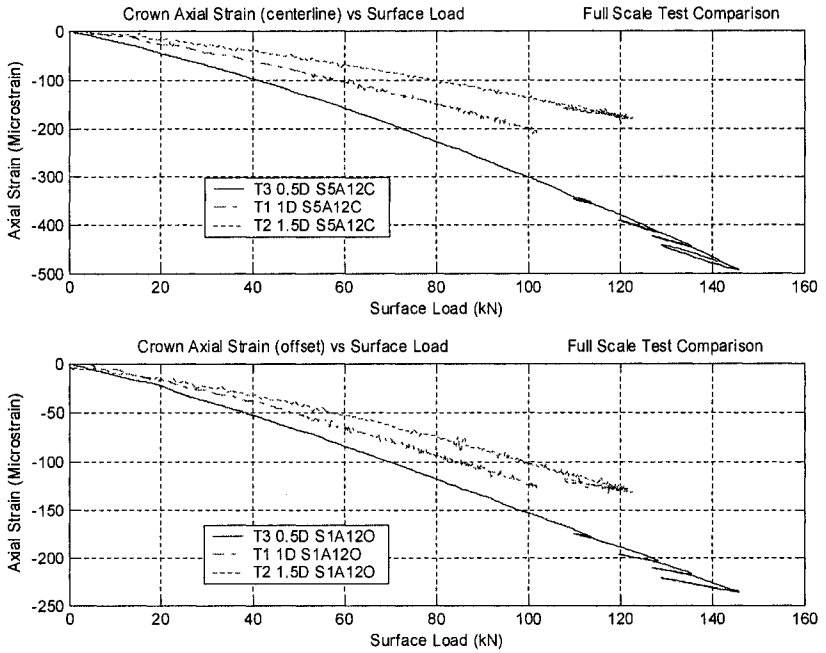

Figure C5: Crown Axial Strain versus Surface Load

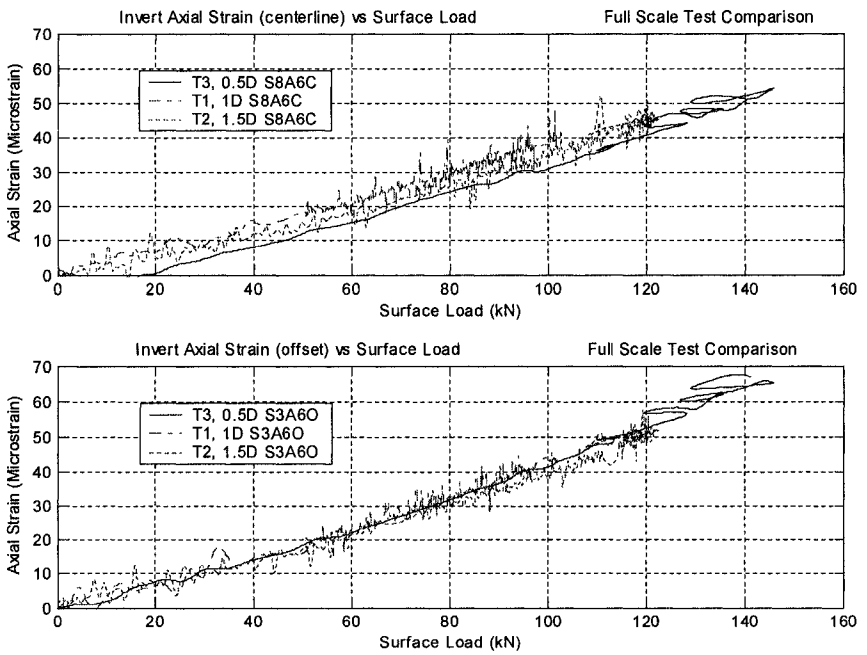

Figure C6: Invert Axial Strain versus Surface Load

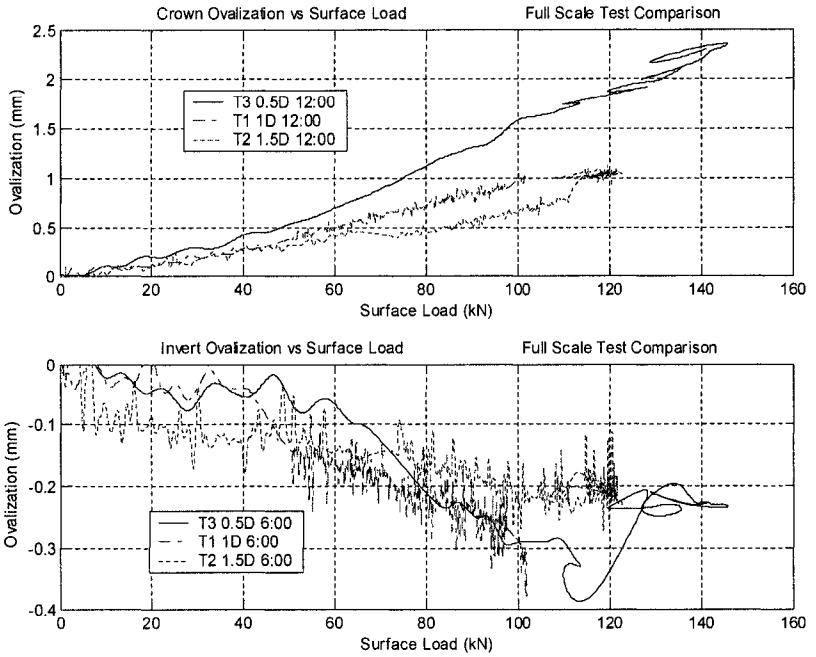

Figure C7: Crown and Invert Ovalization versus Surface Load

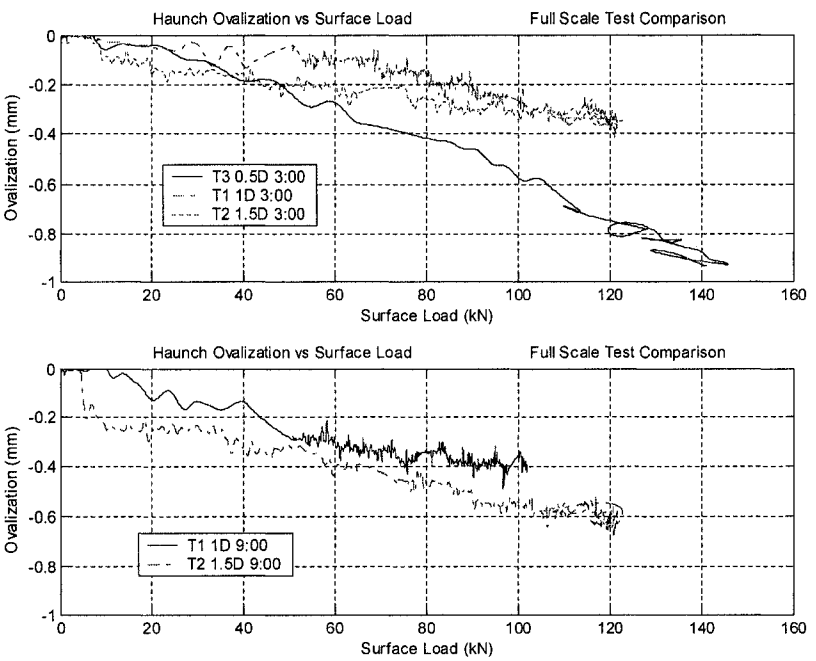

Figure C8: Haunch Ovalization versus Surface Load

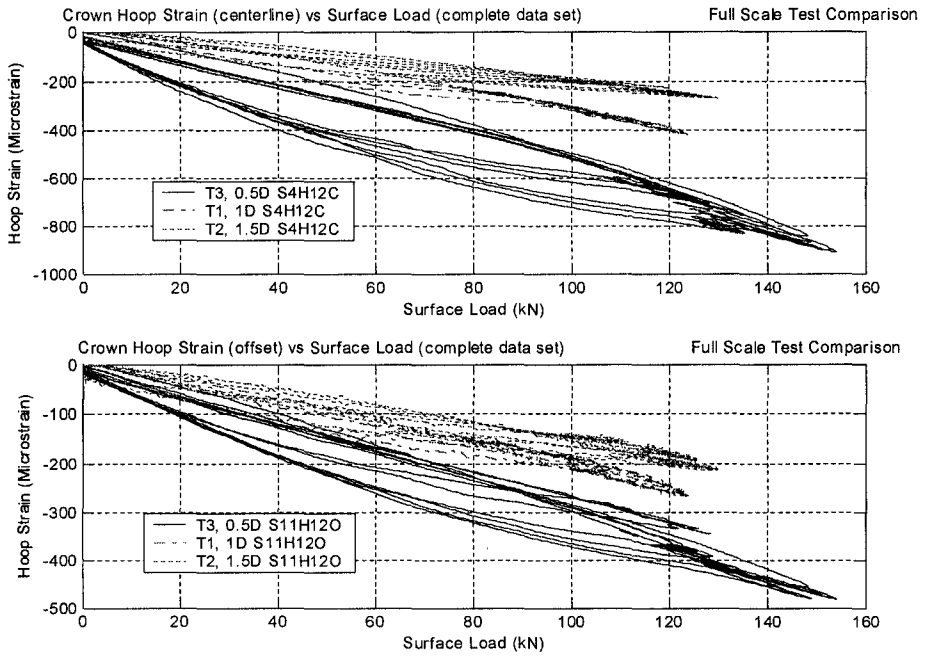

Figure C9: Crown Hoop Strain versus Surface Load

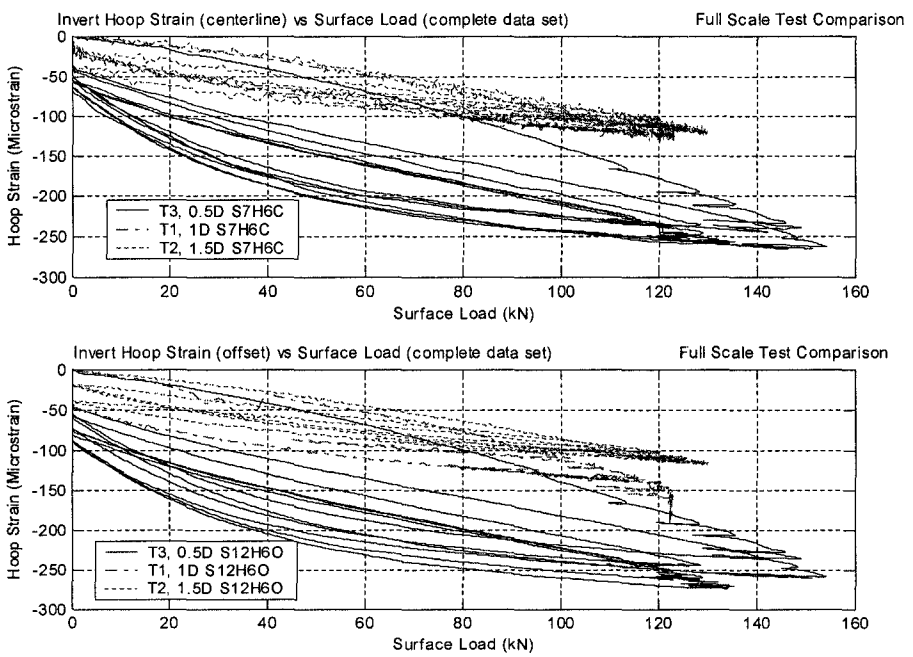

Figure C10: Invert Hoop Strain versus Surface Load

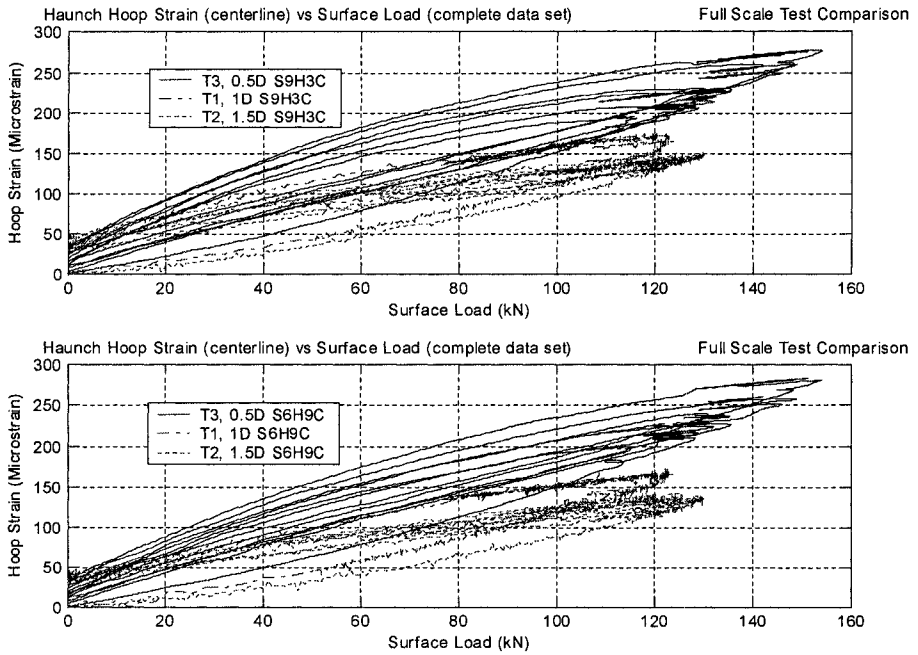

Figure C11: Haunch Hoop Strain versus Surface Load

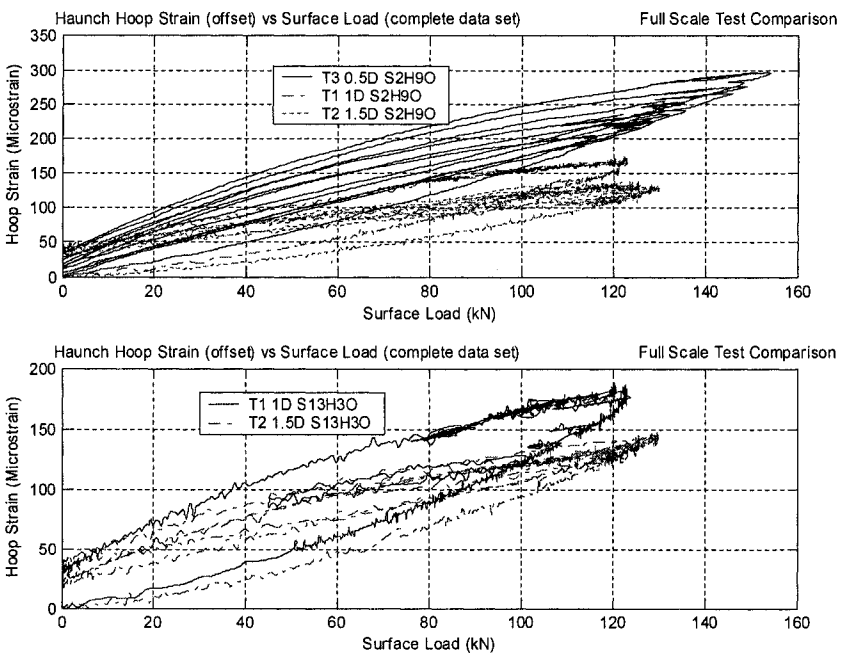

Figure C12: Haunch Hoop Strain versus Surface Load

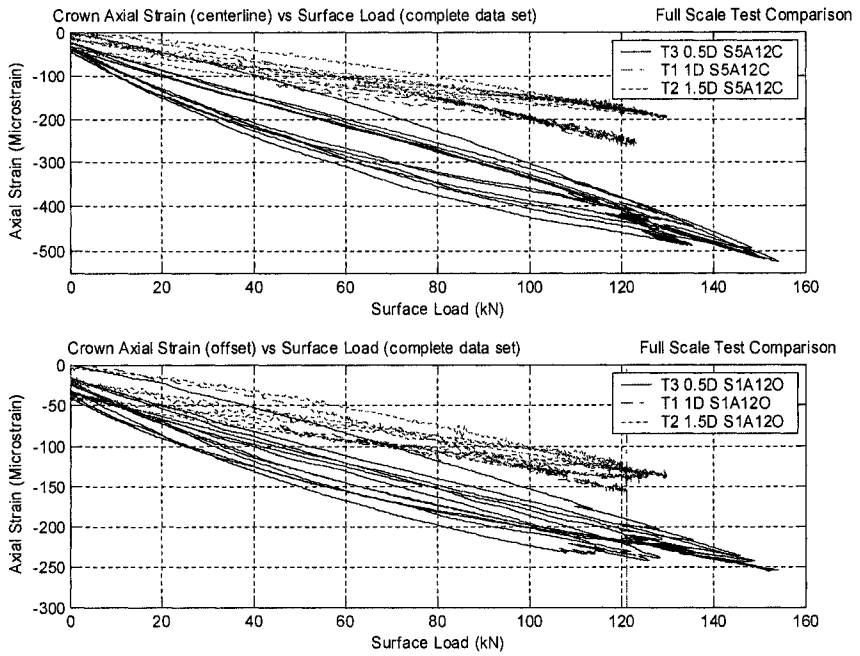

Figure C13: Crown Axial Strain versus Surface Load

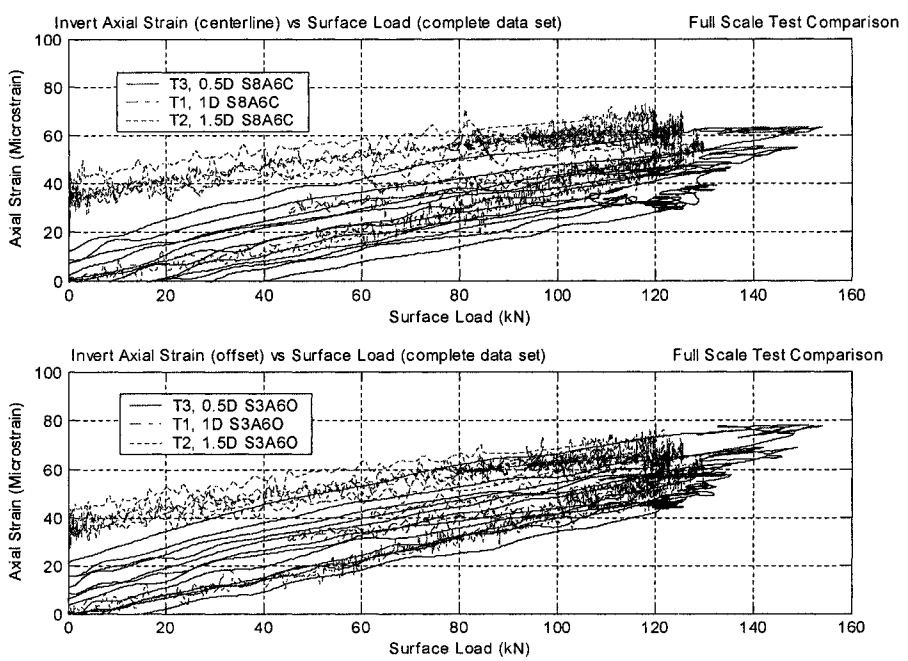

Figure C14: Invert Axial Strain versus Surface Load

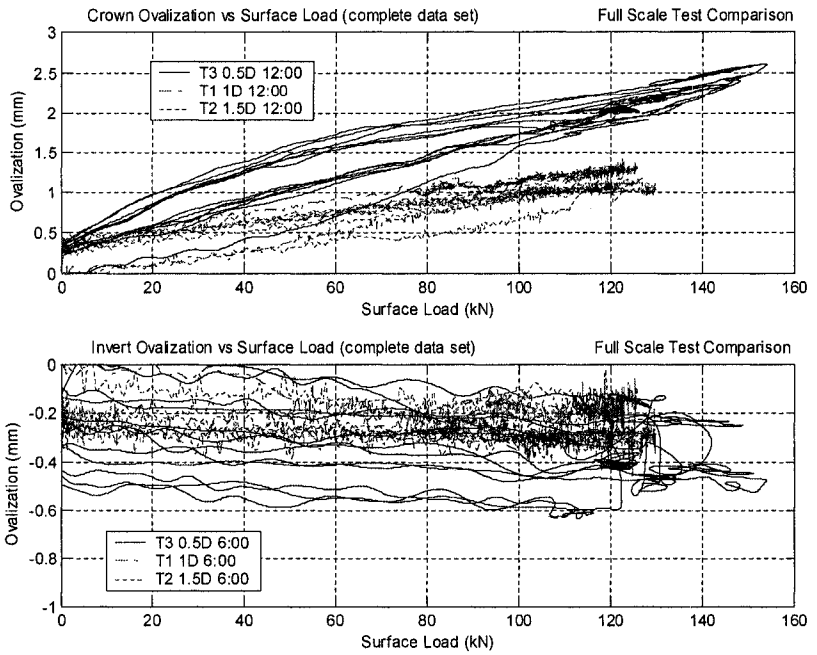

Figure C15: Crown Ovalization versus Surface Load

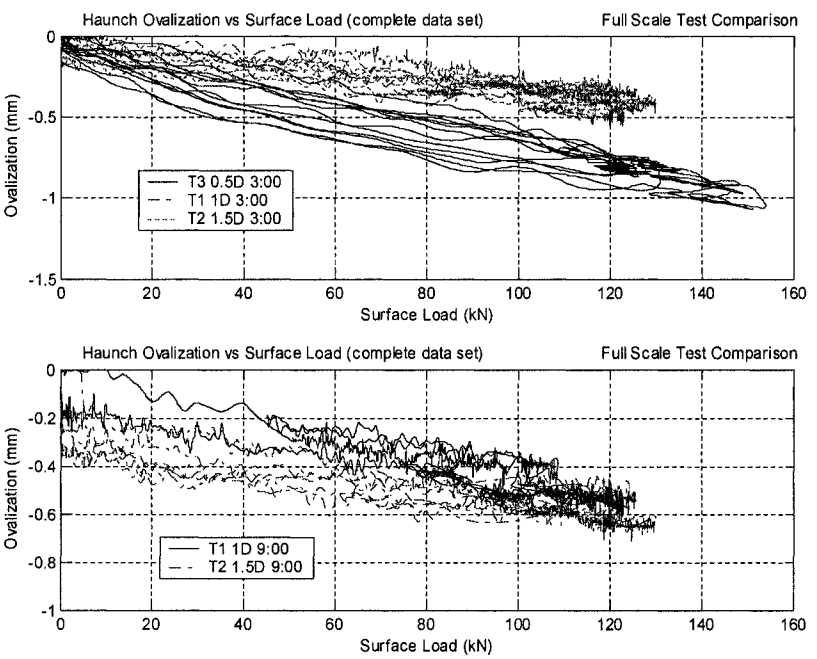

Figure C16: Haunch Ovalization versus Surface Load

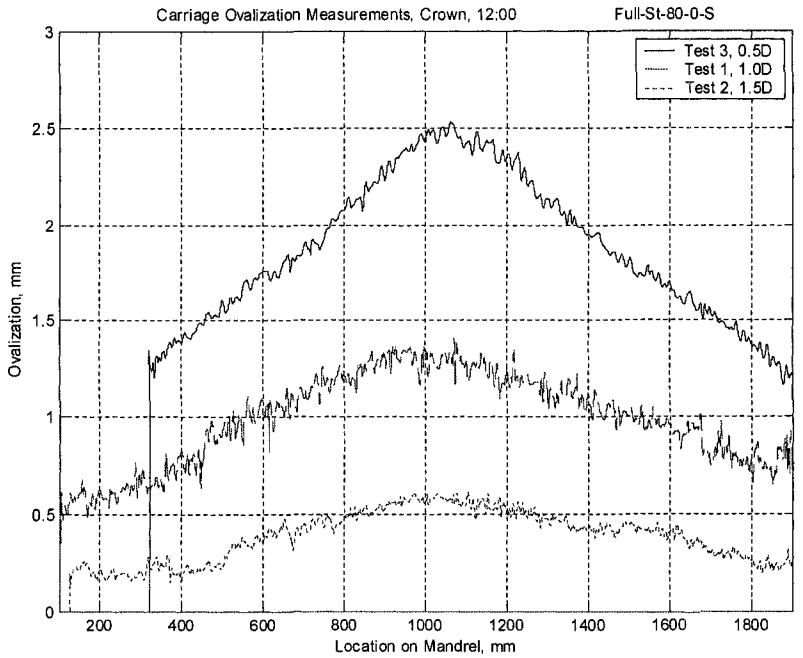

Figure C17: Pipe Ovalization Profiles, Crown

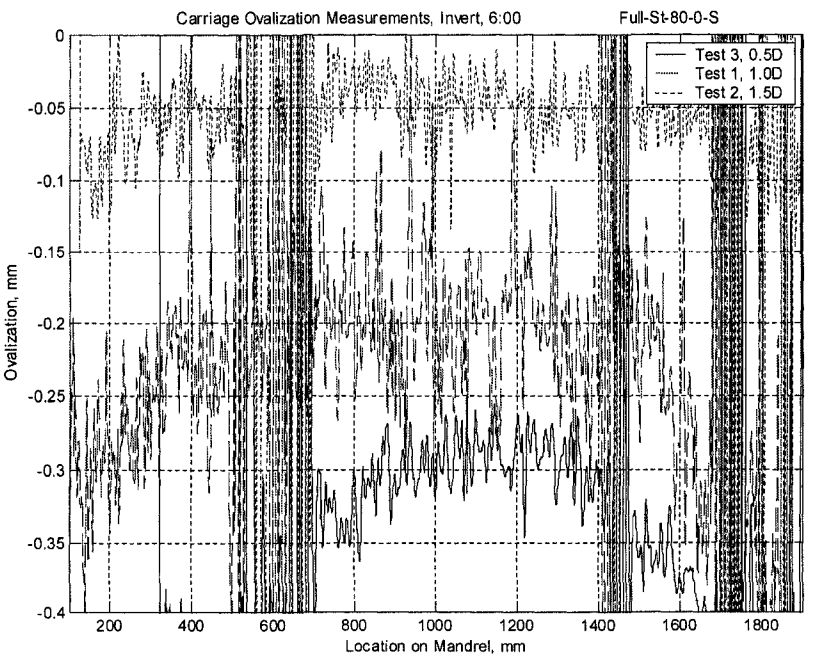

Figure C18: Pipe Ovalization Profiles, Invert

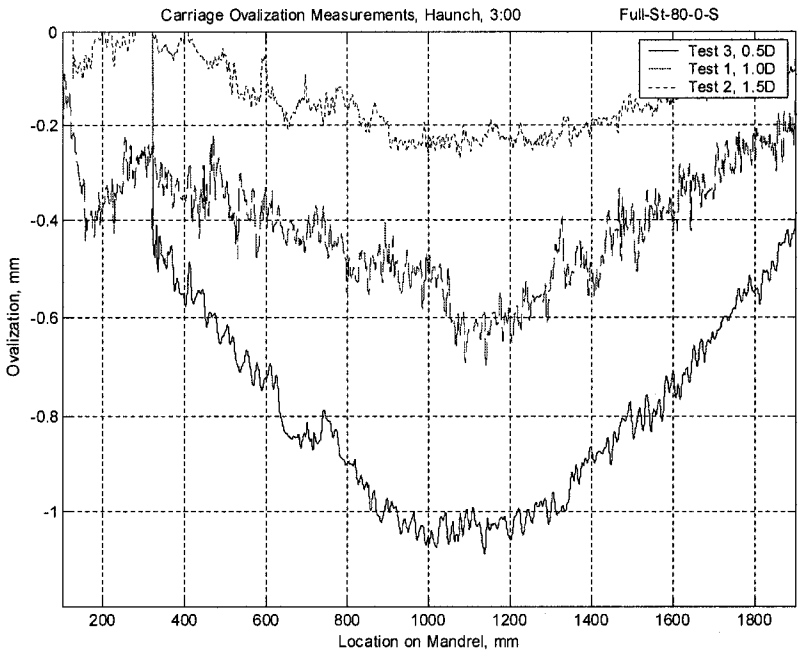

Figure C19: Pipe Ovalization Profiles, Haunch (3:00)

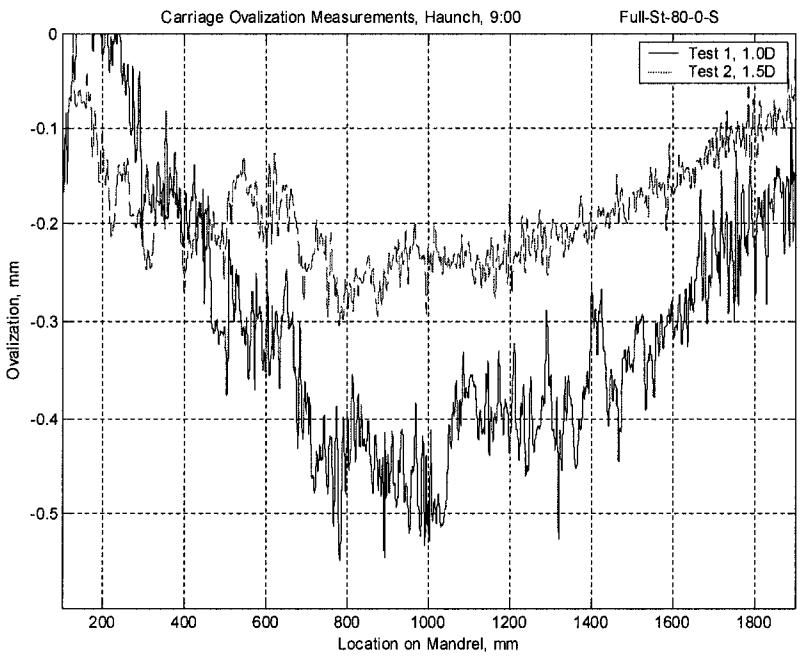

Figure C20: Pipe Ovalization Profiles, Haunch (9:00)

Appendix D
Chapter 5 Plots
Surface Loading of Steel Pipes in the Centrifuge

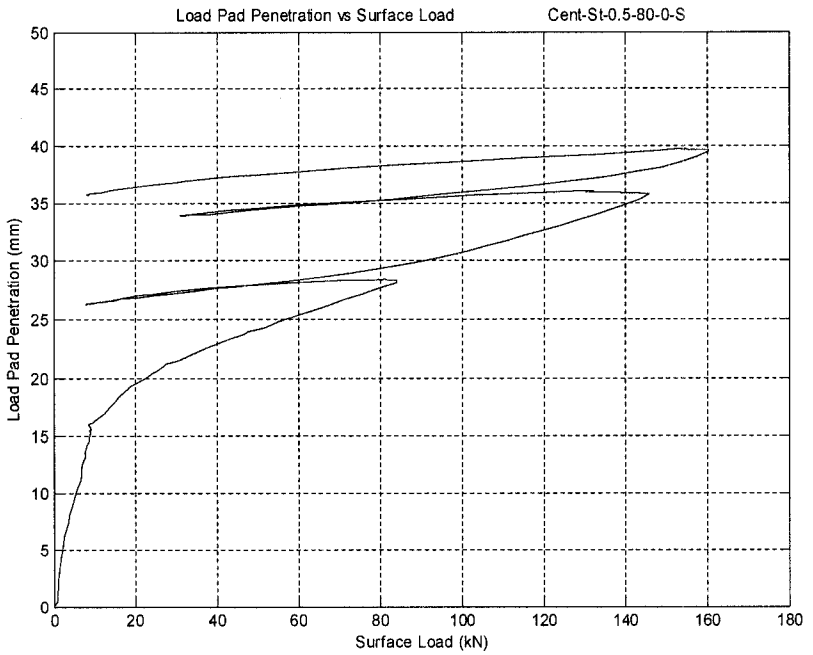

Figure D1: Load Pad Penetration, 0.5D Cover

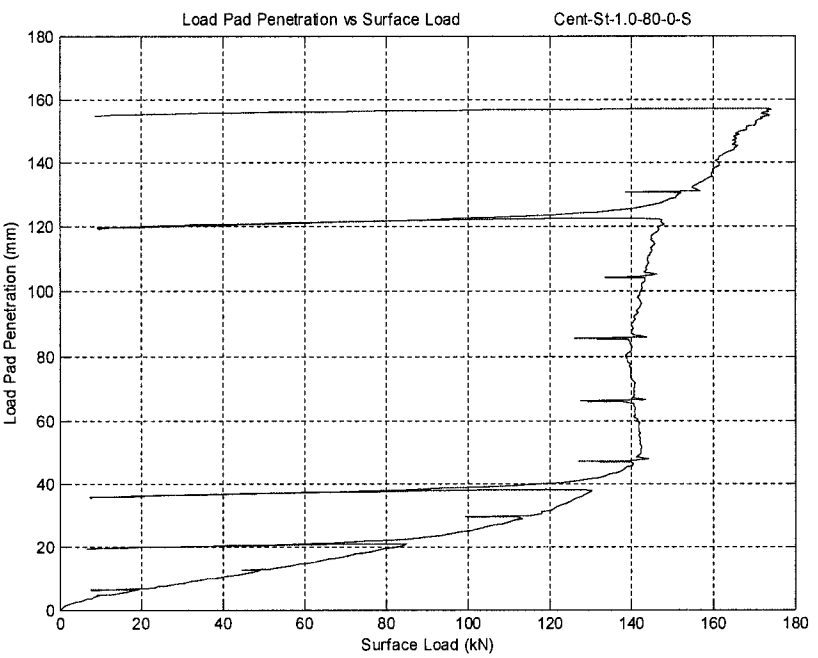

Figure D2: Load Pad Penetration, 1D Cover

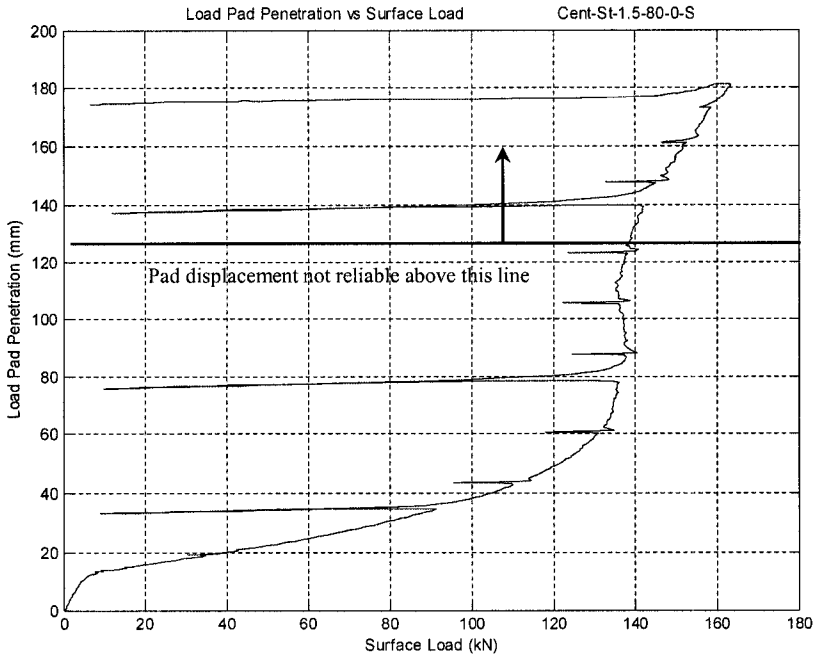

Figure D3: Load Pad Penetration, 1.5D Cover

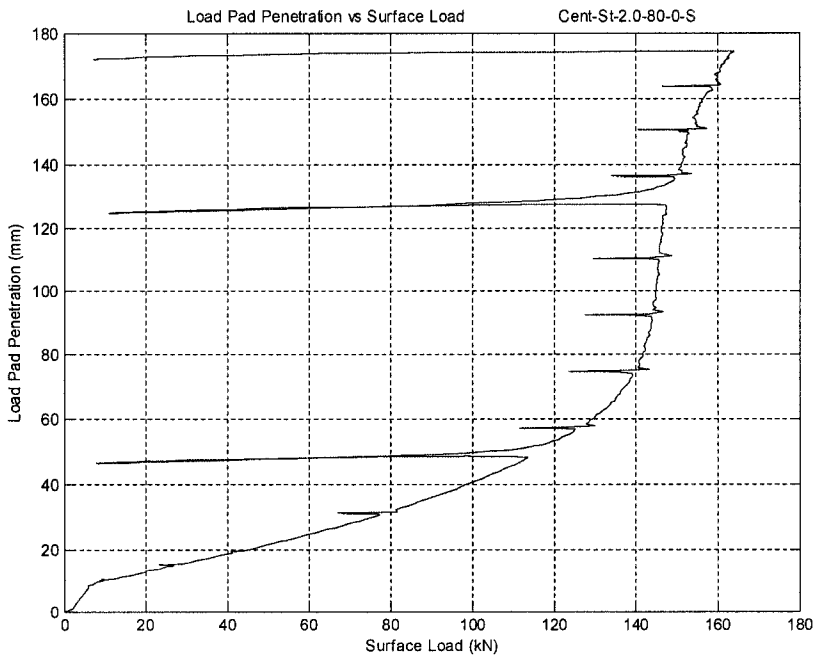

Figure D4: Load Pad Penetration, 2D Cover

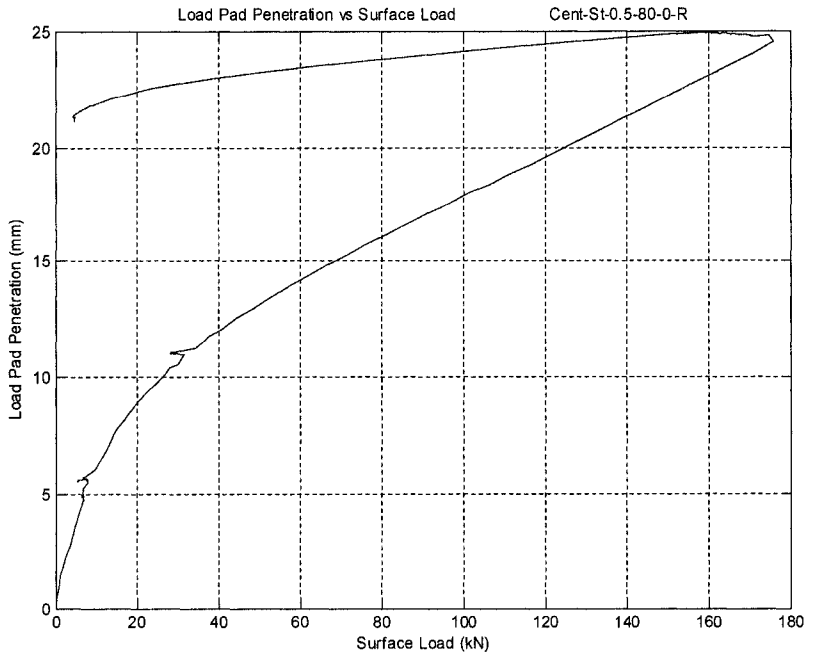

Figure D5: Load Pad Penetration, 0.5D Cover, Rectangular Pad

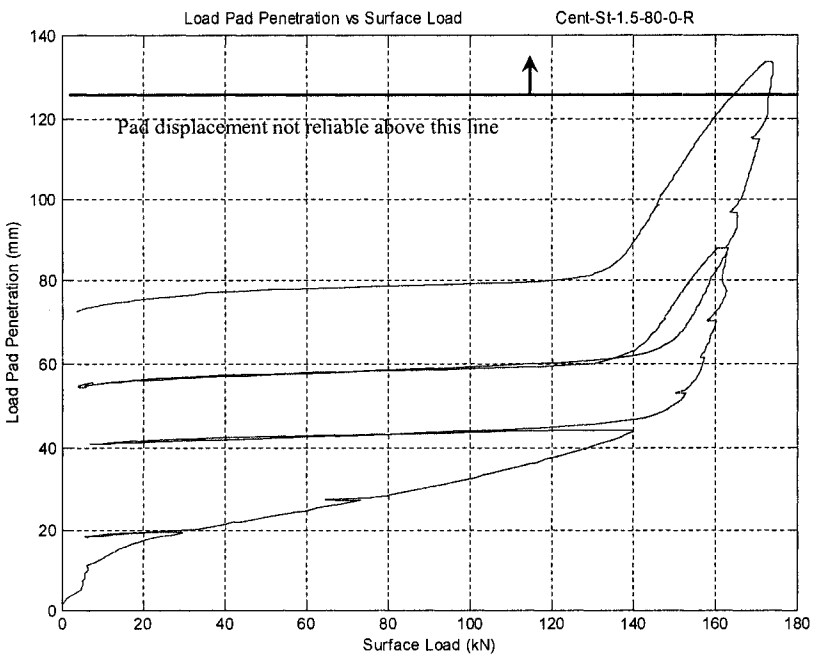

Figure D6: Load Pad Penetration, 1.5D Cover, Rectangular Pad

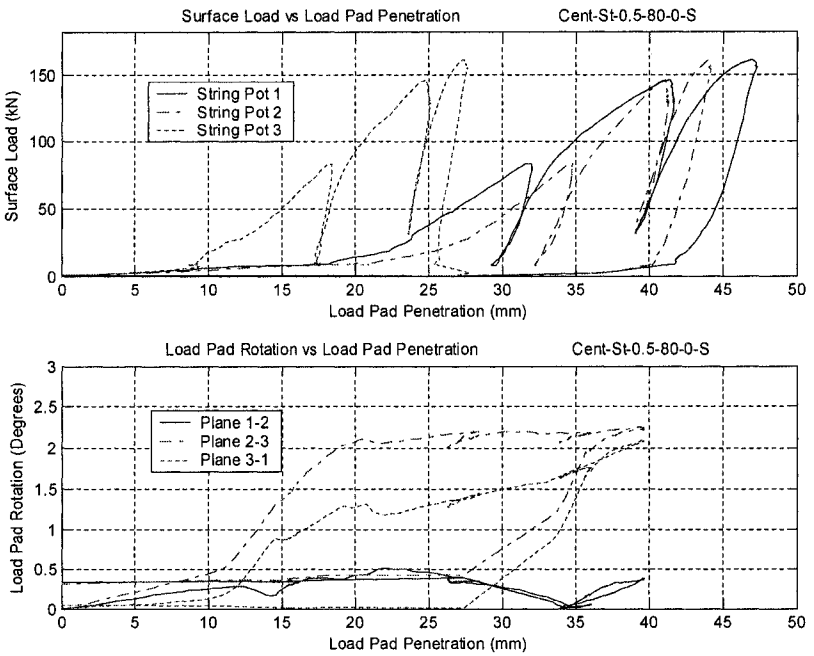

Figure D7: Load Pad Rotations, 0.5D Cover

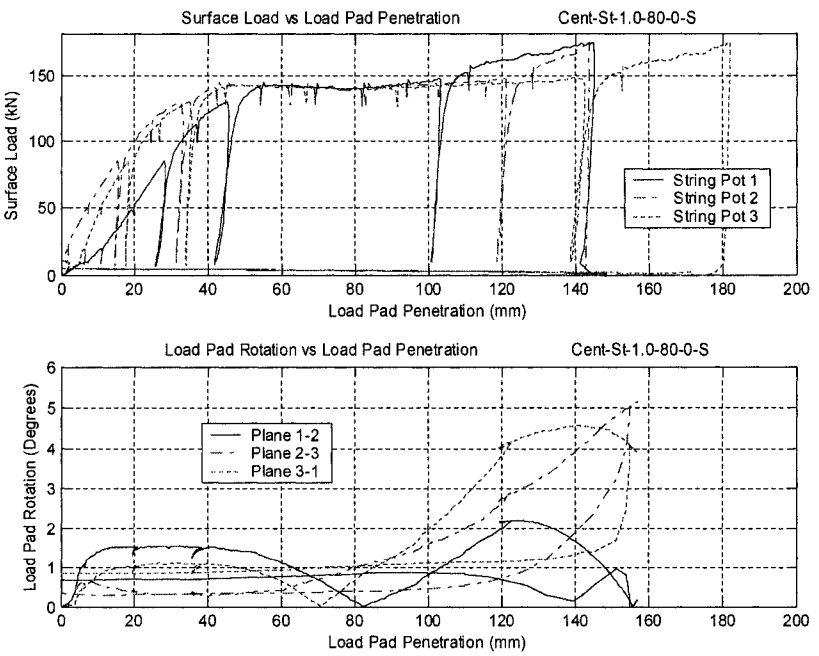

Figure D8: Load Pad Rotations, 1D Cover

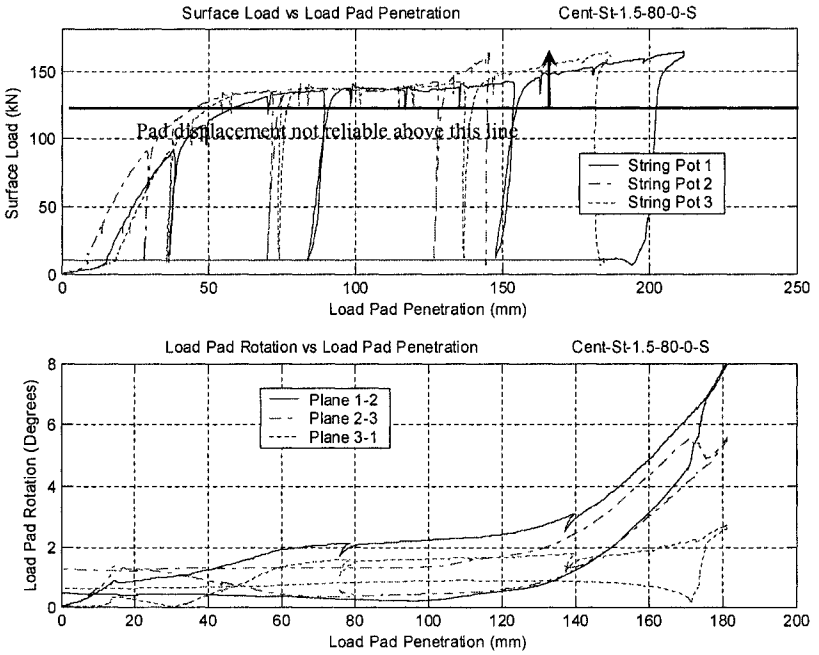

Figure D9: Load Pad Rotations, 1.5D Cover

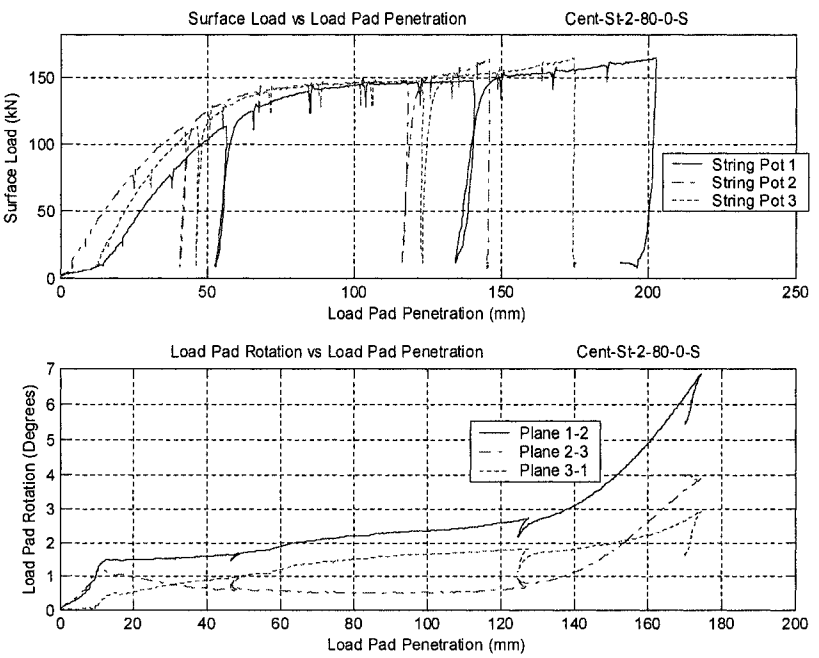

Figure D10: Load Pad Penetration, 2D Cover

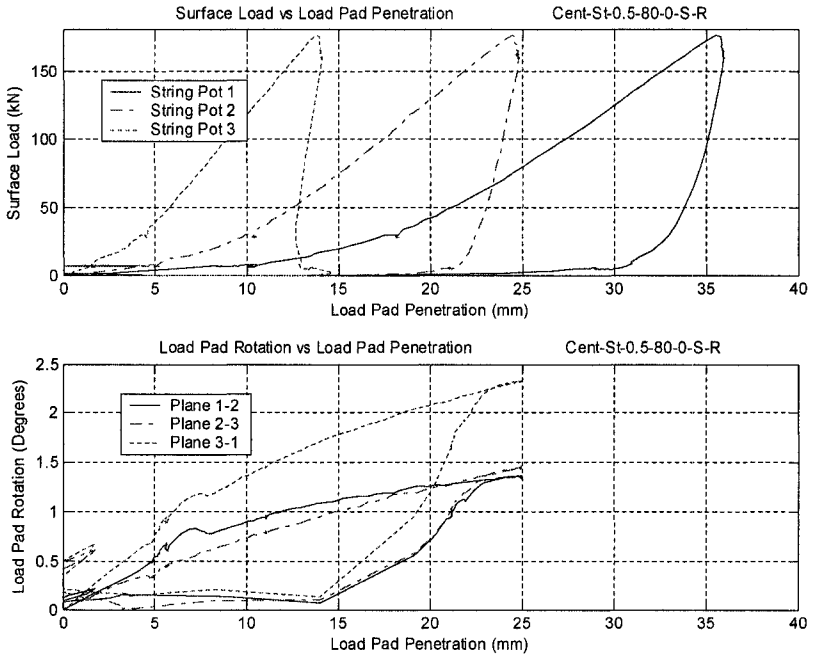

Figure D11: Load Pad Rotations, 0.5D Cover, Rectangular Pad

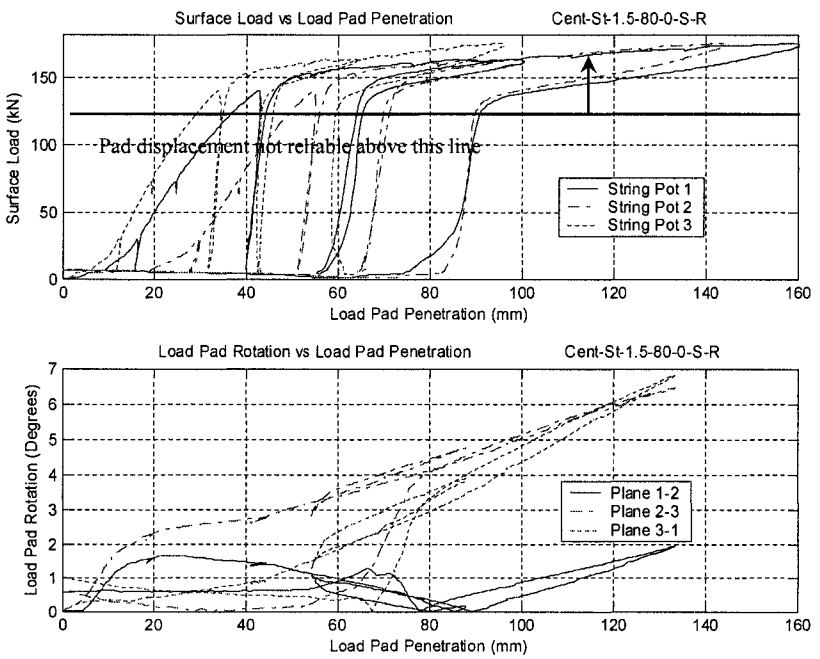

Figure D12: Load Pad Rotations, 1.5D Cover, Rectangular Pad

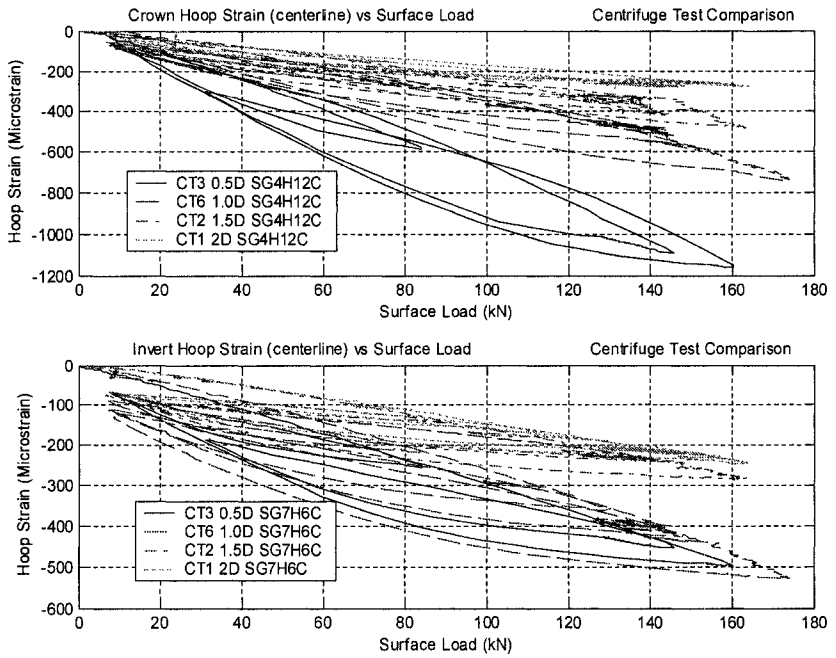

Figure D13: Hoop Strain versus Surface Load, Circular Pad Comparison

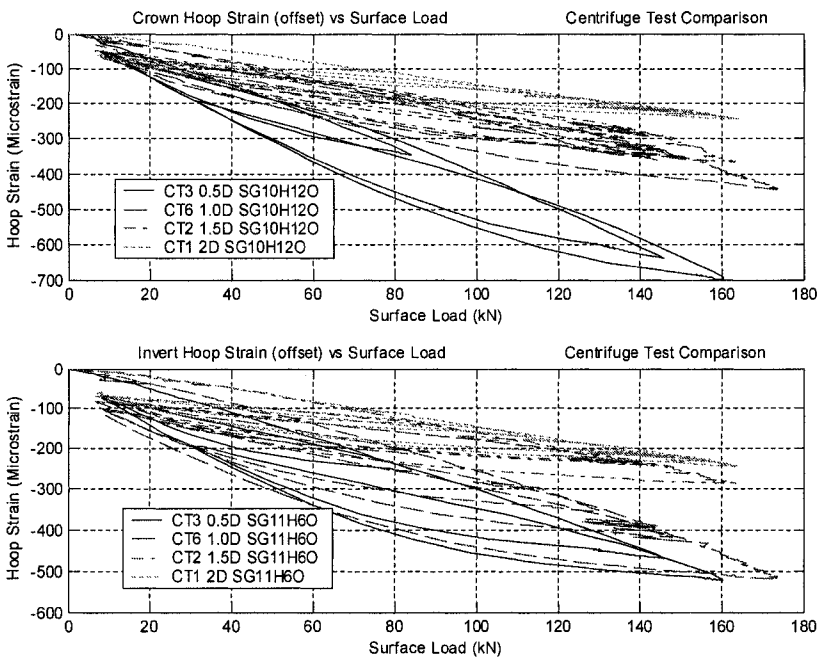

Figure D14: Hoop Strain versus Surface Load, Circular Pad Comparison

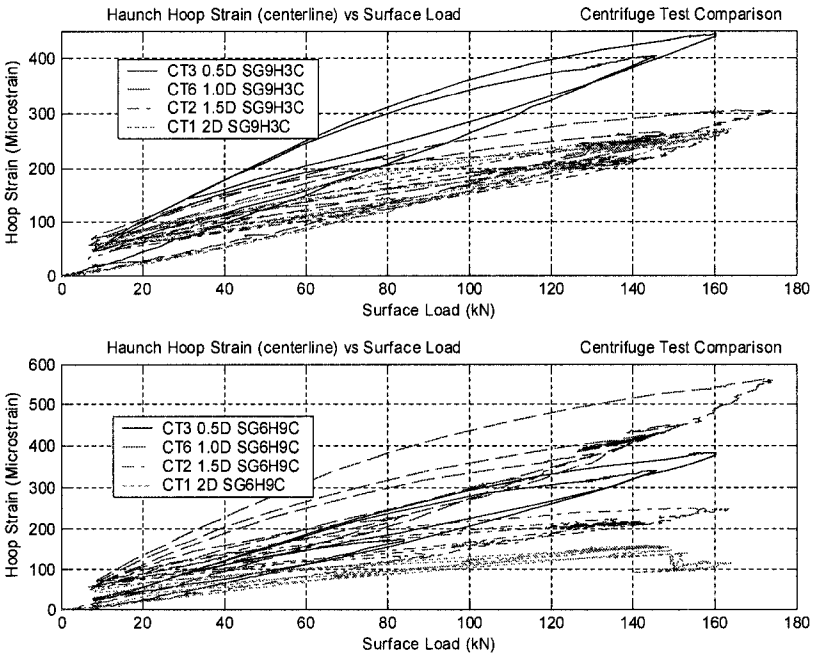

Figure D15: Hoop Strain versus Surface Load, Circular Pad Comparison

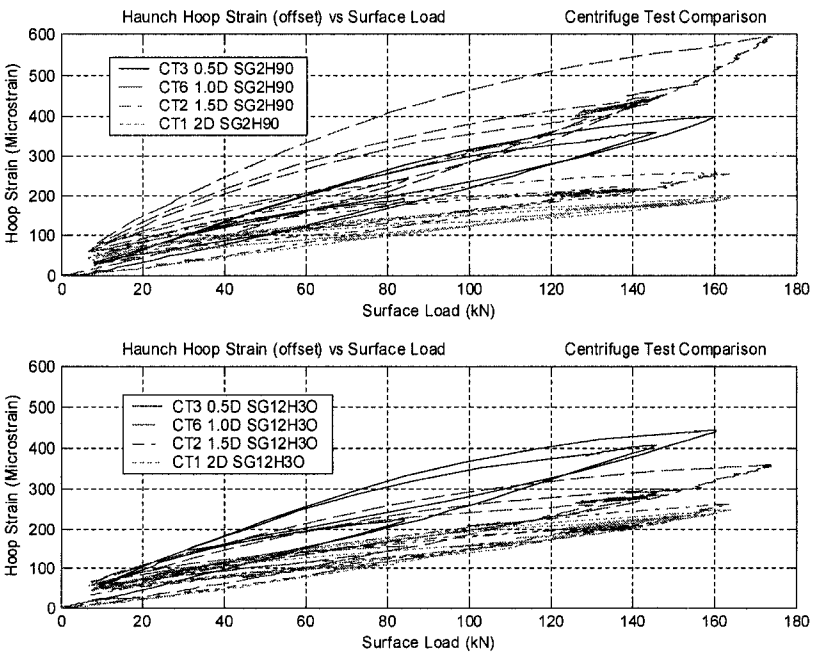

Figure D16: Hoop Strain versus Surface Load, Circular Pad Comparison

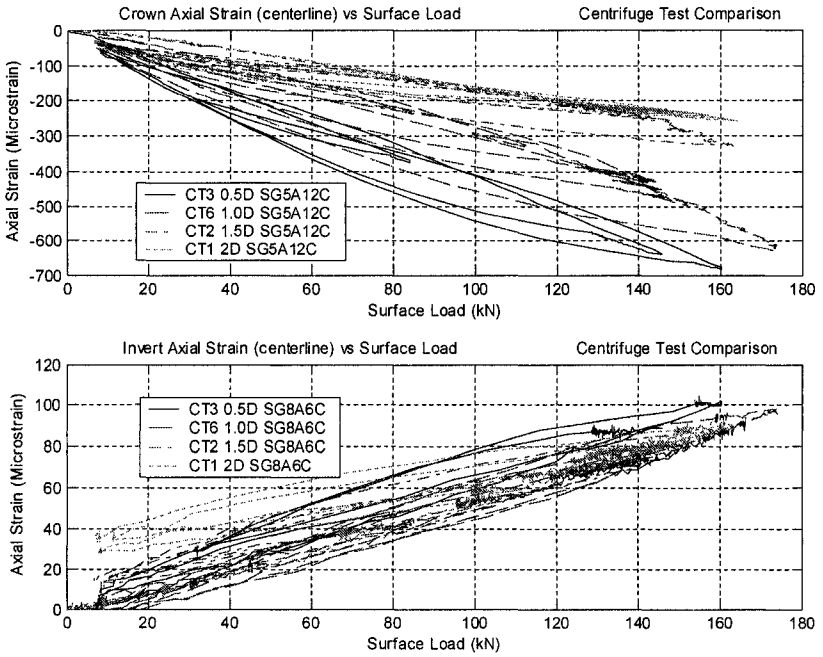

Figure D17: Axial Strain versus Surface Load, Circular Pad Comparison

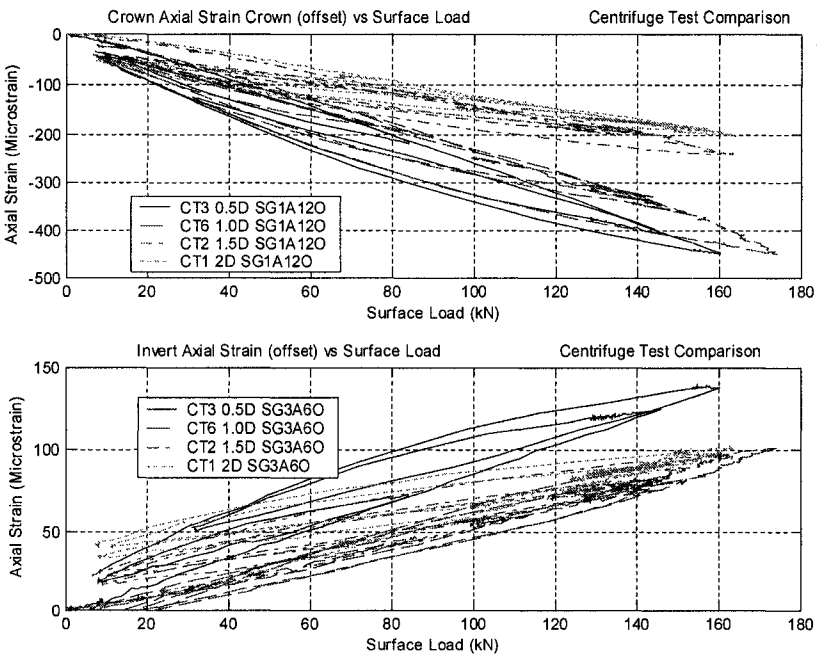

Figure D18: Axial Strain versus Surface Load, Circular Pad Comparison

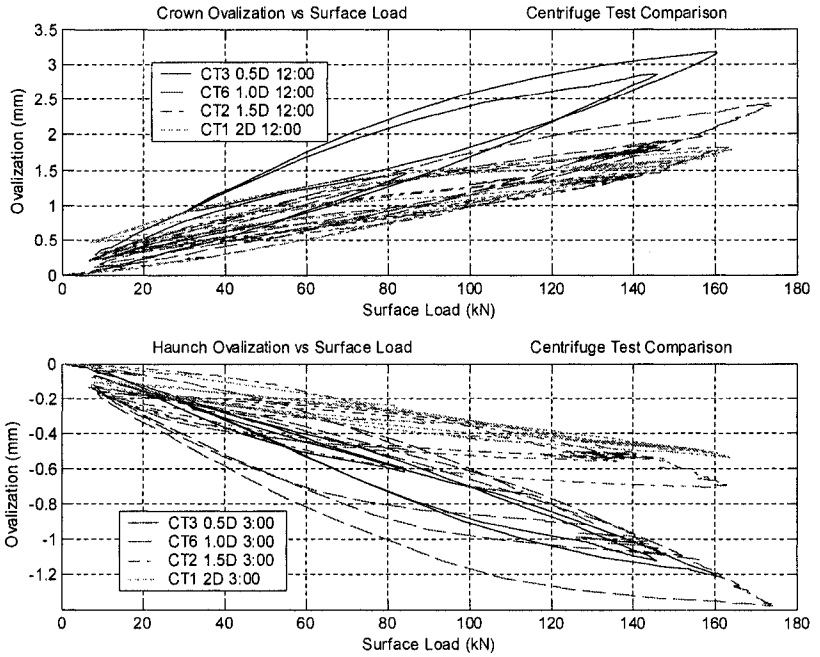

Figure D19: Ovalization versus Surface Load, Circular Pad Comparison

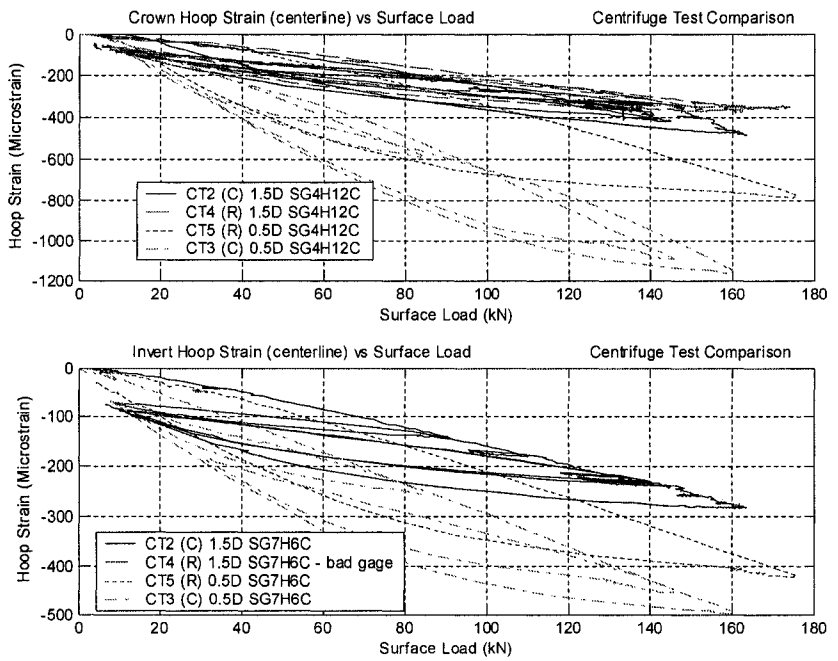

Figure D20: Hoop Strain versus Surface Load, Rectangular Pad Comparison

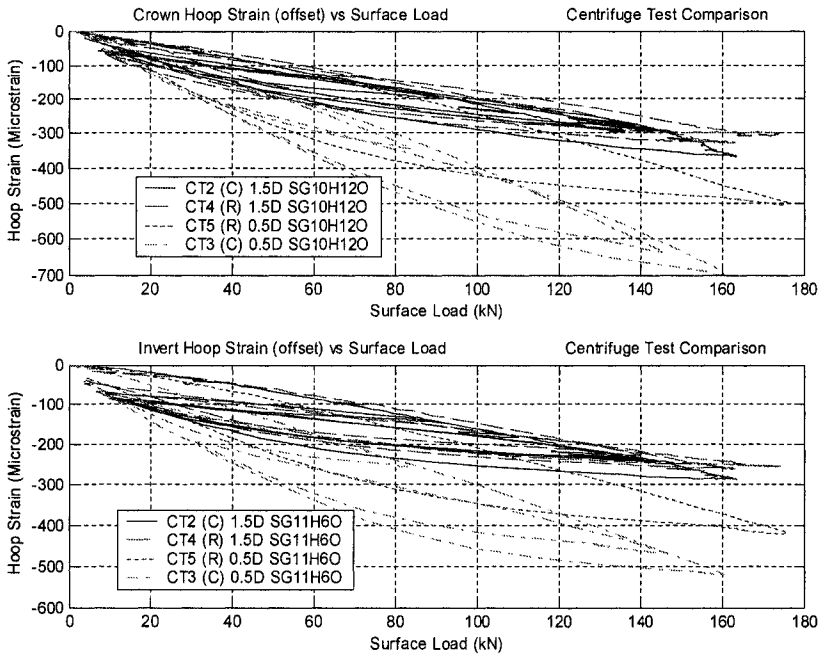

Figure D21: Hoop Strain versus Surface Load, Rectangular Pad Comparison

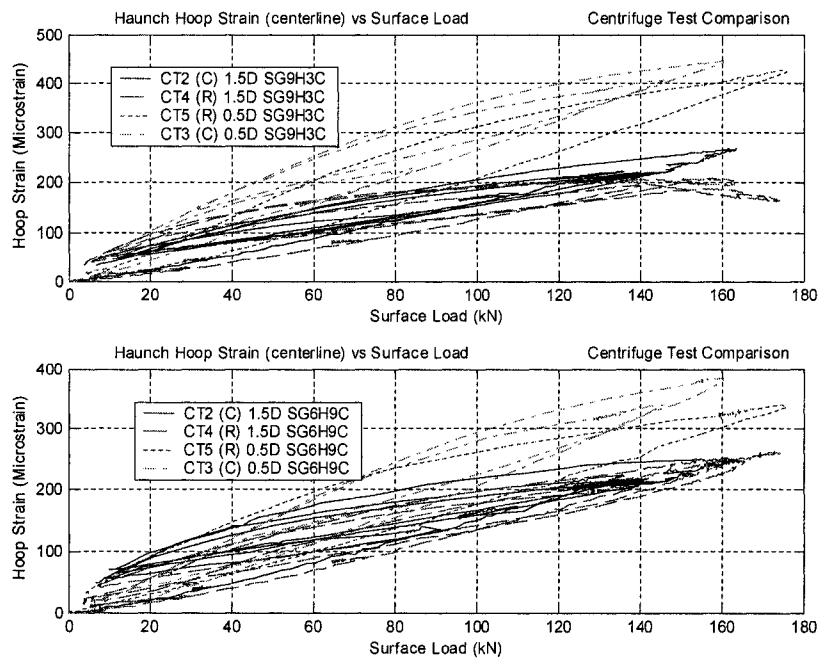

Figure D22: Hoop Strain versus Surface Load, Rectangular Pad Comparison

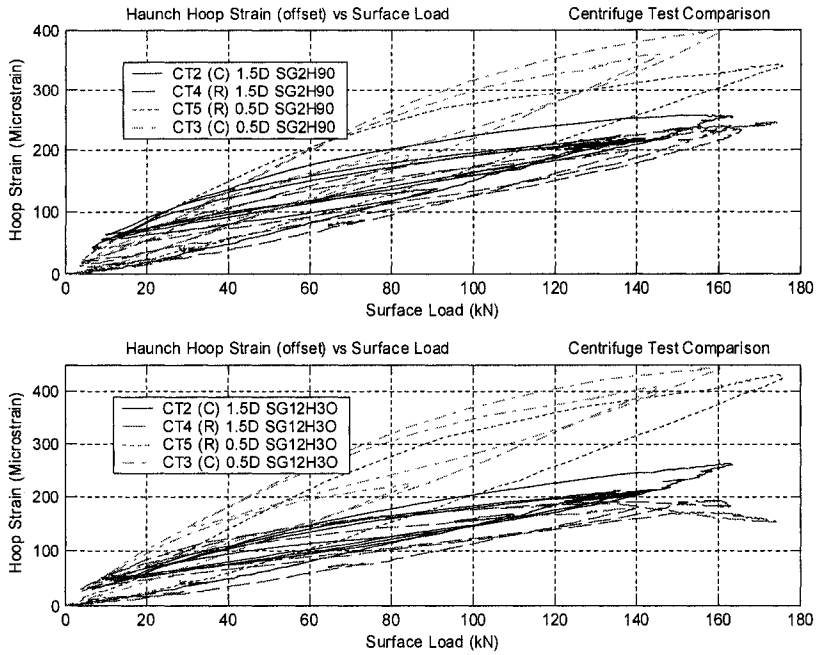

Figure D23: Hoop Strain versus Surface Load, Rectangular Pad Comparison

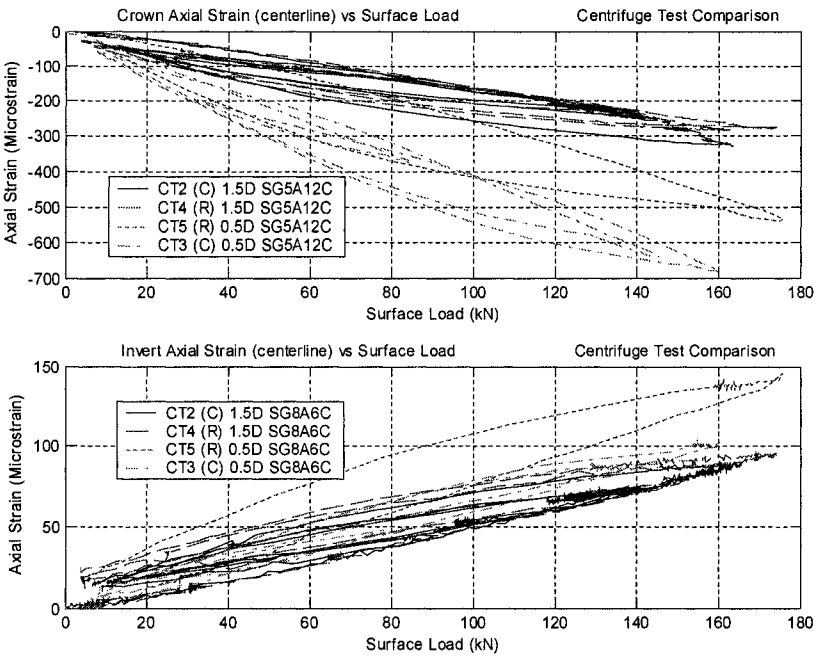

Figure D24: Axial Strain versus Surface Load, Rectangular Pad Comparison

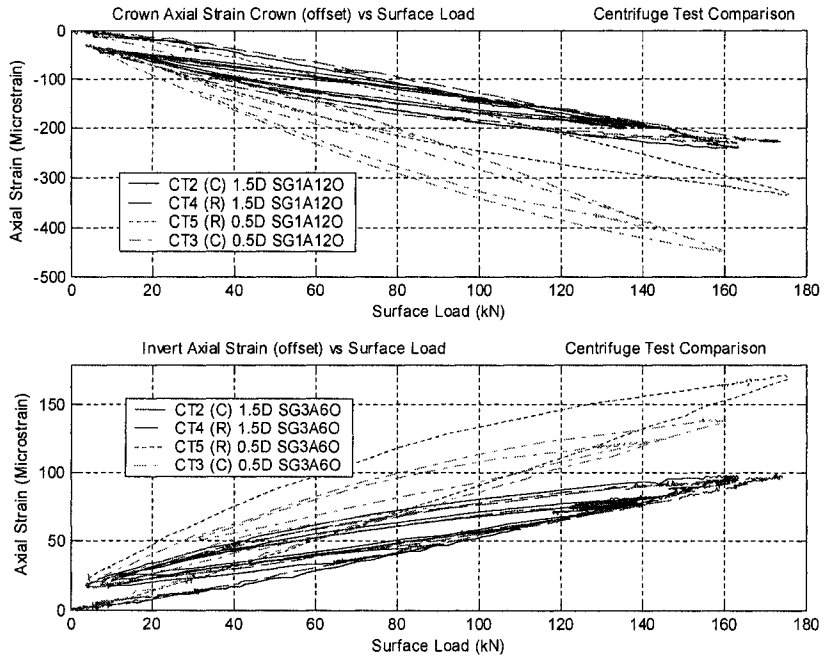

Figure D25: Axial Strain versus Surface Load, Rectangular Pad Comparison

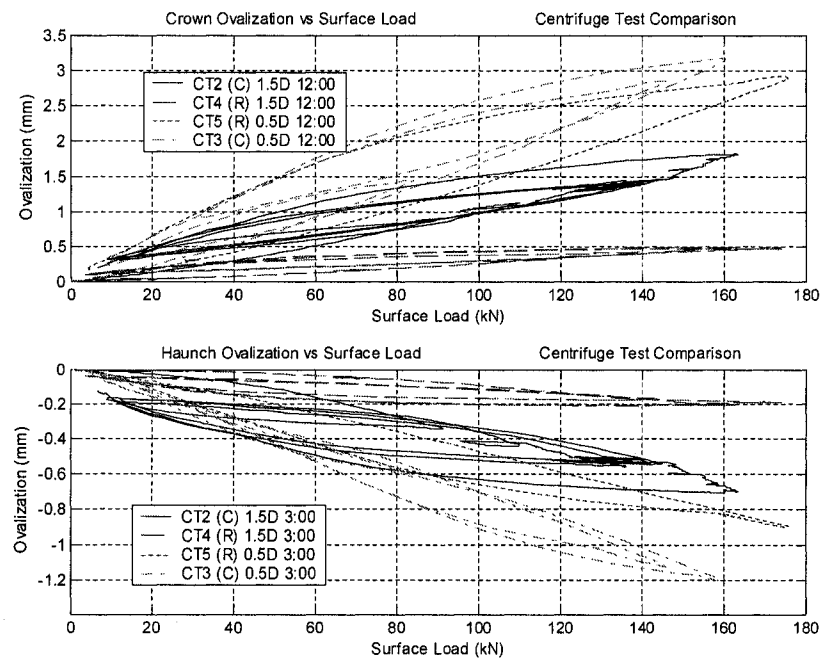

Figure D26: Ovalization versus Surface Load, Rectangular Pad Comparison

Appendix E
Chapter 6 Plots
Comparison of Test Programs

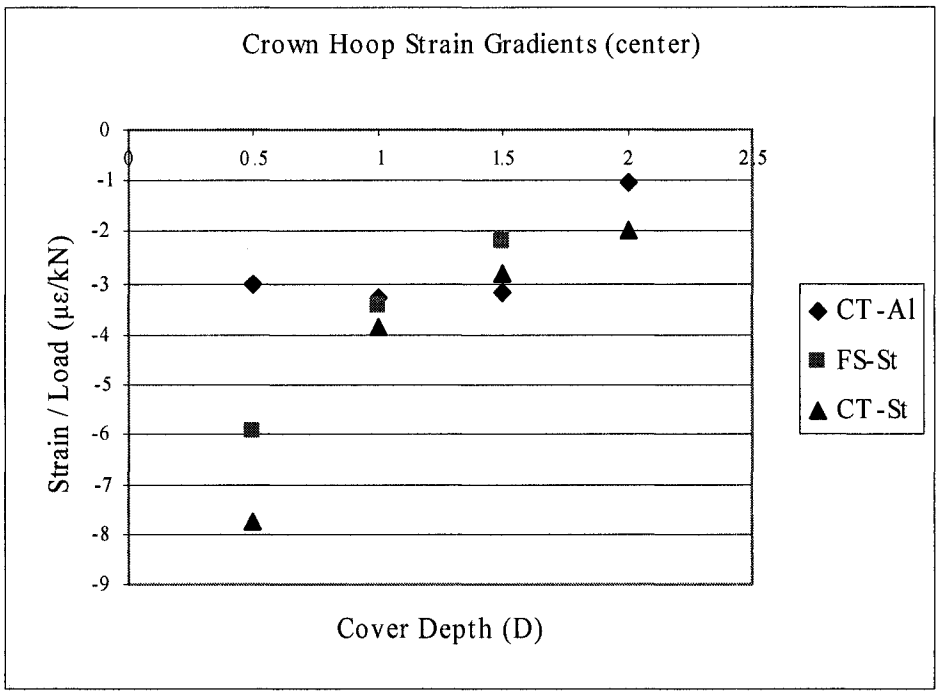

Figure E1: Crown Hoop Strain Gradients (center)

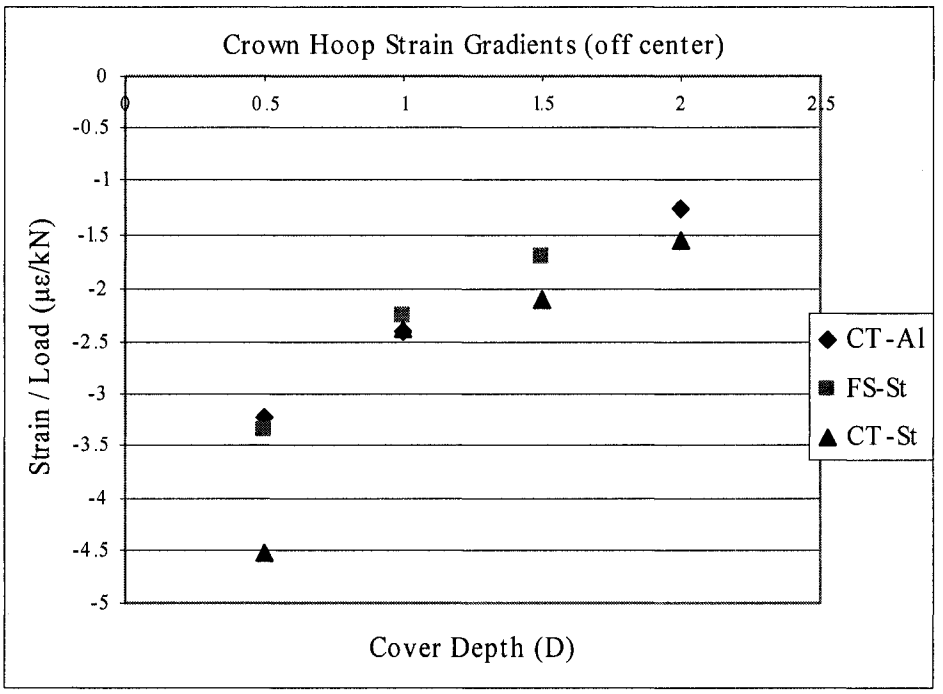

Figure E2: Crown Hoop Strain Gradients (off center)

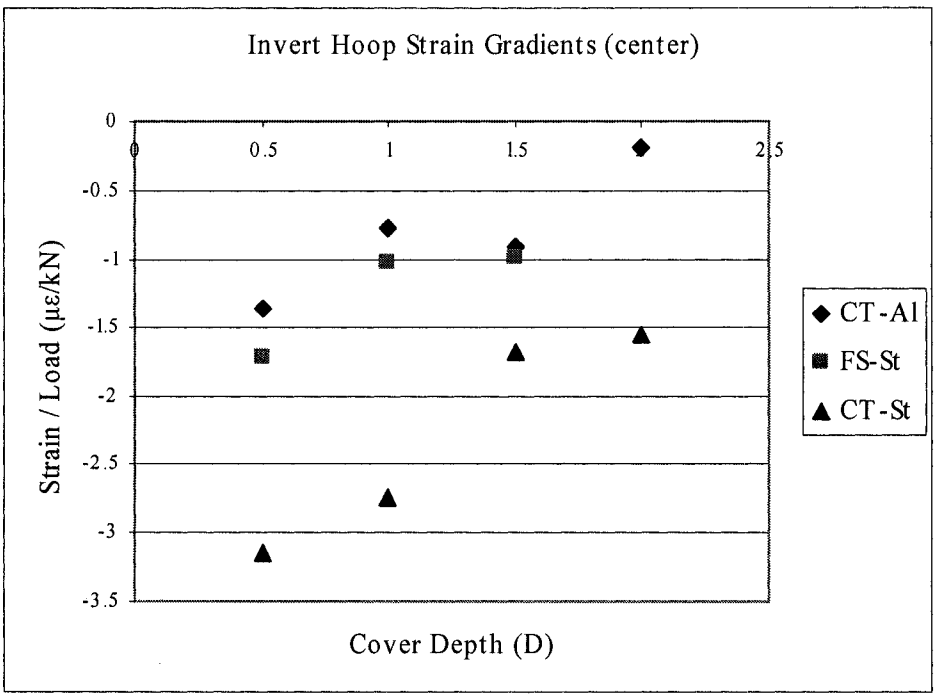

Figure E3: Invert Hoop Strain Gradients (center)

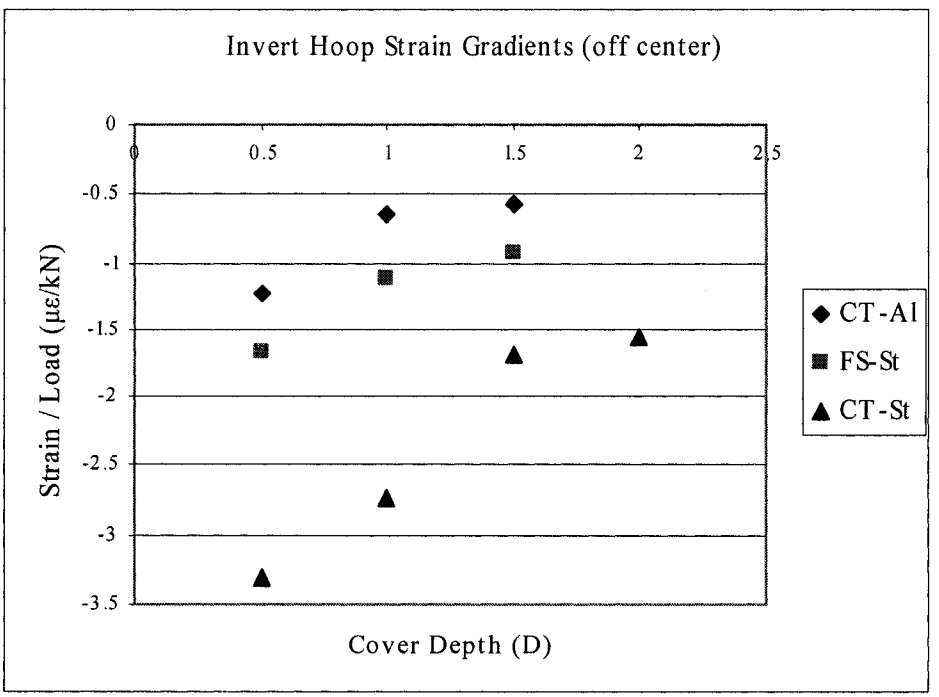

Figure E4: Invert Hoop Strain Gradients (off center)

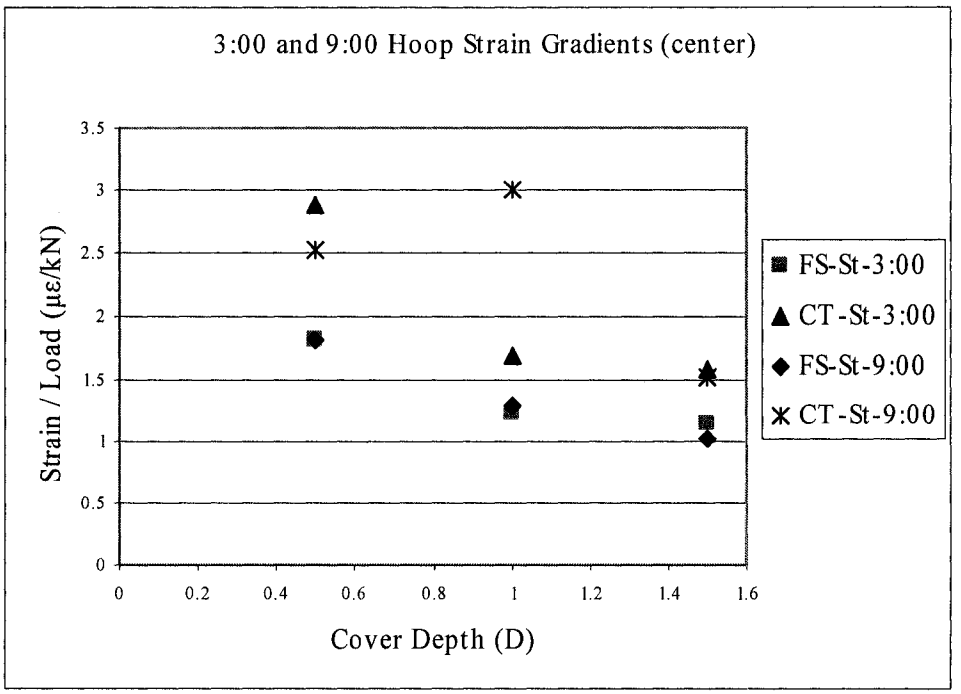

Figure E5: Haunch Hoop Strain Gradients (center)

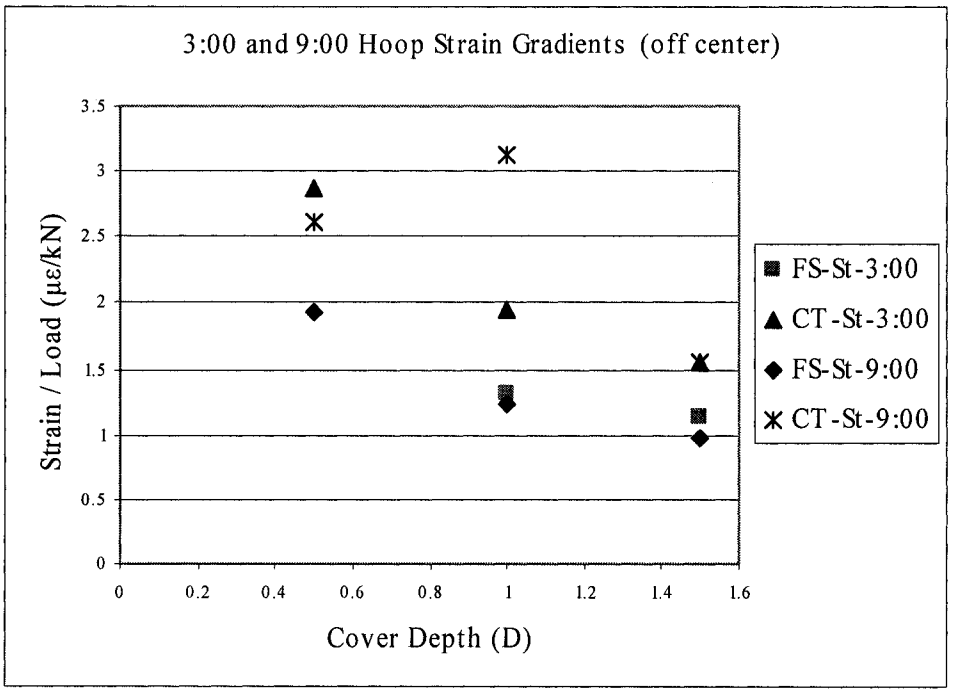

Figure E6: Haunch Hoop Strain Gradients (off center)

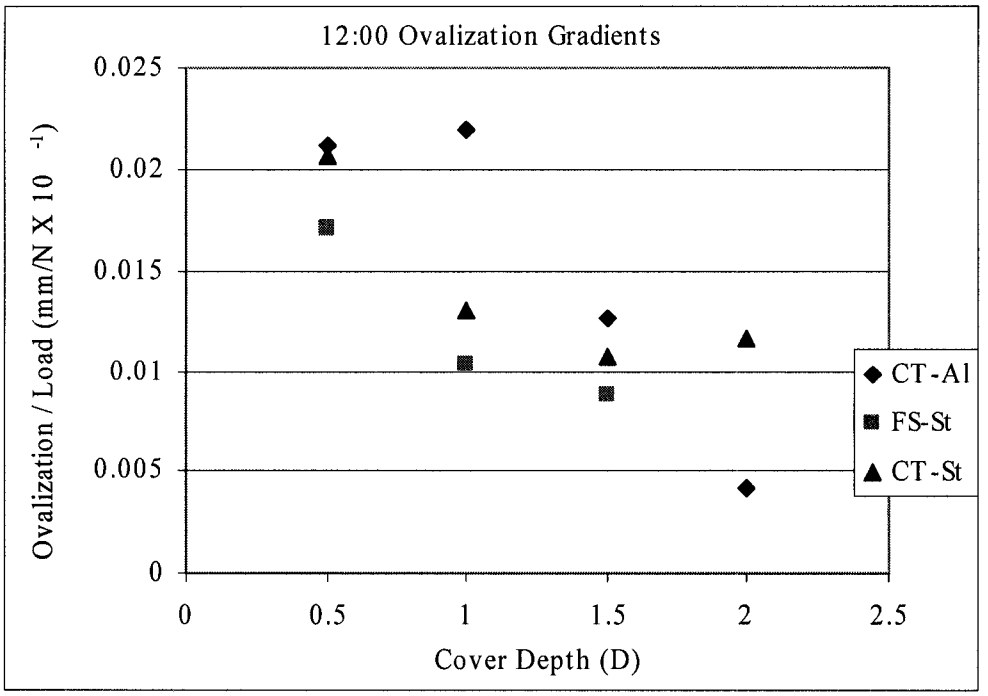

Figure E7: Ovalization Gradients (12:00)

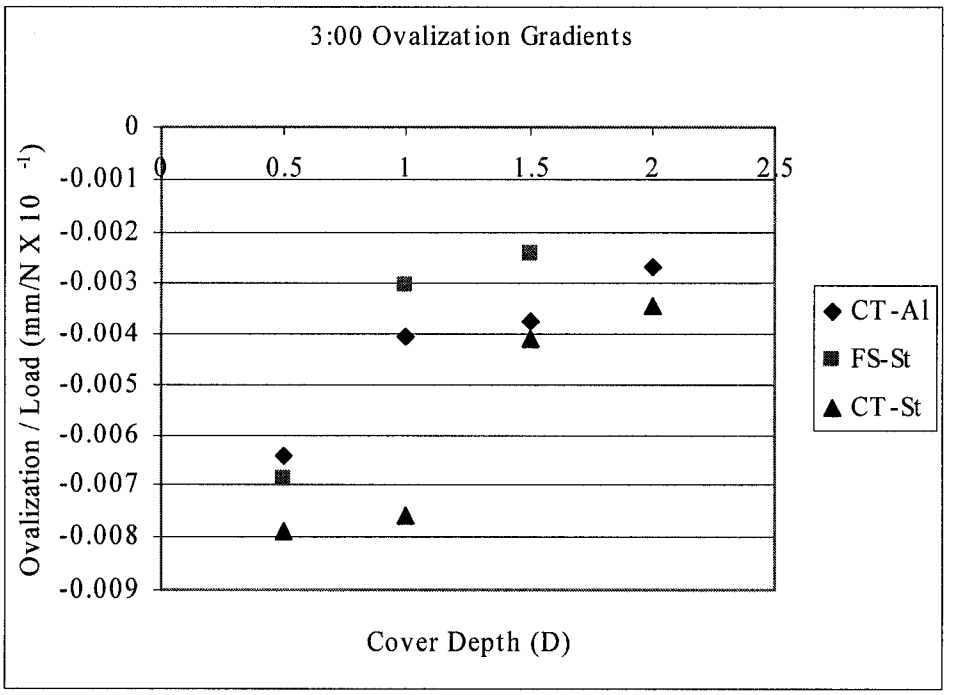

Figure E8: Ovalization Gradients (3:00)

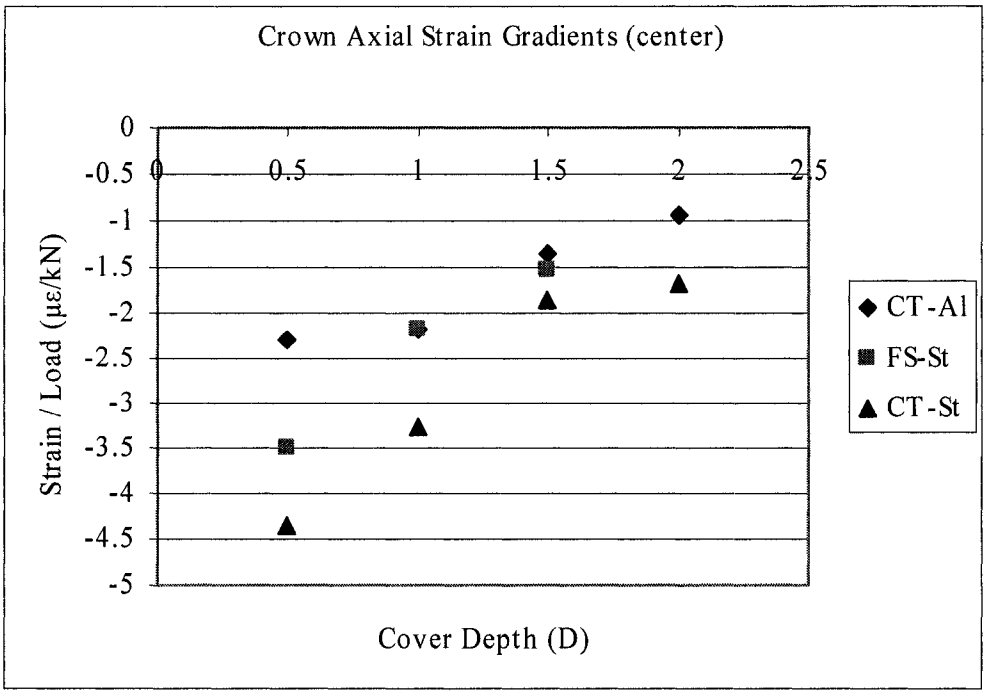

Figure E9: Crown Axial Strain Gradients (center)

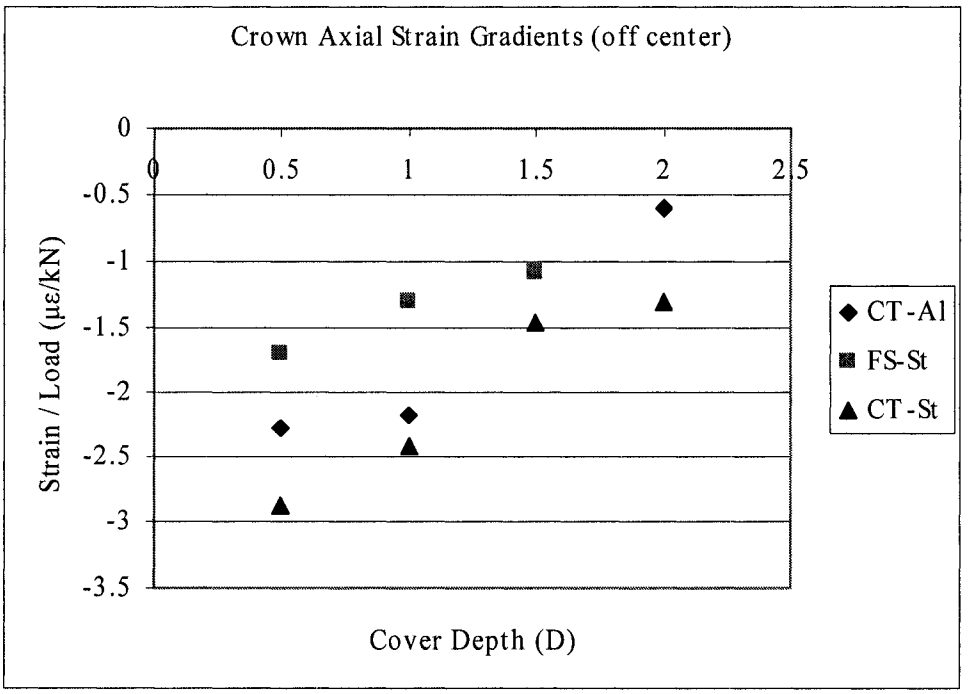

Figure E10: Crown Axial Strain Gradients (off center)

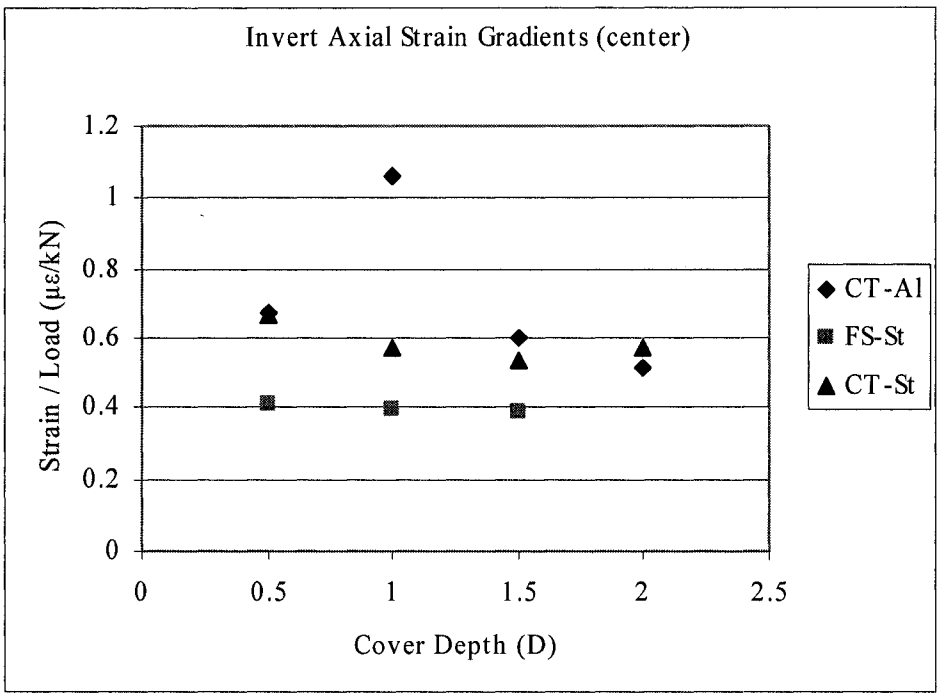

Figure E11: Invert Axial Strain Gradients (center)

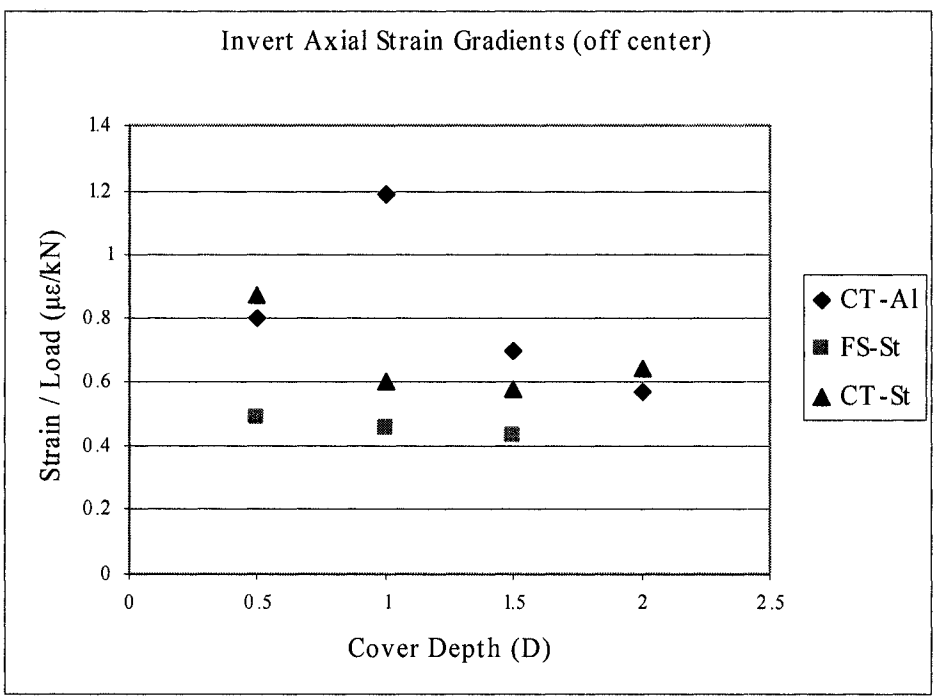

Figure E12: Invert Axial Strain Gradients (off center)

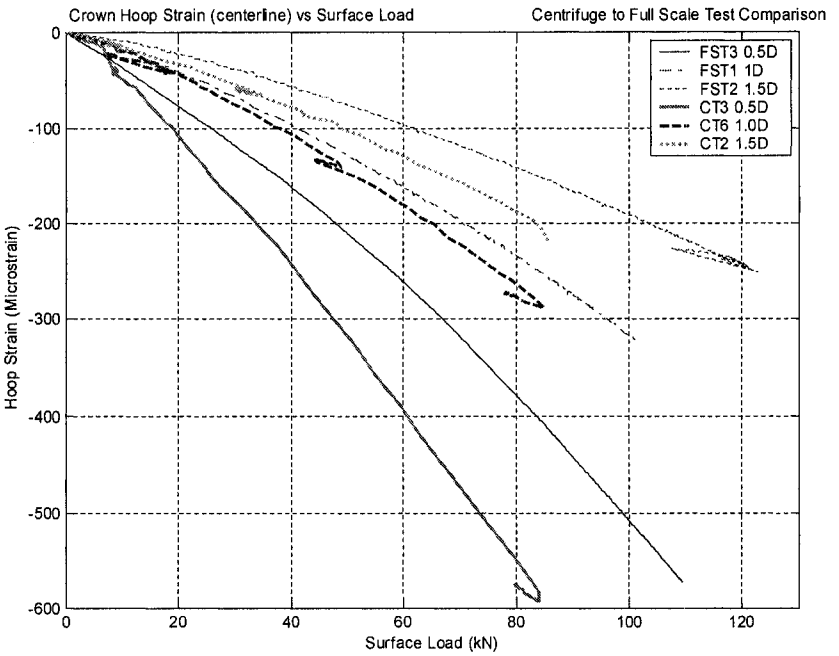

Figure E13: Crown Hoop Strain versus Surface Load (center)

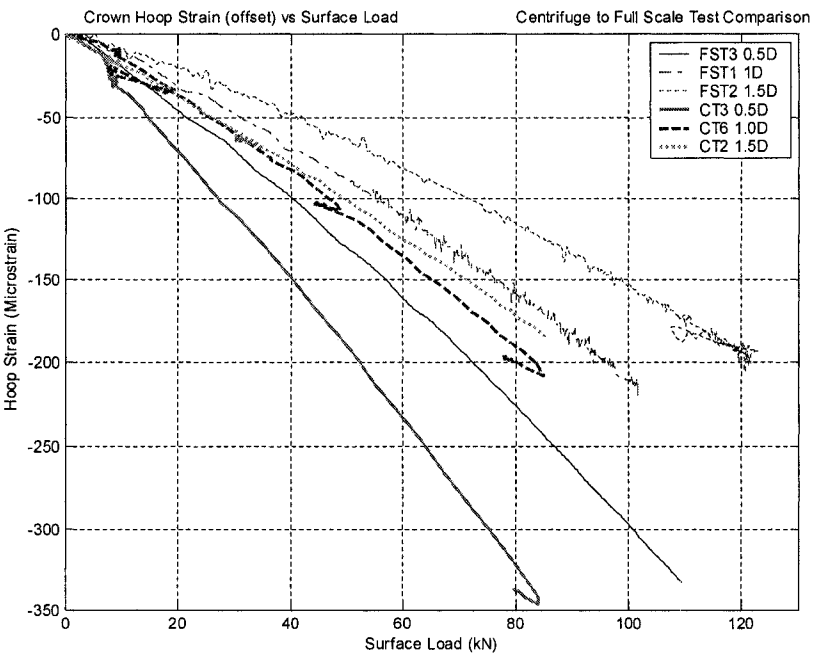

Figure E14: Crown Hoop Strain versus Surface Load (off center)

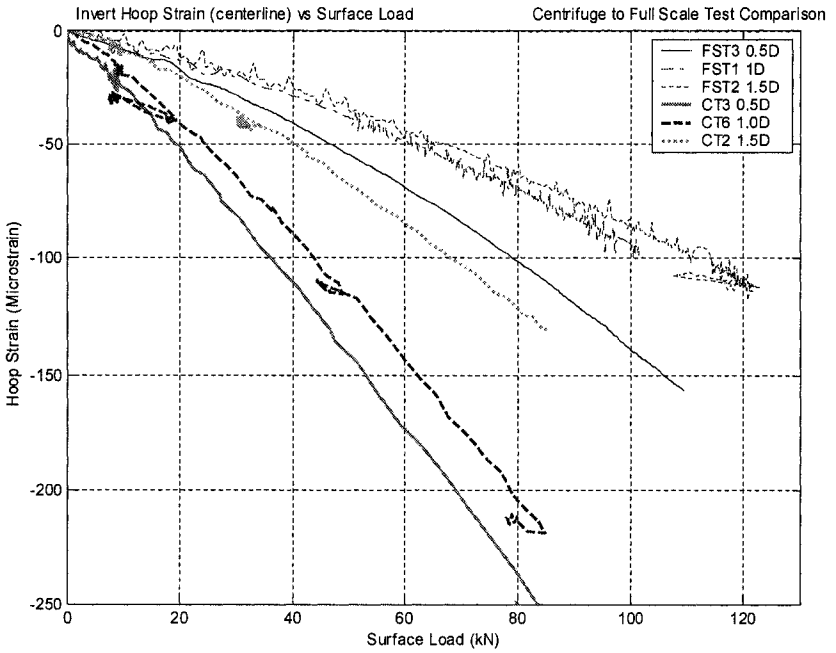

Figure E15: Invert Hoop Strain versus Surface Load (center)

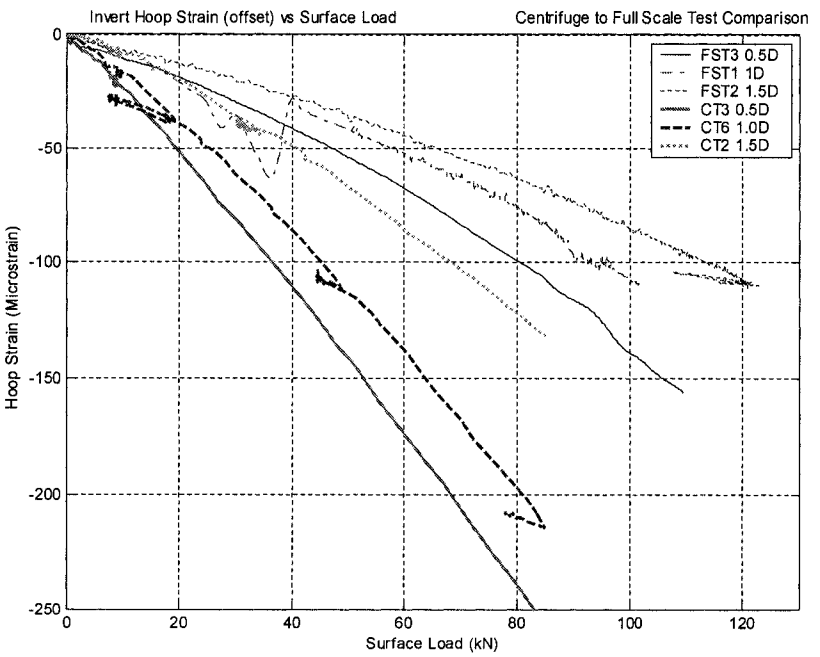

Figure E16: Invert Hoop Strain versus Surface Load (off center)

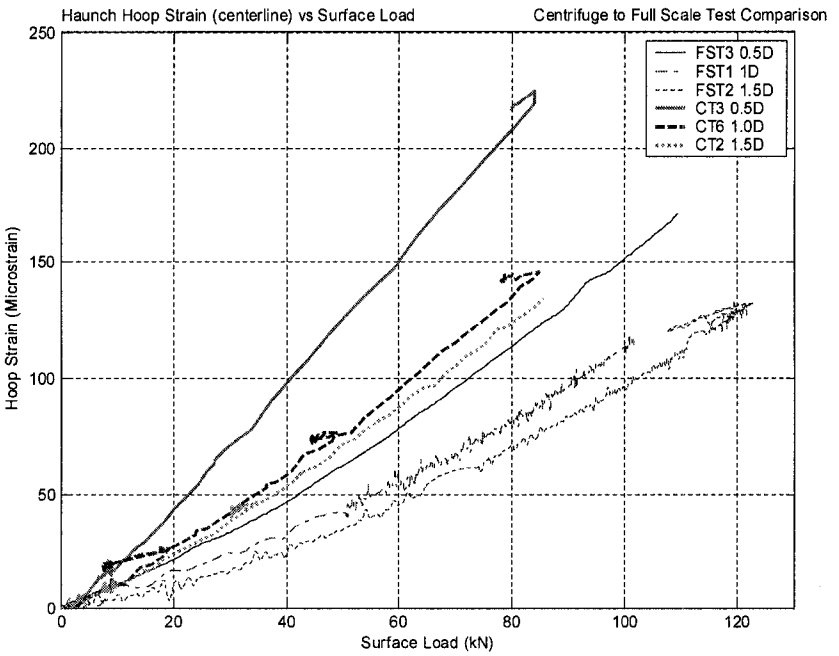

Figure E17: Haunch Hoop Strain versus Surface Load (center, 3:00)

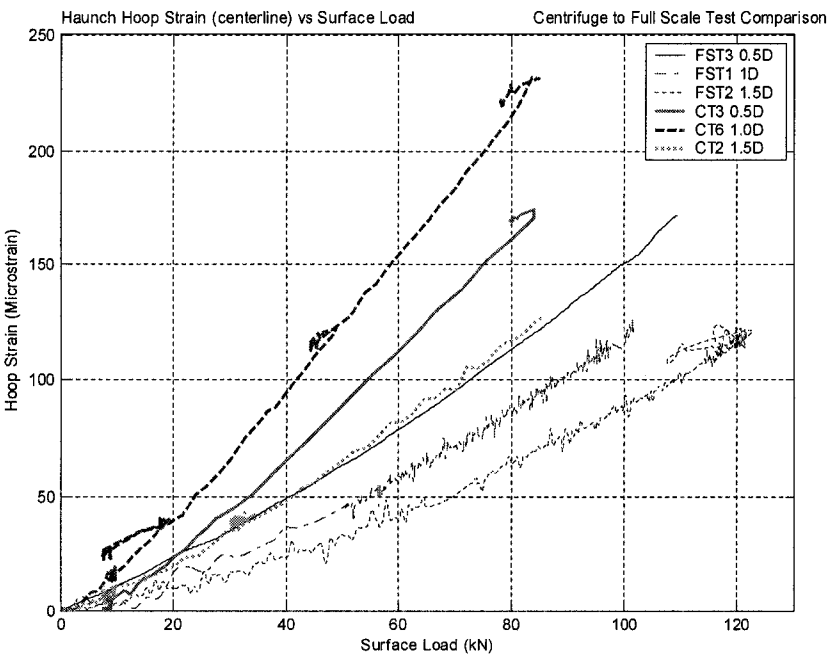

Figure E18: Haunch Hoop Strain versus Surface Load (center, 9:00)

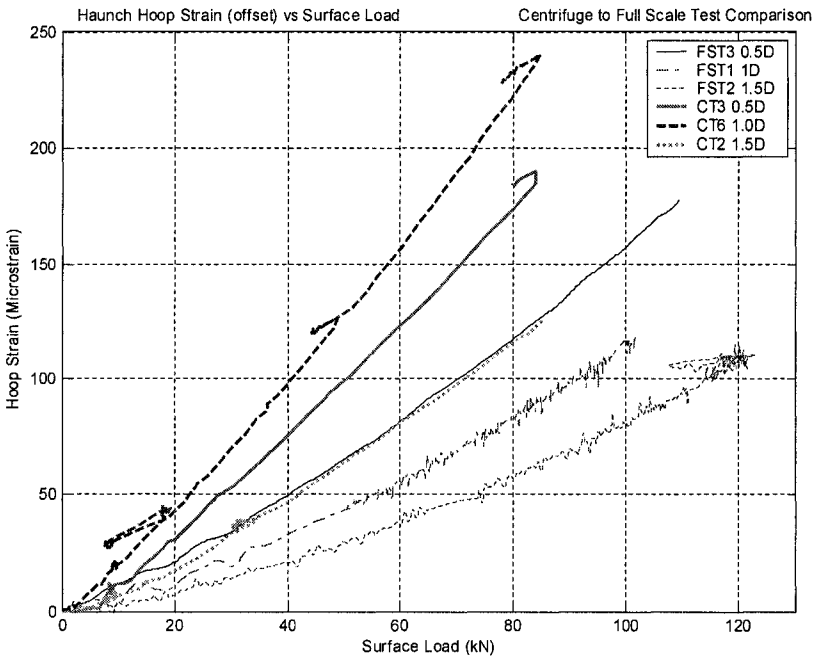

Figure E19: Haunch Hoop Strain versus Surface Load (off center, 3:00)

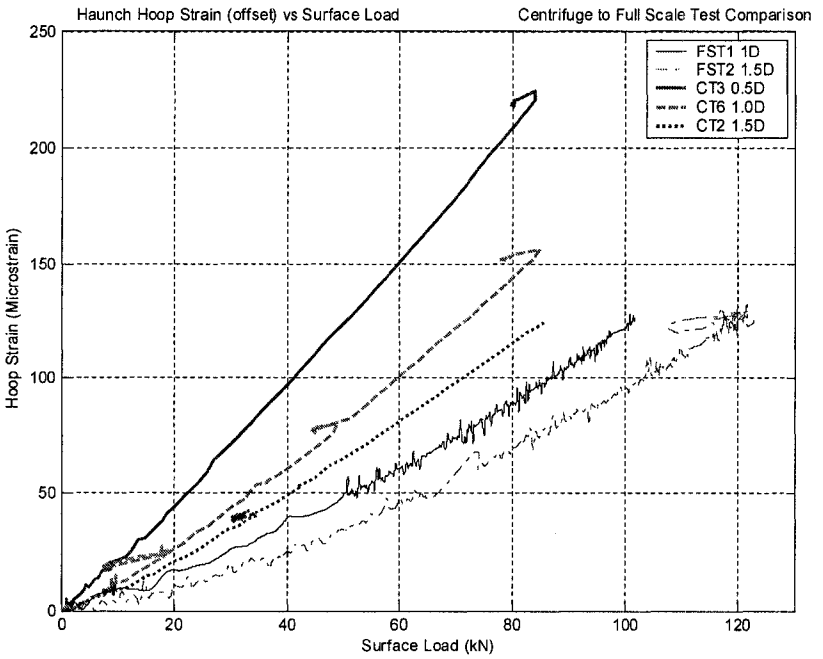

Figure E20: Haunch Hoop Strain versus Surface Load (off center, 9:00)

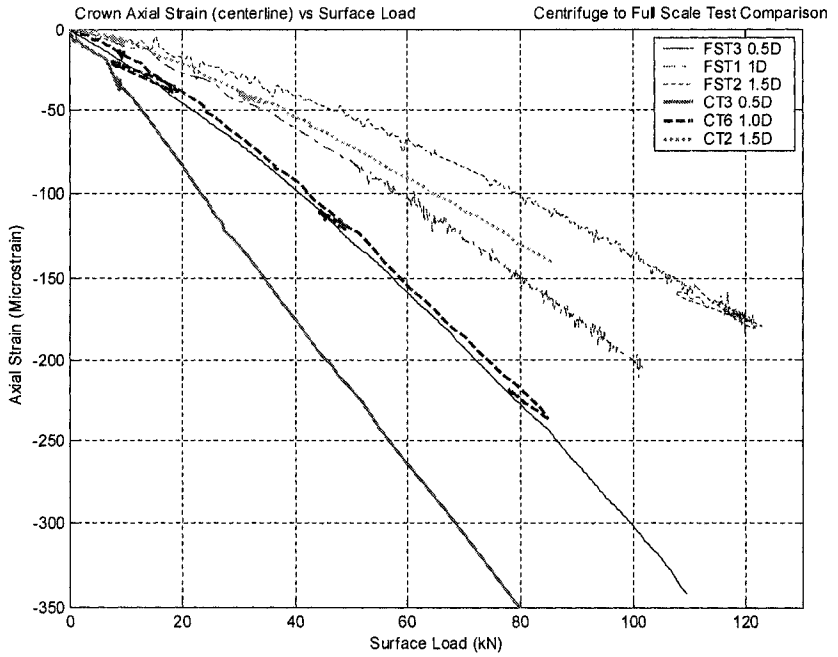

Figure E21: Crown Axial Strain versus Surface Load (center)

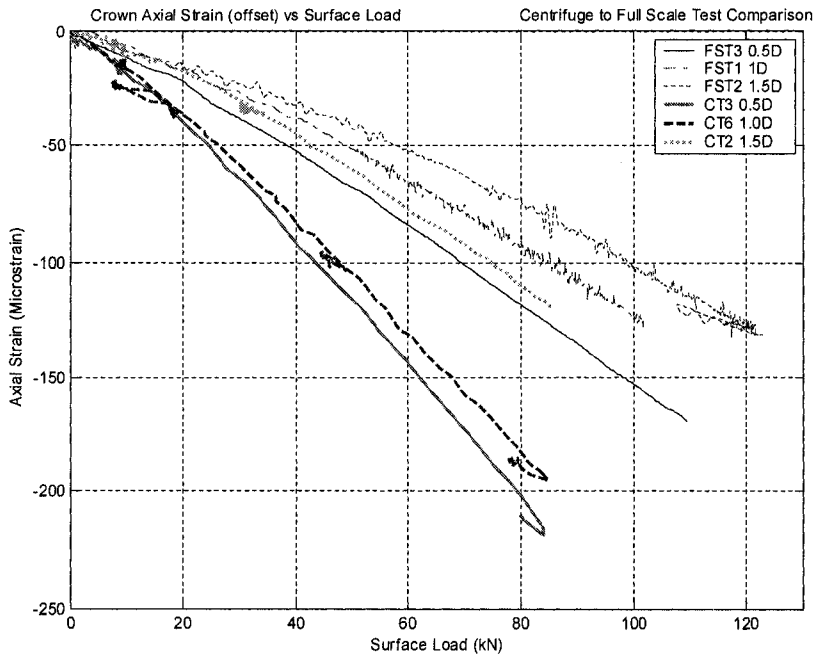

Figure E22: Crown Axial Strain versus Surface Load (off center)

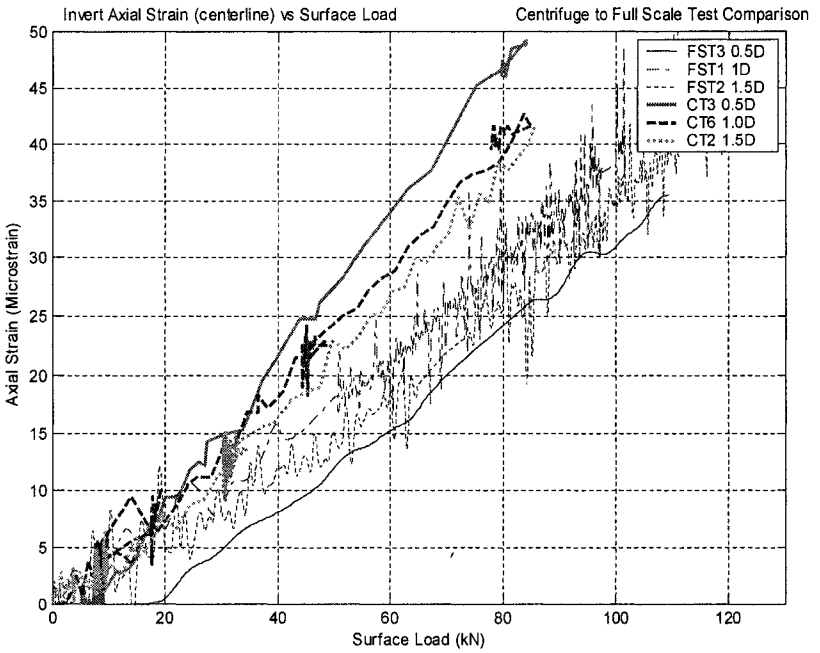

Figure E23: Invert Axial Strain versus Surface Load (center)

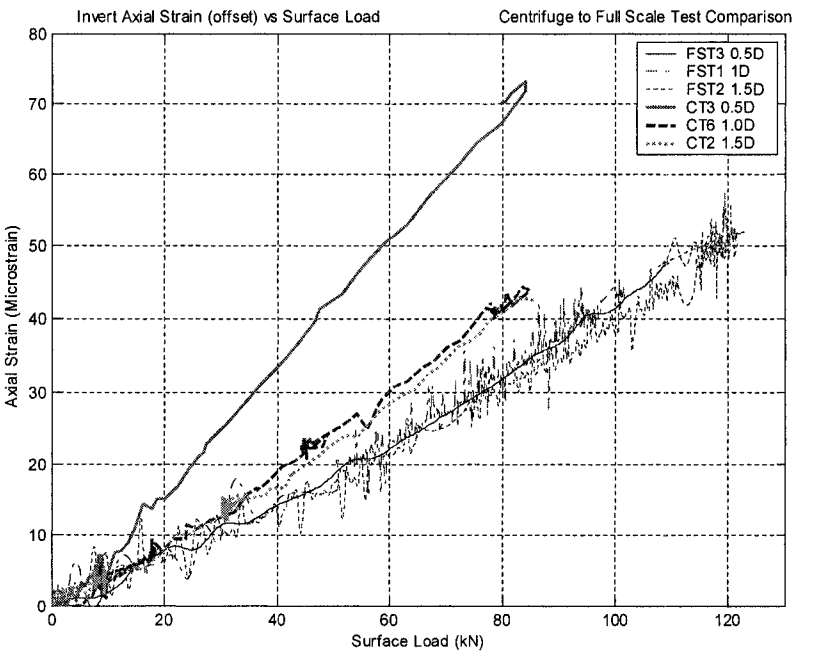

Figure E24: Invert Axial Strain versus Surface Load (off center)

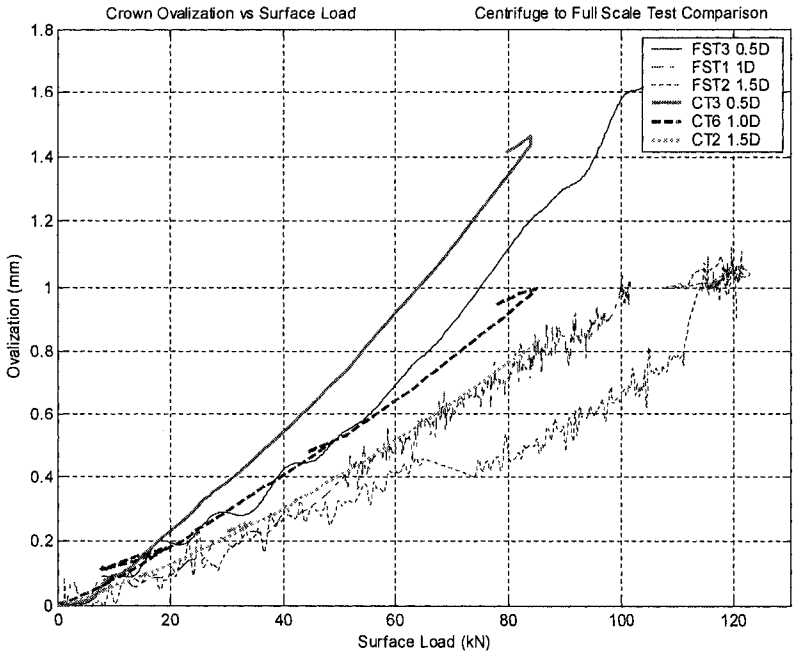

Figure E25: Ovalization versus Surface Load (12:00)

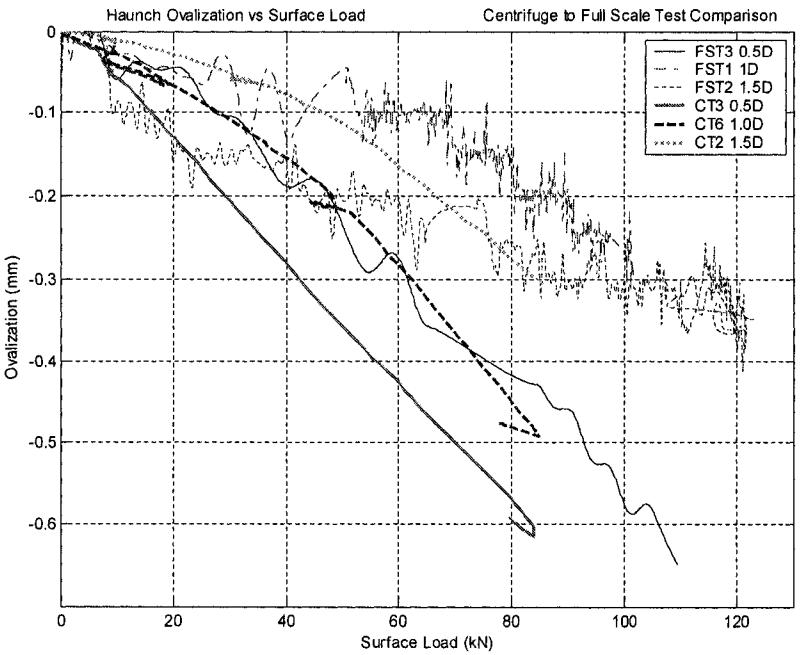

Figure E26: Ovalization versus Surface Load (3:00)